Retrospective Theses and Dissertations

1994

Flocculation kinetics using Fe(III) coagulant in water treatment: the effects of sulfate and temperature

Lim-Seok Kang

Iowa State University

Recommended Citation

INFORMATION TO USERS

This manuscript has been reproduced from the microfilm master. UMI films the text directly from the original or copy submitted. Thus, some thesis and dissertation copies are in typewriter face, while others may be from any type of computer printer.

The quality of this reproduction is dependent upon the quality of the copy submitted. Broken or indistinct print, colored or poor quality illustrations and photographs, print bleedthrough, substandard margins, and improper alignment can adversely affect reproduction.

In the unlikely event that the author did not send UMI a complete manuscript and there are missing pages, these will be noted. Also, if unauthorized copyright material had to be removed, a note will indicate the deletion.

Oversize materials (e.g., maps, drawings, charts) are reproduced by sectioning the original, beginning at the upper left-hand corner and continuing from left to right in equal sections with small overlaps. Each original is also photographed in one exposure and is included in reduced form at the back of the book.

Photographs included in the original manuscript have been reproduced xerographically in this copy. Higher quality 6" x 9" black and white photographic prints are available for any photographs or illustrations appearing in this copy for an additional charge. Contact UMI directly to order.

UMI

Flocculation kinetics using Fe(III) coagulant in water treatment:
The effects of sulfate and temperature

Kang, Lim-Seok, Ph.D.

Iowa State University, 1994

Flocculation kinetics using Fe(III) coagulant in water treatment:

the effects of sulfate and temperature

by

Lim-Seok Kang

A Dissertation Submitted to the

Graduate Faculty in Partial Fulfillment of the

Requirements for the Degree of

DOCTOR OF PHILOSOPHY

Department: Civil and Construction Engineering
Major: Civil Engineering (Environmental Engineering)

Approved:

In Charge of Major Work

For the Major Department

For the Graduate College

Iowa State University
Ames, Iowa

1994

TABLE OF CONTENTS

LIST OF TABLES

v

LIST OF FIGURES

LIST OF NOMENCLATURE AND ABBREVIATIONS

AIA	Automatic Image Analysis
C	scattering cross-section of particles
ε	power input per unit mass
G	root mean square velocity gradient
ΔH_r^o	reaction standard enthalpy
ΔH_f	formation standard enthalpy
Homog.	homogenized kaolin suspension
I	ionic strength
K_1, K_2	equilibrium constant
K^{int}	intrinsic surface complexation constant
K_{os}	stability constant for outer-sphere complex
K_{so}	solubility product
K_w	ion product of water
K_{-w}	water loss rate constant
N	particle number or rotational impeller speed
η	Kolmogoroff microscale of turbulence
NTU	Nephelometric Turbidity Unit
P	power input
PDA	Photometric Dispersion Analyzer
PZC	point of zero charge
r	ratio of $[OH^-]_{added}$ to $[Fe_T]$
R.M.	rapid mixing
T	absolute temperature in Kelvin, ^oK
V_{rms}	root mean square of fluctuating signal around mean voltage (V)
μ, v	absolute and kinematic fluid viscosity
ZP	zeta potential

1. INTRODUCTION

Coagulation and Flocculation have been used to assist in the removal of particulate and dissolved materials in water and wastewater treatment. Coagulation and flocculation are elements of total clarification system used in water treatment that commonly includes sedimentation and filtration. Coagulation and flocculation require a unique combination of chemical reactions and physical transport processes which are used to destabilize and aggregate suspended particles. Therefore, the effectiveness of coagulation and flocculation influences the efficiency of the subsequent sedimentation and filtration processes.

The terms coagulation and flocculation are often used in the literature synonymously. In this discussion, the term coagulation is applied to the overall process including both particle destabilization and aggregation. The term flocculation is used throughout to emphasize the physical transport process which leads to interparticle contact and the formation of particle aggregates.

Each year, the water industry faces increasingly stringent water quality regulations and ever more challenging treatment objectives. Therefore, it is necessary to control and optimize coagulation and flocculation processes that are essential water treatment unit operations in the treatment sequence. Among the coagulants used, aluminum sulfate (alum) has been the most widely used in water treatment and has achieved a satisfactory treated water quality. Recently, however, existing and potential problems associated with high concentrations of aluminum in treated water has raised concern over the use of alum in the

treatment of drinking water. Such problems are associated with the formation of a hydrous Al precipitate in the distribution system and a possible statistical link between Al intake and neurological diseases such as Alzheimer's disease and presenile dementia (Driscoll and Letterman, 1988)(AWWA, 1991).

Attention is therefore increasingly being focused on alternative coagulants to alum such as ferric iron (Fe(III)) salts, organic polymers, and inorganic polymers. This research focuses on the use of Fe(III) salt as a coagulant and includes quantitative studies of the rate at which flocculation processes occur, the factors upon which these rates depend, and the mechanisms involved. Fe(III) salts are receiving attention as alternative coagulants to alum for several important reasons; (1) concerns about residual aluminum concentration in treated waters mentioned previously, (2) possible cost savings compared to other alternative coagulants, and (3) better coagulation efficiency at low water temperature and more efficient removal of color-causing organic materials than alum.

Although the Fe(III) coagulants seems to be the most promising alternative to alum, there are not many water treatment plants using Fe(III) coagulants. Cleasby et al.(1989) reported on detailed studies at 23 successful high rate filtration plants treating surface water. In that report, only two of twenty three plants surveyed had been using ferric chloride as a single coagulant or in conjunction with organic polymer. Therefore, more research is necessary to provide a better understanding of coagulation using a Fe(III) salts for coagulation, leading to more rational process and design decisions.

Many of the experimental techniques (Settling velocity, settled turbidity, refiltration rate) employed for evaluation of coagulation rely solely on measuring the final phase separation of particles from the suspension. While these methods record only the end result of successful coagulation and flocculation, the preceding steps are not followed quantitatively with time, and, therefore, the flocculation kinetics during the preceding steps can not be observed. Treweek and Morgan (1978) indicated that this problem of using indirect measurements alone (i.e., of the end result alone) tends to bias the investigator toward improvement of the physical parameters of the system at the expense of possible chemical alterations that would enhance earlier destabilization stages.

The study of flocculation kinetics is of fundamental interest in the field of water treatment, because rational study of the factors affecting the coagulation process should be based on the rate of particle growth. Therefore, the study of flocculation kinetics can provide a better insight into flocculation mechanisms, the various parameters involved, their impact on the performance of the process, and thereby, the improvement of the design and performance of the coagulation system and the subsequent separation steps. Much attention has been given to the two mechanisms of coagulation in recent years, adsorption-destabilization (A/D) (i.e., adsorption/charge neutralization) and sweep flocculation. However, there has been little work done concerning the differences on flocculation kinetics covering the full range of coagulation domains encompassing the A/D and the sweep flocculation mechanisms. In addition, while some studies have been conducted on the effect

of sulfate ion or cold temperature on flocculation efficiency, little work has been performed using flocculation kinetics observations as a tool to study those effects.

Flocculation is expressly designed to change the particle size distribution of a suspension by causing the aggregation of particles. This research utilizes quantitative measurements of particle size distribution and of the turbidity fluctuations in a flowing suspension to monitor the kinetics of flocculation of a clay suspension following the addition of a Fe(III) coagulant. To accomplish this goal, two sophisticated systems will be used, namely Automatic Image Analysis (AIA) system and Photometric Dispersion Analyzer (PDA). Both of these kinetic measuring systems provide useful information to characterize the rate of flocculation.

In practice, the water treatment industry must operate over a wide range of conditions due to regional and seasonal fluctuations in the physical and chemical characteristics of the surface waters being treated. Water treatment plants of the world must be able to treat surface waters for all seasons of the year. In temperate regions, this includes the winter season with water temperatures near the freezing point of water. In spite of this, published information on the impact of cold water temperature on flocculation is both scarce and contradictory. In particular, very little data are available on the kinetics of flocculation at cold water temperature covering the A/D and sweep floc coagulation domains. Therefore, it is necessary that the impact of low water temperature on flocculation should be investigated to ensure the applicability of coagulation theory to water treatment practice on a year-around basis.

Among the anions dissolved in natural water, sulfate ion is one of the most common anions and its concentration is quite variable from source to source in natural waters. Sulfate ion is an interesting model ion in coagulation for at least four reasons; (1) it is one of the most common anions in natural waters and is known to affect coagulation with metal salt coagulants, (2) it is also the associated anion with commonly used metal salt coagulants, such as alum and ferric sulfate, (3) its use causes the formation of complexes with metal salt coagulants, and (4) in some treatment plants, H_2SO_4 is added for the purpose of pH adjustments in the coagulation process. Some studies have been reported on the effect of sulfate ion on coagulation process using metal salt coagulants, but, no systematic study of the influence of sulfate ion on the rate of flocculation has been reported.

2. OBJECTIVES

This research focuses on the use of a Fe(III) salt as a coagulant for the flocculation of clay dispersion under various experimental conditions. While the use of hydrolyzing metal coagulants has been investigated extensively, there has not been direct measurement of flocculation kinetics spanning the full range of coagulation domains encountered in public water treatment. Furthermore, while a large body of research exists on coagulation and flocculation at warm temperature with a fairly good understanding of the process, there has been very little work done concerning the flocculation process at low temperature. In addition, no attempt has been made to study the effect of sulfate ion on the rate of flocculation of clay dispersion using Fe(III) salt under various experimental conditions. It is believed that rational study of the factors affecting the coagulation-flocculation process should be based on the kinetic aspects of flocculation. In order to try to correct these deficiencies in the study of the coagulation-flocculation process, this research has the following main objectives:

1. to investigate the kinetics of flocculation of clay in water suspension using a ferric nitrate as a coagulant under tightly controlled treatment conditions. Detailed studies of the flocculation kinetics will be done by assessing the rate of change in total particle number, particle size distribution, and the state of aggregation of clay suspension against flocculation time.

2. to assess the effect of low temperature on flocculation kinetics, spanning the full range of coagulation domains including the adsorption/destabilization (A/D) and the sweep

flocculation mechanisms of coagulation. The particle size distribution, degree of turbidity fluctuation, floc strength, and settled turbidity will be used to aid in evaluating the impact of cold water temperature on the flocculation process.

3. to investigate the effects of sulfate ion on the kinetics of flocculation with ferric nitrate as a coagulant, allowing sulfate ion concentration to be controlled as an independent variable, under experimental conditions that cover the two different coagulation mechanisms (A/D and the sweep flocculation) and including experiments at cold temperature as well as room temperature.

In addressing these objectives, jar tests and 2 L batch reactor tests were used in the preliminary stage of this research, and then 18 L batch reactor tests were conducted to evaluate flocculation kinetics under tightly controlled experimental conditions. The information for the state of aggregation of suspension was obtained by measuring changes in particle size distribution using the AIA, also by observing the fluctuation in the intensity of a light beam transmitted through a flowing suspension using the PDA. The research proposed herein should provide the following:

1. improve our understanding of the kinetics and mechanisms of flocculation, and to attain more reliable use of Fe(III) salts in water treatment industry, leading to more rational process and design decisions.
2. give the water treatment industry a better understanding of how the coagulation and flocculation process can be optimized for treatment of cold waters with varying water quality.
3. enable the improvement of the efficiency of flocculation process and reduce the demand for coagulant in water with varying sulfate concentration and varying temperature.

3. LITERATURE REVIEW

In this part, the literature pertaining to the various aspect of metal salts coagulation and flocculation, particularly for Fe(III) coagulant, is reviewed. The discussion is first centered on the chemical aspects of Fe(III) salts as coagulants. This first section discusses the hydrolysis and precipitation process and the effect of hydrolysis on solubility of Fe(III) salts. The second section contains the mechanisms of coagulation and flocculation for the aggregation of the destabilized particles. The third section is about the studies of effects of sulfate ion on flocculation kinetics, and the fourth section is focused on the effects of temperature on flocculation kinetics.

3.1 Hydrolysis and Precipitation Process

In aqueous solution, hydrolysis of free metal ions is a dominant chemical factor of the chemistry of Fe(III) salts because Fe^{3+} is easily hydrolyzed in aqueous solutions in the absence of competing ligands and most trivalent metal ions are already coordinated with OH^- within the pH range of natural waters. Therefore, an understanding of the mechanisms of Fe(III) hydrolysis and the formation of solid species of ferric hydroxide has been viewed as important in the field of destabilization and coagulation of particulates in water. In part, this interest results from the unique properties of certain hydrolysis species of Fe(III) that appear to be present as polymeric ions or colloidal precipitates. These polymeric ions have a strong positive charge and may interact with specific charge sites on surfaces they encounter, and then are

known to be effective in the destabilization of particles. In the discussion of Fe(III) chemistry,

in part, the chemistry of Al(III) will also be discussed because the aluminum ion, Al^{3+}, behaves

very much like Fe^{3+} in aqueous solution.

Since hydrolysis is a classification of complex formation reactions or coordinative

reactions, the knowledge of the complex formation chemistry for Fe(III) salt is essential to an

understanding of its role in the destabilization and coagulation of particulates in water. The

complex formation is simply defined as any combination of cations with molecules or anions

containing free pairs of electrons. The complexes formed modify metal species in solution,

generally reducing the free metal ion concentration so that the effects and properties which

depend on free metal ion concentration are altered (Snoeyink and Jenkins, 1980). Those

effects on coagulation may include such things as the modification of solubility, the variation

of hydrolysis species, and the adsorption ability on particles in solution. In aqueous solution,

free metal ion is actually associated with its surrounding water molecules. In the case of

Fe(III) dissolved in water, there are six such water molecules coordinated with Fe^{3+} ion,

leading to the more refined chemical symbolism $Fe(H_2O)_6^{3+}$ instead of Fe^{3+} for the hydrated

ferric ion.

The coordination reactions in which metal cations participate in aqueous solutions are

exchange reactions with the coordinated water molecules exchanged for some other preferred

ligands (Stumm and Morgan, 1981). The interaction of these hydrated metal ions with acids or

bases is a ligand exchange reaction that is commonly called "hydrolysis" (Snoeyink and

Jenkins, 1980). The following generalized equations can be used to describe the stepwise

hydrolysis of hydrated ferric ion when considering only the formation of mononuclear complexes:

$$Fe(H_2O)_6^{3+} + H_2O \rightleftharpoons Fe(H_2O)_5OH^{2+} + H_3O^+ \tag{3.1}$$

or $\qquad Fe^{3+} + H_2O \rightleftharpoons Fe(OH)^{2+} + H^+ \tag{3.2}$
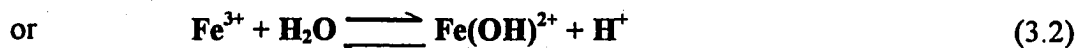
For simplicity, omitting H_2O ligands coordinated to the Fe^{3+} ions,

$$Fe(OH)^{2+} + H_2O \rightleftharpoons Fe(OH)_2^+ + H^+ \tag{3.3}$$

$$Fe(OH)_2^+ + H_2O \rightleftharpoons Fe(OH)_3 + H^+ \tag{3.4}$$

$$Fe(OH)_3 + H_2O \rightleftharpoons Fe(OH)_4^- + H^+ \tag{3.5}$$
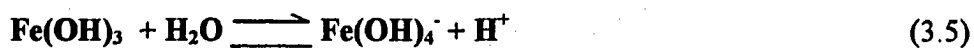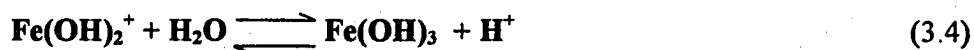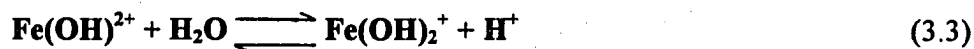
As described in Eqs (3.1) - (3.5), formation of a complex between a metal ion in solution and a ligand requires displacement of one or more coordinated water molecules from the initial aquo complex. Thus, from these equations, the hydrolysis of metal ions is visualized as a stepwise replacement of coordinated molecules of water of hydration by hydroxyl ions. Also, the hydrolysis reactions described in Eqs (3.1) to (3.5) can be viewed as a series of consecutive proton transfer reactions. As described in Eq (3.1), on transferring a proton to a solvent water molecule, a coordinated H_2O is converted to a hydroxyl ion. Therefore, the hydrated metal ions formed by the reactions are acids in view of the Brönsted theory of acids that a proton donor is defined as an acid. Because the hydrolysis reaction is dependent on the acid-base reactions, the solution pH strongly influences the rate and distribution of the various hydrolysis species.

The hydrolysis behavior of Fe(III) salts has been described, thus far, in relatively simplistic reactions. In reality, it is not this simple. According to Baes and Mesmer's discussion about the hydrolysis of cations (1976), because of the number and diversity of the hydroxide complexes which can be formed in solution, the resulting chemical behavior of a given metal cation can be a complicated function of pH and concentration; and, if the identity and stability of the hydrolysis products are not known, it can be quite unpredictable.

The effect of pH on solute-solubility enhancement provides useful information on the mechanism of the interaction between solute and particulates in water. Therefore, it is instructive to evaluate total concentration of all Fe(III) species present as well as to provide a graphical representation of the concentrations of individual Fe(III) species present at various pH values. A solubility diagram of Fe(III) in water at equilibrium with freshly precipitated amorphous $Fe(OH)_{3(s)}$ is presented in Figure 3.1 as a function of pH. Table 3.1 contains Fe(III) equilibria, reaction enthalpy, and stability data used in constructing the diagram.

In Table 3.1, the K and ΔH_r° designate the equilibrium constant and standard reaction enthalpy for the species indicated. The approximate values in Eqs (1) - (7) are typical for 25 °C and corrected to I=0 (Nordstrom et al., 1990). For the solubility diagram, the precipitated $Fe(OH)_{3(s)}$ entity was chosen to be amorphous $Fe(OH)_3$ and K_{so} was chosen as $10^{-38.7}$. In fact, the K_{so} value for ferric hydroxide is ranged from 10^{-38} to $10^{-41.5}$ depending on the structure of ferric hydroxide.

Table 3.1. Hydroxocomplex formation constants for iron(III) at 25°C (Baes and Mesmer, 1976; Nordstrom et al., 1990)

Reaction	ΔH_r^o (kcal/mol)	log K (25 °C)
(1) $Fe^{3+} + H_2O = FeOH^{2+} + H^{+}$ *	10.4	-2.19
(2) $Fe^{3+} + 2H_2O = Fe(OH)_2^{+} + 2H^{+}$	17.1	-5.67
(3) $Fe^{3+} + 3H_2O = Fe(OH)_3^{0} + 3H^{+}$	24.8	-12.56
(4) $Fe^{3+} + 4H_2O = Fe(OH)_4^{-} + 4H^{+}$	31.9	-21.6
(5) $2Fe^{3+} + 2H_2O = Fe_2(OH)_2^{4+} + 2H^{+}$	13.5	-2.95
(6) $3Fe^{3+} + 4H_2O = Fe_3(OH)_4^{5+} + 4H^{+}$	14.3	-6.3
(7) $Fe(OH)_{3(s)} = Fe^{3+} + 3OH^{-}$	20.73**	-38.7

* Ligand and H_2O molecules are omitted for brevity.

** Calculated from the reported values of ΔH_f for $Fe(OH)_3 = -197.0$ kcal/mol, ΔH_f for $Fe^{3+} = -11.4$ kcal/mol, and ΔH_f for $OH^{-} = -54.957$ kcal/mol given by Snoeyink and Jenkins (1980).

Based on the data in Table 3.1, the distribution of the various hydrolysis species of Fe(III) can be computed as a function of pH. The result of such compution is shown in Figure 3.1, in which each number of line represents the behavior of the species with pH in Eqs (1) - (7) in Table 3.1. For constructing Figure 3.1, the possible occurrence of other polynuclear complexes has been ignored. However, such polynuclear complexes have been known not to change the solubility characteristics markedly for the solids considered here (Stumm and Morgan, 1981).

As depicted in Figure 3.1, the Fe(III) species in aqueous solutions are pH-dependent. For any given pH and analytical concentration of Fe(III), the graph shows whether the solid $Fe(OH)_{3(s)}$ is saturated or not, and gives the concentrations of all Fe(III) species in solution. At
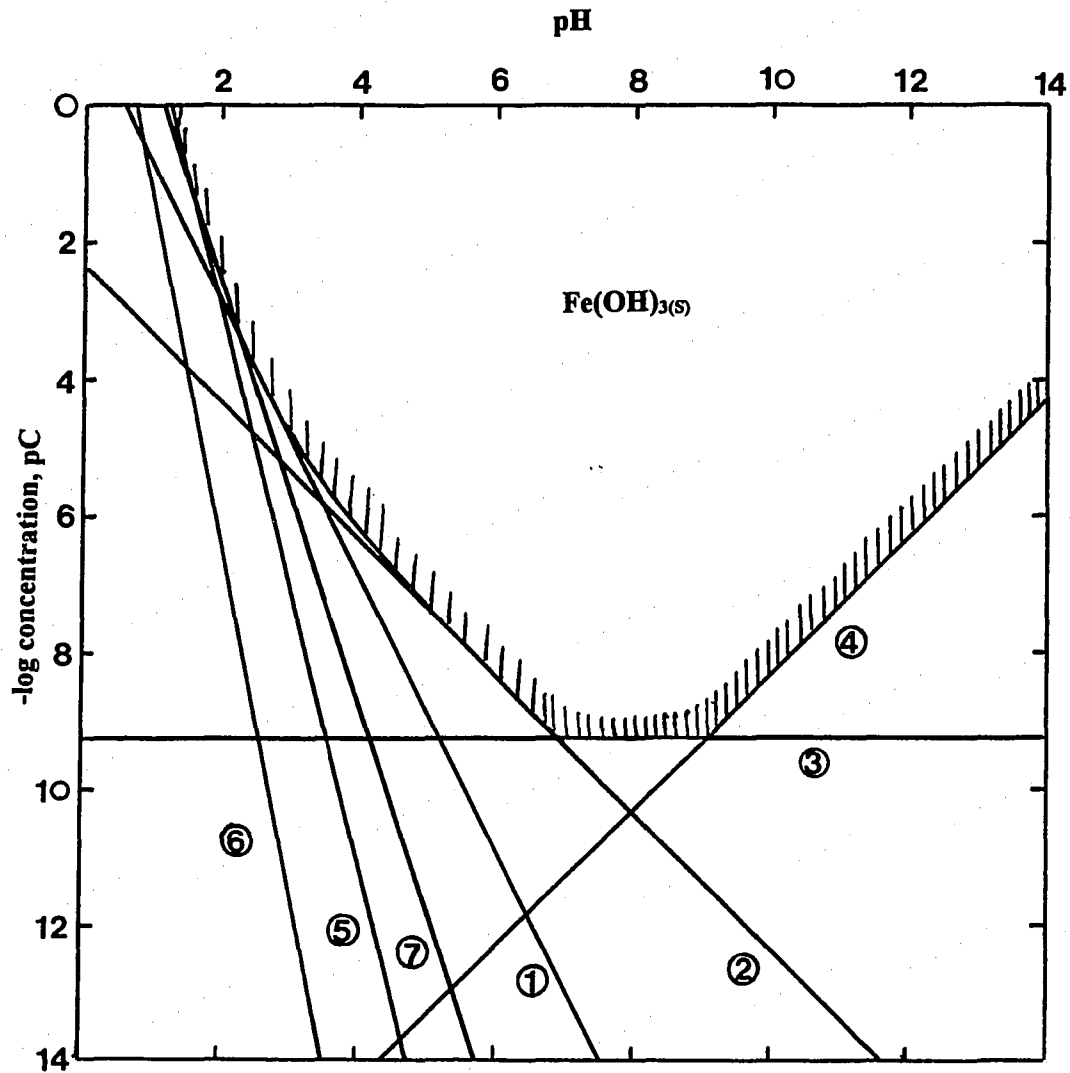
Figure 3.1. Equilibrium concentrations of hydrolysis iron(III) complexes in a solution contact with freshly precipitated $Fe(OH)_{3(s)}$ at 25 °C

low pH, Fe(III) remains unhydrolyzed, the main monomeric species being $Fe(H_2O)_6^{3+}$. As the

pH increases, the hydroxide complexes of Fe(III) account for most of the dissolved iron

concentration throughout the pH range of natural waters

From an inspection of these diagrams one can sketch in the region where any system

whose total Fe(III) concentration and pH yield a point within boundary of the graph is

saturated with respect to $Fe(OH)_{3(s)}$. Thus, the solubility of $Fe(OH)_{3(s)}$ increases under both

acidic and basic conditions. Fe(III) is least soluble at a pH of about 8.0. At lower pH levels

(pH < 6.0), the dominant soluble species are cationic species such as $FeOH_2^+$. At higher pH

values (pH > 8.0), the principal soluble Fe(III) species at equilibrium with solid is the

monomeric anion, $Fe(OH)_4^-$. As can be seen in Figure 3.1, the hydroxide complexes of Fe(III),

not the free ion Fe^{3+}, account for most of the dissolved iron concentration throughout the pH

range of natural waters, However, other dissolved conplexes may dominate the hydroxide

species depending on other ligands dissolved in water. A graph such as Figure 3.1 is thus valid

only when there are no important dissolved Fe(III) species other than the hydroxide

complexes.

Equilibrium diagrams such as Figure 3.1 are useful but incomplete because iron(III)

chemistry in water is generally governed by the kinetics of reactions with water and

contaminants (O'Melia et al., 1989). Snoeyink and Jenkins (1980) gave a word of caution in

the use of the solubility diagram:

First, one must always realize that these diagrams are equilibrium diagrams. For them to
be validly applied to the solution of natural water problems, one must assure oneself that

the solid of interest is present and that a heterogeneous equilibrium truly does exist. Second, for diagram that involves solids containing an anion other than hydroxide, one must stipulate a certain solution concentration for that anion (p. 267).

Let us consider some aspects of stock solutions of Fe(III) salt such as those used in coagulation. Primarily, the species that are formed when a Fe(III) salt is added to distilled water may depend upon the amount of the Fe(III) salt added, solution pH, and anion species. From the dilution, overall, hydroxo and complexed iron(III) species with anion, ferric hydroxide, and protons would be formed. O'Melia (1978) presented equilibrium diagrams of species composition for ferric sulfate and ferric chloride solution as shown in Figures 3.2 and 3.3. In these figures, the species composition (%) is plotted as a function of the concentration of ferric salt where $pFe(III)_T$ is the negative log of the moles per liter of Fe(III) added to system.

It is interesting to note in these two figures that the species composition for the ferric sulfate is quite different from that for the ferric chloride. Particularly, ferric chloride can yield significantly more $Fe(H_2O)_6^{3+}$ and soluble hydroxocomplexes than ferric sulfate. O'Melia (1978) noted that stock solutions of $Fe_2(SO_4)_3$ and $FeCl_3$ prepared with the same total Fe(III) concentration may produce different destabilizing species when used in coagulation. The speciation of stock solutions in practice will also be affected by excess acid in the Fe(III) salt, and by alkalinity and other complex formers in water used to prepare the stock solutions.

The dependence of the speciation of Fe(III) salt on the solution pH and the concentration of Fe(III) solution is also nicely depicted in Figure 3.4 by Baes and Mesmer
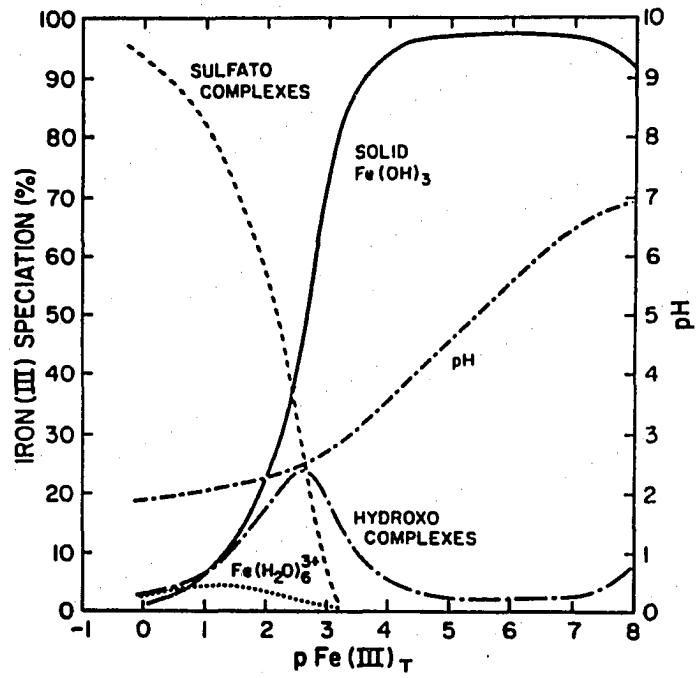
Figure 3.2.   Species composition of ferric sulfate solutions (From O'Melia, 1978)
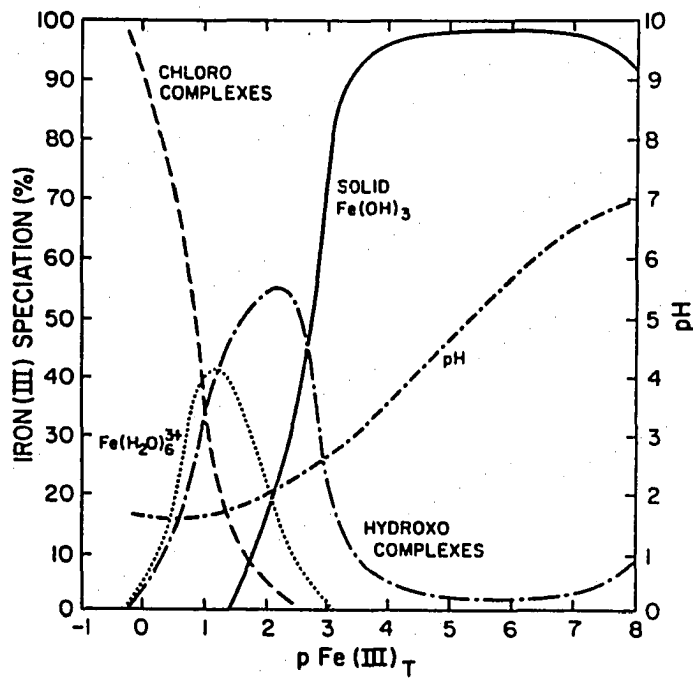
Figure 3.3.   Species composition of ferric chloride solutions (From O'Melia, 1978)
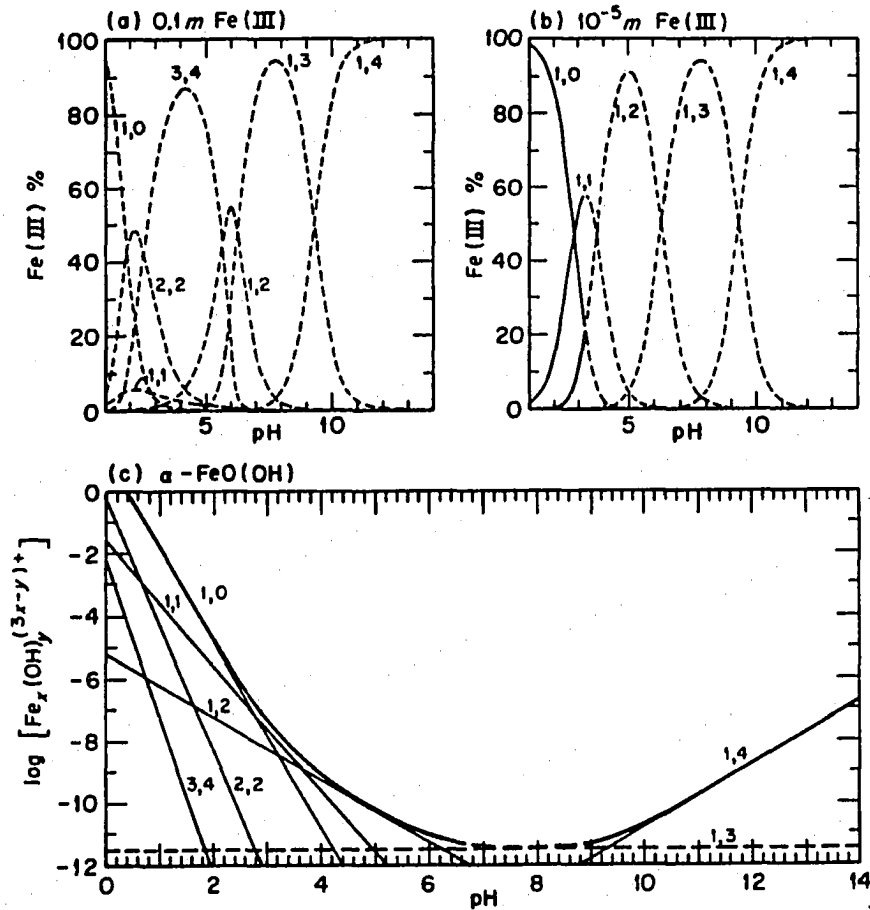
Figure 3.4.   Distribution of hydrolysis products (x, y) at I = 1 M and 25 °C in (a) 0.1 M
Fe(III), (b) 10^{-5} M Fe(III), and (c) solution saturated with α-FeOOH (From
Baes and Mesmer, 1976)

(1976). The number labels on the lines (x,y) indicates the number of iron atoms in the species (x), and the number of hydroxides present in the species (y). That is, curve(1,0) refers to Fe^{3+}, (1,2) to $Fe(OH)_2^+$, and (1,4) to $Fe(OH)_4^{-1}$. The dashed curves in Figures (a) and (b) denote regions supersaturated with respect to α-FeO(OH); the heavy curve in Figure (c) is the total concentration of Fe(III). From Figure 3.4, a binuclear species, $Fe_2(OH)_2^{4+}$, and two mononuclear species, $FeOH^{2+}$ and $Fe(OH)_2^+$ are formed in acidic solutions, while $Fe(OH)_{3(aq)}$ and $Fe(OH)_4^-$ appear in neutral and basic media. Baes and Mesmer (1976) pointed out that there is evidence for the formation of a small amount of $Fe_3(OH)_4^{5+}$ before precipitation occurs. The stable form of precipitated ferric hydroxide is α-FeO(OH), but attainment of equilibrium and interconnection of various other phases are very slow in this system, requiring several years at 25 °C.

It is also of interest to note from Figure 3.4 that $Fe(OH)_{3(s)}$ is the principle species over the pH range of interest in water treatment at both Fe(III) concentrations studied. In addition, the concentrations of the relevant species in 10^{-5}M Fe(III) solution is quite different from those in 10^{-1}M Fe(III) solotion. Stumm and Morgan (1981) reported that the tendency of metal ion solutions to hydrolyze increases with dilution and with increasing pH, and the fraction of polynuclear complexes in a solution decreases on dilution.

The sequence of hydrolysis reactions discussed thus far is by no means complete, and it is well known that several polymeric hydrolysis products can be formed. Actually the polynuclear species are not true equilibrium species, but kinetic intermediates which are in the transition to the precipitation of the metal hydroxide (Flynn, 1984). Stumm and Morgan

(1981) also noted that the existence of polymeric hydrolysis products is a rather general phenomenon for most metal ions. According to their study, the hydrolyzed species such as $[Fe(H_2O)_5OH]^{2+}$ can be considered to dimerize by a condensation process:

$$2Fe(H_2O)_5OH^{2+} = [(H_2O)_4Fe \overset{\text{OH}}{\underset{\text{OH}}{\diagdown \diagup}} Fe(H_2O)_4]^{4+} + 2H_2O \qquad (3\text{-}6)$$
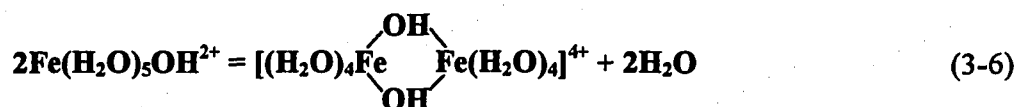
where the metal ions are bound by two hydroxo bridges. The dimer may undergo additional hydrolytic reactions which could provide additional hydroxo groups which then could form more bridges:

$$[Fe_2(H_2O)_8(OH)_2]^{4+} + H_2O = [Fe_2(H_2O)_7(OH)_3]^{3+} + H_3O^+ \qquad (3\text{-}7)$$

$$[Fe_2(H_2O)_7(OH)_3]^{3+} + [Fe(H_2O)_5(OH)]^{2+} = [Fe_3(H_2O)_5(OH)_4]^{5+} + 7H_2O \qquad (3\text{-}8)$$
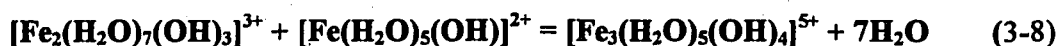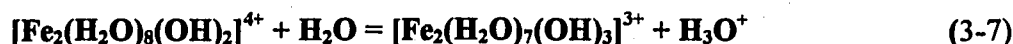
Stumm and Morgan (1971) noted that the tendency toward polymerization increased as the charge of the Fe(III) species decreases through coordination with hydroxo groups because of the decreased repulsion between the ions. In addition, they suggested that a sequence of such hydrolytic and condensation reactions leads, under conditions of oversaturation with respect to the metal hydroxide, to the formation of colloidal hydroxo polymers and ultimately to the formation of precipitates. Schneider (1984) indicated that structually well-defined polynuclear oxohydroxo complexes $Fe_pO_r(OH)_s^{3p-(2r+s)}$ can be obtained

in highly supersaturated solutions under conditions that secure homogeneous nucleation. Heterogeneous nucleation is prevailing in the low supersaturation range in which Fe^{3+}, $Fe(OH)^{2+}$, and $Fe_2(OH)_2^{4+}$ are predominant species.

Nevertheless, polymer formation is much more complicated because the chemistry of Fe(III) in water is governed by the kinetics of reactions with water and contaminants (O'Melia et al., 1989). Also, polymerization and precipitation kinetics are affected by the concentration of stock iron(III) solution; the type, concentration, and method of base addition; ionic strength; temperature; and specific anion effects (van der Woude and de Bruyn 1983; Schneider 1984). As an example, Smith and Hem (1972) concluded that the amount of the aluminum polymer formed in their experimental solutions was, in part, a function of the rate of addition of NaOH solution during preparation. Fast addition tended to produce larger proportions of colloidal precipitates. Slower addition produced less colloidal precipitates and more polymers. They reasoned that this behavior is probably related to the higher initial degree of local supersaturation that occurs during rapid addition of base.

As mentioned earlier, the polynuclear hydrolysis species occur as kinetic intermediates in the usually slow transition to the hydroxide precipitate. That is, the formation of a precipitate can often be considered the final stage in the formation of polynuclear complexes. Precipitation has generally been observed to occur in three steps (Snoeyink and Jenkins, 1980):

1. Nucleation - condensation of ions to very small particles,

2. Crystal growth - crystal formed by the deposition of the precipitate constituent ions onto nuclei,

3. Agglomeration and ripening - additional precipitation to the more stable phase by the change of crystal structure.

Where the nucleation process generally has two different mechanisms depending on the presence of particulates. While homogeneous nucleation and precipitation of ferric hydroxide occur in the absence of foreign particles, there is heterogeneous nucleation of ferric hydroxide onto the initially present seed particles in the presence of foreign particles.

The technical literature contains ample evidence for the precipitation of iron (hydr)oxides in solution through intermediates of monomers and polymers. Ferric hydroxide, also called hydrous ferric oxide, is the solid formed upon rapid hydrolysis of ferric iron solutions at 20 to 30 °C. It was pointed out that four steps in the Fe(III) hydrolysis-precipitation process have been distinguished (Dousma and de Bruyn, 1976): (1) rapid formation of iron hydroxo monomers and dimers, (2) reversible, rapid growth to small polymers, (3) slower formation of large polymers through the oxolation of hydroxo complexes, (4) precipitation of a solid phase. The resulting solid phase has been found to be usually completely amorphous as determined by X-ray diffraction, although a few broad reflections are sometimes observed indicating some crystalline character.

Freshly precipitated ferric hydroxide particles are reported to be approximately spherical and quite small, with particle sizes ranging from 1 to 10 nm (van der Woude and de Bruyn, 1983). The authors reported that this particle size distribution appears to be relatively

independent of pH. As hydrous ferric oxide is aged, however, it coagulates and the resulting
aggregates are highly porous and sometimes micrometer sized (Dzombak and Morel, 1990)

Schneider and Schwyn (1987) reported that at moderate temperatures, a variety of
sols, gels, and amorphous or crystalline precipitates emerge either spontaneously or by
flocculation from the colloidal solutions of iron(III) of the type such as $Fe_p(OH)_q^{3p-q}$ and
$Fe_pO_r(OH)_s^{3p-(2r+s)}$ in aqueous solution. The morphological properties of the products reflect
the pathways of formation in any specific system. The invesgators assert that the prime
variables are the rate of change of pH as a function of time and space and the chemical
components. In a previous work, Schneider (1984) noted that small polycations such as
$[Fe_3(OH)_4]^{5+}$ and $[Fe_4O(OH)_4]^{6+}$ control both nucleation and growth steps by associating in
larger polymers.

Van der Woude and de Bruyn (1983) simply described the precipitation of a hydrous
ferric oxide solid from acidic iron(III)-bearing solutions by the heterogeneous reaction:

$$Fe^{3+}(aq) + 3H_2O \rightleftharpoons Fe(OH)_{3(s)} + 3H^+(aq) \qquad (3.9)$$
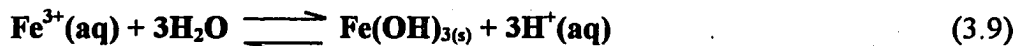
This shows that the process is completed when the ratio of the number of hydroxyls bound per
Fe(III) atom (OH/Fe) equals three. The amorphous hydrous oxide is furthermore known to
transform slowly to a crystalline variety, for example, geothite (α-FeOOH) at room
temperature. The precipitation process is, however, more complicated than is suggested by the
above chemical reaction. Van der Woude and de Bruyn (1983) also noted that relatively high
molecular weight polycations ($Fe_n(OH)_m^{z+}$) are believed to form via hydrolysis-polymerization

reactions and probably serve as precursors for the eventual formation of colloidal dispersions of the metal hydrous oxide and precipitates of the thermodynamically stable solid.

Dousma et al.(1979) proposed the scheme shown in Figure 3.5 to account for the formation of the solid Fe(III) oxide phase from acidified aqueous solution.

$$
\begin{array}{ccc}
\mathbf{1} & \mathbf{2} & \mathbf{3}
\end{array}
$$

monomers $\xrightarrow{\text{polymerization}}$ polymers $\xrightarrow{\text{nucleation}}$ Fe(OH)$_{3(s)}$ $\xrightarrow{\text{growth}}$ FeOOH

dimers $\xleftarrow{\hspace{2cm}}$ $\quad$ growth $\quad\quad\quad$ oxolation

Fe(OH)$_{3(s)}$ $\longrightarrow$ Fe$_2$O$_3$ growth
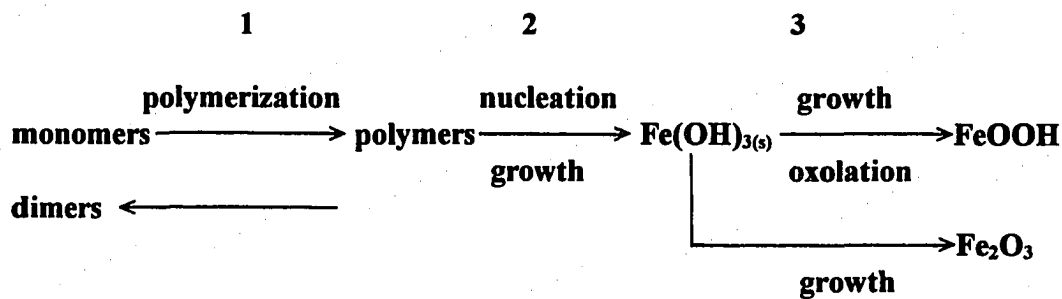
Figure 3.5 The scheme of hydrolysis-precipitation process (Dousma et al., 1979)

The first step in this scheme is the rapid and reversible formation of polynuclear complexes from monomeric and dimeric iron hydroxo-species. The larger polymers can serve as the substrate for a heterogenous nucleation and growth step which starts after a certain supersaturation is reached above the solubility product of the solid phase.

Knight and Sylva (1974) proposed a relatively simple model for the Fe(III) precipitation (Figure 3.6) which is different from the model shown in Figure 3.5, where Dousma et al.(1979) neglected a mechanism for the rapid precipitation (pathway B in Fig. 3.6) at low OH/Fe ratio in their scheme.
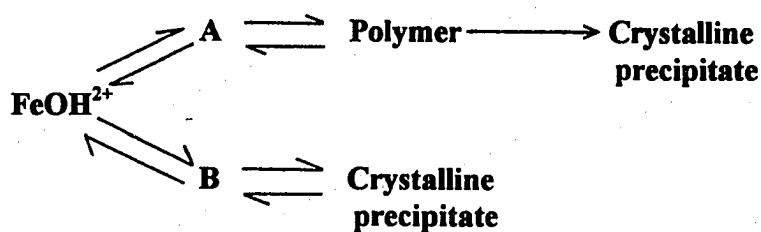
Figure 3.6. The scheme of polymerization and precipitation process (Knight and Sylva, 1974)

From Figure 3.6, A and B represent the low molecular weight precursors of polymer and the crystalline precipitate, respectively. They declared that the precursor A of polymer should be a dimer, $Fe_2(OH)_2^{4+}$ and another precursor B of rapid precipitation should be $Fe(OH)_2^+$. In a base titration of Fe(III) solution, they observed that at low [OH] added to [Fe] in the original Fe(III) solution (low [OH]/[Fe] ratios]), direct precipitation from $Fe(OH)_2^+$ predominates. The rate of this process increases with increasing base addition, to a point at which polycation formation becomes competitively inhibitive.

Tang and Stumm (1987a) proposed to combine the models depicted in Figures 3.5 and 3.6 together using their experimental results in which they used the 0.3 M $FeCl_3$ solution neutralized by injection of 1 M $NaHCO_3$ solution. Figure 3.7 shows this combination as a qualitative scheme of the hydrolysis-polymerization-precipitation process and the main chemical species in various stages. It should be acknowledged that the writer can not see any possible way that B could be -3.4 in this figure.

From Figure 3.7 they pointed out that in the initial stage of hydrolysis, the main Fe(III) species are monomers and complexes with chloride. With the increase of B^* from 0.0 to 0.2,

Type A	Type B	Type C	Type D
$B = -3.4 - 0.1$	$B = 0.1 - 0.4$	$B = 0.5 - 1.0$	$B = 1.0 - 2.3$
$B^* = 0.0 - 0.2$	$B^* = 0.2 - 0.5$	$B^* = 0.5 - 1.0$	$B^* = 1.0 - 2.3$

$$Fe_3(OH)_4^{5+} \rightleftharpoons Fe_4(OH)_6^{6+} \rightleftharpoons Fe_x(OH)_y^{(3x-y)+} \rightleftharpoons Fe_xO_z(OH)_y^{(3x-2z-y)+}$$

$$Fe_2(OH)_2^{4+}$$

$$Fe^{3+} \rightleftharpoons$$

$$FeOH^{2+}$$

$$\longrightarrow \gamma - FeOOH \downarrow \qquad \alpha - FeOOH(am) \downarrow$$

$$Fe(OH)_2^+ \qquad Fe(OH)_3 \text{ (am)} \downarrow \qquad Fe(OH)_3 \text{ (am)} \downarrow$$

$B^* \geqslant 2.3$

$B \geqslant 2.3$

Type E
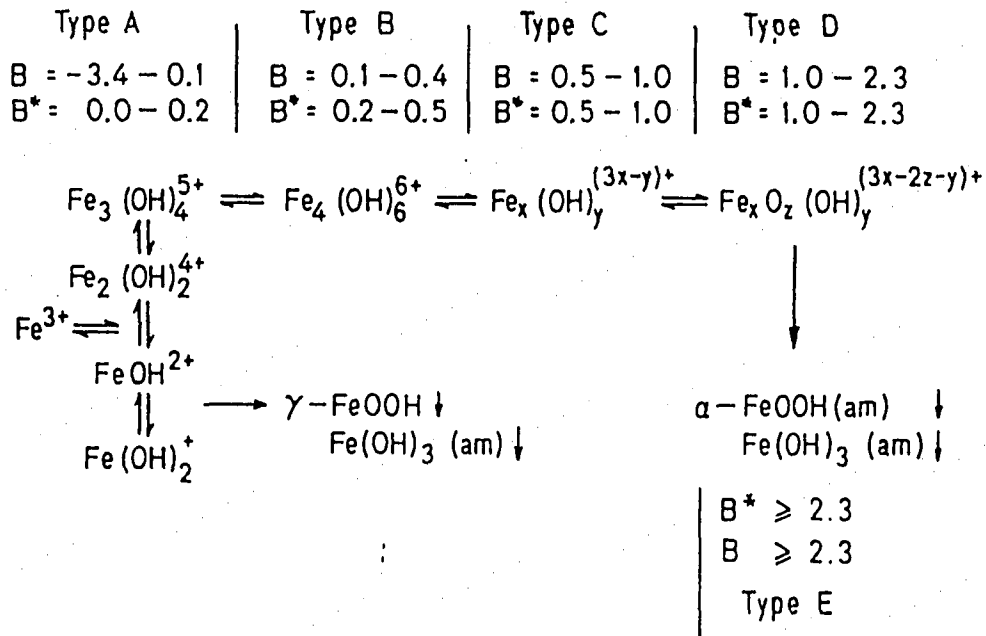
Figure 3.7. A comprehensive scheme of the hydrolysis-polymerization-precipitation process and chemical species ($B = [OH^-]_{added}/[Fe_T]$, $B^* = [OH^-]_{bound}/[Fe_T]$) (Tang and Stumm, 1987a)

the polynuclear species are becoming formed. As B^* approaches about 0.2, at this low OH_{bound}/Fe_T ratios (Type B), rapid precipitation occurs. In type B solutions the two processes, direct precipitation from monomer and polymerization from dimer and trimer are in competition with each other and the former dominates. As the base addition increases over $B^* > 0.5$, the condition of more abundant OH^- is favorable to further polymerization. Then the polymerization process becomes dominant over precipitation. When the high level polymers of type D are produced, their charges become decreased due to deprotonation. Then, a second rapid precipitation from polymers at high OH/Fe ratios appears and the solution turns into type E.

The model proposed by Tang and Stumm(1987a), then, gives a general picture of the hydrolysis-polymerization processes which occur with base addition to supersaturated solution of iron(III) salts. However, the polymeric species and solid phase formed in supersaturated solutions of ferric salts may vary markedly in composition, morphology and colloidal size. Schneider and Schwyn (1987) also suggested that the mode of nucleation, homogeneous versus heterogeneous, determines the extent to which polynuclear species are generated in solution. According to their study, nucleation is heterogeneous at low OH_{added}/Fe_T ratios, but it is homogeneous at high OH_{added}/Fe_T ratios. Although nucleation may be promoted by the presence of contaminant surfaces even at lower OH_{added}/Fe_T ratios.

It is often useful to discuss the overall process of the hydrolysis-precipitation process together based on a titration (neutralization) curve for the Fe(III) salt which has been used for the study of the hydrolysis of various metal cations. van der Woude and de Bruyn (1983)

developed the titration curve of a supersaturated $Fe(NO_3)_3$ solution as presented in Figure 3.8.

In Figure 3.8, solution pH is plotted as a function of base added as denoted by r

($r=OH_{added}/Fe_T$), the number of OH ligands added to solution per iron(III) atom in the

solution. As illustrated in Figure 3.8, a 6.25×10^{-2} M $Fe(NO_3)_3$ solution (3.49 g/L of Fe(III)) is

titrated or neutralized with sodium hydroxide. The authors stated that as base is added to the

iron(III) solution, one can observes changes in color and optical density which reflect the

progress of hydrolysis, polymerization, and the precipitation of an iron(III) solid phase. These

changes are attributed to an increasing r (actually OH_{bound}/Fe_{total}) ratio which usually, not

always, raises the pH.

Van der Woude and de Bruyn (1983) distinguished these four steps in Figure 3.8 in

light of the hydrolysis-precipitation process. In region I, the increase in **r** results in the rapid

formation of monomers such as $FeOH^{2+}$ and small polymers such as $Fe_2(OH)_2^{4+}$. In this

region, polymers larger than the dimer $Fe_2(OH)_2^{4+}$ are not detected. In region II, polymeric

species larger than the dimer are formed, and the solution is seen to undergo a color change

from light to dark yellow. Increasing the ionic strength or the temperature results in the

gradual disappearance of region II (van der Woude and de Bruyn, 1983). In region III, rapid

precipitation of amorphous $Fe(OH)_3$ occurs. The darkening of the solution continues through

bright orange to reddish brown. The formation of the primary solid phase is essentially

completed at **r** = 2.5 for this system. In region IV, additional bases neutralize the positive

surface charge on the precipitate and cause a steep increase in pH.
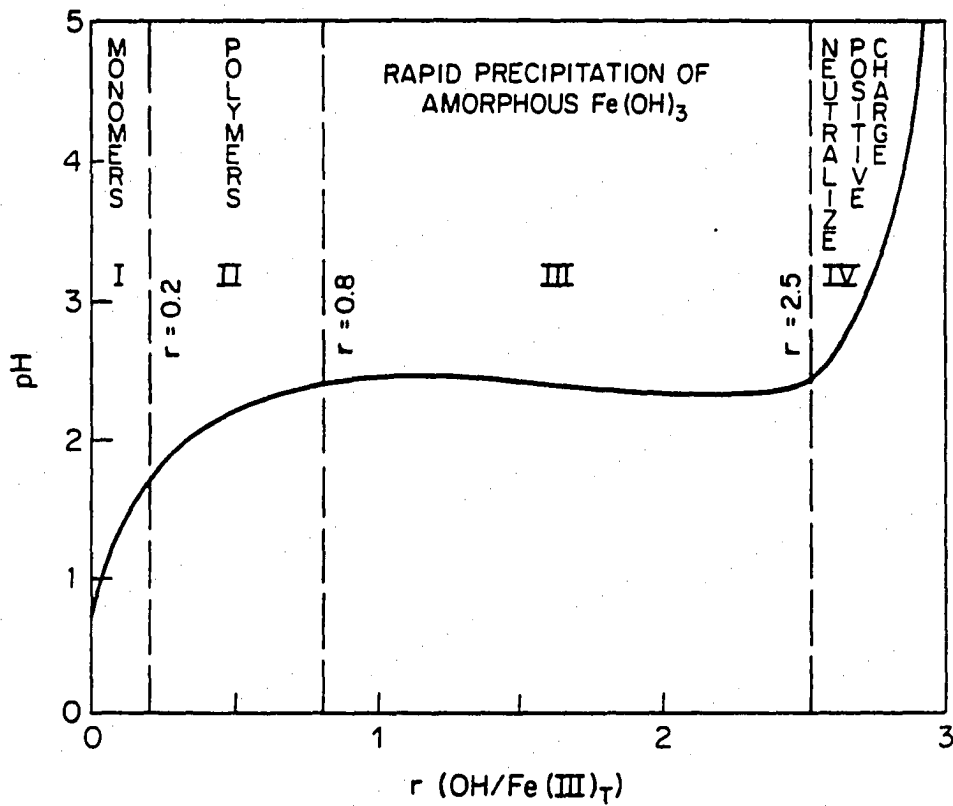
Figure 3.8.   Typical base titration of $Fe(NO_3)_3$ solution, $Fe(III)_T = 6.25 \times 10^{-2}$ M (From van der Woude and de Bruyn, 1983)

Leprince et al.(1984) reported the existence of polymeric species of Fe(III) up to r=2.5 in partially neutralized $FeCl_3$ solutions, indicating that the upper boundary of region II may not be fixed at r=0.8. It is possible that a wide variety of polymeric iron(III) preparations ranging from small cationic polymers to colloidal amorphous iron(III) precipitates can be obtained, depending on the conditions used in their preparation (O'Melia et al., 1989). Schneider (1984) reports that if r exceeds a critical value, usually in the range of 0.5-1.0, polynuclear species such as $Fe_p(OH)_q^{(3p-q)+}$ or $Fe_pO_r(OH)_s^{[(3p-(2r+s)]+}$ form and either precipitate spontaneously or by flocculation. Thereafter, the slow decline in pH reflects the gradual transformation of the solid phase.

Thus far, the Fe(III) chemistry, its hydrolysis, and its implications for water treatment were discussed extensively in the absence of other types of colloidal particulate matters in aqueous solution. However, during water treatment, the injected Fe(III) coagulant hydrolyzes in the presence of other types of colloidal particulate matters that, consequently, affects Fe(III) speciation in a variety of ways. For example, the presence of colloidal matter could interact with Fe(III) species through (Schneider and Schwyn, 1987):

- exchange of surface cations,

- enhanced polymerization of Fe(III) species due to an enhancement in the concentration of these species near colloidal surfaces within the double layer,

- colloid mediated precipitation.

Experimental evidence has indicated that hydrolyzed metal ion species have a particular

affinity for oxide and layer-lattice silicate surfaces, and thus the presence of such minerals in

solutions of metal ions can be effective in promoting the hydrolysis process (James and Healy,

1972b).

Whether the enhancement of hydrolysis at the surfaces of such minerals extends to the

promotion of hydrolytic precipitation is, however, not at all certain. James and Healy (1972b)

indicated that the magnitude of metal hydroxide solubility products at the solid-solution

interface could be significantly lower than those which are obtained in the bulk solution,

owing to differences in the dielectric properties of these two environments. Results obtained

from other experimental investigation (Thompson and Tahir, 1991), however, have indicated

that the conditions required for the precipitation of hydrous oxide in hydrolyzing Fe(III)

solutions are unaffected by the presence of the clay mineral kaolinite. A study by Hem and

Roberson (1990) also explored the effect of mineral surfaces on Al behavior. These

investigators suggested that rate of the aluminum polymer growth to become precipitate

appears not to be affected significantly by the presence of mineral surfaces, such as silica and

clay.

The preceeding discussion of Fe(III) complexation reactions based on equilibrium

arguments provides a good representation of complexation phenomena in aqueous systems.

Here, however, the complexation kinetics, that is, the rate of formation of Fe(III)-ligand

complexes will be briefly discussed to provide insight into whether the kinetics may affect the

overall rates of hydrolysis processes. A few attempts have been made to establish the rate of reactions for Fe(III) or Al(III) salts.

Observed rates of complex formation for most metals are generally consistent with a mechanism in which formation of an outer-sphere complex between the metal and ligand, with the stability constant K_{os}, is followed by a rate-limiting loss of water from the inner coordination sphere of the metal, with the water loss rate constant k_{-w} (Morel and Hering, 1993), e.g.,

$$M(H_2O)_6^{2+} + L^- \overset{K_{os}}{\rightleftharpoons} M(H_2O)_6, L^+ \qquad (3.10)$$

$$M(H_2O)_6,L^+ \overset{k_{-w}}{\longrightarrow} M(H_2O)_5L^+ + H_2O \qquad (3.11)$$
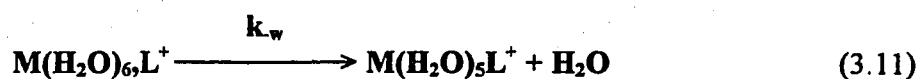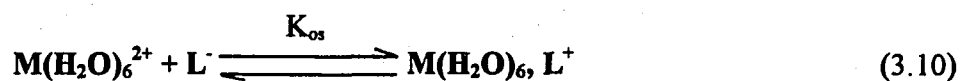
Then, the rate constant for complex formation, k_f, can be written (omitting coordinating waters) as:

$$d[ML^+]/dt = k_f [M^{2+}][L^-] \qquad (3.12)$$

where

$$k_f = K_{os} k_{-w} \qquad (3.23)$$

The stability constant for the outer-sphere complex, K_{os}, is primarily dependent on the charges of the reacting species and the ionic strength of the medium, and its reaction is fast ($K_{os} \cong 10^9$ to 10^{10} mol^{-1}) (Morel and Hering 1993).

Generally, the loss of a water molecule from the primary hydration sphere of a metal ion is often known to be the rate determining step (Morel 1983). Schindler and Stumm (1987) also stated from the studies on the kinetics of adsorption of metal ions on γ-Al_2O_3 that the adsorption rate constants correlate significantly with the rate constants for the release of water molecules from the hydrated metal ions. Therefore, consideration of the kinetics of solvent exchange is important for an understanding of the intrinsic reactivity pattern of a solvated metal ion (Crumbliss and Garrison, 1988). The rate constants for water-loss, k_{-w}, for $Fe(H_2O)_6^{3+}$ are listed in Table 3.2.

From Table 3.2, for instance, the rate of exchange of a H_2O molecule coordinated to Fe^{3+} is 1.67×10^2 sec^{-1}. This is very long in comparison to the Fe(III) hydrolysis species of $FeOH^{2+}$ and $Fe(OH)_2^+$ (1.4×10^5 and 10^7 sec^{-1}), but short in comparison to H_2O molecule coordinated to Al^{3+} (1.29 sec^{-1}).

Table 3.2. Comparison of the rate constants for water exchange on Fe^{3+} *

Metal Ion	Al^{3+}	Fe^{3+}	$FeOH^{2+}$	$Fe(OH)_2^+$	$Fe(OH)_4^-$
$k_{-w}^{298}(s^{-1})$	1.29	1.67×10^2	1.4×10^5	10^7	10^9

* references are to Crumbliss and Garrison (1988) for Fe^{3+} and $FeOH^{2+}$, and to Morel and Hering (1993) for $Fe(OH)_2^+$ and $Fe(OH)_4^-$

It is also noted from the values of k_w that the rate of water loss can be significantly accelerated by Fe(III) hydrolysis. Thus, the exchange of the first coordinated water of $Fe(H_2O)_6^{3+}$ controls the overall complexation rate. The marked enhanced rate of water exchange for $FeOH^{2+}$ (750 times that for Fe^{3+}; Table 3.2) is due to a decrease in the overall charge (Crumbliss and Garrison, 1988). They reasoned that the reduced charge decreases the hold of the control metal ion over the coordinated water molecules, resulting in an increased water exchange rate. Furthermore, the coordinated OH⁻ is known to have a labilizing effect.

While the rate of water exchange seems to help in understanding the critical rate of polymer formation, there seems to be little information on polymerization and precipitation kinetics. It is generally known that polymerization reactions are much slower than the proton transfer reaction (Nordstrom and May, 1989). A study of Al(III) polymerization kinetics was made by Hem and Roberson (1990) using a batch titration experiment and analysis of thermodynamic data collected from several references. They developed a plot of the polymerization rate constants of aluminum versus the controlled pH as shown in Figure 3.9. In Figure 3.9, k_2" represents the rate constant for the formation of aluminum polymeric species from the monomeric species. There is a clear indication in Figure 3.9 of a well defined pH dependence of the nucleation and polymerization rate. The dashed line on the graph represents a third-order pH dependency- that is, a change of 0.5 unit in pH causes a change in k_2" of 1.5 log unit.

Sylva (1972) produced an extensive literature review of iron hydrolysis. He indicated evidence that equilibrium among monomers is approached rapidly, whereas equilibrium among
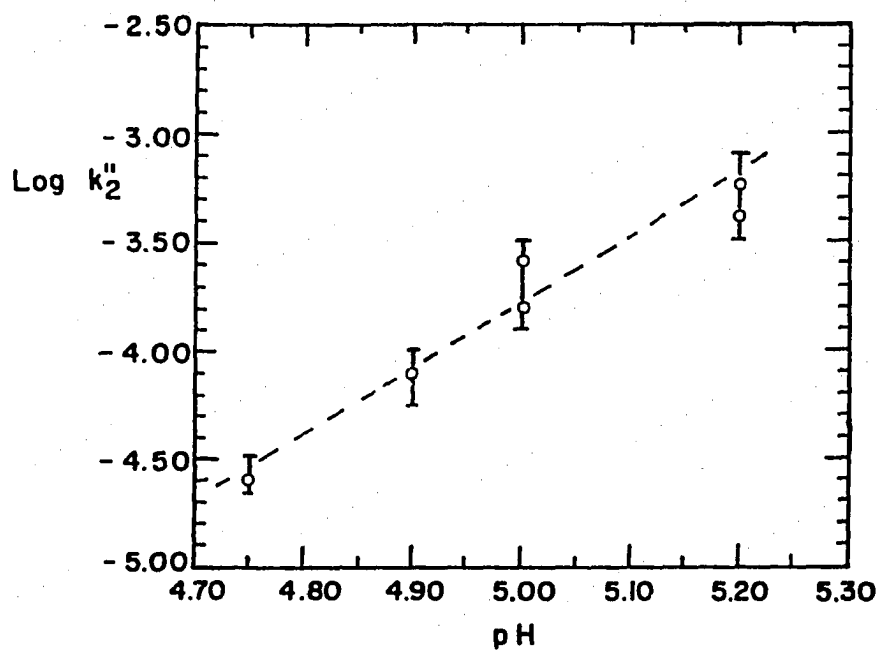
Figure 3.9.   Kinetics of formation of Al$_a$ at 25 °C from pH 4.75 to 5.20. Open circles are
mean values of log k$_2$" measured in six experimental runs, vertical lines
represent range of log k$_2$" values computed for runs at pH's indicated. Units
for k$_2$" are sec^{-1} (Hem and Roberson, 1990)

polymers is attained more slowly. In addition, Hahn and Stumm (1968) also reported that the rate of polymerization of hydrolyzed aluminum species is considerably slower than those reported for the formation of the dimeric iron(III) hydroxo complex from undersaturated solutions.

The rate for the reaction of coagulant formation through hydrolysis and initial polymerization can be gained by considering the time scales involved in the various process steps. From a literature review, Amirtharajah (1987) presented the time scales of the formation of aluminum hydrolysis species as shown in Table 3.3.

Table 3.3. Formation time of aluminum hydrolysis species (Amirtharajah, 1987)

Hydrolysis species	Time scale (sec)
Al(III) monomers	< 0.1
Al(III) polymers	0.1 to 1
Aluminum hydroxide precipitates	1 to 7

As described in Table 3.3, the reactions for the soluble Al(III) hydrolysis products are extremely fast and occur within microsecond without formation of Al(III) hydrolysis polymers and within 1 second if polymers are formed. The formation of aluminum hydroxide precipitate is slower and occurs in the range of 1 to 7 seconds.

3.2 Mechanisms of Coagulation and Flocculation

Although the terms coagulation and flocculation are used in different ways depending on the area of application and on the presumed mechanism of aggregation, in this discussion coagulation is applied to the overall process of particle aggregation, including both particle destabilization and particle transport. The term flocculation is used to emphasize only the particle transport process which leads to interparticle contact and the formation of particle aggregates or flocs. Coagulation and flocculation involve aggregation of particles into larger, more readily removable, aggregates. Aggregation of colloidal particles can be considered to involve two separate and distinct steps (Vik and Eikebrokk, 1989): particle transport to achieve interparticle contact and particle destabilization to permit attachment when contact occurs.

The exact mechanism of particle destabilization in water treatment is a complex process, and then many reactants and reactions are possible, and several are involved in any specific application. Stumm and O'Melia (1968) suggested that coagulation is a time-dependent process including several reaction steps:

1. Hydrolysis of multivalent metal ions and subsequent polymerization to multinuclear hydrolysis species,

2. Adsorption of hydrolysis species at the solid-solution interface to accomplish destabilization of the colloid,

3. Aggregation of destabilized particles by interparticle bridging involving particle transport and chemical interactions,

4. Aggregation of destabilized particles by particle transport and van der Waals forces,

5. "Aging" of flocs, accompanied by chemical changes in the structure of Me-OH-Me linkages, with concurrent change in floc stability and in the extent of floc hydration,

6. Precipitation of the metal hydroxide.

Some of these steps occur sequentially, some overlap, and some may occur concurrently under certain conditions. It is reasonable to assume that different reaction steps may become rate controlling under different conditions (Stumm and O'Melia, 1968).

Therefore, it would be useful to begin discussion of the destabilization process considering the following two predominant mechanisms by which coagulation in water treatment by hydrolyzable metal salts occurs (Amirtharajah and O'Melia, 1990):

1. Adsorption of hydrolysis species on the colloid causing charge neutralization,

2. Enmeshment of the colloid to be coagulated by hydroxide precipitates of the coagulant metal ("sweep" coagulation).

In addition to the above two mechanisms, two other distinct mechanisms have been presented for the destabilization of particles:

3. Compression of the double layer,

4. Adsorption to permit interparticle bridging.

Since the destabilization by the double layer compression has not been considered an important mechanism in typical water treatment conditions, this mechanism will not be discussed further.

Adsorption and interparticle bridging are the mechanisms that provide a useful description of the ability of synthetic organic polymer with high molecular weight to coagulate a colloidal dispersion. Since all of the works in this research were performed using Fe(III) coagulant, this mechanism will not be discussed further.

3.2.1 Adsorption and charge neutralization

It has been well documented that adsorption of charged species for neutralization of the opposite charges on particles is one of the key steps in coagulation. Adsorption of counterions can neutralize the colloidal surface charge, thereby reducing the repulsive energy barrier and encouraging rapid coagulation. Adsorption can continue beyond neutralization to reverse the charge at colloidal surfaces. In this way the repulsive energy barrier to coagulation is reestablished and the colloids are restabilized.

When the destabilization agent and the colloid are of opposite charge, this restabilization is accompanied by a reversal of the charge of the colloidal particles. According to Stumm and Morgan (1962), purely coulombic attraction cannot account for the fact that an attraction of counter-ions proceeds past the point of charge neutralization to cause charge reversal. O'Melia (1987) also stated that while destabilization of colloids is a function of electrostatic colloidal surface properties, these properties are determined primarily by the chemistry of the system.

The chemical structure, the presence of certain functional groups, and the degree of hydrolysis of coagulants influence their adsorption, and hence, destabilizing capacity.

Evidence exists which suggests that all types of hydrolyzed polyvalent metal ions are generally much more efficient in adsorption on colloidal interfaces than unhydrolyzed ions, and the charges they carry may cause charge reversals of the surfaces on which they adsorb (Matijevic and Janauer, 1966; Weber, 1972; Stumm and Morgan, 1981). The qualitative reasons can be given as (Stumm and Morgan, 1962; Stumm and O'Melia, 1968): (1) the species are larger and less hydrated, (2) the presence of coordinated hydroxide groups, (3) the replacement of an aquo group by a hydroxo group may render the complex more hydrophobic and thereby, in turn, enhance the specific chemical adsorption on the surface, (4) more than one hydroxide group can become attached at the interface. These types of adsorptive interactions may be assisted or impeded by electrostatic forces. The charge reversal that accompanies the specific binding of coagulants to colloids is evidence for the fact that short-range chemical adsorption forces may outweigh electrostatic repulsion.

A similar observation was made by James and Healy (1972c) in developing a thermodynamic model for hydrolyzed metal ion adsorption:

> The ion-solvent interactions present a barrier to close approach of highly charged ions to the interface between a low dielectric constant solid (i.e., kaolinite and SiO_2) and water. When the ionic charge is lowered by hydrolysis or ligand complex formation, the ion-solvent interaction is decreased, thus lowering the energy barrier. The ions may then approach closer to the interface which results in greater coulombic and short-range interaction energies, which are more favorable to adsorption (p. 77).

In a study of coagulation of lyophobic colloids by metal chelates, Matijevic and Kolak (1967) found that hydration alone is obviously not the only factor influencing the adsorbability of complex ions. They observed that similar metal chelates (i.e., $Co(en)_3^{3+}$ and $Cr(en)_3^{3+}$, which have different metal centers, but the same organic ligand (ethylenediamine) and net charge) exert very different destabilizing effects. The central metal ion influences the distribution of electrons in the ligands and also the specific chemical groups of the ligand, thus affecting the adsorption capacity of the chelate at the colloid surface. Since work is required to remove the hydration layer of an adsorbing ion, the more hydrated an ion the less it adsorbs.

Now it is clear that adsorption and hydrolysis are well related. Next, the question might be raised related to what extent they both are dependent on known chemical interactions. Several workers have shown that not only is the soluble hydrolysis product considerably more surface active than the free (aquo) ion but also a polymeric charged or uncharged hydrolysis product may be formed at the solid-liquid interface at conditions well below saturation or precipitation in solution (Healy et al., 1968). James and Healy (1972b) presented similar evidence later which indicates that the adsorption of hydrolysis products leads to the formation of a layer or a partial layer (depending on the amount of aluminum, hydrogen ion, Al-complexing ligands, etc., in the system) of amorphous hydroxide precipitate on the particle surface. They referred to this as 'surface nucleation or precipitation' and concluded that it results from a lowered stability of the precipitate at the surface due to the interfacial electric field. To solve the relationship between adsorption and hydrolysis, James

and Healy (1972a) developed a quantitative treatment of adsorption of hydrolyzing metal ions at solid-aqueous solution interfaces. The authors found that there is a critical pH range, usually less than 1 pH unit wide over which the percentage adsorption increases from almost zero to 100 % adsorbed.

One general conclusion is apparent that adsorption and phenomena dependent on adsorption are inextricably related to hydrolysis or to the formation of hydrolysis products. However, a unified interpretation has not yet been accepted. In a recent study using measured $[OH^-]/[Al_T]$ ratios and residual aluminum concentrations, Dentel and Gossett (1988) suggested that destabilization by adsorption is brought about by precipitation of positively charged aluminum hydroxide onto the original particle surfaces.

The approximate stoichiometric relationship typically observed between coagulant dose and the surface area of the colloid is another clear evidence for an adsorptive interaction. O'Melia and Stumm (1967) described coagulation and restabilization as an adsorption phenomenon, and used the Langmuir adsorption isotherm to account for the observed coagulation and restabilization of silica dispersions by the specific adsorption of hydrolyzed Fe(III) species. They pointed out that the coagulation and restabilization phenomena could appear nonstoichiometric in systems where the concentration of surface is small, or in which the fraction of surface covered by the applied Fe(III) is close to 1. Conversely where the surface area is large, or where the fraction of surface covered is close to 0, the coagulation and restabilization induced by adsorption would appear stoichiometric.

Dentel and Gossett (1988) raised some questions about the adsorption isotherm used by O'Melia and Stumm as follows:

> Surface-induced precipitation, such as interfacial tension effects and solvation or dielectric effects near the surface, may provide the appearance of adsorption. In addition, metal hydroxide adsorption becomes multilayered, it may be particularly difficult to distinguish from polymerization directly on a surface or from precipitation. Either of these two phenomena can be visualized as the use of surface sites as a template, inducing polymerization or precipitation (p. 189).

Furthermore, they argued that in practice, actually, it might be difficult to determine the relationship between colloidal surface charge and coagulant dose under a given set of conditions. The difficulty encountered in predicting coagulant dose, depending on the concentration of particles in practice, is that actual treatment conditions can vary outside the set of parameters for which coagulant dose relationships were established.

Let us look at another clear evidence for specific adsorption. Sorbable species that coagulate colloids at low concentrations may restabilize these dispersions at higher concentrations. When the destabilization agent and the colloid are of opposite charge, this restabilization is accompanied by a reversal of the charge of the colloidal particles. If electrostatic interactions were the primary force for destabilization, such an adsorption of an excess of counter ions to produce charge reversal and restabilization would not be possible. Therefore, it is necessary to consider additional energy terms arising from specific chemical interactions in order to explain this restabilization phenomenon.

Stumm and Morgan (1967), in discussing iron salts as coagulants noted that the charge reversal is ascribed to the specific sorption of presumably soluble hydroxo-ferric species. Matijevic and Janauer (1966), in a series of studies of coagulation using ferric nitrate, has also observed that charge reversal is due to adsorption of discrete highly charged polynuclear complexes. In studies of the coagulation of clays with ferric sulfate, Black and Chen (1967) found that the mechanism for charge reversal may be the reversal of the surface potential of the clay particle as a result of specific adsorption of excess polymeric multivalent ferric ions by the ions on the clay surface.

On the other hand, James and Healy (1972b) proposed that the properties of the interfacial region at a charged surface provide one explanation of the phenomenon of charge reversal. According to them, precipitation occurs at a lower pH at the colloidal surface than in the bulk solution generating a new surface with increasing adsorption and surface coverage. For example, using the electrophoretic mobility study of SiO_2 in the presence of Co(II) they found that adsorbed species do not reverse the charge of low dielectric solids such as silver halides, silicates, silicas, etc., until surface precipitation occurs. Therefore, the authors concluded that charge reversal is caused by the particle assuming the properties of a metal hydroxide gel or precipitate covering its surface. In addition, they postulated that there is no evidence that specific chemical interaction sufficient to lead to charge reversal occurs between the adsorbed metal ion and the surface sites of silica, clays, or simpler silicates.

In general, there are often up to three charge reversals observed when an anionic substrate, of which inorganic oxides, silicates, clays, and organic color are examples, is

studied by electrokinetic methods as a function of pH at a fixed added concentration of the

particular metal salt. Shown in Figure 3.10 is the schematic illustration of the general

electrophoretic mobility behavior of colloid systems as a function of pH in the presence and

absence of hydrolyzable metal ions. At low pH, there is a + to - charge reversal (CR.1),

followed by a - to + charge reversal (CR.2), and then finally at high pH a + to - charge

reversal (CR.3). The significance of CR.1 is clear in that for oxides, H^+ and OH^- ions are

potential determining; thus, CR.1 is the point of zero charge (pzc) of the colloidal particle. For

instance, the pzc of the colloidal SiO_2 occurs at pH 2.0. CR.2 occurs in the region of specific

adsorption. According to James and Healy (1972b), CR.2 is the pH of surface precipitation

induced at a pH below bulk precipitation. Matijevic and Janauer (1966) suggested that CR.2 is

due to adsorption of discrete highly charged polynuclear complexes. At high pH charge

reversal CR.3 reflects the adsorption of lower positive charged, even negative charged,

species and/or precipitates on the colloidal substrate. James and Healy (1972b) suggested that

if sufficient metal ion is adsorbed to yield a complete coating of adsorbed metal hydroxide,

then CR.3 is the PZC of the metal hydroxide. Therefore, CR.3 reflects the properties of the

complete or incomplete coating of metal hydroxide nucleated on the surface. However,

Packham (1965) reported that the physical enmeshment of particulates in a metal hydroxide

precipitate brings about the region, CR.3.

O'Melia and Stumm (1967) noted that restabilization is enhanced in solutions which

are slightly oversaturated with respect to ferric hydroxide (pH > 3) due to progressive

hydroxylation and condensation, whereas restabilization becomes retarded or obliterated in
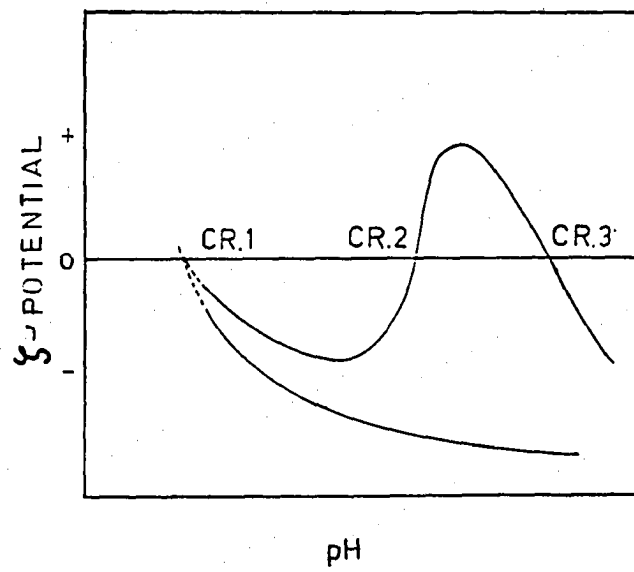
Figure 3.10.   Schematic illustration of the general electrophoretic mobility behavior of
colloid systems in the presence and absence of hydrolyzable metal ions
(James and Healy, 1972c)

solutions that are highly oversaturated with respect to ferric hydroxide (pH > 6). Stumm and

O'Melia (1968) noted that with an increase in pH, the [OH⁻] bound per [Fe(III)] increases and

thus the net positive charge of the hydrolysis species decreases. In addition, the increased rate

of ferric hydroxide precipitation may compete successfully with the adsorption of incipiently

formed soluble iron(III) species.

3.2.2 Sweep coagulation

When a metal salt such as alum or Fe(III) salt is added to water in concentration

sufficiently high to cause precipitation of a metal hydroxide, colloidal particles can be

enmeshed in these precipitates as they are formed and also collide with them afterward

(Amirtharajah and O'Melia, 1990). This process is often referred to as "sweep floc" removal.

That is, in sweep flocculation, physical interaction occurs between the voluminous precipitates

formed and the source water colloids. Packham (1965) revived the concept of a "sweep"

action by the hydrated, gelatinous, metal hydroxides that enmeshed colloidal impurities in their

descent through the water to be purified. Johnson and Amirtharajah (1983) established

boundaries under which conditions for each coagulation mechanism predominate (Figure

3.11). They have superimposed empirically determined coagulation regions onto the Fe(III)

solubility diagram. This diagram provides coagulation domains of mechanistic phenomena

depending on the influences of coagulant dose and solution pH.

Considering the very low solubility product of amorphous ferric hydroxide, $K_{so} < 10^{-38}$,

in virtually all the Fe(III) dosages used in water treatment practice, the applied concentration

of Fe(III) ions is oversaturated with respect to ferric hydroxide. However, according to
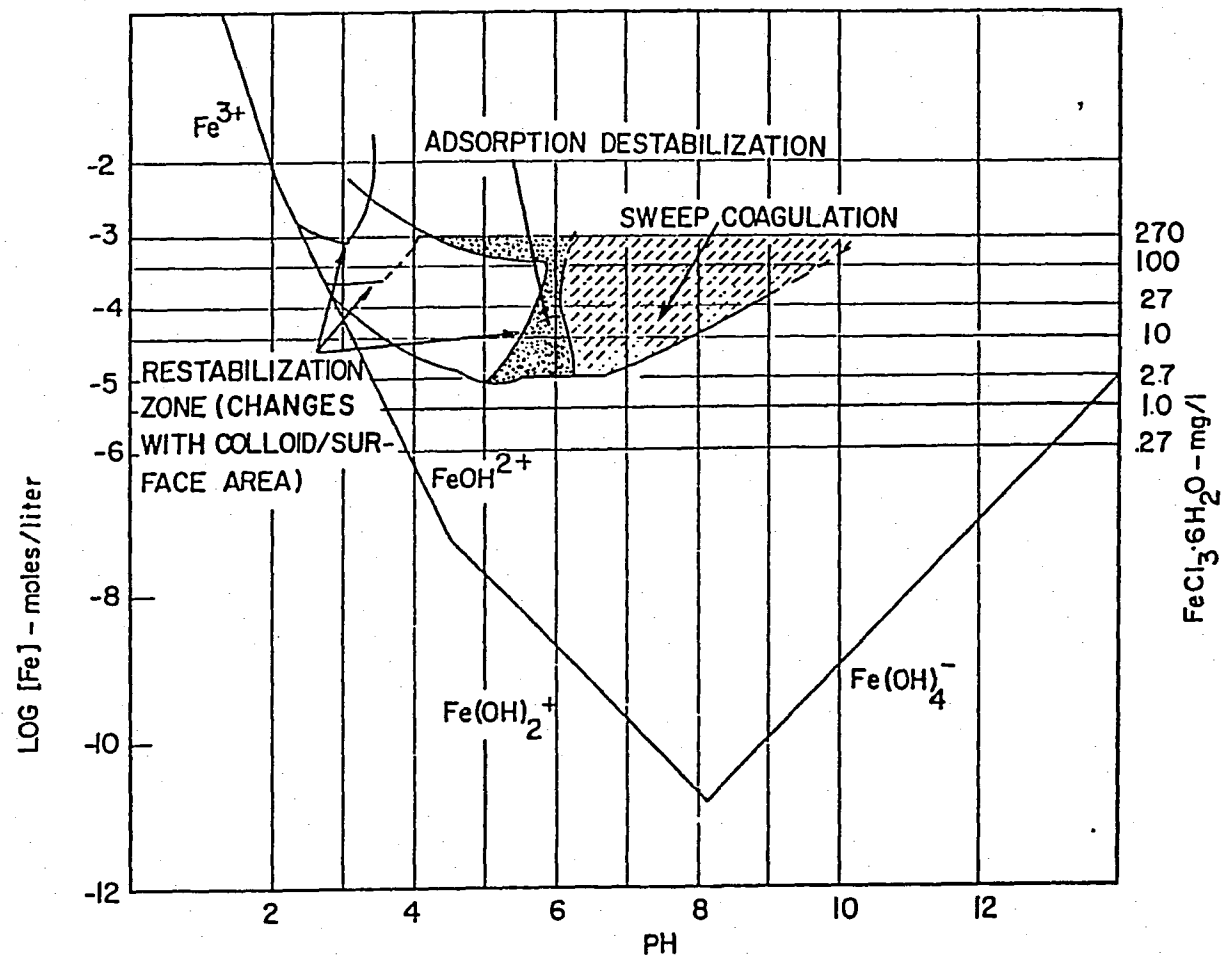
Figure 3.11.   The iron(III) coagulation diagram (Johnson and Amirtharaja, 1983)

Stumm and O'Melia (1968), this oversaturation of the solutions does not necessarily imply that precipitation of the metal hydroxide occurs rapidly. The authors further proposed that some degree of supersaturation must be exceeded before rapid precipitation occurs. This critical supersaturation depends upon several parameters, including temperature, dissolved anions, and the concentration of solid particles already in the solution.

As mentioned earlier, the rate of precipitation is increased by the presence of anions in solution. Sulfate ions are particularly effective. Moreover, the colloidal particles themselves can serve as nuclei for the formation of the precipitate, so that the rate of precipitation increases with increasing concentration of the colloidal particles to be removed (Weber, 1972). It has been known that coagulation under sweep coagulation conditions is no longer stoichiometric. The critical supersaturation necessary for rapid precipitation could in fact decrease with increasing surface concentration, with the colloidal particles providing interfaces for localized oversaturation (Stumm and O'Melia, 1968).

Heterocoagulation, which is particle aggregation caused by collisions between contaminant particles and coagulant precipitates, may also account for observed coagulation. Work by Dentel and Gossett (1988) indicates that an additional possible removal mechanism is that the metal hydroxide first attains a solid state in solution and then heterocoagulates with another solid. They found that these types of precipitation have been shown to be consistent with coagulation results, and then concluded that the destabilization in the sweep coagulation zone is probably caused by precipitate deposition on the surfaces of particles, and hence floc volume increases. In addition, they described the differences of two distinct coagulation

mechanisms. For example, under most conditions common in water treatment, coagulation via charge neutralization is thus achieved by the formation of positively charged precipitates on the particle surfaces, which alter the characteristics of the original particle surface, transforming the overall charge to neutral and then positive values at excessive dosages. It differs from the "adsorption-sweep floc" concept of coagulation in that precipitation precedes charge neutralization. According to them, "sweep floc" coagulation, therefore, is not associated with the onset of precipitation, although it may still be due to the precipitate's overall effect on floc volume fraction and thus the collision rate. Letterman and Iyer (1985) developed a similar model which also describes multilayer coating of particles by precipitate, using several assumptions for complexation of Al(III) on the particle surface to relate coagulant dosage to resultant floc volume.

Several possible pathways by which the metal hydroxide could end up on particle surfaces is shown schematically in Figure 3.12 (Dentel, 1987). However, Figure 3.12 does not clearly define each coagulation mechanism because the pathways neglect the intermediate processes and kinetics. Therefore, kinetic considerations may be especially necessary because of the possible competition between adsorption, complex formation and precipitation of hydrolyzing metal ions. At present there is little fundamental information about these points. James (1981) has stated that one of the challenging problems that remains to be answered is whether the metal hydroxide coating forms by surface condensation of simple ionic species, surface condensation of hydrolyzed species, or whether it is due to adhesion of colloidal hydroxides formed in the solution (i.e., heterocoagulation).

SOLUTION

hydration   polymerization   nucleation /
precipitation

Al (III)➡MONOMERS➡POLYMERS➡PRECIPITATE

⬇ adsorption ⬇   ⬇ hetero-
coagulation

MONOMERS➡POLYMERS➡PRECIPITATE

SURFACE

Figure 3.12.   Schematic representation of the various pathways followed by aluminum hydroxide species in solution or at a surface in contact with the solution (Dentel, 1987)

According to the definitions adopted in this study earlier, enmeshment in a precipitate is both a coagulation and flocculation process since both destabilization and transport are involved. In the treatment of low but objectionable concentrations of colloidal particles in water treatment practice, this process of using high dosages of coagulants, where gelatinous metal hydroxide precipitates are produced rapidly, can be effective, and is used extensively in order to enhance flocculation kinetics. Under the conditions of low turbidity waters, in which flocculation is limited by the number of collisions or contact opportunities, high concentration of precipitates rapidly formed from the metal coagulant can contribute to increase the floc volume, enhance collision opportunities, and produce a settleable floc. According to an AWWA committee report (1989), in typical water treatment practice under sweep coagulation conditions, the water is supersaturated three to four orders of magnitude above the solubility of the metal so that the metal hydroxide precipitates very quickly, in 1-7 seconds. Tang and Stumm (1987b) suggested that the precipitates of metal hydroxides that enmesh colloids is, by kinetic necessity, the only coagulation method possible in waters of very low number concentration of colloids ($N < 10^8$ cm^{-3}).

The major drawback of sweep flocculation using high concentration of metal precipitates would be the costs associated with chemical requirements, the necessity for the sedimentation process before filtration, the disposal of the large quantity of sludge generated, and potential health effects of the residual soluble metal ion remaining in the coagulated water.

3.3 Effects of Sulfate Ion

The presence of certain ions, particularly anions, has been shown to alter the pH range of optimum coagulation, the reaction period for efficient flocculation, the optimum coagulant dose, and the residual coagulant in the effluent (AWWA, 1971). The types of anion present during the hydrolysis of Fe(III) can exert a general ionic strength effect due to double layer compression and a specific chemical effect due to specific adsorption on particulate surface.

Among the ions commonly found in natural waters, sulfate ion is different in the nature of the interaction with the particle surface compared with the interaction of simple ions like K^+, Na^+, Cl^-, and NO_3^- and the particle surface. Flynn (1984) noted that the sulfate ion complexes Fe(III), and thus, affects hydrolysis kinetics; but, this is not the case for Fe(III) salts of nitrate and perchlorate which produce essentially indifferent electrolyte solutions. Hunter (1989) defined clearly this difference in aluminum oxide systems as showing the effect of anions on zeta potential as shown in Figure 3.13. As depicted in Figure 3.13, the monovalent anions reduce the magnitude of zeta potential of aluminum oxide but do not change its sign. By contrast, the divalent counterions (SO_4^{2-} and $S_2O_3^{2-}$) can change the sign of the zeta potential. Several investigators regarded this as unequivocal evidence that the monovalent ions were 'indifferent' while the divalent counterions were specifically adsorbed.

The relative stability of the SO_4^{2-} complexes can be evaluated from the equilibrium

$$FeOH^{2+} + SO_4^{2-} = FeSO_4^+ + OH^- \qquad (3.14)$$
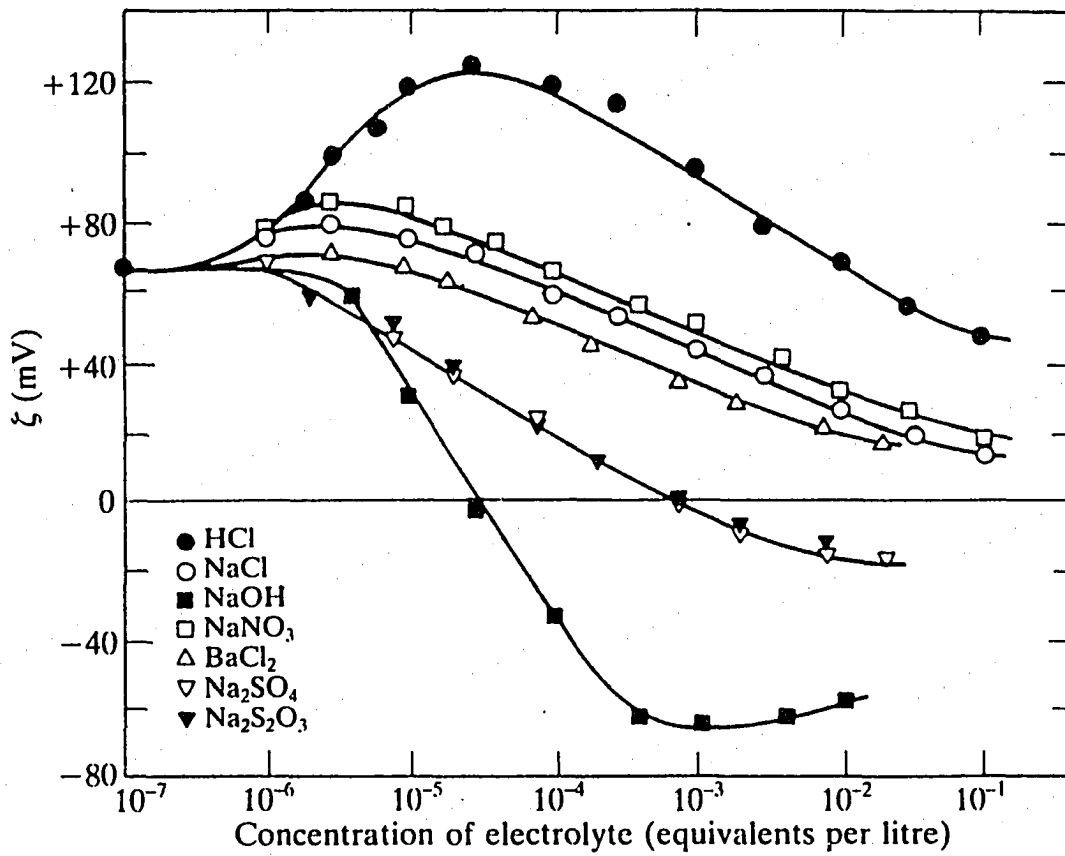
Figure 3.13.   Zeta potential of Al_2O_3 in solutions of various electrolytes. The
concentration unit is equivalents per liter (Hunter, 1989)

where SO_4^{2-} should quickly replace any OH^- held to Fe(III) by single bond. Therefore, hydrolysis reactions of Fe(III) are influenced by sulfate. As described in Eq (3.14), the predicted behavior is generally observed, i.e., a rapid rise in pH occurred following addition of SO_4^{2-} ions. Dousma et al.(1979) also found that the higher $[SO_4^{2-}]$ / [Fe] ratio the smaller the amount of base required to increase the solution pH from a value of 3 to 10. de Hek et al.(1978) cited the works of Hildebrand et al. who also observed that far less alkali was needed to produce the first visible precipitate than when titrating solutions of the chloride or nitrate salts.

In a study of the sulfate adsorption on iron oxides, Parfitt and Smart (1978) reported that sulfate is adsorbed by ligand exchange with exposed surface FeOH groups only in the presence of protons represented here by $FeOH_2^+$. They described the reaction simply as

$$\begin{matrix} \text{FeOH} \\ \\ \text{FeOH}_2^+ \end{matrix} + SO_4^{2-} \longrightarrow \begin{matrix} \text{Fe-O} \\ \\ \text{Fe-O} \end{matrix}\!\!>\!\!S\!\!<\!\!\begin{matrix} O \\ \\ O \end{matrix} + OH^- + H_2O \qquad (3.15)$$
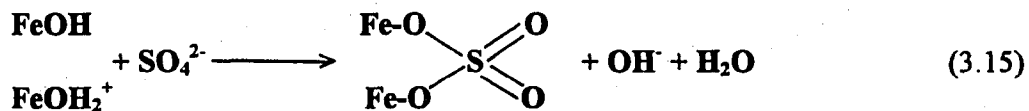
Reaction (3.15) also shows that the adsorption of sulfate results in the release of hydroxyl ion.

Stumm and Morgan (1962) presented alkalimetric titration data of Al(III) and Fe(III) in the presence of anions, and demonstrated that there were very pronounced effects of certain anions on the coagulative behavior. The authors pointed out that if the anions are strong coordinators with the coagulating metal ions, specific chemical equilibria may be more important than double-layer compression. A summary, from the authors:

In case of alkalimetric titration, high concentrations of SO_4^{2-} may compete with OH^- ions for the coordinative sites and may completely or partially substitute for OH^- ions in the charge neutralization reaction of the metal cations. Therefore, the quantity of OH^- ion required was less than the stoichiometric requirements for the neutralization of any excess acid plus precipitation of aluminum hydroxide. Since less OH^- ions have to enter into the lattice if other coordinating anions are present, the pH of optimum coagulation will frequently be lower than it is in the absence of complex forming ligands (p. 985).

The role of sulfate ion on the hydrolysis-precipitation studies of Al(III) solutions was conducted by de Hek et al.(1978). They observed the effect of sulfate ion on destabilizing a suspension already restabilized by an excess coating of aluminum hydrolysis species. They noted that the divalent sulfate ion is known to affect the course of the hydrolysis-precipitation process as well as the composition, texture, and structure of the resultant precipitates. However, they did not observe that the use of other anions (NO_3^- and Cl^-) altered the course of the hydrolysis-precipitation process. They concluded that the observed behavior of the sulfate ion is that expected of a catalyst which accelerates the overall process by lowering the kinetic barriers (energetic and/or entrophic). In order to explain the nature of barriers, they proposed the following reaction scheme:

$$xAl^{3+}_{(aq)} + yOH^- \longrightarrow \text{polynuclear complexes} \qquad (3.16)$$

$$xAl^{3+}_{(aq)} + yOH^- \xrightarrow[\quad SO_4^{2-} \text{ catalyst} \quad]{} \text{precipitate} \qquad (3.17)$$
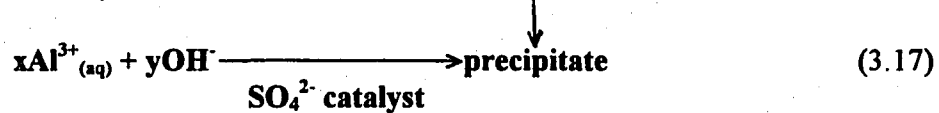
From Eqs (3.16) and (3.17), they stated that the major role of sulfate ion is lowering the free energy of activation for reaction (3.16).

Morel (1983) described how the presence of reactive ligands such as SO_4^{2-} in natural waters affects complexation kinetics:

> The replacement of H_2O by any ligand in the coordination sphere of a metal usually "labilizes" the other water molecules and increases the water exchange rate. In many cases the exchange of one ligand for another (H_2O) may be achieved without intermediate formation of the stable hydrated complex (p. 299).

Bottero and Bersillon (1989) investigated the chemistry of Al(III) coagulants using Al NMR pattern of these dissolved in water. They compared alum with PACl (polyaluminum chloride) and PACS (polyaluminum chlorosulfate) which contains sulfate ions. Comparing Al NMR spectra for these Al(III) coagulants, they observed that alum and PACS make a direct transition between monomers and precipitates after dilution, or upon a sharp increase in pH, while PACl makes polymeric species. They reasoned that the sulfate ions in the alum and PACS form inner complexes with aluminum (i.e., $Al(SO_4)^+$) and inhibit the formation of transient polymeric species, and the polymeric species formed with PACl are not immediately destroyed after the dilution or pH increase.

Flynn (1984) has also found that addition of base at room temperature to $Fe_2(SO_4)_3$ solution produces polymeric species and precipitates; however, the precipitation process occurs at a lower pH value and at a greater rate than in solutions of Fe(III) salts with

monovalent anions such as nitrate, perchlorate, or chloride. The author observed that through

the precipitation processes, hematite (α-Fe$_2$O$_3$) and goethite (α-FeOOH) were identified in the

solids precipitated from sulfate solutions. Sylva (1972) also observed that addition of sulfate

salts to the polymers formed by adding NaHCO$_3$ to solutions of Fe(III) perchlorate or nitrate

causes rapid precipitation.

Dousma et al.(1979) cited the work of Wendt et al., who found higher values of rate

constants for the formation of iron sulfate complexes (i.e., FeSO$_4^+$) than for the formation of

the chloride or bromide complexes. Also, the formation of dimers, Fe$_2$OH$_2^{4+}$ was shown to

occur more rapidly in the presence of sulfate ions. Dousma and his co-workers also reported

that the major difference between sulfate system compared with chloride or nitrate systems is

the catalytic effect of SO$_4^{2-}$ in promoting nucleation and growth at lower supersaturation.

Dzombak and Morel (1990) also reported on the effect of sulfate on the hydrolysis and

precipitation of Fe(III). They reported that the presence of sulfate results in precipitation at a

greater rate and at lower pH values or [OH$^-$]/[Fe] mole ratios than in solutions with only

uninegative anions.

Through investigating the rate of chemical complexing in the formation of ferric

colloidal dispersions, Matijevic (1976) noted that the particle shape and composition depend

most strongly on the pH and on the nature of the anions contained in the systems. In

observing the role of sulfate, he noted that the anions responsible for the characteristic of the

particles frequently were not found in the solid phase, indicating that solute complexes

involving such anions must act as precursors to the nucleation stage. For example, they found

that the presence of sulfate ions was essential in order to produce uniform colloidal spheres of chromium hydroxide, yet sulfate was not a constituent species in the final particles.

Thompson and Tahir (1991) investigated the hydrolysis and precipitation of Fe(III) in simple inorganic electrolyte solutions and in aqueous dispersions of the clay mineral montmorillinite. The following observations of interest for the sulfate system in comparison with other anion systems came out of their work:

- More rapid hydrolysis-precipitation evidenced by the pH titration curves for the sulfate system,

- The amount of dissolved Fe(III) from sulfate solutions containing dispersed clay were found to be generally much lower than in the case of the other electrolyte systems,

- The morphologies of solid phases formed in the presence of sulfate ion were found to differ significantly from those encountered in chloride systems (i.e., more gelatinous phase comprised of much bigger spherical particles (20-50 nm dia.) with crystalline structure in the presence of sulfate),

- More reduction in the value of electrophoretic mobility and lower point of zero charge.

Specifically sorbing anions may form complexes either in solution or on the surface of (hydr)oxides. Specific sorption of anions on hydrous oxides occurs via ligand exchange reaction in which hydroxyl surface groups are replaced by other coordinating ligands (Sigg and Stumm, 1981). Likewise, there is now a considerable body of evidence to show that sulfate in aqueous solution involves in a reaction with either iron or aluminum ions on the surface of particulates in water. Specific sorption of anions on (hydr)oxide surfaces has been studied based on the surface complexation concept. In the surface complexation approach,

reactions between solutes and functional groups on the solid surface are effectively

coordination reactions that are analogous to the formation of soluble complexes. This

approach postulates a set of specific surface reactions and formulates equilibrium constants as

a product of intrinsic and electrostatic contributions.

To explain the effects of the adsorbed aluminum hydrolysis products and the specific

adsorption of sulfate on the particle surface, Hohl et al.(1978) proposed the following

ionization and complex formation reactions for hydrous aluminum oxide where '≡' represents

an ionizable, complex-forming site on the surface of particle:

$$\equiv AlOH_2^+ + OH^- \longleftrightarrow \equiv AlOH + H_2O \qquad (3.18)$$

$$\equiv AlOH + OH^- \longleftrightarrow \equiv AlO^- + H_2O \qquad (3.19)$$

$$\equiv AlOH + SO_4^{2-} \longleftrightarrow \equiv AlSO_4^- + OH^- \qquad (3.20)$$

$$2\{\equiv AlOH\} + SO_4^{2-} \longleftrightarrow \equiv Al_2SO_4 + 2OH^- \qquad (3.21)$$
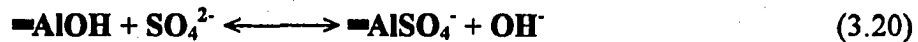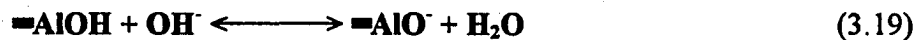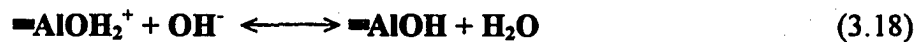
According to both types of reactions, increasing the pH and/or the sulfate concentration

decreases the charge of the aluminum hydroxide surface by increasing the number of neutral

($\equiv AlOH$ and $\equiv Al_2SO_4$) and negative ($\equiv AlO^-$ and $\equiv AlSO_4^-$) surface groups. As described in Eqs

(3.18) to (3.21), changes with pH in the degree of protonation of anions sorbed on surfaces

can be expected.

Contradictory conclusions exist in the literature about the anion sorption mechanism in ferric oxide. Double-layer adsorption of counterions to a surface positively charged due to H^+ ion adsorption, ligand-exchange adsorption involving the replacement of surface OH groups, and adsorption by hydrogen binding to surface OH_2^+ and OH groups have been suggested (Davis and Leckie, 1978; Ghominy et al., 1993). These authors reported that exchange with surface OH groups (or ligands) seems to be the main mechanism for anion sorption on ferric oxide gel. Sigg and Stumm (1981) suggested that possibly, the initial SO_4^{2-} adsorption is specific (i.e., at the edges of α-FeOOH surface), but subsequently, at higher concentrations, SO_4^{2-} behaves like an indifferent electrolyte (i.e., double layer compression).

As mentioned previously with Eqs (3.18) to (3.21), the extent of surface complex formation (adsorption) is, as with metal ions, strongly dependent on pH. Since the adsorption of SO_4^{2-} is coupled with a release of OH^- ions, adsorption is favored by lower pH values (Stumm, 1992). Also, competitive complex formation equilibria (SO_4^{2-} vs. OH^-) explain the strong dependency of anion binding on pH. Dzombak and Morel (1990) showed the pH dependence of SO_4^{2-} adsorption on ferric (hydr)oxide surface as illustrated in Figure 3.14. The curve is calculated from equilibrium constants for $[SO_4]_T = 1 \times 10^{-5}M$ using the surface complexation reactions and complexation constants presented in Table 3.4. Figure 3.14 shows how the adsorption of sulfate on amorphous iron oxide exhibits pronounced maxima at low pH. For example, the adsorption of SO_4^{2-} on $Fe(OH)_{3(am)}$ is greatly increased at more acidic pH range and is almost absent at pH < 7.
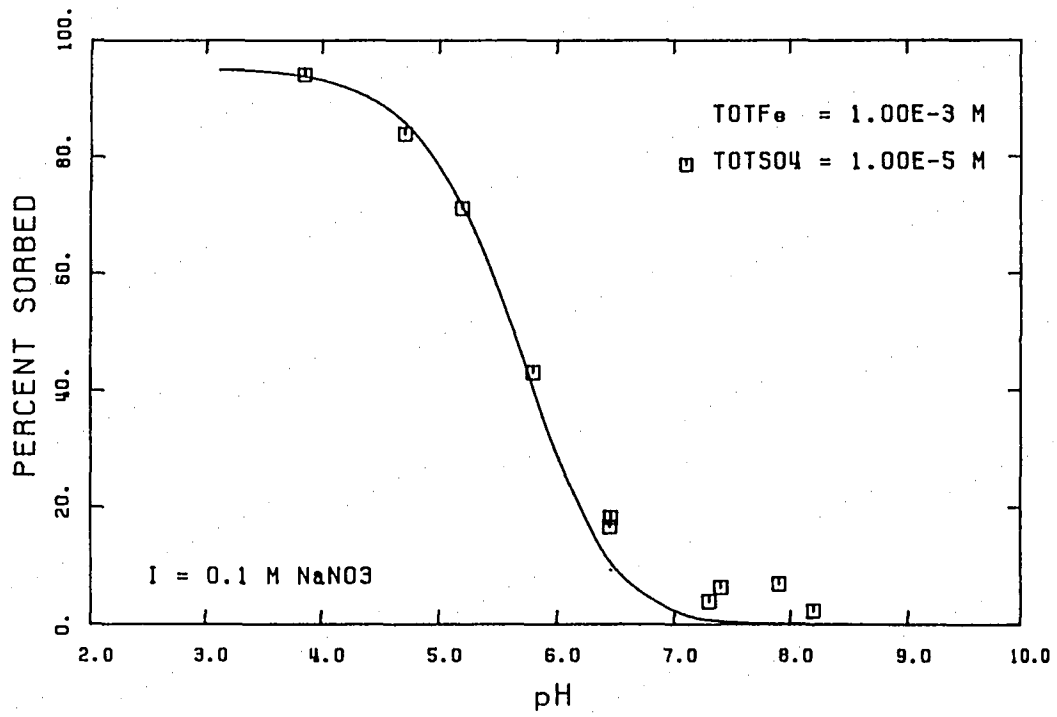
Figure 3.14. Adsorption of sulfate on amorphous iron oxide, $[Fe(OH)_3]_T = 10^{-3}$ M (Dzombak and Morel, 1990)

Table 3.4. SO_4^{2-}/Hydrous ferric oxide surface complexation reactions and intrinsic surface complexation constants (From Dzombak and Morel, 1990)

Reaction	log K^{int} *
$\equiv FeOH^0 + SO_4^{2-} + H^+ = \equiv FeSO_4^- + H_2O$	7.78
$\equiv FeOH^0 + SO_4^{2-} = \equiv FeOHSO_4^{2-}$	0.79

* equilibria are defined as: $K^{int} = [\equiv FeOHSO_4^{2-}] / [\equiv FeOH^0][SO_4^{2-}]$

The effect of the adsorbed aluminum hydrolysis products and the specific adsorption of sulfate on particle surface is schematically described in Figure 3.15 presented by Letterman and Vanderbrook (1983). Figure 3.15 shows that the particles are destabilized by the adsorption of the hydrolysis species(region II) and then restabilized due to excess adsorption of the species(region III). Region IV illustrates the effect of sulfate ions on destabilizing a suspension already restabilized by an excess coating of aluminum hydrolysis species.

Several studies have shown that sulfate ions produce dramatic effects on the coagulation and flocculation efficiencies achieved by metal coagulants. For example, Packham (1965) carried out experiments with various compounds of iron and aluminum. The results of coagulation tests on 50 mg/L kaolin suspensions using aluminum salts and iron salts are shown in Figure 3.16 and Figure 3.17, respectively. In these figures the values of $D_{t/2}$, the coagulant dose required to halve the turbidity after flocculation and settling, were plotted against the pH measured after coagulation. From Figure 3.16 and 3.17, it is observed that values of $D_{t/2}$ increase more sharply at acid pH values for aluminum chloride than for
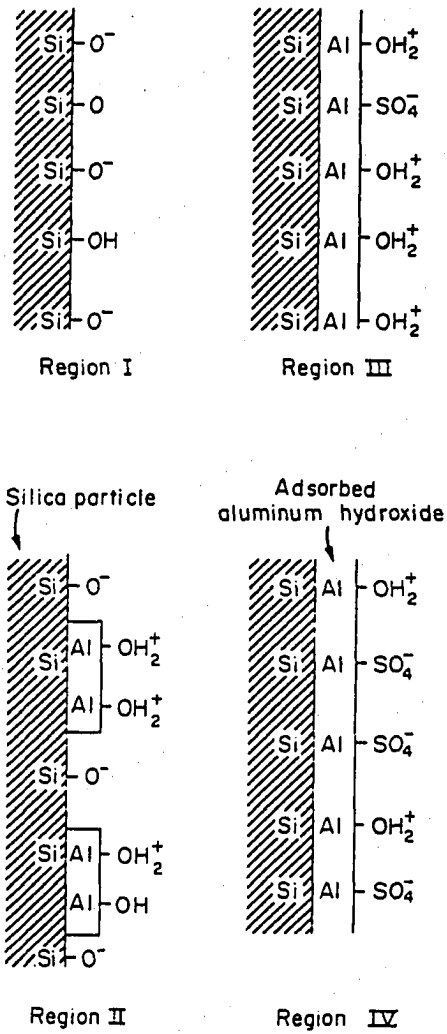
Figure 3.15. Schematic diagram of the aluminum treated particle surface (Letterman and Vanderbrook, 1983)
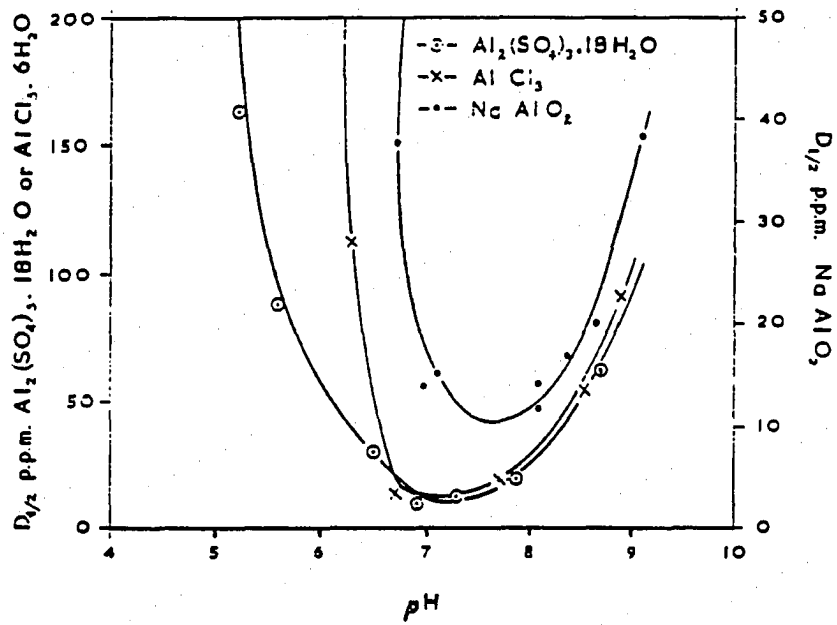
Figure 3.16.   Coagulation of 50 mg/L kaolin with aluminum compounds (Packham, 1965)
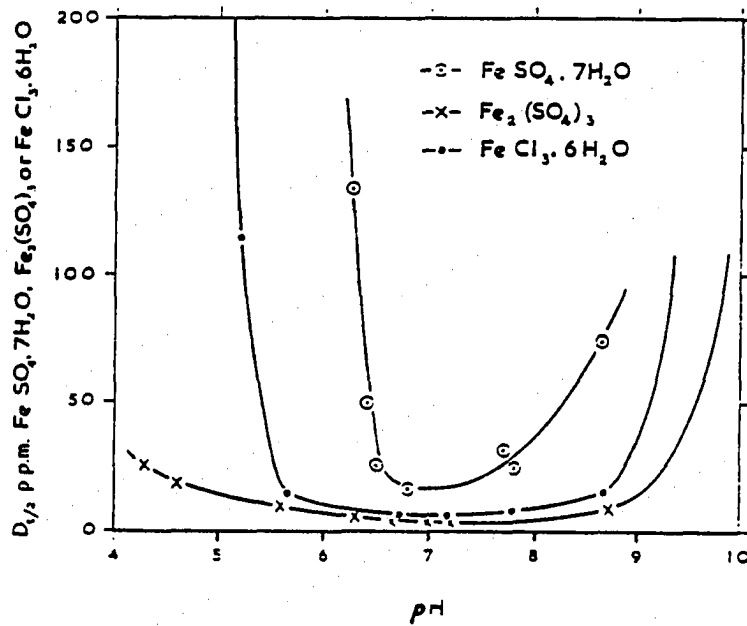
Figure 3.17. Coagulation of 50 mg/L kaolin with iron compounds (Packham, 1965)

aluminum sulfate, and aluminum chloride has a narrower optimum pH range than that of aluminum sulfate. With ferric chloride and ferric sulfate, $D_{t/2}$ are minimal over a wider pH range than the corresponding aluminum salts, again with a tendency for the sulfate to have a wider pH range than the chloride. Packham explained the effect of sulfate ion on the optimum pH range for coagulation that the sulfate ion enters into the coordination sphere of the aluminum ion in place of hydroxyl ions forming complexes that precipitate at a lower pH than aluminum hydroxide.

Hanna and Rubin (1970) investigated the coagulation of E.coli by aluminum sulfate under the same conditions reported for the aluminum nitrate to observe the effect of anion, especially sulfate ion. They observed that sulfate ion produced a dramatic effect of significantly widening the sweep zone to the acid side; and furthermore, the restabilization zone, so prominent in the neutral pH range for aluminum nitrate, never appeared. They reasoned for the effect of sulfate that:

The widening due to sulfate is attributed to complexing of sulfate within aluminum. This might be due to the complexing between aluminum and sulfate in terms of Lewis acid-base theory whereby the strongly acid aluminum can accept an electron pair from the weakly basic sulfate ion. Therefore, insoluble aluminum hydroxo sulfato precipitate will form at a pH lower than necessary for the formation of insoluble $Al(OH)_3$ since a lesser hydroxide ion concentration is required. Upon increasing the pH, sulfate is displaced from the lattice by the more basic hydroxide ion, and then this results in the formation of insoluble $Al(OH)_3$ (p. 319).

Amirtharajah and Mills (1982) also pointed out that in the coagulation diagram for alum,

significant background concentration of anions such as sulfate ion could eliminate all traces of

a restabilization zone.

Figure 3.18 presented by Letterman and Vanderbrook (1983) demonstrates the effect

of sulfate ion by comparison with a familiar figure from Weber (1972). It is seen from Figure

(A) that with particle concentrations S_2 and S_3, the particles will be destabilizd as coagulant

concentration increases (zone 2)and then restabilized due to overdosing (zone 3), but will then

be destabilized again in the sweep floc zone (zone 4). Figure (B) shows the regions of

restabilization disappear with a high sulfate concentration, for example, 3×10^{-4}M. They

pointed out that this is apparently a result of the total particle volume fraction of the

suspension. That is, solution pH and specifically adsorbed anions such as sulfate have an

important effect on the charge and amount of the adsorbed precipitate and hence on the net

charge, volume concentration and stability of the composite particles.

Sricharoenchaikit and Letterman (1987) investigated the effect of sulfate ion on

flocculation kinetics. Diluted suspensions (2×10^7 particles/L) of 9.8 μm diameter polystyrene

latex spheres were destabilized at pH 6.0 using aluminum nitrate, and then sodium sulfate was

injected into the reactor at the start of the flocculation reaction. The total particle

concentration measurements using a HIAC particle counter were used to determine the rate of

flocculation. They noted that at pH 6.0 and low sulfate concentration, the kinetics of

orthokinetic coagulation of the polystyrene particles can be described using the first order rate

equation with respect to particle number derived from a simplification of Saffman and
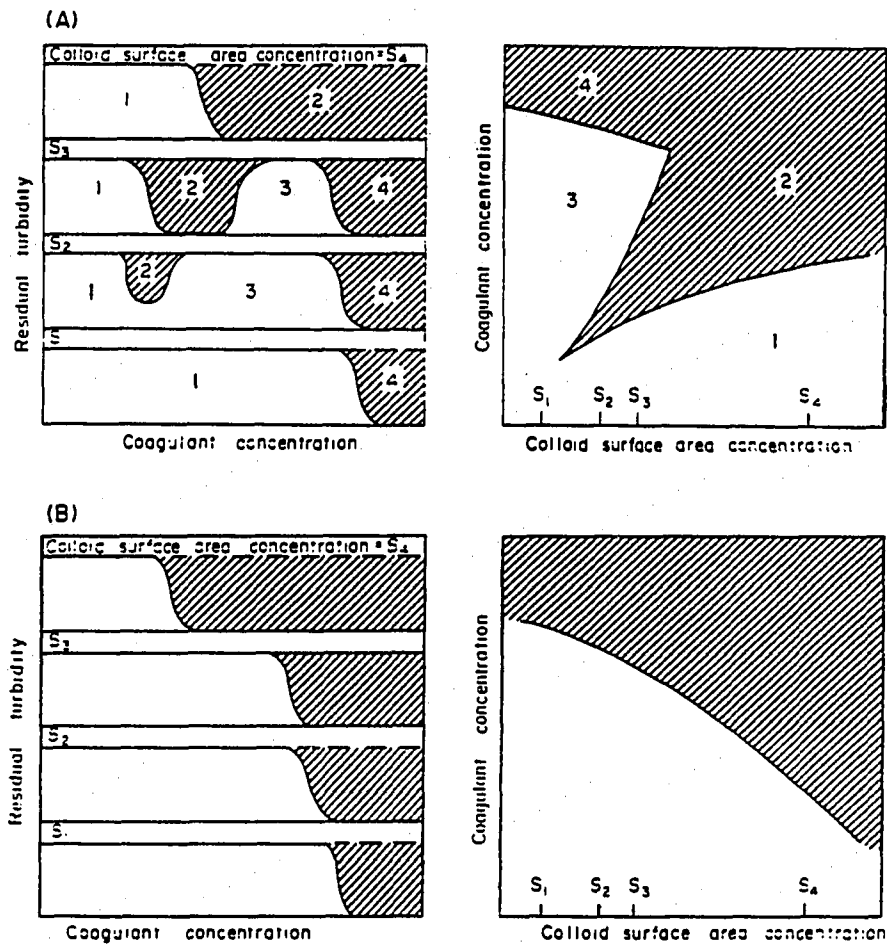
Figure 3.18. (A) Schematic diagrams illustrating the effect of colloid surface area concentration on the residual concentration relationship, (B) Schematic diagram showing the effect of a high back-ground sulfate ion concentration on the feature of (A) (Letterman and Vanderbrook, 1983)

Turner's second order rate equation. However, at higher sulfate ion concentrations, i.e.,

$\geq 3 \times 10^{-4}$ M, the kinetics of aggregation were enhanced and were no longer first order. A

similar enhanced kinetics of aggregation was also obtained by increasing a mixing intensity.

In summary, the sulfate ion appears to tend to alter the behavior of hydrolyzed metal

coagulants through the reaction with the metal ions and charged sites on the metal hydroxide

precipitate. Thus, the sulfate ion may enhance the hydrolysis-precipitation of metal coagulants.

In general, it was noted that the sulfate ion may suppress charge reversal and accelerate the

kinetics of precipitation of metal hydroxide. Accordingly, the sulfate ion present in particulate

suspension is an important factor in the kinetics of flocculation.

3.4 Effects of Temperature

A number of water treatment plants experience significant operational problems when

the water temperature approaches the freezing point. There are reports of decreased turbidity

removal efficiency and deteriorated effluent quality at very low temperature. However,

published information on the effect of temperature on the mechanism of flocculation is both

scarce and contradictory. In particular, little data are available on the kinetics of flocculation

using Fe(III) coagulants, not even with alum, at low temperature. Therefore, It is necessary

that the impact of low water temperature on flocculation should be studied to ensure the

applicability of coagulation theory to water treatment plant practice on a year-around basis.

The following factors in Table 3.5 can be considered to be affected by the varying

temperature and may, in turn, affect the process of flocculation.

Table 3.5. Possible factors affecting flocculation kinetics with varying water temperature

Factors	Parameters
Physical	• viscosity and density of fluid (flow field characteristics)
	• strength of particulate aggregates
Physico-chemical	• electrokinetics of particulates (changes in surface charges)
Chemical	• rate and distribution of hydrolysis species of metal coagulant
	• solution pH due to the change in ion product of water

3.4.1 Physical effects

The destabilization of particles can be produced by a number of different mechanisms. But, when considering only physical aspects of flocculation (i.e., transport aspects of flocculation), the rate of particle collision in terms of diameter of particles for the description of the kinetics of flocculation can be expressed as follows (Lawler 1994),

For Brownian Motion:
$$\beta_{Br}(i,j) = \frac{2kT}{3\mu}\left\{\frac{1}{d_i}+\frac{1}{d_j}\right\}(d_i+d_j) \qquad (3.22)$$

For Fluid Shear:
$$\beta_{Sh}(i,j) = \frac{1}{6}(d_i+d_j)^3 G \qquad (3.23)$$

For Differential Sedimentation:
$$\beta_{DS}(i,j) = \frac{g\pi}{72\mu}(\rho_p-\rho_l)(d_i+d_j)^3|d_i-d_j| \qquad (3.24)$$

In Eqs (3.22) - (3.24), β is the rate of collision between particles of different diameter i and j, i and j are subscripts denoting particle size classes, d is the particle diameter, k is Boltzmann's constant, T is absolute temperature, μ is the absolute fluid viscosity, G is the average velocity gradient, g is the gravitational constant, and ρ_p and ρ_l are the particle and liquid mass densities, respectively.

The driving forces for the these transport processes are kT for the Brownian motion (perikinetic), the fluid velocity gradient for the fluid shear (orthokinetic), and relative settling velocity of particles for the differential sedimentation. First, the physical effects on the rate of flocculation for the perikinetic and differential sedimentation mechanisms include such terms as temperature and/or viscosity in equation for rate of particle aggregation during flocculation. That is, the rates of flocculation in perikinetic and differential settling flocculation decrease with decreasing temperature. By observing the progress of flocculation of a ferric floc in the absence of other particles, using a light beam passed through the jar, Camp et al.(1940) concluded that the Brownian phase of flocculation, which is temperature (viscosity) dependent, was completed in 6 to 10 seconds. Accordingly, the authors stated that if considering the time required for the particles to become plainly distinguishable, the time of temperature dependence is negligible in comparison to the total flocculation time. In addition, it has been known that the orthokinetic collision rate greatly exceeds the rate due to brownian diffusion for particles whose effective diameters are larger than 1 μm, even at fairly low velocity gradient (Ives, 1978). For larger particles and higher shear rates, the orthokinetic rate becomes much greater. In practice, since the size of particles grows well above 1 μm during

flocculation and quite high shear rate is applied, the influence of temperature on perikinetic

flocculation would have little effect, or only initial effect, on the overall flocculation kinetics.

Another physical factor to be considered is the effect of temperature on the

flocculation mixing intensity. For orthokinetic flocculation, the flocculation efficiency can be

affected by the varying temperature because of the term, G in Eq (3.23). Camp and Stein

(1943) developed the root mean square velocity gradient (G) that can be calculated from the

power input, P, to the fluid and the viscosity as follows:

$$G = (\frac{P}{V\mu})^{1/2} = (\frac{\varepsilon}{\upsilon})^{1/2} \qquad (3.25)$$

where P/V is the mean value of the work input per unit time per unit volume being mixed, ε is

the power input per unit mass, and μ and ν are the dynamic and the kinematic viscosity,

respectively. Camp and Stein stated that G is valid for both laminar and turbulent fluid flow.

Therefore, the rate of flocculation would be dependent on temperature because of the

viscosity change. However, in an earlier study of an effect of temperatures on the rate of

flocculation, Camp et al. (1940) observed that if mixing velocity is high enough to mask the

effect of convection currents and produce a stable flow pattern, the speed of coagulation is

independent of temperature.

Recently, however, based on the understanding of turbulent mixing characteristics,

some researchers have raised questions about the effectiveness of using a spatially-averaged

velocity gradient or energy dissipation rate to describe interparticle collisions (Cleasby, 1984; Clark, 1985; Han and Lawler, 1992).

Cleasby (1984) argued that this approach can only apply to particles smaller than Kolmogoroff microscale of turbulence, η. This microscale is a characteristic size of the eddies below which the energy is dissipated primarily by viscous effects. The size of microscale depends on the energy input and the viscosity of the fluid. The collision rate for turbulent flocculation of raindrops in a cloud proposed by Saffman and Turner (1956) are also dependent on the kinematic viscosity. However, they assumed that the rain drops were at least one order of magnitude smaller than the Kolmogoloff length scale of turbulence. From the literature reviewed, Cleasby (1984) suggested that if eddy sizes smaller than the Kolmogoroff microscale are important in flocculation, flocculation efficiency should be temperature dependent as evidenced by the viscosity term in G, if eddies larger than the microscale are important, flocculation efficiency may be independent of temperature since no viscosity term is included in any of the aggregation equations reviewed.

Gregory (1989) also suggested that in practice, flocs can grow considerably larger than Kolmogoroff microscale which, for the kind of turbulence found in stirred tanks and similar units, is of the order of 100 μm and collisions of such flocs and the collision rate of such flocs should be independent of viscosity and hence of temperature. In contrast, Vik and Eikebrokk (1989) ascribed the poor coagulation result to the poor rapid-mixing conditions caused by lower temperature. For example, They reported that decreasing the temperature from 20 to 0 °C increases the viscosity 50 %. When the viscosity increases, the possibility of

obtaining an even distribution of coagulants in the water decreases. Francois and Bekaert (1986) also pointed out that the slowed floc growth at low temperature (at 5 °C) might be due to the slowing the formation of insoluble aluminum hydroxide or poor homogeneous distribution of the insoluble hydroxide throughout the clay suspension.

Several researchers (Cleasby, 1984; Clark, 1985; Han and Lawler, 1992) have commented on the effects of temperature on the hydrodynamic aspects of flocculation, and some even drew conclusions about temperature effects, but no one has ever done a cohesive set of experiments which demonstrated the temperature dependence of flocculation until the work of Hanson and Cleasby (1990). They tried to demonstrate whether one measure of turbulence intensity is better than another, i.e., G, ε, or η, when attempts were made to correct flocculation mixing intensity for temperature effects. They concluded:

- None of the three energy parameters used was able to eliminate the effect of temperature on alum flocculation kinetics,

- Much of the difference seen between the 20 and 5 °C alum flocculation is related to floc strength and not to turbulent flow field characteristics,

- The system chemistry was found to be much more important than the choice of energy input parameters on flocculation kinetics at different water temperatures.

3.4.2 Physico-chemical effects

Particles could be destabilized by the compression of the double layer. In flocculation due to the compression of the double layer, the dominant forces are electrostatic repulsion and London-van der Waals attraction, whose combined interactions are the essence of the DLVO (after the four scientists - Deryaguin, Landau, Verwey, and Overbeek - who were largely responsible for its development) theory. The total potential energy of the interaction can be estimated from the electrokinetic (or zeta) potential.

Mohtadi and Rao (1973) found that the zeta potential of kaolinite and bentonite clays coagulated with alum at a given dose and constant pH (pH 5.0) did not change with temperature variation from 1 to 25 °C. They also observed no measurable change in the stability of kaolinite or bentonite suspensions, which was measured by the light absorption index, with varying temperature (1 - 25 °C). Similarly, Stumm and O'Melia (1968) also observed negligible effect of temperature on ZP measurement for the kaolinite dispersions used in their study. These investigators indicated that many coagulant-colloid interactions can overshadow electrostatic effects in the destabilization of colloids. Thus, according to the authors, the particle-particle interaction resulting from double layer compression is expected to be relatively constant or negligible over the temperature changes normally encountered in water treatment flocculation.

3.4.3 Chemical effects

As reviewed in previous section, the Fe(III) hydrolysis process can be viewed as a complexation reaction involving hydroxyl ion, and hence, significantly influenced by a solution pH. As the temperature of the water being treated changes, both the equilibrium concentrations of the various coagulant species and the hydrolysis reaction kinetics may change. Accordingly, the changes in the chemical structure, the presence of certain functional groups, and the degree of hydrolysis of metal salt coagulants can influence their adsorption and/or precipitate formation, and hence, their destabilizing capacity.

The simplest thermodynamic expression available for estimating changes in solution species distributions is the integrated form of the van't Hoff equation with the reaction enthalpy (ΔH_r) taken to be independent of temperature,

$$\log(\frac{K_2}{K_1}) = (\frac{\Delta H_r}{2.303R}).(\frac{1}{T_1} - \frac{1}{T_2}) \tag{3.26}$$

where K_1 and K_2 are the reaction equilibrium constants at temperature, T_1 and T_2 (Kelvin), respectively; R is the ideal gas constant. Thus, if the reaction enthalpy can be determined and the reaction equilibrium constant is known at one temperature, the equilibrium constant at a second temperature can be calculated.

Table 3.6 contains chemical equilibria and stability data and reaction enthalpy for monomeric iron(III) and ferric hydroxide complexes.

Table 3.6. Iron(III) hydrolysis equilibrium constants and corresponding reaction enthalpy (Baes and Mesmer, 1976; Nordstrom et al., 1990)

Reaction	ΔH_r° (kcal/mol)	log K (25 °C)	log K (5 °C)
(1) $Fe^{3+} + H_2O = FeOH^{2+} + H^+$ [a]	10.4	-2.19	-2.74
(2) $Fe^{3+} + 2H_2O = Fe(OH)_2^+ + 2H^+$	17.1	-5.67	-6.57
(3) $Fe^{3+} + 3H_2O = Fe(OH)_3^0 + 3H^+$	24.8	-12.56	-13.84
(4) $Fe^{3+} + 4H_2O = Fe(OH)_4^- + 4H^+$	31.9	-21.6	-23.28
(5) $Fe(OH)_{3(s)} = Fe^{3+} + 3OH^-$	20.7	-38.7	-39.79 [b]

a; Ligand and H_2O molecules are omitted for brevity.

b; solubility product (K_{so}) calculated from van't Hoff equation using values of ΔH_f for $Fe(OH)_3 = -197.0$ kcal/mol, ΔH_f for $Fe^{3+} = -11.4$ kcal/mol, and ΔH_f for $OH^- = -54.957$ kcal/mol given by Snoeyink and Jenkins (1980).

The data in Table 3.6 can be used to compare equilibrium iron(III) solubility as a function of pH at two different temperature. It should be emphasized that the polymeric species are metastable reaction intermediates, and do not directly participate in the reversible equilibrium controlling ferric hydroxide equilibrium solubility (Stumm and Morgan, 1981). The results of such calculations for amorphous ferric hydroxide are given in Figure 3.19. In Table 3.6 the K and H_r° designate the equilibrium constant and reaction enthalpy for the species indicated. The approximate values in Eqs (1) - (5) in Table 3.6 are typical for 25 °C and corrected to I=0. For the solubility diagram, the precipitated $Fe(OH)_{3(s)}$ entity was chosen to be amorphous $Fe(OH)_3$ and K_{so} was chosen as $10^{-38.7}$.
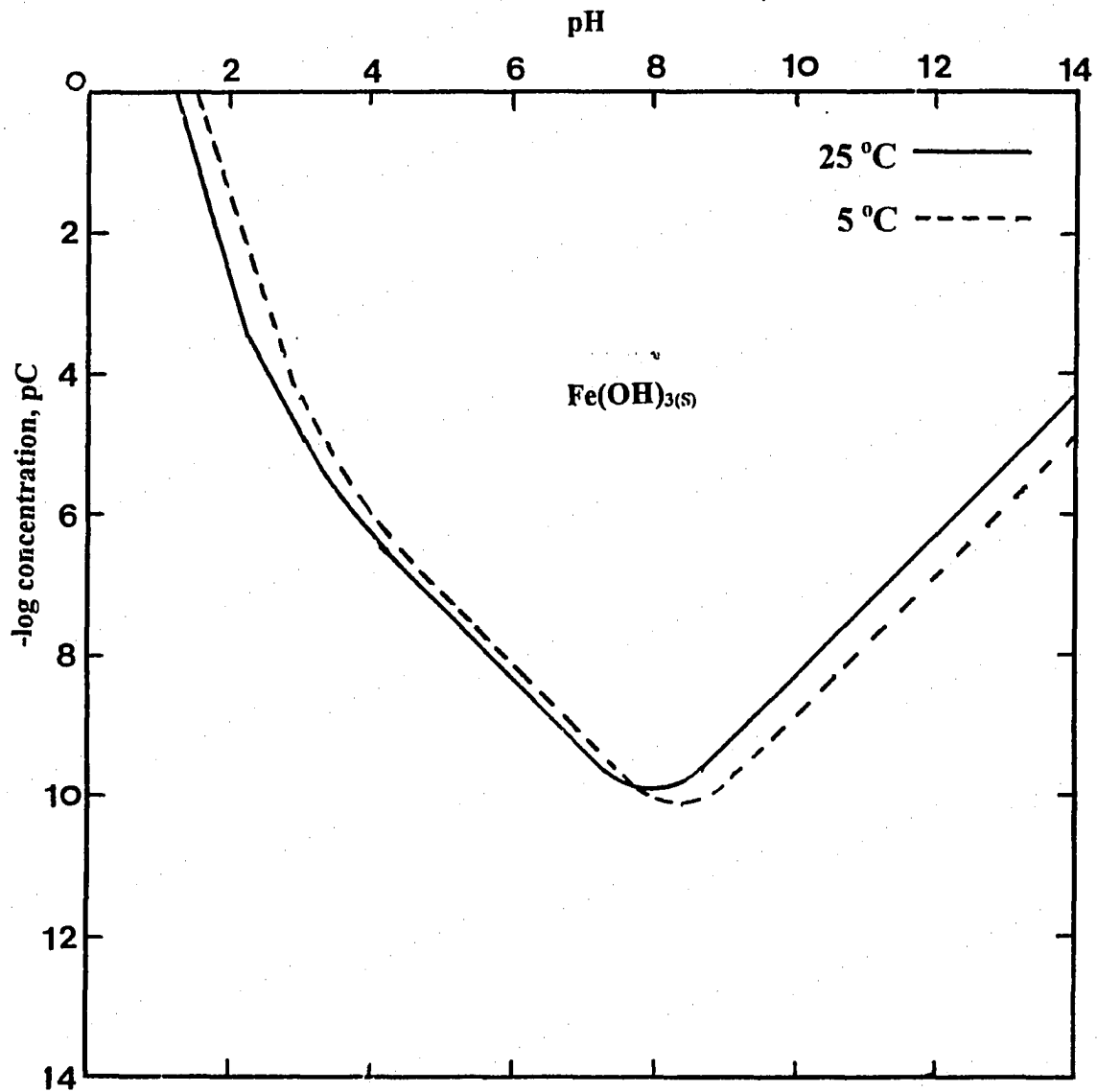
Figure 3.19.   Equilibrium concentrations of hydrolyzed iron(III) complexes in a solution
in contact with freshly precipitated $Fe(OH)_{3(s)}$ at 25 and 5 °C using both
reported and calculated values for the hydrolysis constants

Constructing a solubility diagram of the ferric hydroxide in solution at different temperatures using the equilibrium equations in Table 3.6 requires the corresponding changes in solution pH with temperature. That is, the pH of a aqueous solution changes with temperature through changes in the ion product of water, K_w. This change can also be calculated for various systems employing the van't Hoff equation, Eq (3.26). Since the ion product of water, K_w, changes with temperature, the pH of neutrality also changes with temperature. The pK_w values calculated at 5 °C and 25 °C for pure water give 14.73 and 14.0, respectively. Then, the calculated change in pH from 5 °C to 25 °C with constant pOH is 0.73 unit. Otherwise, simply, the change in pH with temperature to maintain constant pOH may be determined from the temperature dependence of the dissociation constant for water, K_w which is given by,

$$\log K_w = -4470.99/T + 6.0875 - 0.01706\ T \qquad (3.27)$$

where T is the absolute temperature in Kelvin (Stumm and Morgan, 1981).

As depicted in Figure 3.19, the effect of temperature on the $Fe(OH)_{3(s)}$ solubility is distinguishable. Overall, the 20 °C temperature decrease from 25 to 5 °C results in lowering the boundary of the equilibrium $Fe(OH)_{3(S)}$ solubility by 0.2 log unit and shifting it about 0.4 pH unit to the alkaline side. However, the shift in the solubility boundary gives a different effect of temperature on ferric hydroxide solubility at different pH ranges. For example, at the pH range below the pH of minimum solubility at 25 °C (≤ 8.0), the solubility of $Fe(OH)_{3(S)}$ increases with decreasing temperature. Conversely, in alkaline side above pH 8.0, the solubility decreases with decreasing temperature. Therefore, precaution should be taken when

interpreting the changes in K_{so} with temperature. That is, as shown in Table 3.6, even the calculated K_{so} values decreases at lower temperature, the solubility of $Fe(OH)_{3(S)}$ decreases mostly in acidic solution ($\leq$ pH 8.0).

Also, to illustrate changes in the concentration and speciation of Al with variation in temperature, Driscoll and Letterman (1988) showed the simulation of Al concentration in equilibrium with amorphous $Al(OH)_3$ at 5 °C and 25 °C (Figure 3.20). As shown in Figure 3.20, variation in temperature produced marked changes in concentration and speciation of Al. The solubility of Al is increased at low temperature below the pH of minimum solubility. Driscoll and Letterman (1988) observed that the formation of amorphous $Al(OH)_3$ decreases at lower temperature in the acidic pH range, since the solubility of Al^{3+} from the dissolution of amorphous $Al(OH)_3$ increases with decreasing temperature.

Using reported enthalpic data and equilibrium constants for the monomeric hydrolysis species of aluminum, Dempsey (1987) also showed the theoretical solubility curve of $Al(OH)_{3(s)}$ shifting 0.6 to 0.8 pH units to alkaline side and lowering about 5 times of soluble aluminum concentrations with the temperature changes from 25 to 1 °C (Figure 3.21). Based on Figure 3.21, he stated:

> There is greater expected supersaturation with respect to $Al(OH)_{3(s)}$ for pH > 7
> and as the temperature decreases. If applying the concepts of nucleation and
> crystal growth theory, alum forms smaller flocs under these conditions, a possible
> result of much faster formation of nuclei (p. 35).
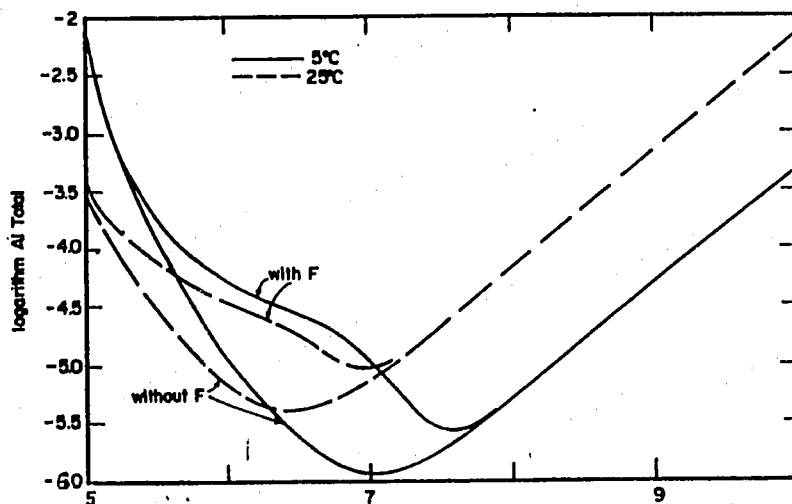
Figure 3.20.   Solubility of Al in equilibrium with amorphous Al(OH)$_3$ with and without 58 μmol/L F^{-1} at 5 and 25 °C (Driscoll and Letterman, 1988)
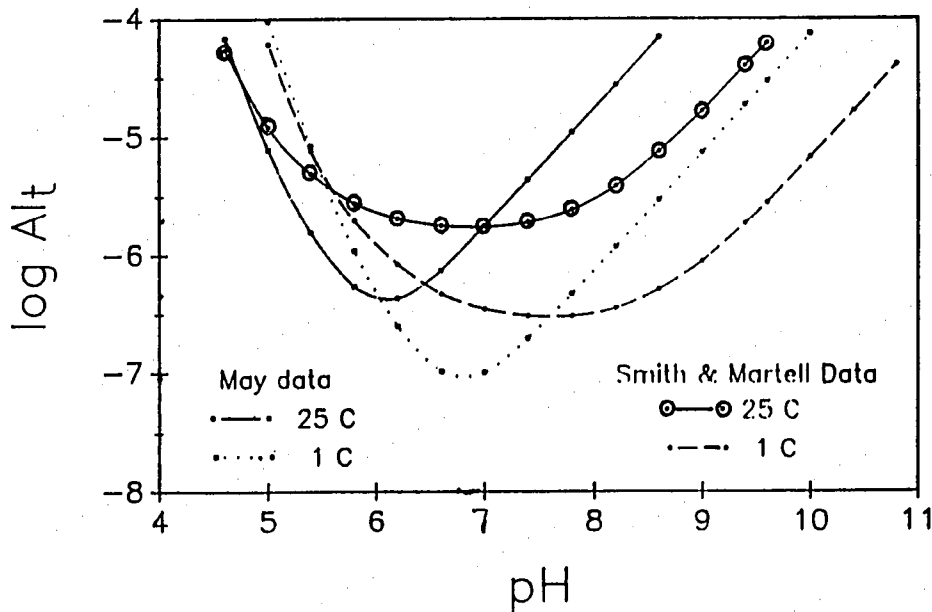
Figure 3.21.   Calculated monomeric Al vs. pH for two temperatures and using alternative reported values for hydrolysis constants (Dempsey, 1987)

In a recent study of aluminum hydrolysis reactions, Hem and Roberson (1990)

investigated hydrolysis and hydroxide polymerization reactions of aluminum using total Al

concentrations between 2×10^{-4} and 5×10^{-4} molar and holding pH ranges between 4.0 to 6.0.

The authors nicely described the changes in the equilibrium aluminum solubility as a function

of pH at several temperatures as shown in Figure 3.22. In Figure 3.22, the C_{Al_a} represents a

summation of the concentrations of monomeric Al species, such as Al^{3+}, $Al(OH)^{2+}$, $Al(OH)_2^{+}$,

and $Al(OH)_4^{-}$. As described in Fig 3.22, over the 30 °C range from 5 to 35 °C the solubility at

pH 4.00 changes by more than 2 log units, with the highest solubility at the lowest

temperature. The temperature effect is still nearly as great at pH 5.00 but is much less at pH

6.00. Another interesting feature indicated by this plot (but not fully evident) is the

displacement of the minimum solubility for each pH level to a lower pH as temperature

increases. These authors also found a strong temperature effect on the rate constants for the

aluminum hydrolysis reactions.

The strong effect of temperature on $Al(OH)_{3c}$ (gibbsite) solubility and aluminum solute

species was also noted by Apps and Neil (1990) who evaluated the solubility of gibbsite in

alkaline solutions between 20 and 350 °C. The authors investigated gibbsite solubility data and

calculated the stability constants (K_{s4}) for aluminate ion from gibbsite in alkaline solutions

using the following equation,

$$Al(OH)_3 + OH^- = Al(OH)_4^- \qquad K_{S4} = \frac{[Al(OH)_4^-]}{[Al(OH)_3][OH^-]} \qquad (3.28)$$
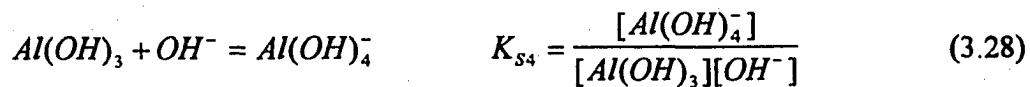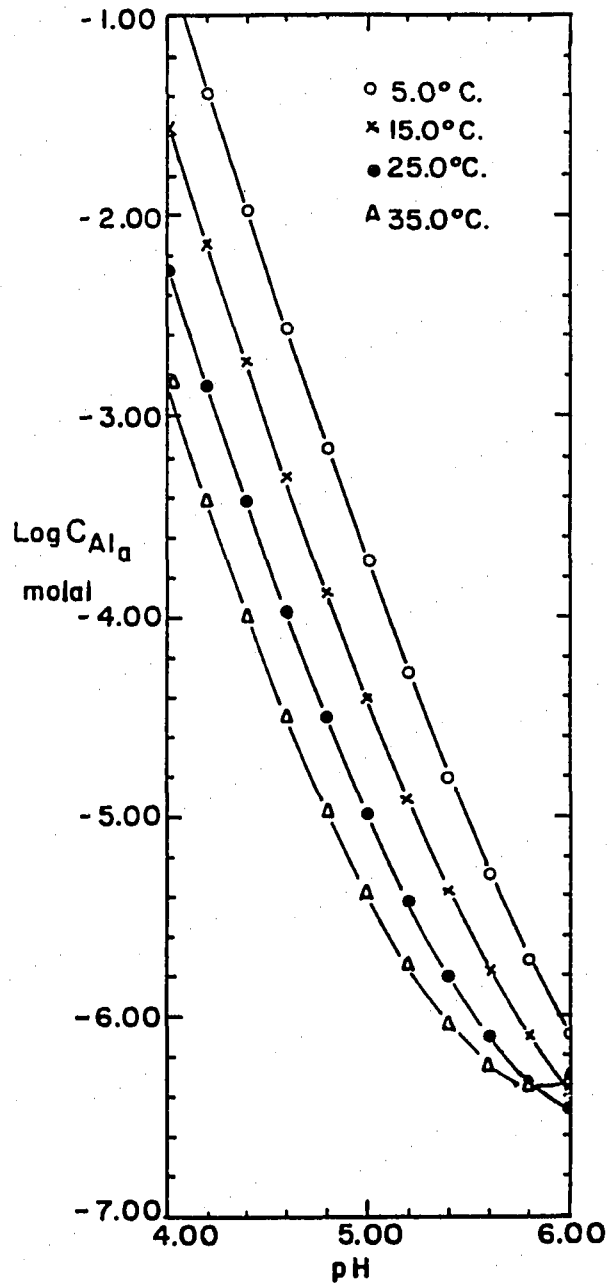
Figure 3.22. Equilibrium solubility of microcrystalline gibbsite at four different temperatures and 1 atm pressure. Ionic strength 0.010 (Hem and Roberson, 1990)

The resulting K_{S4} values together with the data collected from references for gibbsite are plotted against the reciprocal of absolute temperature in Figure 3.23. As shown in Figure 3.23, log K_{S4} values for aluminum hydroxide increases with increasing temperature. For instance, the solubility of aluminum hydroxide at 25 °C (log K_{S4} = -1.28) is about a factor of 2 greater than the value for 5 °C (log K_{S4} = -1.60). The authors also observed that the rate of approach to the equilibration concentration of aluminum hydroxide with the aqueous phase is greatly accelerated in strongly alkaline solutions and with increasing temperature.

Water temperature may also have an effect on the distribution of the hydrolysis species of Fe(III) by altering the rate and extent of reactions involved. For example, Flynn (1984) noted that at elevated temperatures, the rate of hydrolysis of Fe(III) salts was increased and the life time of the Fe(III) polymers decreased. van der Woude and de Bruyn (1983) also studied the kinetics of precipitation of a ferric hydroxide phase from supersaturated acidic Fe(III) solutions and found that the reaction rate increases with temperature, and the length of the formation time of polymeric species is seen to decrease rapidly with increasing pH and temperature. Work by Hem and Roberson (1990) that included kinetics of the formation of polymeric Al species indicated that the rate constant for the polymeric species formation increases in 1.0 log unit with a change in 20 °C from 10 to 35 °C.

As discussed thus far, at cold water temperature, it is reasonable to assume that the hydrolysis reactions are much slower than at moderate temperature. Accordingly, this change in the rate of the hydrolysis reactions will result in the changes in solution species distribution with temperature, and hence, this will influence the type of Fe(III) species adsorbed on
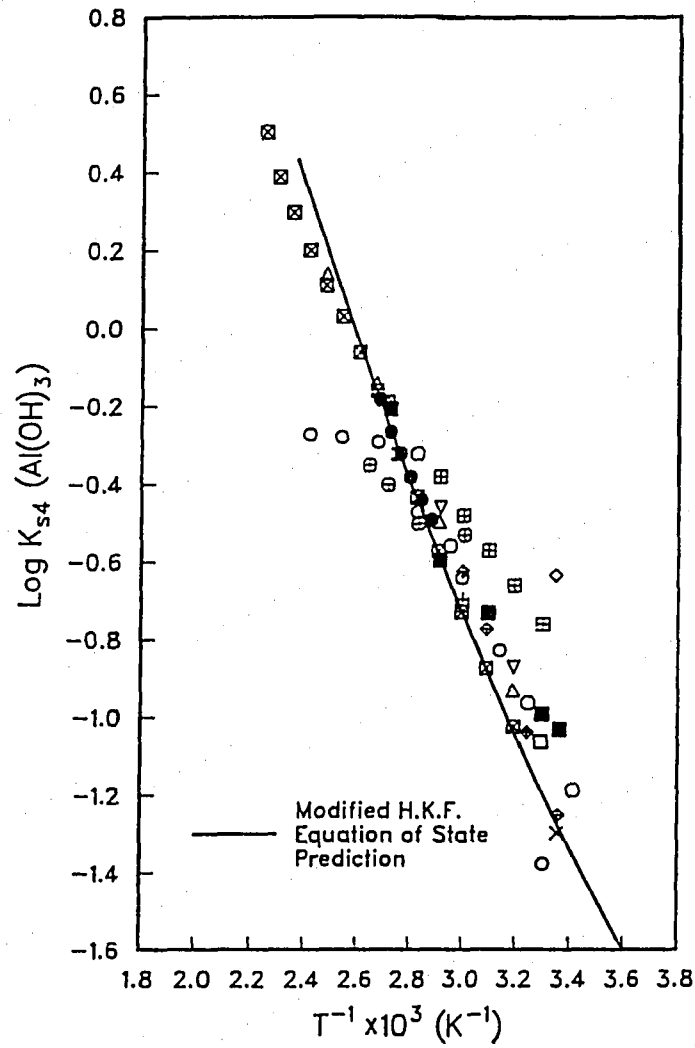
Figure 3.23. Plot of log K_{s4}, $Al(OH)_4^-$ versus the reciprocal of absolute temperature, in which solubility measurements attributed to gibbsite are compared (Apps and Neil, 1990)

particle surfaces because the amounts adsorbed depend on the predominant form of a species present.

Machesky (1990) investigated the effect of temperature on ion adsorption by hydrous metal oxide, such as α-Fe_2O_3 and γ-Al_2O_3 using adsorption enthalpy data and standard thermodynamic relationships. The author reached the following generalizations which were derived from the comparative studies at several temperatures. First, the zero point of charge (pH_{ZPC}) of hydrous metal oxides increases as temperature decreases and vise-versa. For example, as temperature decreases from 20 °C to 5 °C, the pH_{ZPC} of α-Fe_2O_3 increases from 8.60 to 9.50. The author reasoned for the cause of the shift in the pH_{ZPC} that equilibria between solution forms of an absorbing ion are temperature dependent and then the adsorbed to solution phase ratios of cations and anions will vary with temperature. It should be noted that the temperature dependence of pH_{ZPC} of hydrous oxide will alter the pH range of positive and negative surface charge with varying temperatures. Second, specific adsorption of anions appears to increase and metal cation adsorption to decrease with decreasing temperature.

Even though the effects of temperature appear to be clear in the changes of chemical characteristics of metal salt coagulant, it is uncertain how much the rate of hydrolysis-precipitation reaction or adsorption of the hydrolysis species on particle surfaces at cold temperature will affect the degree of flocculation. If we consider the time scales of the formation of aluminum hydrolysis species presented previously in Table 3.3, the hydrolysis steps are completed within a second or a few second at most, whereas, floc growth is a rather slow process taking many minutes. Thus, it may be hypothesized that the changes of chemistry

in Fe(III) coagulant due to cold temperature may have little affect the kinetics of flocculation

or affect only the early stage of coagulation. Similarly, from a study of chemical effects on

coagulation, Hahn and Stumm (1968) suggested:

> The coagulation rate is given by the product of the collision frequency as determined
> by conditions of particle transport and the collision efficiency factor as affected by
> hydrolysis and specific adsorption of coagulant. The effect of chemical parameters on
> the transport step, owing to concentration changes which cause slight alteration in the
> viscosity of the suspending medium, are negligible. In a similar way, the influence of
> the temperature upon the rate of hydrolysis and polymerization of aluminum has no
> effect upon the collision efficiency as long as the rate of destabilization is much larger
> than the rate of transport (p. 92).

Now, keeping in mind the general physical, chemical, and physico-chemical effects on

flocculation with varying temperature, The following pages go over the published studies on

the effects of temperature on flocculation.

In a study of the various aspects of mixing in the flocculation of Lake Michigan waters

with turbidities in the range of 12 to 20 JTU, Leipold (1934) used an alum dose of 17 mg/L at

pH 8 over a temperature range 2 - 24 °C. Leipold concluded that alum floc formation was not

prevented or retarded by cold temperature in 30 minutes of mixing. In contrast with the result

of Leipold's work, Velz (1934) noted that flocculation efficiency was affected noticeably with

colder temperatures. In his experiment, he used the coagulant range from 10.9 to 49 mg/L of

alum to coagulate a natural water containing 34 to 38 ppm color at pH range from 5 to 7.

Velz found that if the pH was held constant, lower alum dosage was required at cold

temperature for good color removal. However, if the dose was held constant and the pH was adjusted (i.e., 0.9 pH unit increase with 11.5 °C temperature drop) for optimal color removal, the effect of temperature on color removal efficiency disappeared.

In a well-controlled laboratory tests using ferric sulfate applied to particle free distilled water over a temperature range 1.0 to 28.3°C, Camp et al.(1940) drew the following conclusions:

- Changes in temperature have no measurable effect upon the time of formation of floc, if coagulation takes place at the optimum pH value,

- The optimum pH value is shifted by changes in temperature and the amount of coagulant used, and the influence of temperature is greatest for the smaller coagulant doses.

In addition, Camp and his co-workers also observed some very interesting results. First, they reported that difficulties in maintaining optimum turbidity removals throughout the winter months were due primarily to a decreased settling rate caused by an increase in the viscosity of water. Second, if the mixing velocity is high enough to mask the effect of convection currents and produce a stable flow pattern, the speed of coagulation was independent of the temperature.

Matijevic and Janauer (1966) also studied the effects of temperature on the coagulation of silver bromide sol and the reversal of charge of silver bromide and polystyrene latex by using ferric nitrate. Coagulation effectiveness was evaluated by comparing the turbidity after addition of coagulant. The turbidity was measured at 546 nm of light wavelength during the 10 minutes of flocculation time to check particle growth. Within their

Fe(NO$_3$)$_3$-pH domain of coagulation over the temperature range of 3 - 25°C, it was shown

that the critical coagulant concentration (i.e., the lowest dosage resulting in the onset of

flocculation) was about 3 to 5 times less at 3°C than at 25°C over pH range from 4 to 7. The

authors concluded that the temperature effects reflect the variation in the composition of the

coagulant solution rather than a change in the coagulation or the reversal of charge process.

Maulding and Harris (1967) conducted jar tests to observe the effect of temperature

on the coagulation of color-causing organic compounds using ferric sulfate as a coagulant.

Tests were performed using naturally colored water(405 C.U.) at pH range 3.0 - 4.4 for the

temperature range 3 - 42 °C employing 85.5 ppm of ferric sulfate. They found that the best pH

for optimum color removal was shifted to higher pH at lower temperatures. Their result

indicates an optimum pH shift of 0.8 pH units over 40 °C difference. They noted that although

some change in the pH of optimum coagulation is due to the change of pH with temperature,

some other factors also must be considered. They observed that one such fact may be a

change in the distribution of iron hydrolysis products due to a change in the rate of hydrolysis.

An increase in optimum pH with decreasing temperature was also noted by Mohtadi

and Rao (1973). They used either 20 to 50 mg/L of alum or 0.1 to 1.25 ppm of cationic

polyelectrolyte to flocculate 200 mg/L of bentonite or 450 mg/L of kaolinite clay at pH 4 to 9.

Although the zeta potentials of both bentonite and kaolinite coagulated with alum at a given

dose and constant pH did not change with temperature variation from 1 - 25 °C, higher

coagulant dosage was required to achieve the same degree of residual turbidity when

temperature was lowered at constant pH. However, they noted that reduction in temperature

does not necessarily mean an increase in the required coagulant dosage, provided that the pH

of the dispersion is maintained at the optimum value. In their study, optimum pH was shifted

1.5 pH units lower with changing temperature from 1 to 20 °C. In contrast, when using

cationic polymer, the authors found that temperature had no significant effect on the optimum

pH, the coagulant dosage, or the rate of flocculation. The different result observed between

alum and cationic polyelectrolyte may illustrate that the changes of hydrolysis of alum due to

varying temperature cause the primary impact on the flocculation efficiency.

The prior conclusions of the several investigators, who found a higher optimum pH at

lower temperatures, agree well with the findings and conclusions made by Hanson and

Cleasby (1990) and van Benchoten and Edzwald (1990a). The authors indroduced the idea of

using a constant pOH to correct system chemistry for temperature effects. The use of constant

pOH is, in effect, maintaining hydroxyl ion concentration constant as temperature changes.

The coagulation study by Hanson and Cleasby (1990) utilized 5 mg/L of alum or 4

mg/L of ferric sulfate to flocculate 25 mg/L of kaolinite clay at temperatures of 5 and 20 °C.

The pH at 20 °C was 5.5 for the ferric sulfate experiments, and 6.8 for alum experiments.

Both were selected to be in the range of the A/D coagulation mechanism. The flocculation

efficiency was measured by the removal of primary particles. They observed that with ferric

sulfate as a coagulant, the flocculation results at 20 and 5 °C were nearly identical when pOH

was held constant. However, flocculation efficiency was markedly decreased at the cold

temperature when the pH was held constant. With alum as a coagulant, the authors noted that

flocculation at 5 °C with constant pOH also yielded better efficiency than constant pH

conditions (see Fig 3.24 and 3.25), even though flocculation performance at low temperature was poorer than of ferric sulfate.

van Benschoten and Edzwald (1990a) examined hydrolysis reaction of alum using a dosage of 13.5 mg/L as Al applied to particle-free deionized water at 25 and 4 °C. The tests were conducted in jars with experimental conditions of rapid mixing at 100 rpm and 30 minutes of slow mixing at 20 rpm, followed by 1 hr of settling. Using the data collected from the measurements of turbidity, electrophoretic mobiiity, and Al solubility, they observed a two-fold effect of low temperature as shown in Figure 3.26. First, the pH at which Al precipitate occurs was increased from 4.6 to 5.5, which was illustrated by the shift of peak in turbidity and decrease in the concentration of dissolved aluminum. The second effect was that Al precipitates at 4 °C appeared to maintain a positive charge at higher pH than at 25 °C, which was shown by the shift of the isoelectric point of Al precipitates from pH 7 at 25 °C to pH 9 at 4 °C. The authors noted that some of adverse effect due to cold temperatures may be offset by an increase in the coagulation pH, by using pOH as the independent variable rather than pH. In another study of coagulation of fulvic acid using alum, van Benschoten and Edzwald (1990b) reported similar findings for the temperature effects and concluded that the aluminum hydrolysis and solubility are affected by temperature, primarily through changes in the ion product of water.

In a study of the precipitation kinetics of alum at pH 6, 7, and 8, and of ferric chloride at pH 8 over temperature range 3.6 to 28.3 °C, Morris and Knocke (1984) determined that low temperature condition did not significantly inhibit the aluminum or iron(III) precipitation
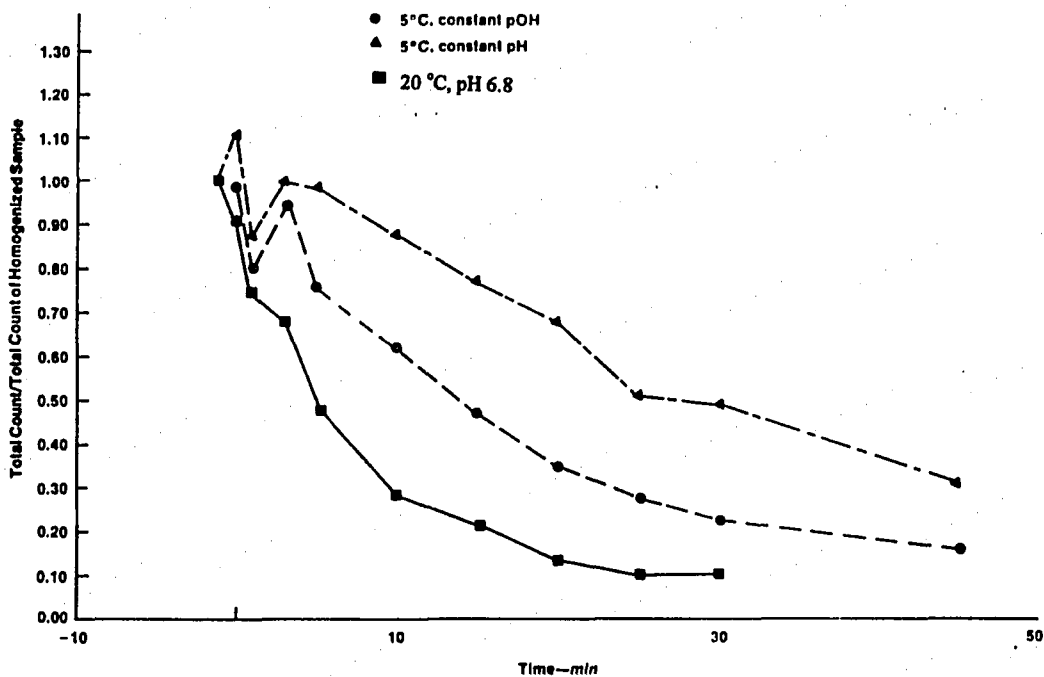
Figure 3.24. Effect of system chemistry on alum flocculation under high-energy conditions (G = 60 sec^{-1}, constant ε) (Hanson and Cleasby, 1990)
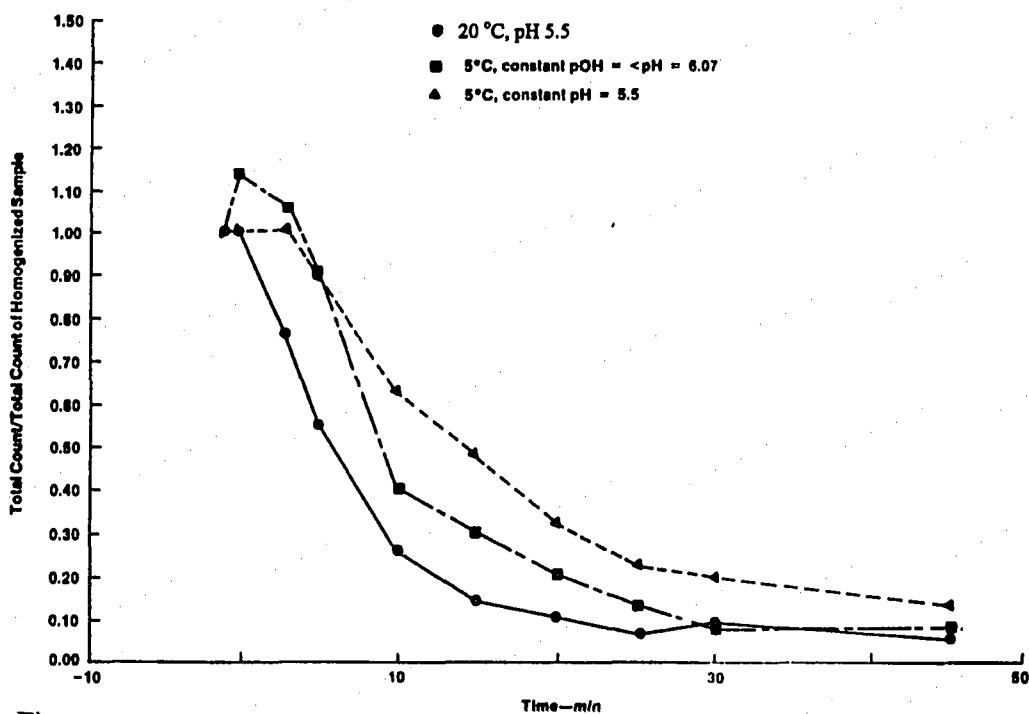
Figure 3.25. Effect of system chemistry with ferric sulfate under high-energy conditions (G = 60 sec^{-1}, constant ε) (Hanson and Cleasby, 1990)

92

Turbidity (NTU)

8
6
4
2
0

ALUM   ● T = 4°C
        o T = 25°C

3   4   5   6   7   8   9   10
pH

EPM (μm/s/V/cm)

2
1
0
-1
-2

3   4   5   6   7   8   9   10
pH

Al (mg/L)

15
10
5
0

3   4   5   6   7   8   9   10   11
pH
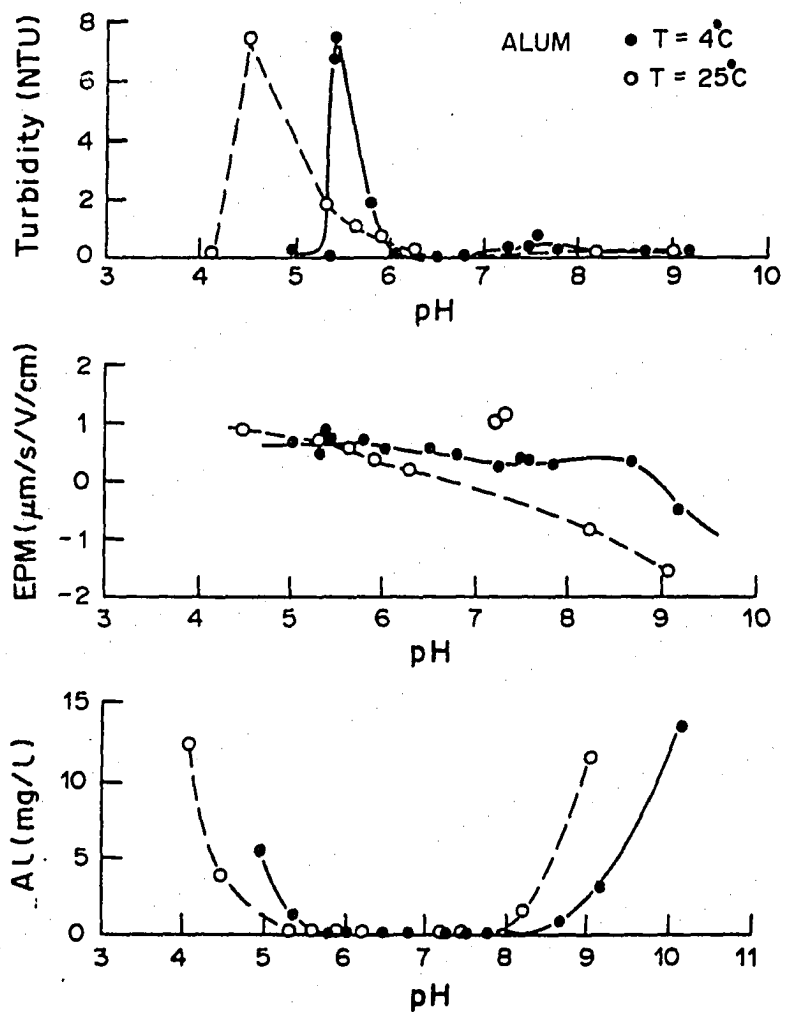
Figure 3.26.   Experimental results for alum (5 X 10^{-4} M Al) in deionized water at two temperatures (van Benchoten and Edzwald, 1990a)

rate, and that the impact of low temperature on turbidity removal efficiency was not related to reduced metal hydroxide precipitation rates. In contrast, they observed treatment plant failures at temperatures below 4 °C. Treatment failure was characterized by increased finished water turbidity and by decreased consumption of alkalinity by alum, indicating less efficiency of the alum reactions. However, they noted that the use of ferric sulfate as the primary coagulant at cold water temperature improved turbidity removal and increased alkalinity destruction to values near the theoretical prediction.

In addition, under controlled jar tests with kaolinite suspensions having an initial turbidity of 10 NTU, Morris and Knocke (1984) demonstrated that turbidity removals were diminished at low temperature for alum and ferric chloride. Particle size distribution data obtained with a HIAC particle counter indicated that for the same coagulant dosage, cold-temperature conditions produce smaller flocs than do 20 °C conditions. They also noted that ferric chloride was a much more effective coagulant at low temperatures than was alum, owing to the formation of large flocs that settled more efficiently. One of the conclusions formulated by the investigators is that decreased turbidity removal efficiency under low-temperature conditions could be related to fundamental changes in floc characteristics. Similarly, Hutchison and Foley (1974) found that water temperature below 3.3 °C led to slowly forming flocs that required flocculation times longer than 10 min in direct filtration; whereas under normal temperature conditions the flocculation times shorter than 10 min were acceptable for direct filtration.

In a later study, Knocke et al. (1986) again observed good treatment of natural organic matters with a Fe(III) coagulant in comparison with alum under low-temperature conditions, particularly under higher dosage conditions. The authors ascribed the better performance of Fe(III) coagulant to the faster rate of precipitation with Fe(III). Similarly, Leprince et al.(1984) found that a polymeric iron chloride (PICl), which was made by partially neutralizing ferric chloride before use, was much more effective than ferric chloride for turbidity removal at low temperature, but the improvement achieved by the use of PICl tended to disappear as the temperature increases. They reasoned that at low temperature, the hydrolysis reactions are much slower than at moderate temperatures.Therefore, the use of PICl instead of $FeCl_3$ allows the hydrolysis reactions to be bypassed.

A similar observation was made by Haarhoff and Cleasby (1988) who studied the use of alum and ferric chloride to treat 3 °C water containing a turbidity of less than 2 NTU. They noted that the flocs formed at lower temperatures were weaker than those formed at higher temperature, and the ferric chloride was more effective at removing turbidity than alum at a same molar dosage of Fe^{3+} or Al^{3+}. The differences of floc strength at two different temperatures (5 and 20 °C) for alum and ferric sulfate were also observed by Hanson and Cleasby (1990). They observed that both iron and alum flocs formed at 5 °C with kaolin clay, even with constant pOH, were much weaker than those at 20 °C.

The coagulation efficiencies of alum, ferric chloride, and polymeric metal coagulants in synthetic waters containing turbidity or natural organic material at pH 5.5 and 7.0 and at temperatures of 4 and 20 °C have been compared by O'Melia et al. 1989. For the low-turbidity

water (7.2 NTU) containing 1 mg/L of 0.198 μm latex particles, the required alum dosage at

pH 7.0 was lower at 4 °C than 20 °C, whereas at pH 5.5 it was slightly higher. In contrast, for

high-turbidity water (538 NTU) containing 100 mg/L of 0.198 μm latex particles, a

completely opposite result in alum dosage was observed. Thus, the required alum at pH 7.0

was higher at 4 °C than at 20 °C, whereas it was less at pH 5.5 and 4 °C than at 20 °C. When

using ferric chloride, although low temperature had an effect on coagulation as with alum, its

effect was quite minimal regardless of concentrations of humic material. O'Melia and co-

workers also suggested that slowing the hydrolysis and precipitation reactions of metal

coagulants in lower-temperature water is beneficial to some conditions, perhaps by permitting

hydrolysis species to react more extensively with turbidity and with humic substances. In

addition, the authors concluded that difficulties encountered in practice in treating waters at

cold temperatures may then be the result of physical limitations such as short-circuiting in

such processes as sedimentation or, in some cases, the result of changes in raw water quality.

In summary, system chemistry appears to be an important factor in the effect of

temperature on coagulation and flocculation. Probably, the increased viscosity at low

temperatures of water probably can cause some detriment to flocculation efficiency, resulting

from less homogeneous distribution of the coagulant. It has been found in literature that the

changes in solution temperature affect both the kinetics of formation and the equilibrium

distribution of the hydrolysis products of metal salt coagulant, and hence, the flocculation

efficiency. In general, since the hydrolysis and precipitation reactions of metal salt coagulant in

water are retarded at cold temperature, the retarded reactions may permit hydrolysis species

to react more extensively with particles before the precipitation reaction consumes the coagulant. That is, if a suspension requires an enhanced charge neutralizing capacity of metal salt coagulant, cold temperature may be beneficial; whereas, if a suspension requires higher interparticle collision efficiency with the help of voluminous precipitates, low temperature conditions would impair the kinetics of flocculation. This hypothesis can be supported by the observation by Morris and Knocke (1984) who noted that for the adsorption mechanism of coagulation, the effect of low-temperature conditions on alum coagulation was less severe. With the use of optimum chemistry such as the use of constant pOH or use of a Fe(III) salt coagulant instead of alum, the impact of cold temperature on the flocculation of turbidity and/or humic substances by metal coagulants could be eliminated, or at least diminished.

4. MATERIALS AND METHODS

The work was comprised of two main groups of experiments. In the first group, coagulation experiments were conducted in conventional jar tests using various concentrations of $Fe(NO_3)_3.9H_2O$ and pH ranges from 5 to 9 for the removal of turbidity. From the jar tests, optimal coagulation conditions, spanning the A/D and sweep floc coagulation mechanisms, were chosen and used throughout the subsequent flocculation kinetics studies. In the second group of experiments, the kinetics of flocculation was studied for systems of kaolin dispersions destabilized by ferric nitrate coagulant in an 18 liter batch reactor under tightly controlled treatment conditions.

The experimental setup used in flocculation kinetics studies is shown schematically in Figure 4.1. The kinetics of flocculation was monitored by using two-sophisticated systems. For the first method, a sample stream was withdrawn continuously during flocculation at a rate of 15 mL/min (5 cm/sec velocity) through a glass tube of 2.5 mm internal diameter by a peristaltic pump connected in series with an Photometric Dispersion Analyzer (PDA). The PDA monitors the fluctuations in the intensity of light beam transmitted through a flowing suspension. Using the PDA, the ratio value of the root mean square value of the fluctuating signal (V_{rms}) to the voltage corresponding to the mean transmitted light intensity (V) was found to increase substantially as particle aggregation occurs, and provided a sensitive measure of the extent of flocculation. This system is described in detail later in this section.
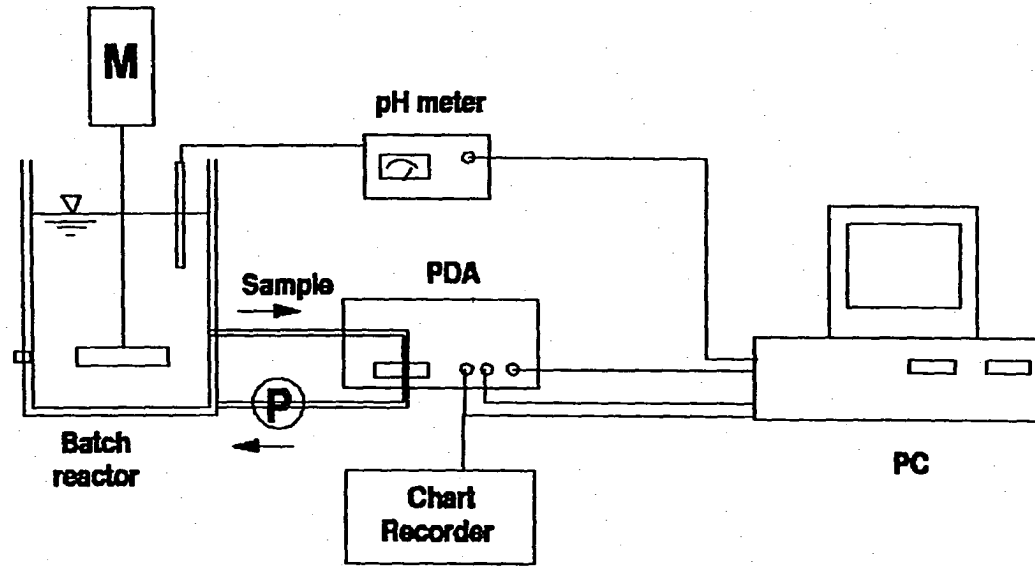
Figure 4.1. Schematic diagram of experimental setup

The glass tube was passed through a cell of the PDA and the flowing sample was monitored directly, before being returned to the flocculation reactor. The delay between the suspension leaving the reactor and entering the monitor was about two seconds.

The second method involved drawing 1 mL samples at several times during the progress of flocculation for analysis using an Automatic Image Analysis (AIA) system. The samples were withdrawn using a 1 mL syringe with a needle through a sampling port. The flocculation kinetics were quantified by measuring particle size distribution and the rate of disappearance of primary particles with mixing time during the flocculation process utilizing the AIA system. This system is also described in detail later in this section.

As shown in Figure 4.1, leads from the output socket on the PDA, the pH meter, and the thermocouple were connected to the analog card of the ACPC-16 Analog Connection personal computer based data acquisition/control system (Strawberry Tree Computers, Sunnyvale, CA). This data acquisition/control system controlled the temperature inside the constant temperature room by appropriately switching a refrigeration compressor on and off. The output signals from these instruments were installed in a personal computer after the analog to digital data conversion. The data acquisition/control system received and logged the data from the PDA, pH meter, and thermocouple at 5 sec intervals throughout each experiment. The ratio value (V_{rms}/V), among the available output signals from the PDA, was also monitored continuously on a chart recorder for on-line monitoring. All these systems were placed inside the constant temperature room for experiments at room temperature and 5 °C.

4.1 Material Preparation

4.1.1 Clay suspension

Turbid water was simulated with a suspension of kaolinite clay (Kentucky Ball Clay) in a water of controlled dissolved mineral content. The AIA system equipped with a microscope was used to count this clay sample. For a 25 mg/L of kaolin suspension, it consistently counted a mean of 8.9×10^6 particles per mL with standard deviation of 3.7×10^5 per mL. A primary particle size distribution for 25 mg/L of kaolinite suspension is illustrated graphically with Figure 4.2 being typical of the raw data collected from the AIA system. This clay suspension has a mean equivalent circular diameter equal to 1.8 μm. In this graph, the number of particles per mL of sample in each size class is plotted against the equivalent circular diameter of each size class. In general, particles smaller than 2.9 μm dominated the total number concentration for the particle size distribution of a homogenized sample. In other words, particles smaller than 2.9 μm contributed approximately 90% of the total particle number concentration.

The kaolin clay was dried overnight at 103 to 105 °C in a drying oven before use. The stock clay suspension was prepared at a concentration of 800 mg/L in distilled water in a 60 liter plastic tank equipped with a mixing device (Figure 4.3). The pH of the stock clay suspension was brought to pH 7.0 using the necessary amount of 0.1 N NaOH to avoid a possible aggregation of clay during storage in the tank. This large volume of stock clay suspension provided a reproducible means of adding the clay particles to the water. The clay
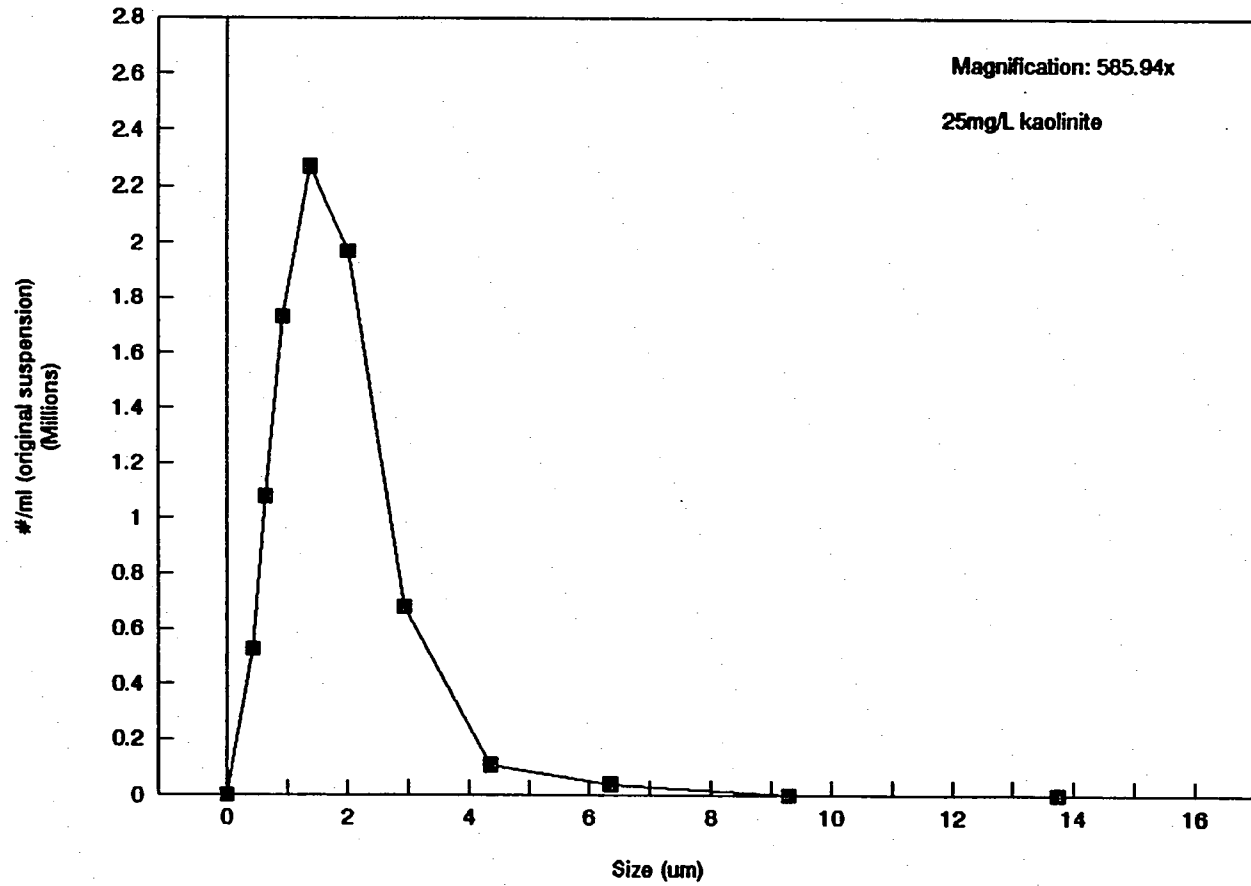
Figure 4.2.   Typical particle size distribution for 25 mg/L of clay primary particles
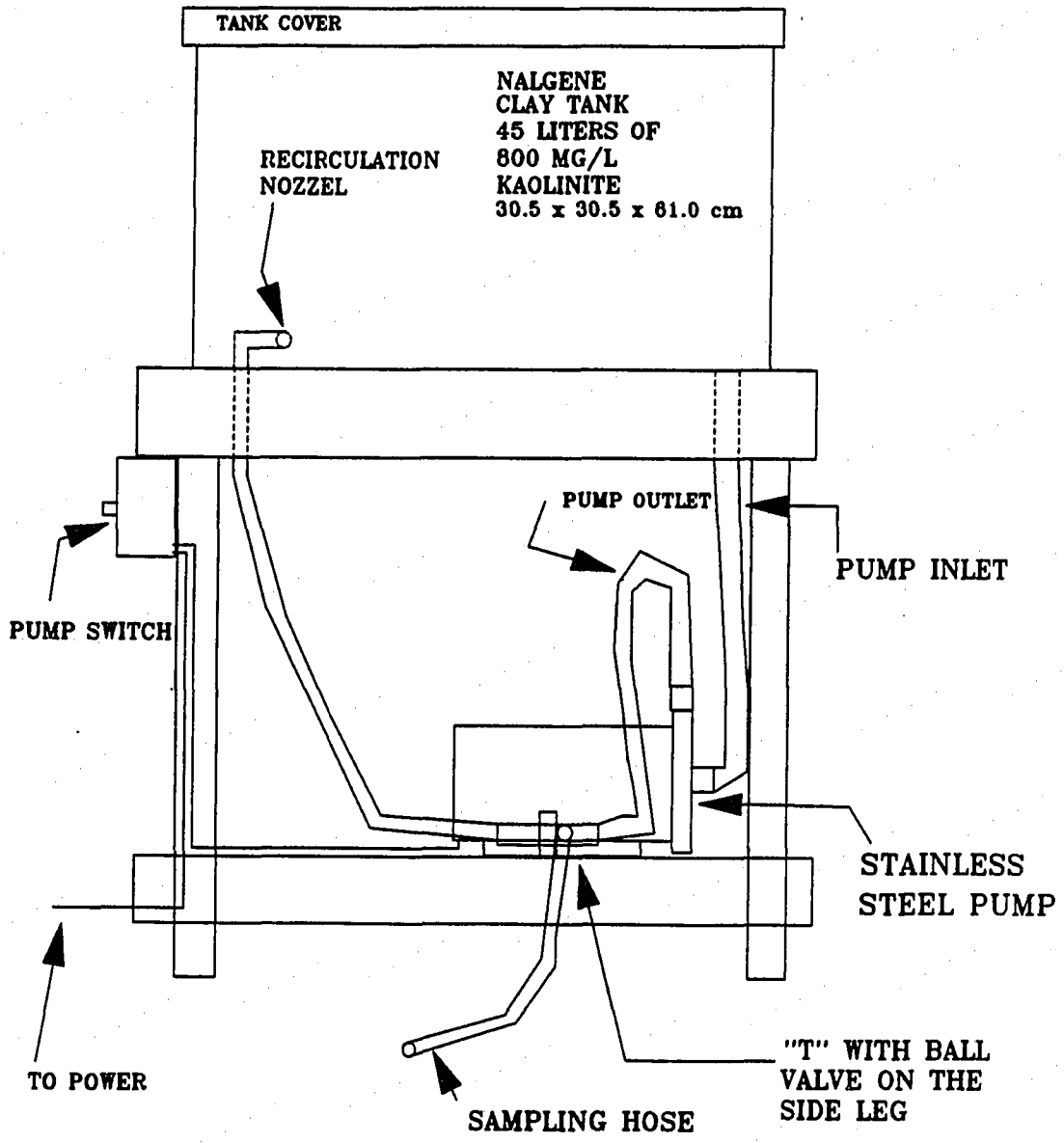
Figure 4.3.   Schematic of clay dispersion mixing system

suspension diluted from the stock clay suspension in this manner gave consistent turbidities, particle numbers, and ZP values during the course of experiments conducted. The following method was used to make stock clay suspension and to make a desired concentration of clay suspension sample:

- The plastic tank was rinsed thoroughly,
- Approximately 30 liters of distilled water was run into the tank,
- Stainless steel recirculation pump was turned on,
- 36 g of dry clay, which had been dried overnight at a 103 to 105 °C drying oven, was added slowly in the tank,
- The distilled water was brought up to the 45 liters mark,
- Continue mixing the suspension for an hour and maintain the pH of the clay suspension to 7.0 with 0.1 N NaOH,
- The sample hose was used to scour out the corners during mixing and insure that all of the settled clay was in suspension,
- The recirculation pump was turned off and let stand overnight,
- Before each experiment, the recirculation pump was turned on again for at least 30 minutes and the sample hose was often used to scour out the corners,
- An appropriate aliquot was withdrawn through the sample hose into a graduated cylinder after purging briefly to waste.

After using around 30 liters of stock clay suspension the remaining suspension was drained to waste in order to insure homogeneity of clay suspension throughout all experiments. By using this method of preparation, no aggregation of particles was observed during storage in the tank.

4.1.2 Dilution water

Distilled water was used to make a desired concentration of clay suspension using the stock clay solution for each experiment. The distilled water was stored in 300 liters polyethylene tank before use, while it was being brought to equilibrium with atmospheric CO_2 and temperature. For the experiments at 5 °C, the water was placed in 20 liters carboys, and then the carboys were placed in the 5 °C constant temperature storage room before use.

When diluting the clay suspension, a desired amount of 1 M $NaNO_3$ was added to achieve 0.005 M of $NaNO_3$, which gives 0.005 M ionic strength in the diluted suspension. The choice of 0.005 M $NaNO_3$ was based on the results obtained from preliminary tests. According to the result of preliminary tests, the changes in ionic strength between 10^{-3} to 10^{-2} M with the addition of $NaNO_3$ did not induce any aggregation of clay suspension and did not affect the ZP values of kaolin particles. Therefore, the medium ionic strength, 0.005 M was chosen to avoid any sign of aggregation of clay particles due to destabilization caused by double layer compression, and to facilitate consistent measurements of the ZP. The 1 M $NaNO_3$ stock solution was stored in a polythene container, because it had been observed that the prolonged storage of $NaNO_3$ solution in glassware prior to use caused the silicate from the glass container to be dissolved in the solution and shifted the isoelectric point of a substrate (Hunter, 1981).

4.1.3 Coagulant

Ferric nitrate was used as a coagulant to allow sulfate concentration to be controlled as an independent variable. The stock solution containing 0.25 M $Fe(NO_3)_3.9H_2O$ was stored at room temperature. The dosing solution of 10 mg/mL (2.48×10^{-2} M) as $Fe(NO_3)_3.9H_2O$ was prepared volumetrically from the stock solution the day before each experiment was to be conducted, and was stored at room temperature overnight to avoid coagulation differences due to a potential aging, and to ensure consistent speciation in the coagulant dosing solution. The pH of the stock and dosing solutions were checked periodically to check for potential aging of Fe(III) in the solution.

The conditions in all flocculation experiments were such that no iron hydroxide precipitated in the stock or dosing solution within the period of observation and reproducible coagulant species were obtained. The pH values of 0.25 M stock solution and 2.48×10^{-2} M (10 mg/mL) dosing solution were found to be always in the ranges 1.29 ± 0.01 and 2.05 ± 0.02, respectively. The pH values of ferric nitrate solutions are very important so that hydrolysis-precipitation of iron(III) does not occur during storing, e.g., precipitation was evident in the case of 1.0 mg/mL of dosing solution (pH 2.60) within 2 hours of storage at room temperature (23 ± 1 °C). At the end of each experiment the remaining dosing solution was discarded, and the volumetric flask used was rinsed with 0.1N HCl solution to remove any possible iron stuck on the glass, and then rinsed in distilled water again.

4.1.4 Other chemical solutions

Suspension pH was adjusted to the desired target pH by using 0.02 to 0.05 N NaOH

or 0.01 HNO$_3$ as necessary. A stock solution of 1 M Na$_2$SO$_4$ solution was used as a source of

sulfate for the study of sulfate ion effect.

4.2 Equipment and Methods

4.2.1 pH adjustment

The pH of the system was measured using a 12 mm diameter pH probe and a Fisher

Accumet no. 610 pH meter. The pH meter was standardized using a pH 7 buffer first, and

then a pH 4 buffer. For accuracy, the temperature of the buffer solutions and the samples was

maintained to be identical. The pH meter was checked at both the beginning and the end of

each experiment. A major interference problem was caused by the current of the mixing

motor. This interference was readily identified because as the motor rpm was increased above

around 100 rpm for both jar test and batch reactor experiments, the pH meter reading was

also increased with increasing motor speed. For the batch reactor experiments, this problem

was solved by connecting a non-metallic coupler and impeller shaft to the motor. However,

this interference problem was not solved for the Phipps and Bird jar test apparatus because

replacing of metal coupler and shaft was not possible. During the jar tests, therefore, pH

measurements were done at low motor rpm (around 50 rpm) after rapid mixing. The details of

pH adjustment during the experiments are presented in this Section titled Experimental

Procedures.

4.2.2 Batch reactor system

Flocculation tests were carried out in an 18 liter bench scale batch reactor identical to

that used by Argaman and Kaufman (1968) and Hanson (1989) in their studies on flocculation

kinetics. This permitted the use of their studies for physical characteristics of turbulence in the

reactor and direct comparison of experimental data. The reactor system consisted of a reactor,

an impeller, a motor and motor controller, and a tachometer. The features of the plexiglass

reactor are shown in Figure 4.4. The stirrer was a 1/4 inch diameter plexiglass shaft onto

which a flat (1/16 inch thick) stainless steel blade was mounted using a screw. When mounting

the shaft, the center line of the turbine blade should be positioned at the identical level with

the chemical injection port (sampling port). This stirrer was rotated, via plexiglass coupler, by

a electric motor and a speed controller (Master Servodyne motor and motor controller

manufactured by Cole-Parmer Instrument Company of Chicago, IL).

The motor was mounted on a wooden support which was rigidly attached to the top of

the reactor during experiments. Provisions were made for connecting a tachometer sensor to

the top of shaft on the motor so that the stirrer rotation speed could be measured. The

tachometer sensor was an encoder type and was connected to an Ametek Model 1736

tachometer. The wooden support for the motor also had holes for a pH probe and a

thermocouple. All of these systems were placed inside the constant temperature room.

108

PLAN VIEW

3" DIAMETER GLASS
VIEWING WINDOW

ELEVATION VIEW

All Dimensions are in inches.
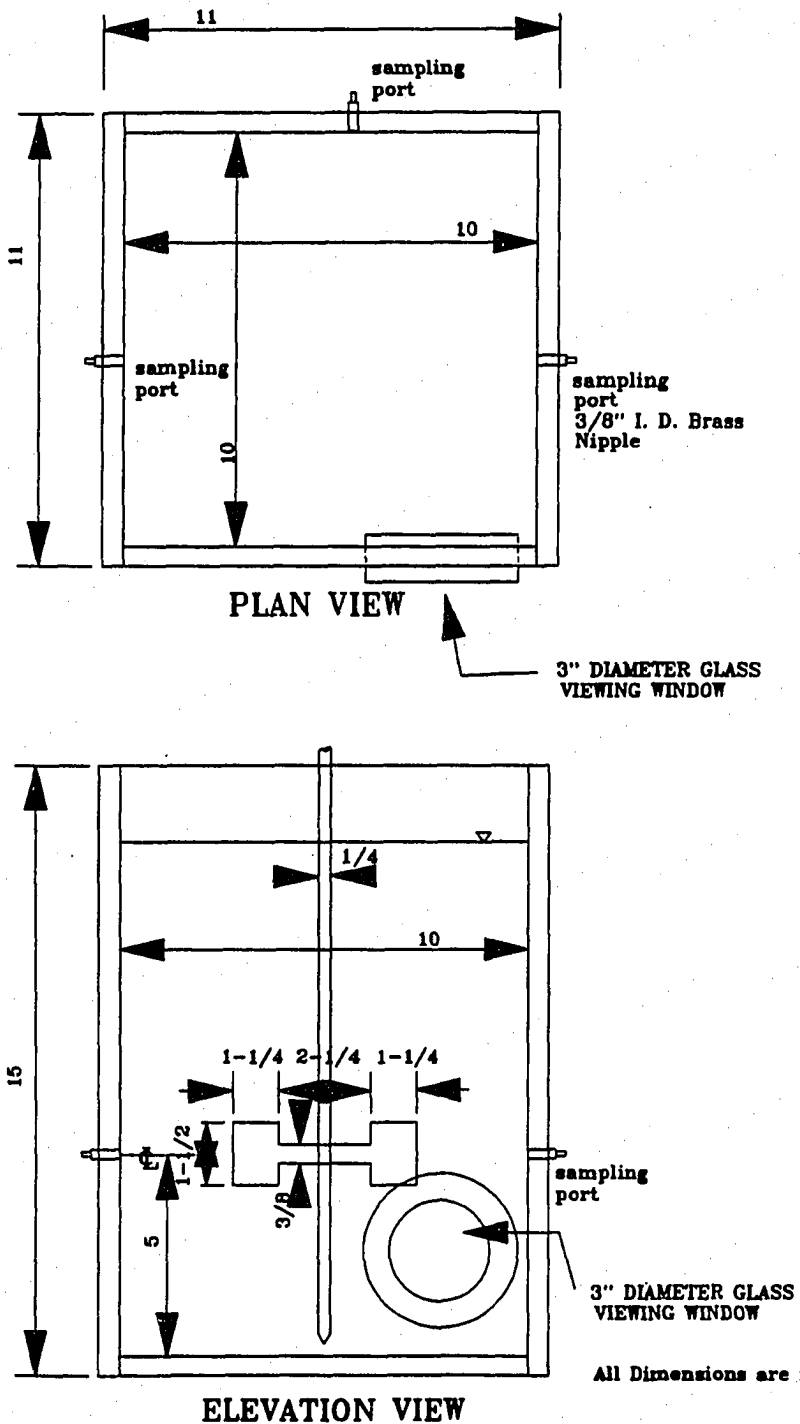
Figure 4.4.   Schematic of 18 liters batch reactor

The stirring power input to the reactor was determined experimentally by direct measure of the torque on the impeller shaft at various rotating speeds measured by the tachometer. Because of the wide range of torques measured for both slow and rapid mixing, two different torque meters, each with a different measuring range capability, were used (Bex-O-meter, Model 38 (0 to 5 and 0 to 50 oz-in) (The Bex Company, San Francisco, CA). The relation between power, torque, and rotational speed is given by

$$P = \tau.\omega \qquad (4\text{-}1)$$

$$= 2\pi.N.\tau \qquad (4\text{-}2)$$

where P is the power input, τ is the torque, and ω is the angular velocity of the rotating impeller (radians/sec) with rotating speed, N (revolutions/sec). Using the P value, a calibration curve showing the rotating speeds and the root-mean-square velocity gradients (G) for the 18 L reactor is given in Figure 4.5. From the curve, G was found to be related to the rotation speed by

$$G = 0.135 \, N^{1.471} \quad \text{(at 23 °C, with N in rev/min)} \qquad (4\text{-}3)$$

Hanson (1989) had shown previously that the power required was independent of temperature due to full turbulence in this 18 L reactor. Therefore, the impeller speed (rpm) was used as the operational control parameter to maintain constant power input,ε, but with a lower resulting G value at the lower temperature.
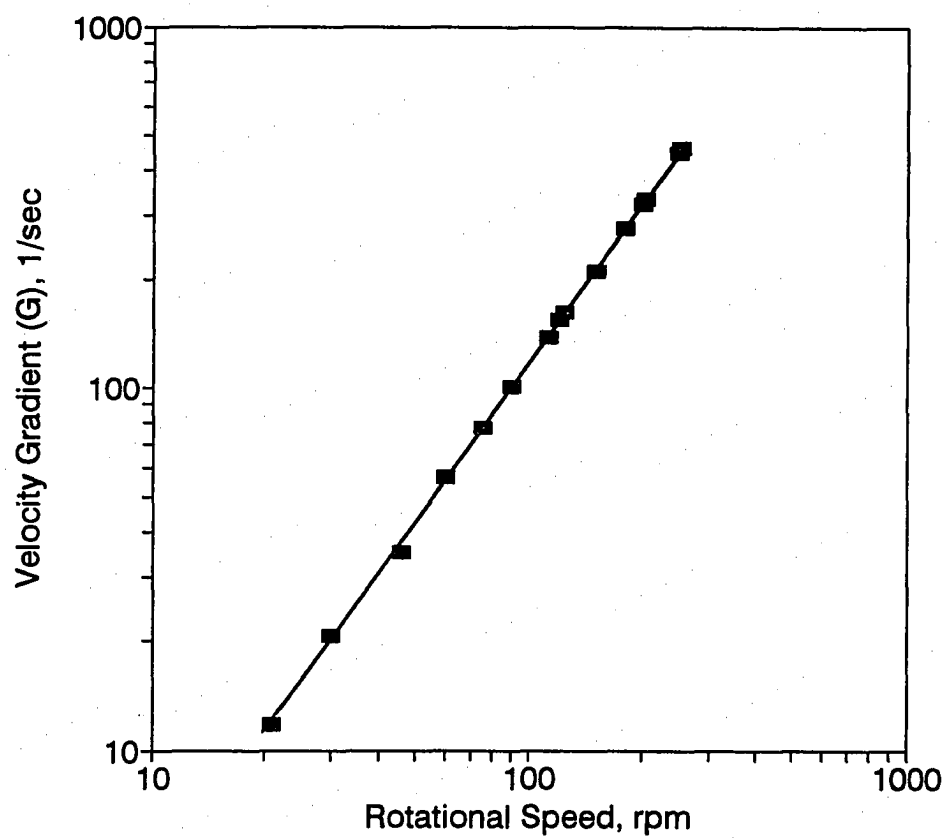
Figure 4.5.   Velocity gradient, G versus paddle rotating speed (18 L reactor at 23 °C)

4.2.3 Sample collection

The sampling port of the reactor consisted of a 3/8 inch brass hose fitting threaded into the wall of the reactor at the centerline of the turbine impeller blade. The port was fitted with a disposable septum. The samples from the flocculation work to be subjected to image analysis for particle size distribution were withdrawn from the reactor through a side port using a 1 mL disposable syringe. The syringe had a no.13 gauge Perfectum PS 13 Hospi-Luer 4 inch stainless steel hypodermic needle. The needle used to withdraw the samples had an inside diameter of 1.96 mm and a length of 8.96 cm. The sample collection was initiated 5 sec prior to sampling time, and a total of 20 sec was used to draw a 1 mL sample. Care was given not to cause floc rapture during withdrawal of the sample, which might be caused by flow in needle. A simple evaluation of the flow condition inside the needle was made from which the rms velocity gradient, G, was calculated inside the needle to be 48 sec^{-1}. Although it is well known that the breakup of floc may be caused by turbulent flow conditions or rapid change in velocity and the inertia of the floc particles (AWWA, 1991), it is impossible to predict with certainty whether the calculated G (48 sec^{-1}) caused the breakup of flocs inside needle during withdrawal of the sample. But the calculated G was comparable to the G values used in the turbulent reactor, and breakup during the laminar flow sample withdrawl is considered unlikely.

The samples withdrawn from the reactor were immediately placed in a specially constructed glass cells of the kind shown in Figure 4.6. Each sample cell was covered with 45 x 50 mm Number 1-1/2 (0.16-0.19 mm thick) Fisherbrand Microscope Cover Glass. During the placement of the slip cover, caution was taken not to scratch the cell surface and to avoid

depth d: 0.9 to 1.1

d

elevation view

thickness: 3

76.2

25.4

50.8

plan view
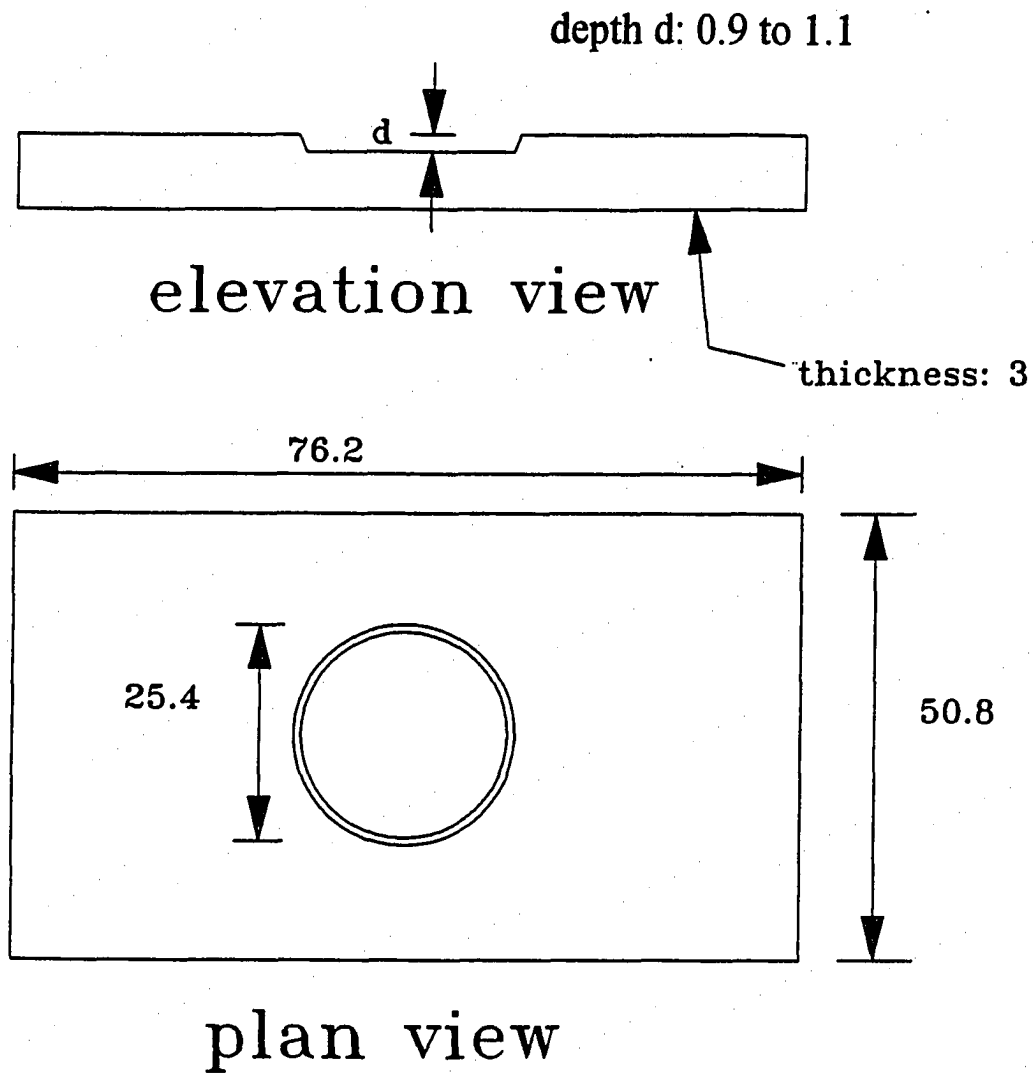
COUNTING CELL FOR
USE WITH AIA
ALL DIMENSIONS IN MM

Figure 4.6.   Schematic of the sample counting cell used with the AIA

air bubbles in the cell. Once the sample cell was loaded and covered it was allowed to sit overnight to make sure all the particles settled to the bottom of the cell which was the selected focal plane of the microscope used for the image analysis observations. The cell depth measurement was done by measuring the focal length difference between the top surface of cell (underside of the cover slip) and the bottom surface with the same microscope used in the image analysis observations.

After counting the particles the counting cells were rinsed, first with tap water, and then with high pressure water from the distilled water tap. After rinsing, the cells were placed in an ultrasonic bath containing cleaning solution and vibrated for 30 min. Once the cells had been washed in the ultrasonic bath, they were again rinsed with a high pressure jet of distilled water. After rinsing, the cells were dried with lint free paper towels.

4.2.4 Turbidity measurement

The turbidity of the sample was measured by a Hach Model 18900 Ratio Turbidimeter. For the 18 L reactor experiments, turbidity was measured on both the homogenized sample before coagulant addition and the rapid mixed sample immediately following rapid mixing to use as a quick and surrogate check of the kaolinite primary particle concentration. Supernatant turbidity was measured for the samples from the jar tests to check the effectiveness of the flocculation. Also, supernatant turbidity was measured for some selected 18 L reactors tests to relate it with the differences in flocculation kinetics. The turbidimeter was standardized according to the manufacturer's recommendations before every

test using "Gelex" secondary standards. It was also calibrated periodically against Formazin

Standards as part of the Environmental Engineering laboratory on-going QA/QC routine

operation.

4.2.5 Zeta potential

Zeta potential (ZP) measurements were used throughout this study in order to reveal

any significant differences in the electrokinetic properties of the primary particles and formed

flocs. A Model 102 Lazer Zee Meter, manufactured by Pen-Kem, Inc. of Croton-on-Hudson,

NY, was used to measure the ZP. The electronics in the zeta meter have been upgraded to

Model 104 electronics, but the optics were still original. ZPs were measured on both the

homogenized sample and the coagulated sample immediately following rapid mixing for both

jar test and batch reactor experiments.

The measurement techniques detailed in the manufacturers literature were followed

closely. Particularly, it is important to check the location of stationary layer in the ZP cell

before every measurement so that the ZP values can be reproducible throughout the

experiments. The checking of the stationary layer consisted of focusing at a fixed point inside

of the cell. In order to adjust the stationary layer, first set the fine focus of the microscope to

image on the inside of top surface of the cell using bubbles formed by breathing into the cell.

Record the setting of the fine focus adjustment. Next, turn the fine focus knob toward you,

raising the microscope stage, to add the calibration constant determined by the manufacturer

for each cell. This results in focusing at the stationary layer of the cell. The calibration of the

instrument was checked periodically using a standard colloid suspension purchased from Pen

Kem Inc. The ZP values measured on the standard colloid (-62.2±1.5 mV) and for the primary

kaolin particle in the distilled water with I=0.005M showed very consistent values throughout

the experiments (e.g., -31 ± 1 mV). A precaution was taken to avoid temperature increase in

samples during the measure of ZP for the samples taken at 5 °C. Before taking a sample into

the ZP cell, it was rinsed with cold distilled water to bring down the temperature of the cell.

4.3 Measuring Flocculation Kinetics

The studies of the flocculation kinetics require a method of assessing the state of

aggregation of suspension as a function of flocculation time. The process of flocculation can

be simply characterized as the growth of aggregates resulting in a decrease of primary particle

number. Therefore, the quantitative measure of change in aggregate sizes can be used to

assess the kinetics of flocculation or, alternatively, the decrease in number of primary particles

due to the growth of aggregates can be used to assess the kinetics of flocculation. In this

research, two methods were used to assess flocculation kinetics. One was the direct

quantitative measure of the changes in the particle size distribution by use of the Automatic

Image Analyzer (AIA) system (Lemont OASYS, Lemont Scientific Inc., Science Park, Pa).

The other was the rather indirect qualitative measurement using the Photometric Dispersion

Analyzer (PDA) in which the degree of turbidity fluctuation due to the continuous changes in

the number concentrations and sizes of particles can be obtained and related to the rate of flocculation.

4.3.1 Automatic Image Analysis System

In this study, particle size distributions were determined for some experiments using an automatic image analysis system, coupled directly to a research-quality Olympus BH-2S upright, transmitted light microscope (Olympus Corp., Lake Success, NY) via a video camera. The analyzed samples were used to evaluate the degree of particle flocculation for some of experiments conducted in the 18 L batch reactor. In studies of flocculation using the image analysis system, Hanson and Cleasby (1990) indicated that it is absolutely necessary to use a system capable of measuring primary particles if basic flocculation research is to be performed. They gave two main reason for this. First, the majority of flocculation models are written in terms of primary particle disappearance. Second, the primary function of flocculation is to remove particles from the 1 μm size range and place them into the 10+ μm size range. A schematic of the image analysis system is shown in Figure 4.7.

The image to be analyzed by the AIA is input to the system through a TV/video camera mounted on a microscope. After input, the digitized images can be mathematically manipulated to enhance desired aspects of the image by edition of the analyzed image using features of the AIA, such as small feature enhancement, dilation, and erosion. Once an object in the image can be extracted from the surrounding background, it can then be measured for

high resolution
graphics monitor

control
terminal

microscope
with video
camera

computer
system
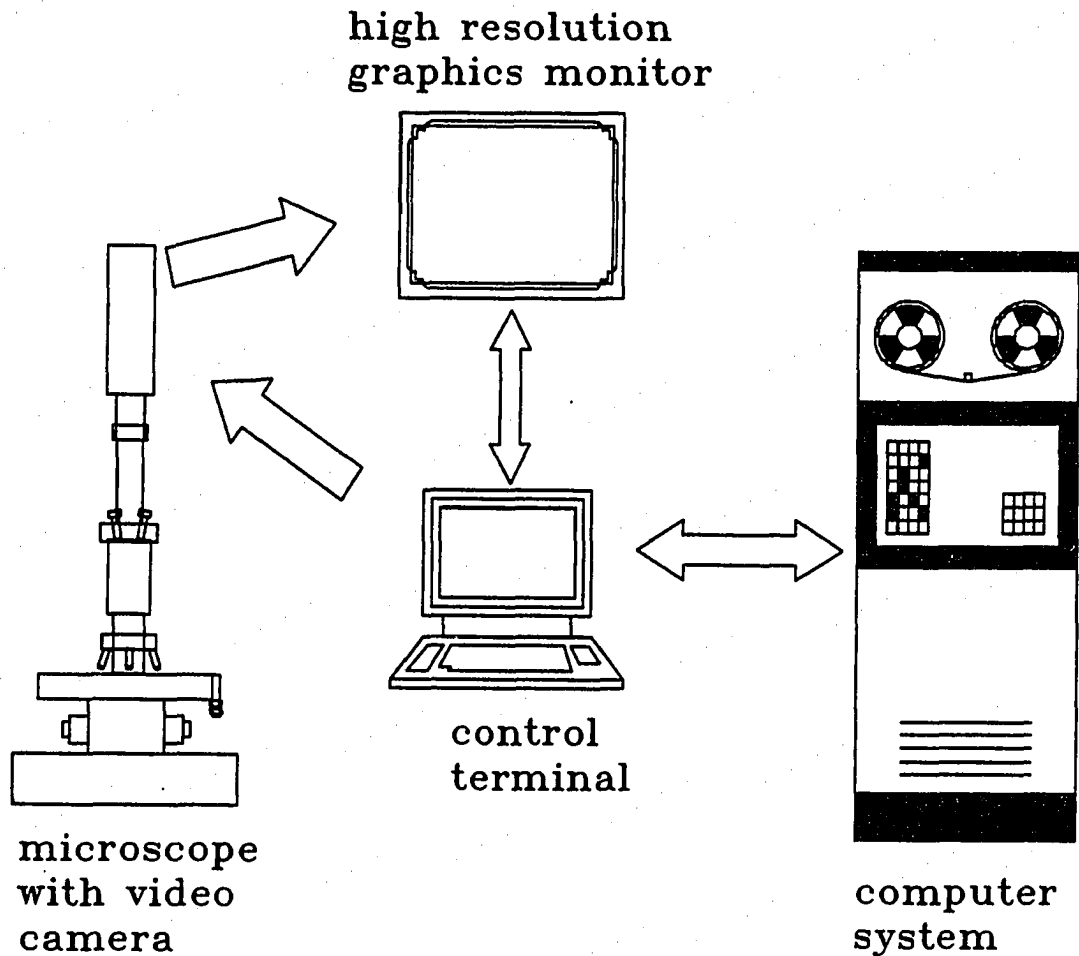
AUTOMATIC IMAGE ANALYSIS SYSTEM

Figure 4.7.   Schematic of Automatic Image Analysis system (AIA)

various types of parameters. These include geometric parameters (i.e., size, shape) and entire field parameters (i.e., reference area, total area, counts).

Although the AIA makes it very expedient to measure particle size distributions automatically, it does not completely eliminate the judgement of the operator in assigning a size for a particle. Therefore, the quality of optical image visible in the microscope is the important key to achieve good resolution, and thereby, to obtain reproducible data. The optical image can be varied depended on the optical system of the microscope. The pertinent optical system selected for reasonable technical resolution of the microscope was as follows:

- Dry dark field condenser : to produce a light microscope image with high contrast which is valuable for locating extremely small features in a microscope field
- Optic system magnification : high (546.87X) and low magnification (36.91X)
- Each optic magnification used : 20X and 5X objectives, 15X and 2.5X NFK lens (video eyepiece), 1.25X Normarski DIC intermediate tube, and 1.46+ X video lens inside video camera (this magnification can be changed by changing the location of the video lens inside video camera)

After appropriate focusing, brightness, and magnification have been determined, the optical image visible in the microscope was input to the AIA through the video camera for analysis. The AIA identifies and measures objects based on the contrast between the object and the background, which is represented by the level of gray in the field of view. There are 256 levels of gray, from black at level zero, to white at level 256, to be used according to the characteristics of object. Usually the background is dark gray, the object is light gray and

there is a transition zone of varying shades of gray at the object boundary, making the edges fuzzy. A distinct gray level of the actual object boundary should be selected and set before the AIA stores and digitizes the object image. After identifying the threshold gray level, the AIA starts to analyze the image. Automatic analysis of image features is provided by the programs in AIA. The AIA program algorithm measures image features by sequentially examining pixel data on a line by line basis where a feature consists of 512 x 480 individual dots (pixels).

Image processing used in this study consisted of four major steps, such as set level for analysis, image acquisition, edit displayed image, and frame analysis. Before the image processing, the magnification was calibrated for the microscope-AIA combination using a standard stage micrometer (Nikken 0.01 mm objective micrometer). The stage micrometer was placed under the optical microscope, and a pair of cursors in the monitor are placed on the micrometer scale at a known distance apart. The calculated magnification of the displayed image is determined by the AIA and then used by the AIA to analyze the image features.

The first step in image processing is to set levels for analysis. This option allows the operator to set upper and lower thresholds for gray level. When a feature of interest has the thresholds set properly, the AIA can correctly identify, count, and size the feature. The set level for kaolinite particles used in this study was low level 88 and high level 255. After setting the gray level, the image acquisition step is entered. The image acquisition is to acquire an optical image from the selected video camera. The AIA directs the video signal to the imaging screen. Because anything in the field of view of the lens is transmitted to the screen, we should then adjust the lighting and focusing control to gain the clearest possible images.

Then, the AIA prompt: "number of times to average the image?". Averaging a live image

clarifies the image or removes noise from the live image before it is displayed on the monitor.

After proper averaging the image manually, the video image is frozen for processing or

analysis.

Image editing operations are then performed for the displayed image on the screen.

For editing the image, first the small feature enhancement is processed. This operation

amplifies the gray level at locations of rapid change, where the edges of small features are

detected and presented on the screen by increasing contrast of the dark field. Next, erode and

dilation options are sequentially performed to lead to a more accurate feature count during

analysis. The final enhanced image is analyzed by the AIA, and then the raw information is

stored to disk or sent to a microcomputer via a telephone line for the final data processing.

The final data processing was all accomplished on a micro computer.

To ensure that sufficient particles are counted for each sample to give reproducible

results of the particle size distribution, the following guidelines modified from Hanson (1989)

were followed:

- a goal of a minimum of 1000 features measured, if they can be measured in less than 20 microscopic fields,
- a goal of a minimum of 10 microscopic fields, if 1000 features are measured with less than 10 microscopic fields,
- a goal of a minimum of 30 microscopic fields, if they can not measure 300 features within 30 microscopic fields,

- an absolute minimum of 10 microscopic fields, when low magnification was used, because a field of view for low magnification (2709 μm) was much greater than for high magnification (183 μm).

4.3.2 Photometric Dispersion Analyzer System

The state of aggregation of particles in a flowing suspensions is monitored with the PDA. An optical sensor in a cell of the PDA, which is connected directly through a tubing to a flocculation reactor, is sensitive to fluctuations in the flowing suspension's turbidity caused by random variations in the number and size of particles in the light beam. The essential point is that these turbidity fluctuations increase markedly as particle aggregation occurs, and provide a simple and sensitive means of monitoring the rate of flocculation. In the PDA instrument, the signal from the transmitted light detector consists of a large dc component corresponding to the average transmitted light intensity (related to the turbidity of a suspension), and a much smaller fluctuating ac component due to random variations in particle number, as shown in Figure 4.8. In the PDA instrument, the ac component is separated from the dc component and amplified to be analyzed.

It has been shown that the root mean square (rms) value of the fluctuating signal varies with the square root of the particle concentration and linearly with the size of the suspended particles in a rather complex manner (Gregory and Nelson, 1986). Assuming that variation in particle number follows a Poisson distribution, Gregory (1985) derived formulas for the relationship between the PDA output and concentration of suspended particles using a
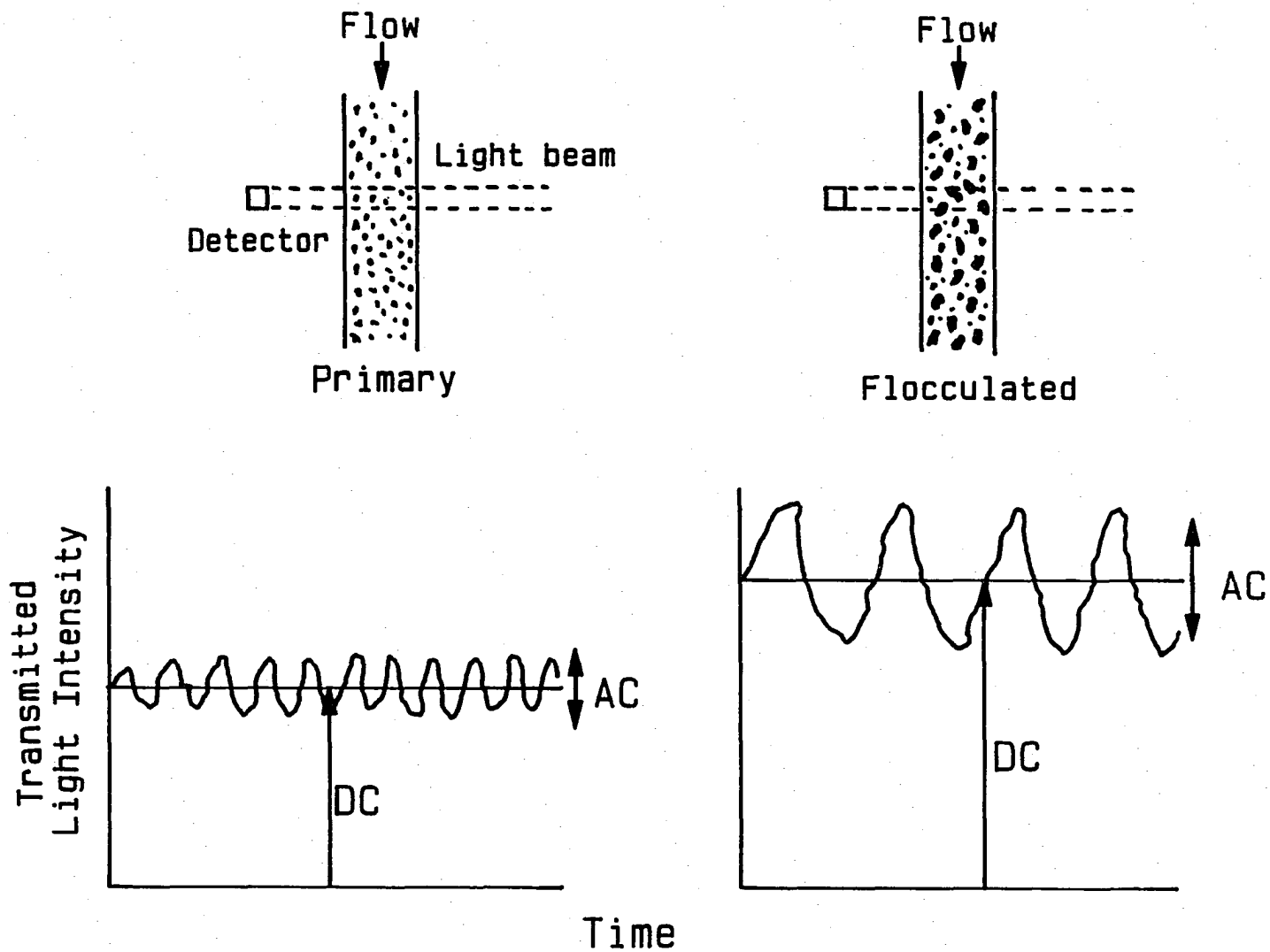
Figure 4.8.   Schematic diagram showing the principle of the turbidity fluctuating
technique used with the PDA

modified Lambert-Beer law. The basis of the technique to flocculation monitoring can be discussed starting from the Lambert-Beer law. According to the Lambert-Beer law, the intensity of transmission of light, T, through a particle suspension is defined as:

$$T = I/I_0 = V/V_0 = \exp(-NCL) = \exp(-\tau L) \tag{4.5}$$

where

I_0 = incident light intensity (i.e., that transmitted through particle free-water)

I = light intensity transmitted through a suspension of optical path length

N = number of particles in suspension per unit volume

C = average scattering cross-section of suspended particles

τ = scattering coefficient (= NC, also called turbidity)

V, V_o = light intensity converted to a voltage at a detector with and without particles

L = optical path length.

Considering a suspension of particles flowing through a cell with a light source, the average number of particles in the beam, ν, is given by

$$\nu = N.A.L \tag{4.6}$$

where A is effective cross-sectional area of the light beam.

Then, Eq (4.5) can be expressed as,

$$V/V_0 = \exp(-\nu C/A) \qquad (4.7)$$

It has been known that local variations in composition of a suspension follow the Poisson distribution, so that the standard deviation about the mean is equal to the square root of the mean value. That is, the rms of a fluctuating signal (V_{rms}) is equivalent to the standard deviation of the voltage about the mean value V, in which V_{rms} can be related to the particle number fluctuations about the mean, and the rms value of the fluctuating voltage signal is given by (Gregory, 1985):

$$V_{rms} = V(\nu^{1/2}C/A) \qquad (4.8)$$

Now, Eq (4.8) can be expressed in terms of particle number concentration, N ($= \nu/AL$):

$$V_{rms} = V(NL/A)^{1/2}C \qquad (4.9)$$

For a given PDA apparatus, the term L/A is constant so that V_{rms} from Eq (4.9) varies with particle concentration and particle size. Using the PDA, both V_{rms} and V can be measured experimentally and the ratio of these two quantities is obtained directly from Eq (4.9):

$$V_{rms}/V = (NL/A)^{1/2}C \qquad (4.10)$$

This ratio value varies directly with square root of particle number, $N^{1/2}$, and with the average scattering cross-section of particles. Combining Eq (4.5) with Eq (4.10) can eliminate the scattering cross-section, C, and provide Eq (4.11) in terms of the total particle number:

$$\frac{\ln(V_0/V)}{(V_{rms}/V)} = (NLA)^{1/2} \tag{4.11}$$

Since all of the quantities on the left hand side are measurable by the PDA, the average number in the sample volume can be easily calculated. However, it should be emphasized that this result applies only to a monodisperse suspension.

Since the suspensions of practical interest are heterodispersed as particles are aggregated, the equations derived are limited to a single particle size in the suspension. For heterodispersed suspensions, Eq (4.10) has to be replaced by:

$$V_{rms}/V = (L/A)^{1/2} \, (\Sigma \, N_i C_i^2)^{1/2} \tag{4.12}$$

where N_i and C_i represent the number concentration and scattering cross-section of particles of type i and the sum is taken over all types of particles. The nature of the sum in Eq (4.12) is such that smaller sizes of particles contribute relatively little to the ratio value and that, in an aggregating system, the larger aggregates have a greater influence on the ratio, V_{rms}/V.

Therefore, in this flocculation kinetics study, the rate of increase in the ratio is taken as an empirical measure of the rate of flocculation, and the ratio value is referred as 'flocculation index' for the sake of illustration and discussion. Assuming the particles are spheres, Gregory (1985) derived the equivalent results for a continuous size distribution:

$$V_{rms} / V = (N_T \, L/A)^{1/2} \, \pi \left\{ \int a^4 f(a) Q(a)^2 \, da \right\}^{1/2} \tag{4.13}$$

$$\ln(V_0 / V) = N_T L \pi \int a^2 f(a) Q(a) \, da \tag{4.14}$$

where

  N_T = total number of particles per unit volume

  $f(a) da$ = fraction of particles with radius in the range a to a+da

  $Q(a)$ = scattering coefficient for particles of radius a

From Eqs (4.13) and (4.14), the following equation was derived by Matsui and Tambo (1991):

$$N_T = \frac{1}{LA} \left\{ \frac{\ln(V_0 / V)}{V_{rms} / V} \right\}^2 \frac{\int a^4 f(a) Q(a)^2 \, da}{\left\{ \int a^2 f(a) Q(a) \, da \right\}^2} \tag{4.15}$$

This result shows that the number concentration of particles can be calculated by providing the particle size distribution and the particle scattering coefficient of a suspension.

Light scattered from a coagulating system can be evaluated using such scattering theories as Rayleigh, Reyleigh-Debye, or Mie, depending on the size regime of the aggregates, the refractive index of particles, and the wavelength of the light (Treweek and Morgan, 1980). Treweek and Morgan (1980) made a detailed comparison of these theories for the turbidity of a suspension of aggregates coalesced from singlets. They found that the application of the coalesced-aggregate to the Mie scattering regime allowed the calculation of the turbidity per size interval caused by particulates in the coagulated suspension. They also demonstrated the use of Mie scattering theory via the coagulation of E.coli (equivalent spherical dia. = 1.3 μm). Gregory (1985) also applied Mie theory for the scattering coefficient for polystyrene latex particles (dia. = 0.72 - 2.03 μm).

In reality, the light scattering properties depends on the structure of the reflecting surface and the formation of insoluble hydroxide, and thus on floc structure. However, a relation between scattering coefficient and floc structure, especially iron floc, is currently unknown. Although Matsui and Tambo (1991) applied an extension of the PDA theory (particularly, Eq (4.15)) in order to obtain the size information of coagulated particles, and proposed some formulae which gives floc size information from the PDA output. In order to obtain the formulae, they applied a number of modifications to Eq (4.15) to calculate the scattering coefficient of the suspension and the total volume concentration of particles in the suspension. By comparing the mean size of alum flocs calculated from the output of the PDA

with the photographically measured diameter in batch and continuous flocculation, the authors

concluded that the floc size obtained from each of the two methods was satisfactorily

coincident.

4.4 Experimental Procedures

In this study two series of experiments were conducted. The first series was conducted

by using jar tests. The second series was conducted in the 18 L batch reactor using the results

of jar tests to guide the choice of conditions to be studied.

4.4.1 Jar tests

The jar tests were conducted to evaluate the coagulation mechanism and to determine

the optimal coagulant dose and pH to be used in subsequent batch reactor experiments. The

jar tests were conducted using a Model 7790-300 Phipps & Bird 6 Paddle Stirrer, which

utilized 2-liter square acrylic plastic jars called Gator jars, each jar with a flat, two blade

turbine mixer. The jar has a sample tap at a point 10 cm below the water line for withdrawal

of sample. In this experiment, pH and applied ferric nitrate dosage were the major controlled

parameters to be considered. A certain amount of stock clay suspension was diluted in a 15 L

reactor equipped with a mixer, and $NaNO_3$ was then added to produce an ionic strength of

0.005 M. During the mixing, 2 L of the diluted suspension was transferred to each jar via a 2

L-volumetric flask. A predetermined amount of 0.05 N NaOH was added to each jar in order to initially adjust solution pH before coagulant addition. A selected dosage of the coagulant was added during rapid mixing to each jar via a syringe near the tip of the rotating impeller.

After the coagulant addition, the jars were mixed rapidly for 1 min at a mixing speed of 250 rpm, and then stirred for 30 minutes at 30 rpm, followed by 30 min of sedimentation. The target pH was measured in all six jars immediately after rapid mixing. Samples were collected following rapid mixing and at the end of sedimentation for measuring ZP and settled turbidity, respectively. For a qualitative monitoring, floc sizes were measured using a 30-power hand-held monocular microscope with an optical micrometer.

4.4.2 Flocculation kinetics tests in 18 L batch reactor

These experiments were conducted using the experimental conditions selected from the jar test results. From the jar tests the optimum pH and coagulant concentration values were chosen for the comparison of flocculation kinetics when utilizing either of the two main coagulation mechanisms, namely the adsorption/destabilization (A/D) mechanism and the sweep flocculation mechanism. In the batch reactor tests, pH, applied ferric nitrate dosage, and mixing intensity for flocculation were the major controlled parameters considered. In addition, temperature and sulfate concentration were the additional controlled parameters for the studies of their effects on flocculation. The experimental parameters are summarized in Table 4.1.

Table 4.1. Summary of experimental conditions

Parameter	Description
Primary particle	Kaolin clay (1.8 μm mean equivalent circular dia.)
Particle concentration	25, 50, and 100 mg/L of kaolin clay
	(Turbidity, NTU: 24, 52, and 105, respectively)
Dilution water	distilled water with 0.005 M $NaNO_3$
Coagulant	stock solution: 0.25 M $Fe(NO_3)_3.9H_2O$
	dosing solution of 10 mg/mL as $Fe(NO_3)_3.9H_2O$
Temperature	room temperature (23 $\pm$ 1 $^{\circ}C$) and 5 $^{\circ}C$
Rapid mixing	250 rpm (G = 455 sec^{-1} at 23 $^{\circ}C$) for 1 min
Slow mixing	30, 45, and 60 rpm (G = 20, 37, 56 sec^{-1} at 23 $^{\circ}C$)
Suspension pH	6.0, 6.5, 6.8, 8.0 selected from experiments
Sulfate concentration	0 to 2 x 10^{-3}M using 1 M Na_2SO_4 solution

Before initiating a batch reactor test, it was necessary to determine the amount of acid or base required to obtain the target pH. This work was done using a titration technique in the 18L batch reactor.

The following are the stepwise procedures used in the batch reactor tests:

- On the day prior to the experiment, the 10 mg/mL coagulant dosing solution was prepared and stored in the constant temperature room. When a work was needed at lower temperature, the dilution water was withdrawn from the 500 L tank into several 20-liter carboys, and then stored in the constant temperature room to allow the dilution water to come to constant temperature,

- On the day of the experiment, approximately 15-16 L of the dilution water were placed in the reactor, and the pH meter was standardized using the pH 7 and 4 buffer, the PDA was turned on for 30 min before test for warming up and the rms gain, which sets the main amplifier gain between 1 and 10, was adjusted to the predetermined value to bring the ratio output to a suitable baseline. The optimum ratio output was necessary to obtain optimal signal sensitivity for a certain particle concentration and to avoid overload conditions as particle aggregation occurs. From the preliminary experiments by trial and error, the initial rms gain setting dial was adjusted to settings of 50, 50, and 20 for clay concentrations of 25, 50, and 100 mg/L, respectively. These settings had been found to be the most suitable gain settings for optimal response of the PDA,

- Before adding the stock clay suspension into the dilution water in the reactor, the DC gain control was adjusted with the particle-free dilution water flowing through the tube inside the PDA so as to give an incident voltage of 10 V,

- The clay suspension tank was turned on to mix for at least 30 min to insure complete homogeneity in the clay tank. After the clay stock suspension was mixed thoroughly, the sample hose was purged briefly to waste, and a desired amount of 800 mg/L stock suspension was collected into a graduated cylinder. The measured stock suspension and an amount of 1 M $NaNO_3$ were added into the reactor, and the volume of suspension in the reactor was then brought up to 18 L so as to give a desired concentration of clay suspension and ionic strength. In addition, when sulfate addition was desired, an appropriate amount of 1 M Na_2SO_4 was added and the total ionic strength due to the addition of $NaNO_3$ and Na_2SO_4 was maintained to 0.005 M,

- The wooden supporter equipped with the electric motor and the tachometer sensor was placed on the reactor, and then the pH probe and thermocouple were inserted into the holes on the supporter,

- The motor controller, the tachometer, and the pH meter were turned on, and the impeller speed was set to 250 rpm in order to have a homogenous clay suspension of kaolinite in the reactor,

- As mixing was being done at 250 rpm, acid or base was injected into the reactor so as to give a desired target pH, and a sample was started to be pumped out through the tube to the PDA flow-through monitor, and then the mixing was continued for about 5 min to insure the equilibrium of suspension with acid and/or base applied,

- After 5 min of mixing, a 60-mL homogenized sample of this suspension was drawn from the sampling port, by using the 60-mL syringe with a needle, to be used for measuring the turbidity and the zeta potential. This sample was also used for the particle analysis by the AIA. All the needles used for sampling were Perfectum PS 13 Hospi-Luer 4 inch stainless steel hypodermic needles,

- A dose of coagulant and a predetermined amount of NaOH was loaded into individual plastic syringes equipped with 4 in long needles, and then both were injected simultaneously through two rubber septa into the reactor near the tip of the rotating impeller while it was being rapid-mixed. Then, if necessary, a small amount of the acid or base was injected for final small pH adjustment during a period of 1 min of rapid mixing,

- After the 1 min of rapid mixing (2 min in some experiments), the impeller speed for the reactor was then reduced accordingly to its desired flocculation speed as rapidly

as possible followed by a flocculation period of 30 min. After the impeller speed was reduced, 60 mL of sample was extracted by inserting a 4 inch long needle, attached to a 60 mL of plastic syringe, through the sampling port to collect a sample for turbidity, ZP, and particle size analysis. In addition, pH was monitored continuously throughout the rapid mixing period using the pH meter. At the conclusion of the rapid mixing period, if the target pH was not attained within ±0.05 pH units, the experiment was abandoned,

- During the flocculation period, 1 mL samples were collected for some experiments (not all) at the following times for analysis of the particle size distribution : 1, 3, 5, 10, 15, 20, and 30 min after slow mixing began. The samples from the reactor were collected and transferred into the sample cells in the manner described earlier,

- During the course of the experiment, it was useful to describe the visual observations that were occurring as the flocculation progressed. These observation included naked-eye observation of the "smoke" disappearance time and microscopic observation of larger flocs with the hand-held monocular microscope,

- After the end of 30 min flocculation, a floc break-up test was performed in some experiments (not all); the impeller speed was increased to the 250 rpm immediately, which was the same impeller speed used for rapid mixing, and a sample was then taken at the end of 1 min of this repeated rapid mixing. In addition, after the end of flocculation period the pH of the suspension was again measured,

- In some experiments, the supernatant turbidity following settling was measured instead of performing the floc break-up test. In such experiments, the mixing was shut off after the end of flocculation and the suspension was allowed to settled for 30 min, and supernatant samples were withdrawn at several times during the 30 min of

settling through the sampling port located 14 cm below the water surface for measuring settled turbidity,

- All of the collected samples for the particle size analysis were then kept in a closed wooden box, and allowed to sit undisturbed overnight before being analyzed by the AIA,

- After all samples were collected, the PDA, the motor, the tachometer, and the pH meter were switched off. The batch reactor was then drained into the drain pipe and washed thoroughly. After each experiment, the pH of coagulant dosing solution was measured to check whether a change had occurred due to overnight storage,

- During these flocculation and floc break-up processes, the flowing suspension in the tube was also monitored continuously by the PDA.

For the experiments at 5 °C, system pOH was sometimes used as a control parameter since pOH was known as the appropriate control parameter to adjust water chemistry for changes in water temperature conditions (Hanson and Cleasby, 1990; van Benschoten and Edzwald, 1990). The pOH's were calculated using the temperature-corrected pK_w as presented earlier, and repeated here for convenience (Stumm and Morgan, 1981):

$$pKw = -6.0875 + 4470.99/T + 0.01706T \qquad (3.27)$$

where T is absolute temperature in °K.

5. RESULTS AND DISCUSSION

The experimental results obtained in this research are presented in this section. Two groups of experiments were performed. In the first group, conventional jar tests were conducted using a dosage range of ferric nitrate coagulant from 3 to 20 mg/L, a pH range from 5.0 to 9.0, and a kaolin clay concentration range from 5 to 500 mg/L under controlled slow- and rapid-mixing conditions. The results of these jar tests were used to delineate the experimental conditions which affect the kinetics of flocculation of the suspended clay particles. Then, a more limited set of pH and dosage experiments for the different clay concentrations would be selected for the flocculation kinetics comparisons using 18 L batch reactor tests. Performance for the flocculation of particles during the jar tests would be evaluated by measuring supernatant turbidity after 30 min of settling and by the measuring ZP values of the rapid mixed suspension.

The second group of experiments were flocculation kinetics tests conducted in an 18 L batch reactor. The desired dosages and pH values for optimal performance were selected from the results of the prior jar tests so as to cover the A/D and sweep floc mechanisms of coagulation. The flocculation kinetics was evaluated by the changes in particle size distribution measured with the AIA and/or by the degree of fluctuating turbidity in the flowing suspension measured with the PDA. Based on the results obtained from the flocculation kinetics tests, the effects of sulfate and temperature on the flocculation kinetics were assessed.

5.1 Jar Test Experiments

Most of the comparison of the jar test results presented herein is based on the supernatant turbidities and ZP values as a function of pH and coagulant dose. The supernatant turbidity, which is the turbidity remaining in the supernatant after 30 min of sedimentation, is expressed as the percentage of initial turbidity (Ti). The coagulant dosages that are quoted in the remainder of these results are expressed as mg/L of $Fe(NO_3)_3.9H_2O$. The concentration of clay particles, another important parameter for flocculation process, ranged from 5 to 500 mg/L to simulate low, medium, and high turbidity waters that are encountered in water treatment practice. The clay suspension pH ranged from 5 to 9 and the coagulant dosages ranged from 3 to 20 mg/L were selected to span the two predominant coagulation mechanisms, i.e., the A/D and sweep floc mechanisms. All of the jar tests were conducted at room temperature.

Results of the jar tests for treating a water with average 5 NTU of turbidity produced by 5 mg/L of kaolin clay are presented in Figures 5.1(a) and (b). In these figures, the percent of turbidities remained and ZP values are plotted against suspension pH measured immediately after rapid mixing over 5 to 20 mg/L coagulant dose. Figure 5.1(a) shows that at 5 mg/L of clay concentration, the effectiveness of flocculation was improved at higher pH and higher coagulant dose. As shown in Figure 5.1(b), there is reduction of negative ZP of kaolin particles with increased dosages, even a charge reversal at lower pH for all of the coagulant doses used. At 5 mg/L of coagulant dose the simple attainment of charge neutralization of negative charged clay particles did not result in efficient flocculation, and thereby resulted in
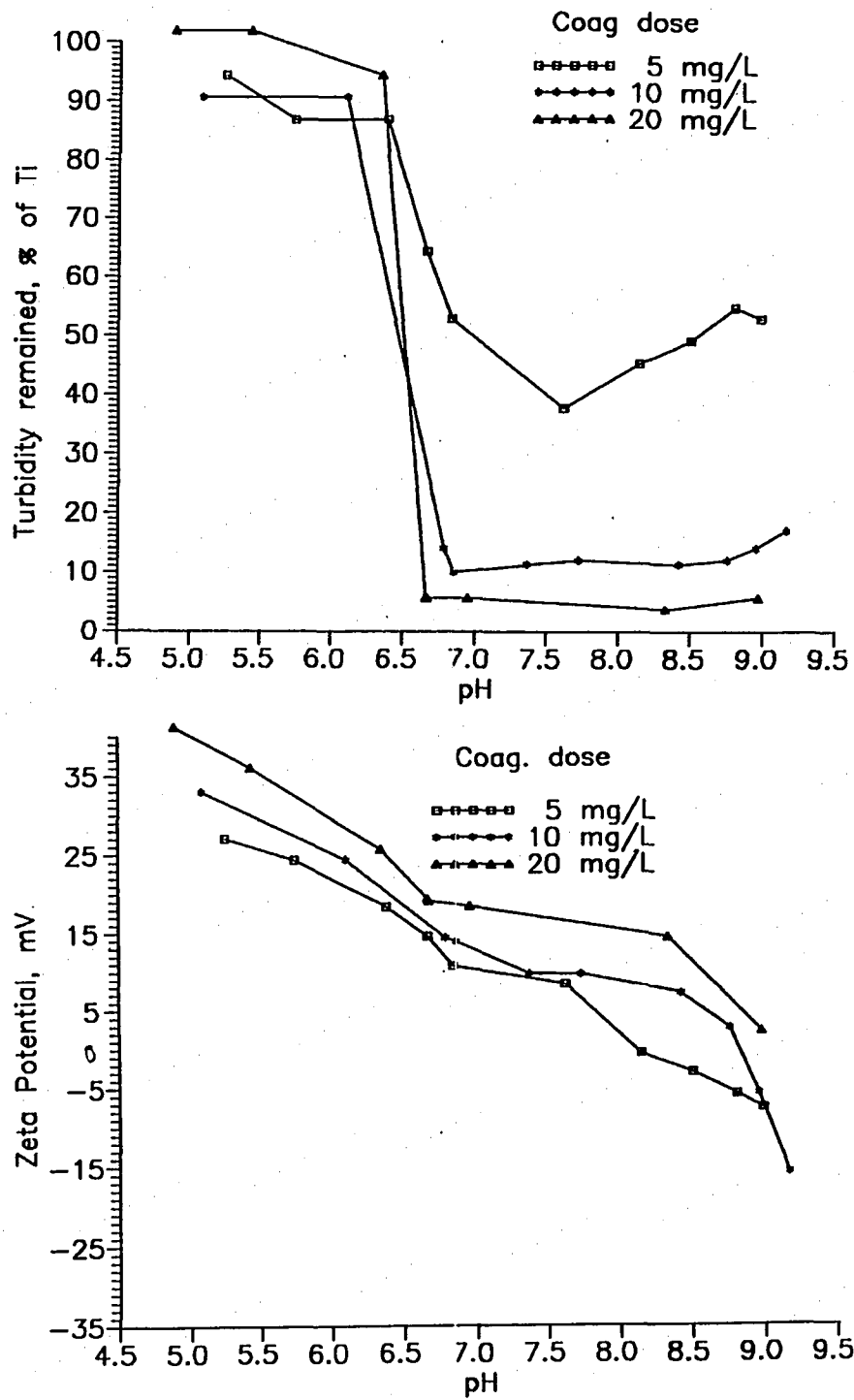
Figure 5.1.   Jar test results (clay: 5 mg/L, 5 NTU); (a) supernatant turbidity vs. pH, (b) zeta potential vs. pH

poorer sedimentation. These results indicate that because of the low concentration of particles in this suspension, the overall process of flocculation was limited by the rate at which interparticle contacts were produced. That is, effective flocculation was accomplished by precipitates of ferric hydroxide formed due to increased pH and/or increased coagulant dose, which increased the interparticle collision rates and hence enhanced aggregation of particles.

Plots of supernatant turbidity and ZP as a function of pH for different dosage of coagulant at a clay concentration of 25 mg/L (turbidity = 24 NTU) are presented in Figures 5.2(a) and (b). These results indicate that efficient turbidity removals occurred only when pH of the suspension was in the range from 6.7 to 8.2 and ZP is between about ±10 mV, except with higher coagulant dose (20 mg/L) where good turbidity removal was obtained even at more extreme ZP values (+15 to -13 mV). Beyond this region, two distinct restabilization zones are apparent, as evidenced in the ZP values. First, in the acidic pH range (< pH 6.5), the restabilization was induced by highly positive charged Fe(III) species. Second, on the alkaline side (> pH 8.5) the restabilization was induced by negative charged species. Previously, as shown in Figure 3.1, the solubility diagram of Fe(III) indicated that the negative iron(III) species, $FeOH_4^-$, is dominant at the pH level above 8.0, when competing ligands are absent. The comparison of these results to those observed at 5 mg/L of clay concentration suggests that destabilization of the particles is associated with surface charge neutralization under more favorable interparticle contact opportunity resulting from higher concentration of clay particles. It is noteworthy that adequate aggregation of particles occurred in a very
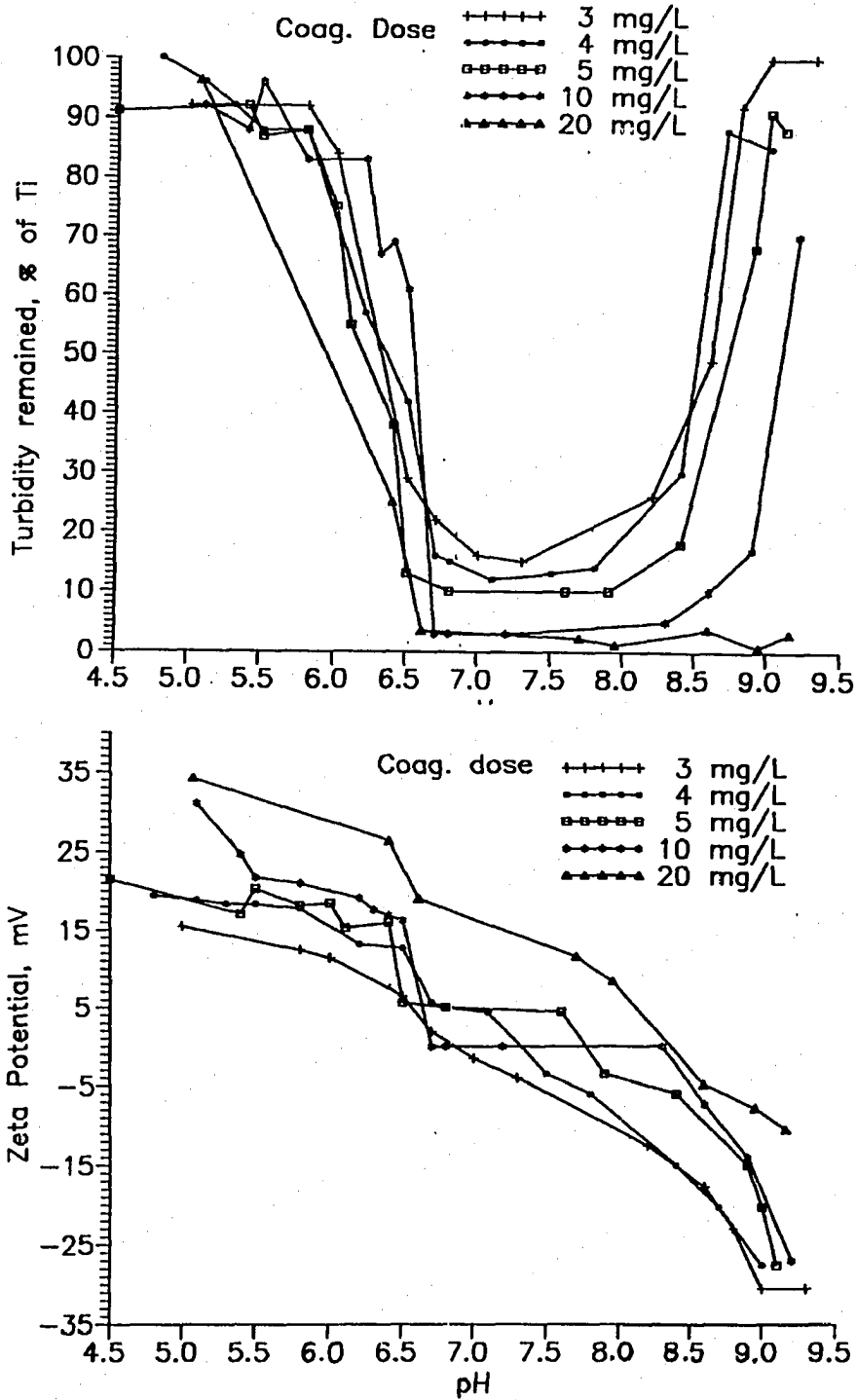
Figure 5.2. Jar test results (clay: 25 mg/L, 24 NTU); (a) supernatant turbidity vs. pH, (b) zeta potential vs. pH

limited pH range of 1.5 units, and that the poor coagulation apparent at higher pH was avoided with the addition of higher dosage of coagulant, i.e., 20 mg/L dose.

Figures 5.3(a) and (b) represent the jar test results obtained with 50 mg/L of clay concentration (turbidity = 52 NTU) under the same experimental conditions as the lower clay concentration. Comparison of Figure 5.3(a) with Figure 5.2(a) for 25 mg/L clay concentration indicates that the restabilization that was observed at lower pH range with 25 mg/L of clay has shifted to a slightly more acidic pH with 50 mg/L of clay. This may be explained by considering the production of higher positively charged Fe(III) species at more acid pH levels. That is, more positive charge is required for the restabilization due to charge reversal with higher concentration of negatively charged clay. It is noteworthy that the restabilization that occurred at higher pH range with 25 mg/L of clay disappeared for all the coagulant doses used with 50 mg/L of clay. Overall, the supernatant turbidity curves in Figure 5.3(a) indicates that a suspension containing the relatively high concentration of particles, which is probably less collision limited, gives good turbidity reduction over broader range of pH and coagulant dose.

The flocculation of high turbidity water was simulated with 500 mg/L of clay concentration which resulted in an average turbidity of 590 NTU. With this high clay concentration, collision limitation should not be a factor in flocculation kinetics. The results of the turbidity removal and the ZP are presented in Figures 5.4(a) and (b), respectively. In this high clay concentration, the supernatant turbidity instead of the percent remained turbidity is depicted as a function of pH. These results indicate that good turbidity removal was achieved at near zero and negative ZP values. As shown in Figure 5.4(b), the amount of coagulant
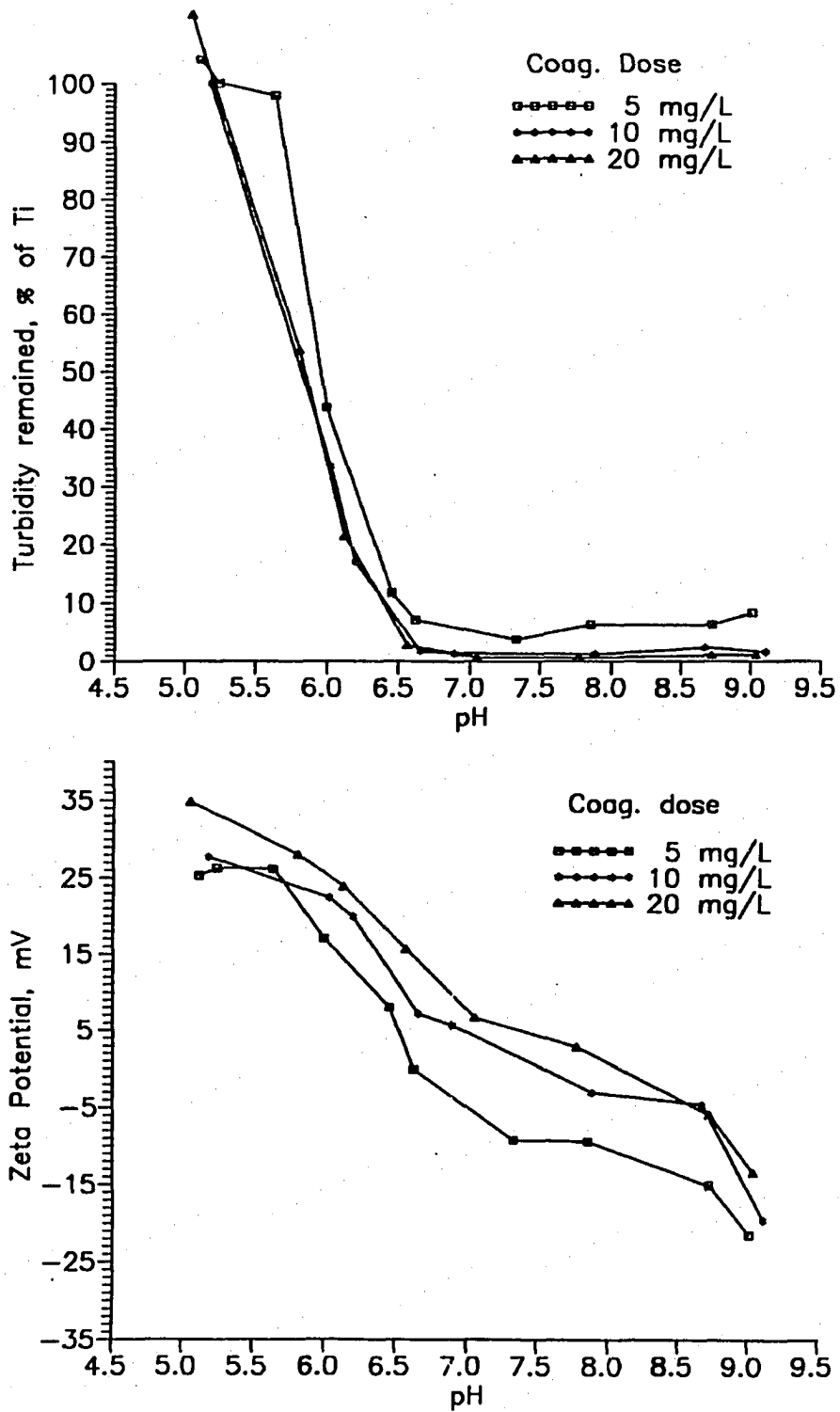
Figure 5.3. Jar test results (clay: 50 mg/L, 52 NTU); (a) supernatant turbidity vs. pH, (b) zeta potential vs. pH
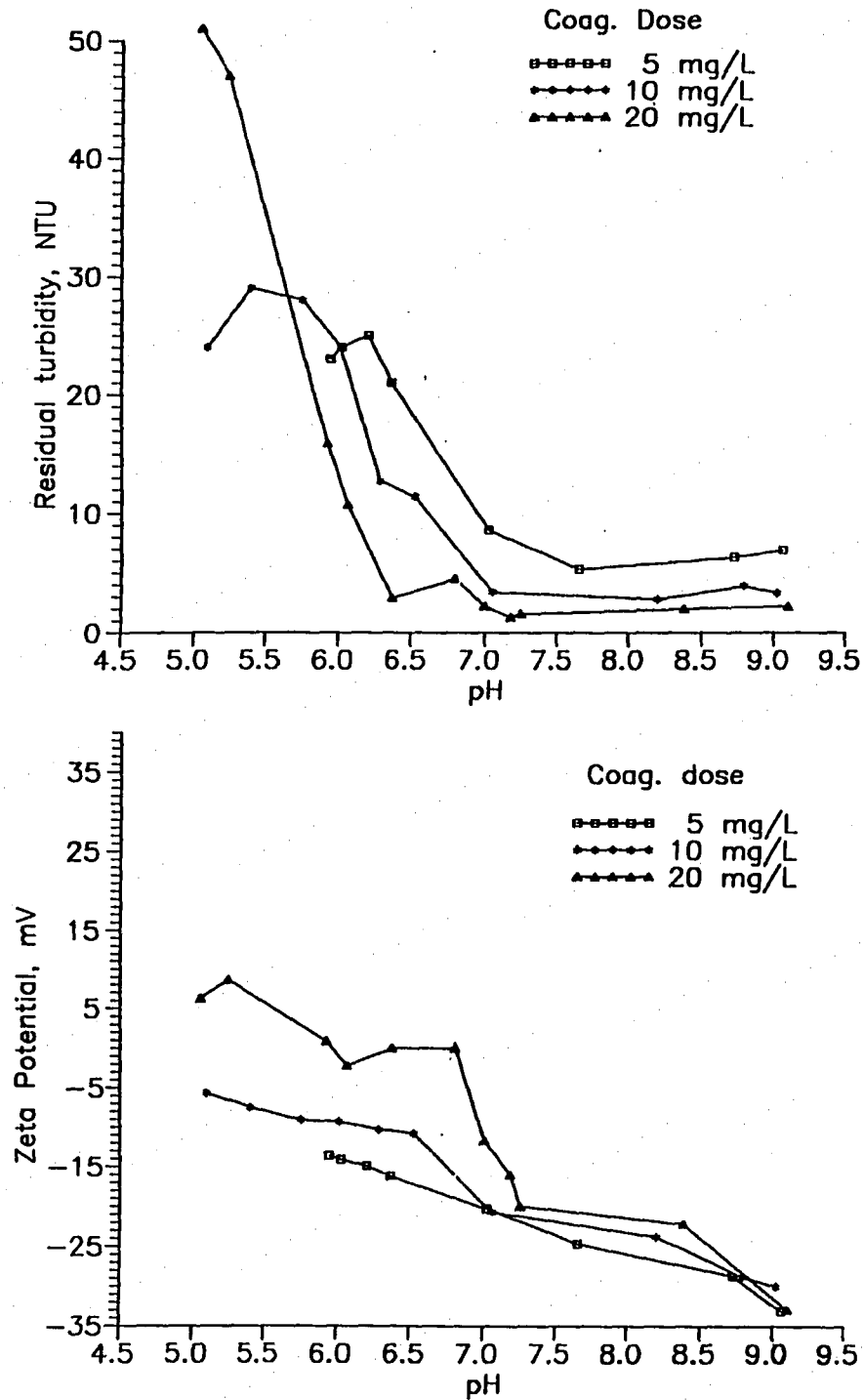
Figure 5.4. Jar test results (clay: 500 mg/L, 590 NTU); (a) supernatant turbidity vs. pH, (b) zeta potential vs. pH

dosage required for the complete charge neutralization would be above 20 mg/L at or below pH 6.8 for this high turbidity water. It is noteworthy that with this highly turbid water, better turbidity removal is still observed at high pH range, which favors the presence of lower positively or even negatively charged Fe(III) species and the rapid formation of ferric hydroxide precipitates. This result suggests that even at this high clay concentration (500 mg/L), flocculation due to heterocoagulation and/or enmeshment interaction caused mainly by Fe(III) precipitates might act more effectively in the aggregation of the particles.

5.2 Batch Reactor Test

Bench-scale batch flocculation tests were conducted using the 18 L reactor. The objectives were to evaluate flocculation kinetics using the experimental conditions selected from the results of jar tests. The experimental conditions for the flocculation tests conducted are summarized in Table 5.1.

The experimental parameters were chosen to span the full range of coagulation mechanisms including the A/D and sweep floc mechanisms, and varied clay concentration to simulate low, medium, and high turbidity waters. The maximum and minimum mixing intensities applied during the flocculation process were selected based on preliminary tests not to cause breakup of flocs or to result in significant settling during the slow mixing process. In addition, a minimum pH of 6.0 was selected for one pH value on the basis of preliminary tests because flocculation at this pH was found to be caused mainly by the A/D mechanism. Stated another way, the formation of highly positive charged Fe(III) species is expected to be

Table 5.1. Summary of experimental conditions for 18 L batch test

Fixed parameters	Description
Primary Particles	Kaolin: 1.8 μm mean equivalent circular diameter
Dilution Water	Distilled water
Ionic Strength	5×10^{-3} M (0.005 M $NaNO_3$)
Coagulant	Stock solution, 0.25 M $Fe(NO_3)_3 \cdot 9H_2O$
	Dosing solution, 10 mg/mL $Fe(NO_3)_3 \cdot 9H_2O$
Coagulant Dosage	1 to 10 mg/L as $Fe(NO_3)_3 \cdot 9H_2O$
Rapid Mixing	250 rpm (G = 455 sec^{-1} at 23 °C) for 60 sec.
Varied Parameters	Description
pH	6.0, 6.5, 6.8, and 8.0
Clay Concentration	25, 50 and 100 mg/L (24, 52, and 105 NTU)
Sulfate	0 to 2×10^{-3} M SO_4^{2-}
Temperature	room temperature (23±1 °C) and 5 °C
Flocculation Intensity :	30, 45, and 60rpm (G=20, 37, and 56 sec^{-1} at 23°C) for 30min.

predominant and the formation of hydroxide precipitate is expected to be very slow or none at this low pH. A maximum pH of 8.0 was selected for the highest pH level on the basis of preliminary tests that showed the aggregation of particles was mainly caused by the interaction between clay particles and rapidly formed hydroxide precipitate. In addition, $Fe(OH)_{3(s)}$ is least soluble at around pH 8.0.

In the jar tests, flocculation has been evaluated indirectly by the measurement of the supernatant turbidity after 30 min of sedimentation and by the ZP after rapid mixing. With only these measurements, however, it is difficult to observe the effect of changes in the flocculation kinetics of the process because the supernatant turbidity measured after 30 min of sedimentation can not reveal the rate of particle aggregation directly. Therefore, for most of the experimental results presented herein, flocculation kinetics was monitored by using two-sophisticated systems. For the first system, flocculation kinetics was determined from the rate of decrease in the total number of particles in the flocculating suspension, owing to aggregation of particles measured with the AIA system. To assess the rate of decrease in the total particle number in the flocculating suspension, the total number of particles was first counted in the homogenized sample, which is the one taken before adding coagulant, and compared with the total number of particles counted in each sample taken at several different flocculation times. A particle size distribution is illustrated graphically with Figure 5.5 being typical of the raw data collected from the AIA using a high magnification (547x) of the microscope. Each particle size distribution in Figure 5.5 represents a sample taken from a reactor at a different flocculation time. In this graph, the number of particles per mL of sample in each size class is plotted against the equivalent circular diameter of each size class. As illustrated in Figure 5.5, the number of particles with equivalent circular diameter smaller than 3.0 μm is gradually decreased as flocculation proceeds, resulting from the growth of aggregates.
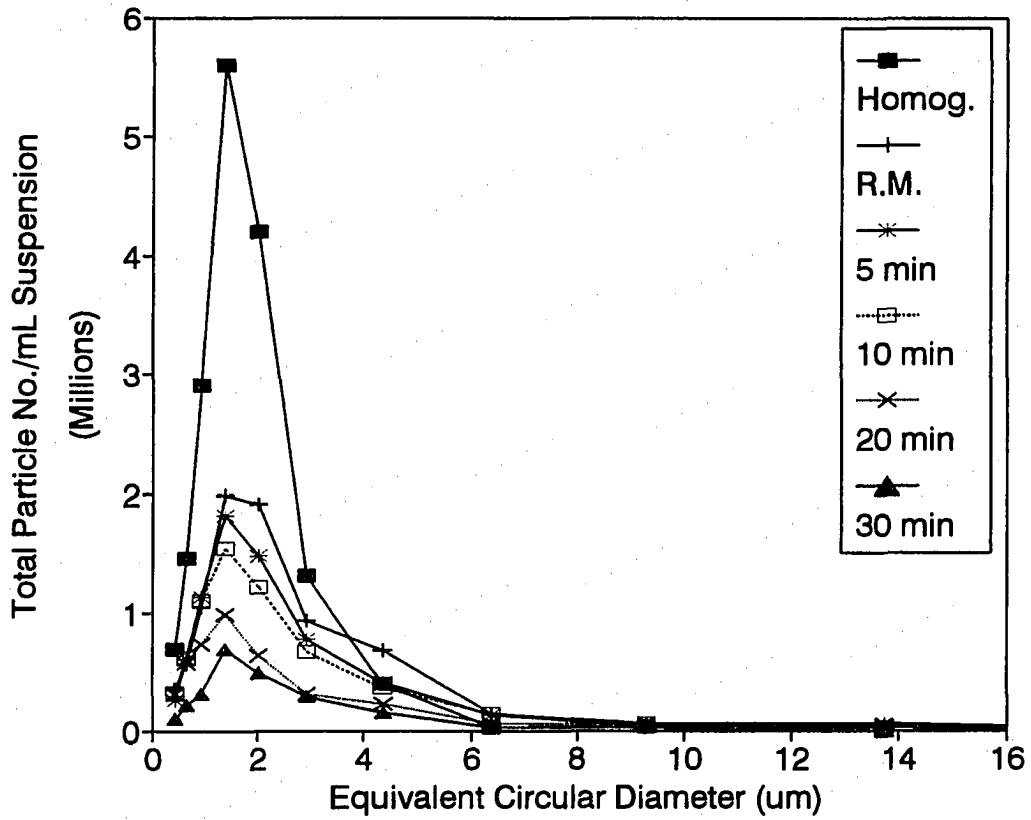
Figure 5.5. Changes in particle size distribution as a function of flocculation time (pH 6.8, clay: 25 mg/L, dose: 5 mg/L as $Fe(NO_3)_3.9H_2O$, 30 rpm)

For the second system, the PDA instrument was utilized to investigate the state of aggregation of kaolin particles in a flowing suspension. This instrument measures the fluctuation of transmitted light intensity for an aggregating suspension whose composition is continuously changing with flocculation time. To establish the validity of the PDA signals, the normalized values of the voltage corresponding to the mean transmitted light intensity (V) versus kaolin concentration, and the ratio of the root mean square of the voltage fluctuations around the mean value to the mean value (V_{rms}/V) versus the square root of particle concentration, respectively, are shown in Figures 5.6 and 5.7. Figure 5.6 indicates that the mean transmitted light intensity, V is linearly changed with the concentration of primary clay particles. As discussed previously with Eq (4.10), $V_{rms}/V = (NL/A)^{1/2}C$, should vary directly with the square root of the particle concentration, assuming a monodispersed suspension. As shown in Figure 5.7, it is noted that V_{rms}/V is directly proportional to the square root of particle concentration in the clay suspension used, even though some departure from monodispersity would be expected for the clay suspension used in these experiments.

The presentation of the flocculation kinetic results obtained in the 18 L batch reactor using kaolin suspension is given as follows:

- The effect of changing suspension pH on the flocculation rate with various clay concentrations
- The effect of slow mixing intensity on the flocculation rate
- The effect of coagulant dose on the flocculation rate
- The effect of sulfate ion on the flocculation rate
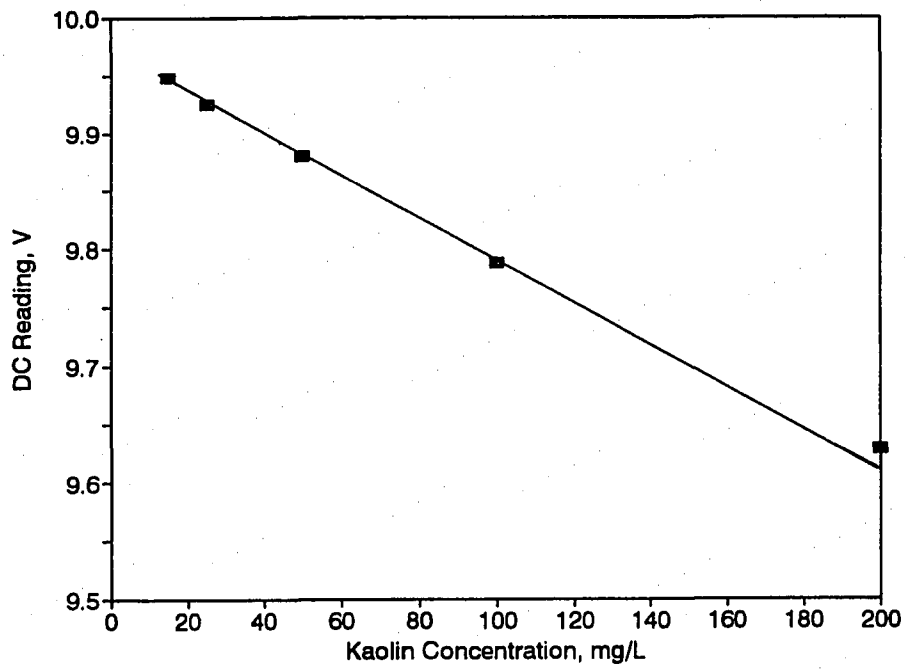- The effect of low water temperature on the flocculation rate

Figure 5.6. Measured values of V as a function of kaolin concentration

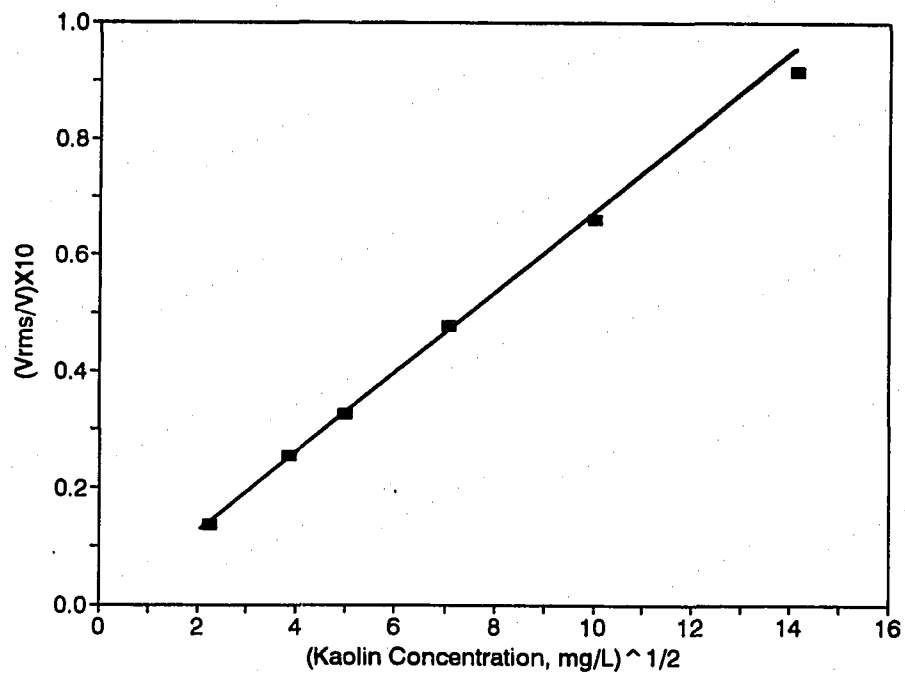
Figure 5.7. Measured values of V_{rms}/V as a function of kaolin concentration

5.2.1 Flocculation kinetics

Figures 5.8 and 5.9 show the effect of pH on flocculation kinetics at 30 rpm slow mixing speed. A comparison of particle count measurements by the AIA and the growth of aggregates expressed as the signals of the PDA was made to assess the reliability of both kinetics measuring techniques. The kinetics of flocculation was measured simultaneously by using the AIA and PDA. First, for Figure 5.8, the particle size distribution obtained from the AIA, previously as shown in Figure 5.5, was manipulated to plot the total particle count fraction which was obtained as the ratio of the total particle number per mL of suspension at any given time to the total particle number per mL of suspension measured in the homogenized sample. In the X-axis, the zero time in these figures refers to the beginning of the flocculation period immediately following the 1 min rapid mixing, thus the negative time represents the rapid mix time duration. Generally, Figure 5.8 shows the decrease in the total number of particles in suspension during the flocculation time owing to aggregation of primary particles into flocs. Second, Figure 5.9 shows the PDA monitor responses collected at every 5 seconds. The ratio, V_{rms}/V, was plotted as a function of flocculation time. In this study, the ratio value was referred as 'flocculation index' for the sake of illustration and discussion. Figure 5.9 indicates that the ratio, V_{rms}/V, always increases in the course of aggregation until a limiting value is reached.

Figures 5.8 and 5.9 show the dramatic impact of solution pH on the rate of flocculation, as evidenced by both the decreases of total particle count fraction and marked increase of flocculation index, respectively. Overall, under the same coagulant dose, the plots
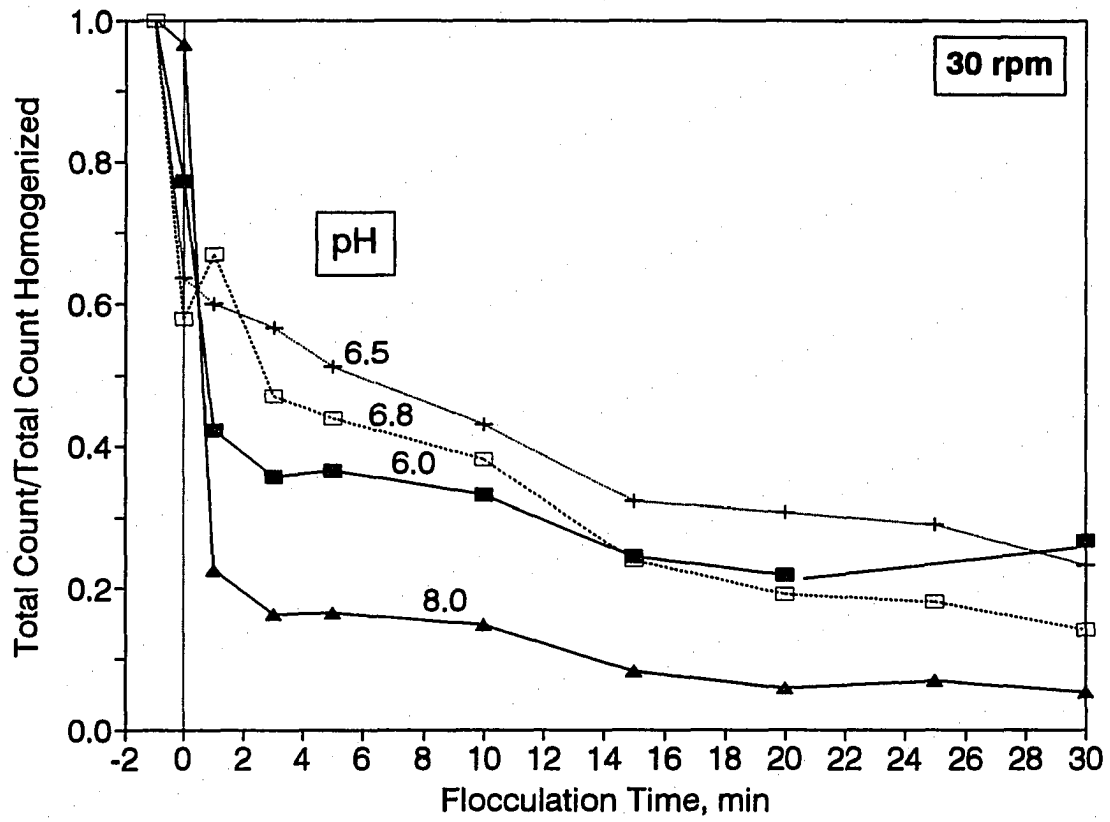
Figure 5.8.   Effect of pH on the rate of flocculation (clay: 25 mg/L, dose: 5 mg/L, 30 rpm)
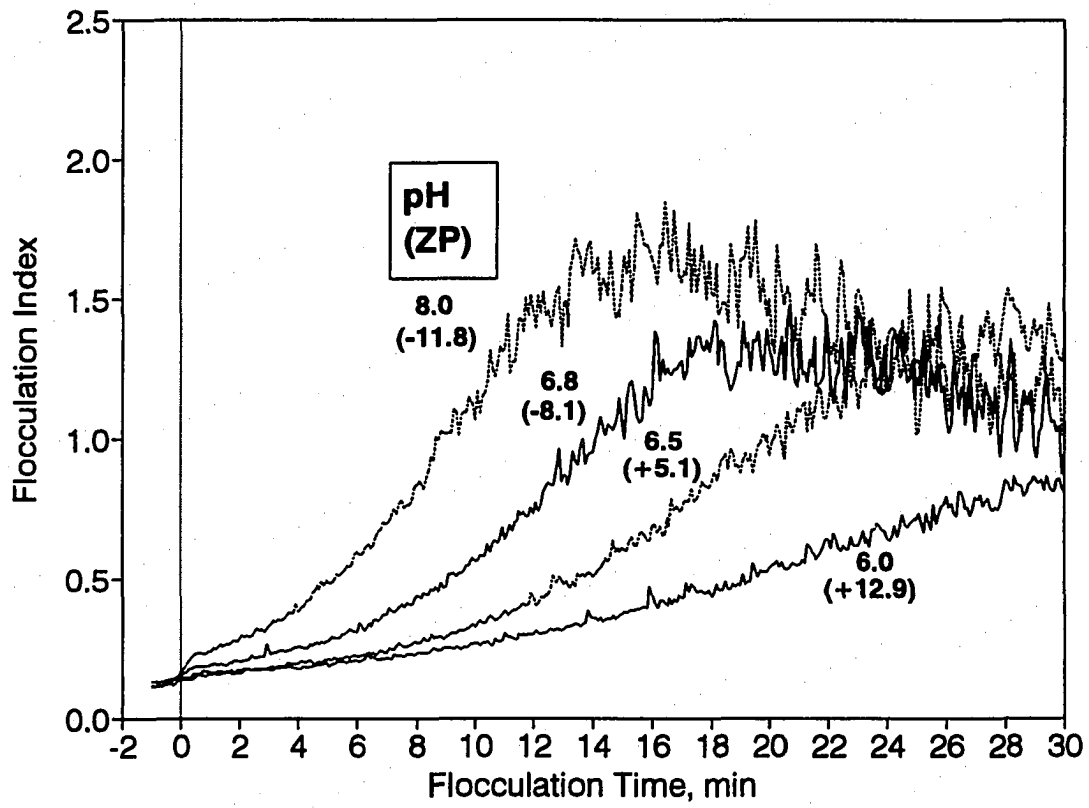
Figure 5.9. Effect of pH on the rate of flocculation (clay: 25 mg/L, dose: 5 mg/L, 30 rpm)

in Figures 5.8 and 5.9 show marked increases in the rate of flocculation as the suspension pH increases from pH 6.0 to 8.0. The higher pH favors the faster rate of flocculation. The ZP values measured immediately after rapid mixing are also shown in Figure 5.9. The ZP value at each pH indicates that the surface charge resulting from the addition of coagulant is more negative at the higher pH; whereas, at lower pH, complete charge neutralization and even charge reversal are achieved with a 5 mg/L of coagulant dose. To some extent, the faster rate of flocculation at higher pH relative to the rate at lower pH may be attributed to a general effect of precipitation of iron hydroxide. This precipitate forms more rapidly at higher pH and hence enhances particle-particle interaction resulting in faster rate of flocculation. As shown in Figure 5.9, the measurable differences in the rate of flocculation are demonstrated clearly by the flocculation index. However, as shown in Figure 5.8, the result at pH 6.0 shows slightly greater decreases in particle count fraction than at pH 6.5 and 6.8 during the initial 15 min of flocculation period.

Figures 5.10 and 5.11 present comparison between experiments performed over the pH range 6.0 to 8.0 at 60 rpm slow mixing speed but with otherwise identical conditions to Figures 5.8 and 5.9. Under this high mixing intensity, once again, it is evident from the plots in Figures 5.10 and 5.11 that the suspension pH produces pronounced effect on the rate of flocculation. Again, the higher pH results in faster aggregation of the primary particles, as evidenced by rapid disappearance of primary particles and rapid growth of flocs. It is interesting to compare the rate of flocculation at pH 8.0 observed in Figures 5.10 and 5.11. Figure 5.10 shows that around 80 % reduction of total particle number was accomplished
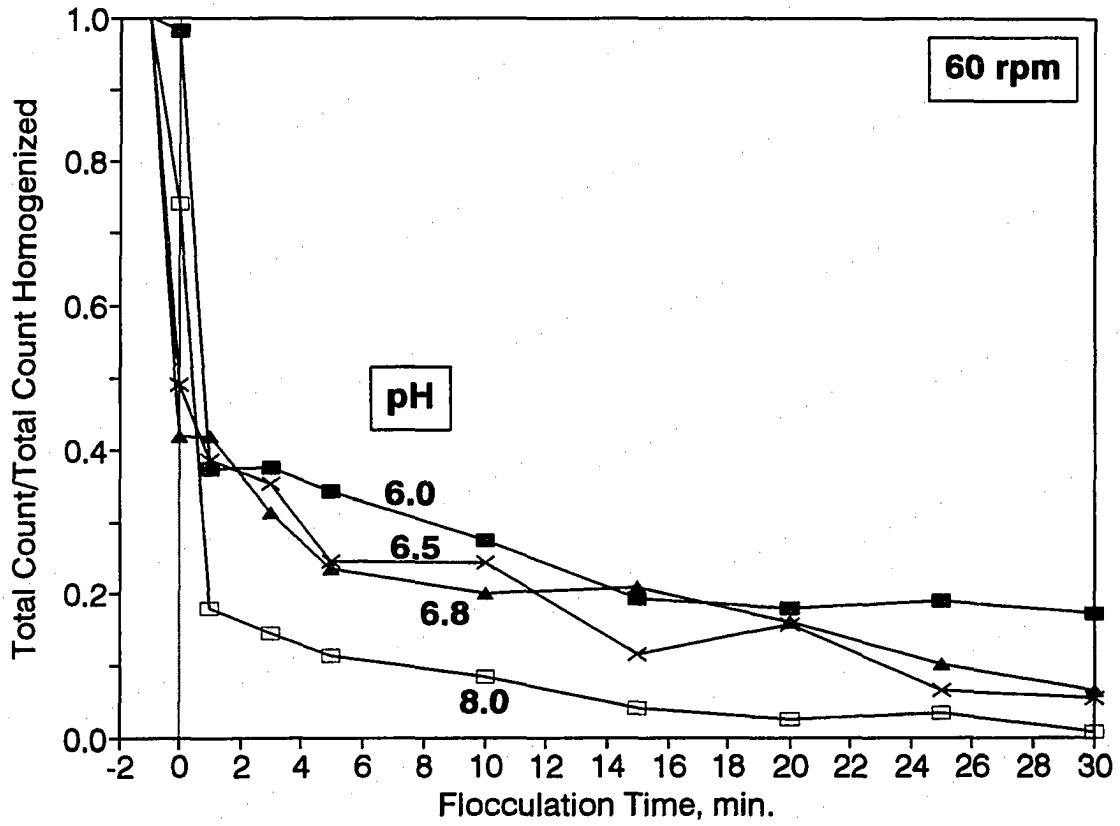
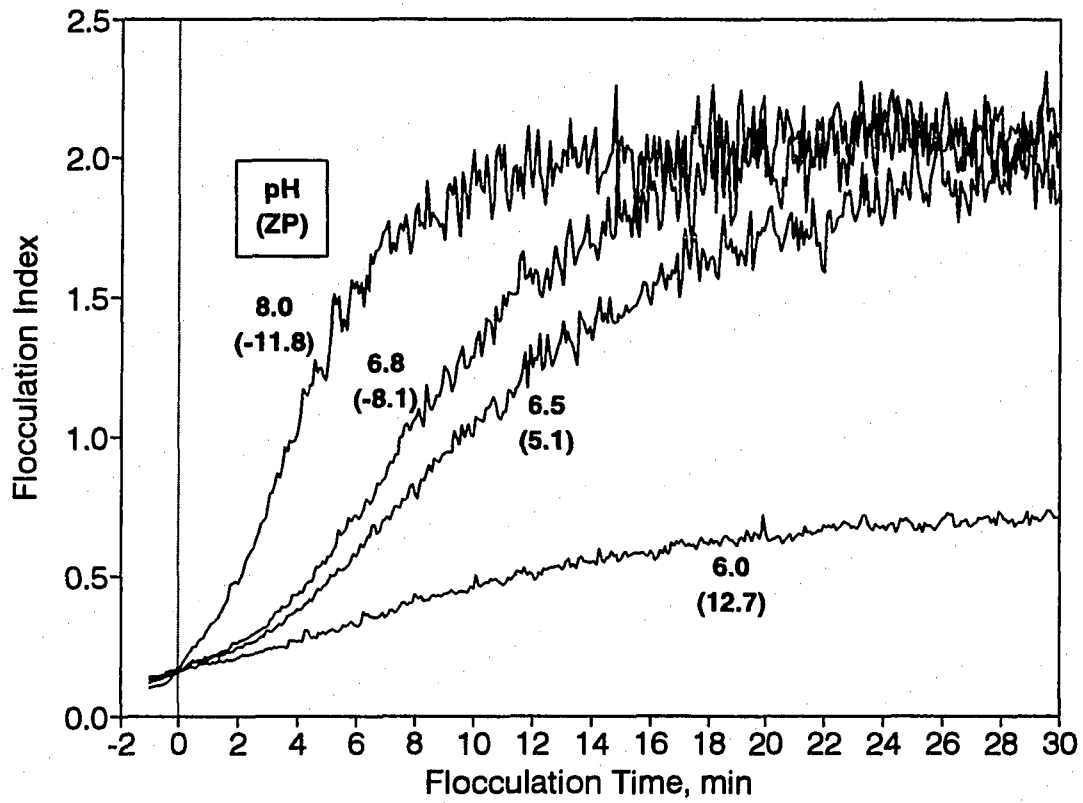Figure 5.10. Effect of pH on the rate of flocculation (clay: 25 mg/L, dose: 5 mg/L, 60 rpm)

Figure 5.11. Effect of pH on the rate of flocculation (clay: 25 mg/L, dose: 5 mg/L, 60 rpm)

after just 1 min of flocculation period; whereas, Figure 5.11 shows that the flocs tended to grow most rapidly in the first 8 min of flocculation period. However, it can be seen that in both kinetic measuring systems, the flocs reached their ultimate size after approximately 15 min of flocculation period. In general, the flocculation rate evidenced by the flocculation index shows a rapid increase in the rate of flocculation (particularly at the higher pH levels) followed by a leveling-off, indicating a decrease in particle collision frequency, and thereby, flocculation rate. The cause of leveling-off of the flocculation index can not be simply explained, but it is believed that the flocs eventually reach a limiting size, depending on the mixing intensity and the floc strength. However, at low mixing speed used in Figure 5.9, a number of bigger sized flocs were observed to be settled toward the end of mixing, resulting in gradually decreased flocculation index values following the maximum index values. Unfortunately, attempts to avoid both sedimentation of flocs and significant breakup of flocs were unsuccessful. Therefore, the settling of flocs within the reactor seemed to be inevitable at low mixing intensity under a certain experimental conditions. Therefore, when the decrease in the flocculation index is observed after the peak in the curve, the part of rising limb on the index curve should be considered to be the most significant in assessing the kinetics of flocculation.

Figures 5.12 to 5.15 are comparisons of flocculation rate at different mixing intensities under experimental conditions of pH 6.0 and 6.5, respectively. The mixing intensities applied during flocculation are 30 and 60 rpm, which correspond to $G = 20$ sec^{-1} and 56 sec^{-1} at 23 °C, respectively. At pH 6.0, as shown in Figure 5.12 and 13, the results of the total particle count fraction exhibit slightly faster flocculation kinetics at the higher shear rate. The flocculation
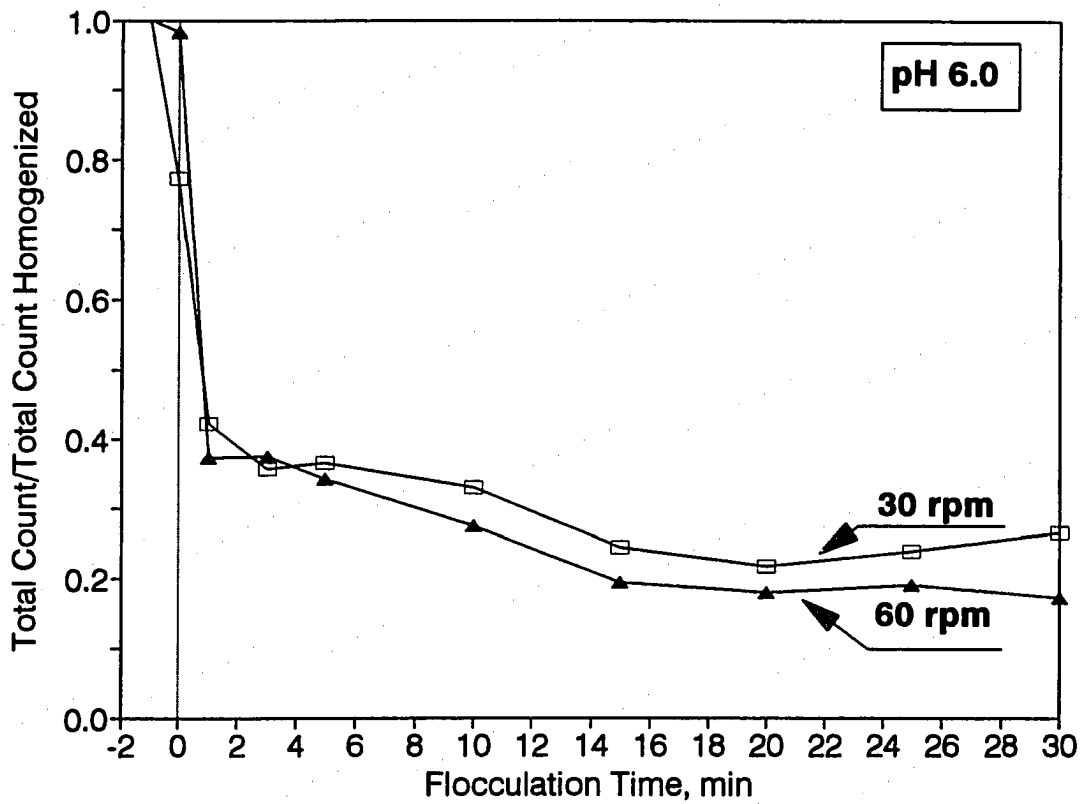
Figure 5.12. Effect of flocculation mixing intensity on the rate of flocculation (pH: 6.0, clay: 25 mg/L, dose: 5 mg/L)
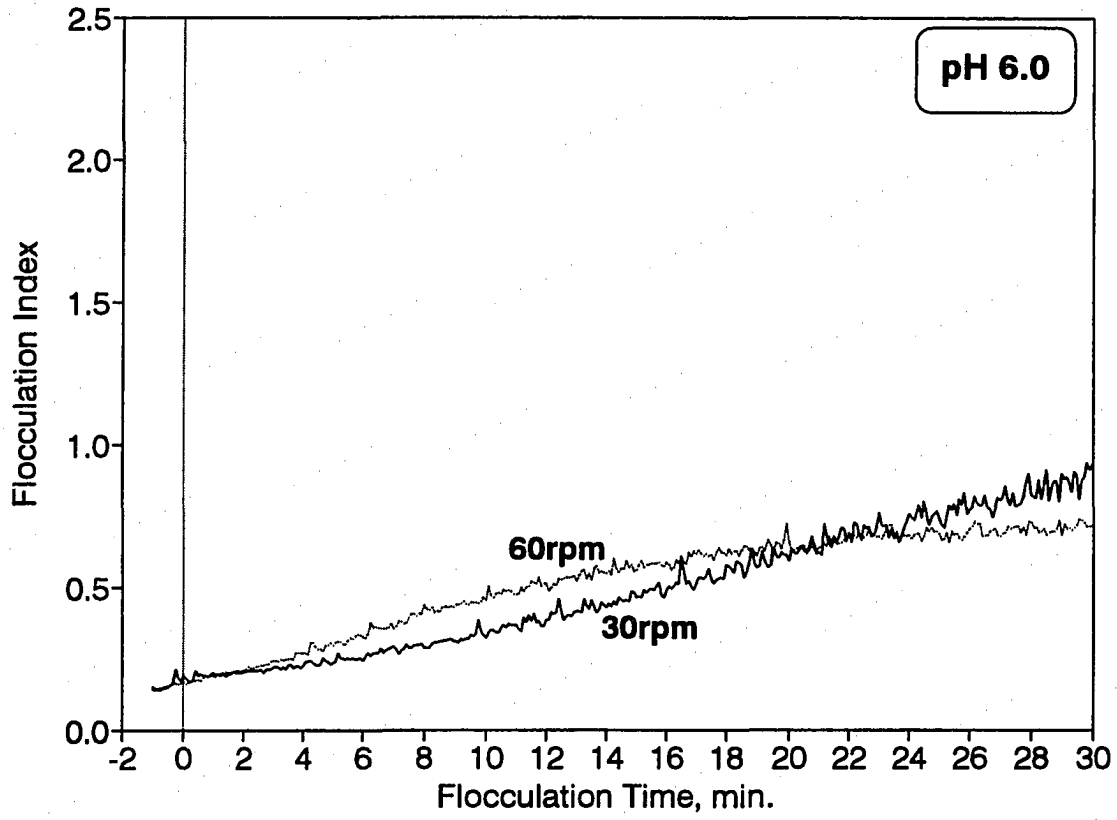
Figure 5.13. Effect of flocculation mixing intensity on the rate of flocculation (pH: 6.0, clay: 25 mg/L, dose: 5 mg/L)
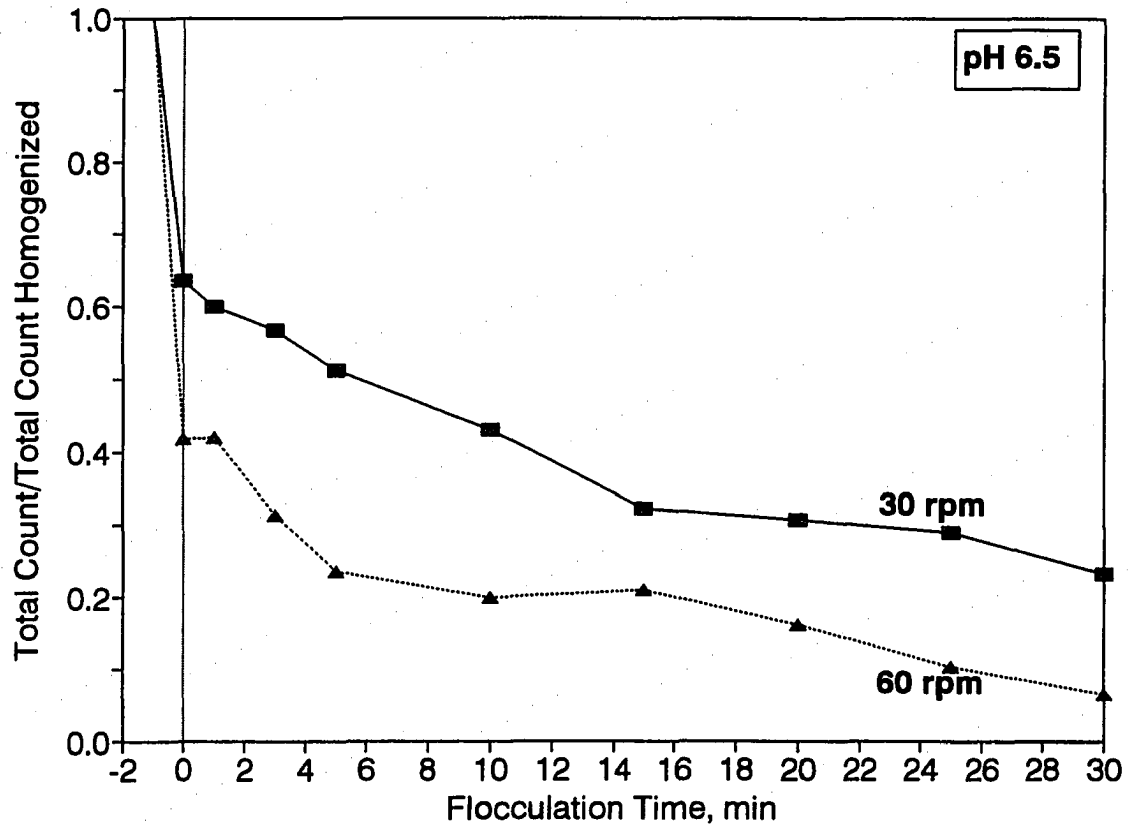
Figure 5.14. Effect of flocculation mixing intensity on the rate of flocculation (pH: 6.5, clay: 25 mg/L, dose: 5 mg/L)
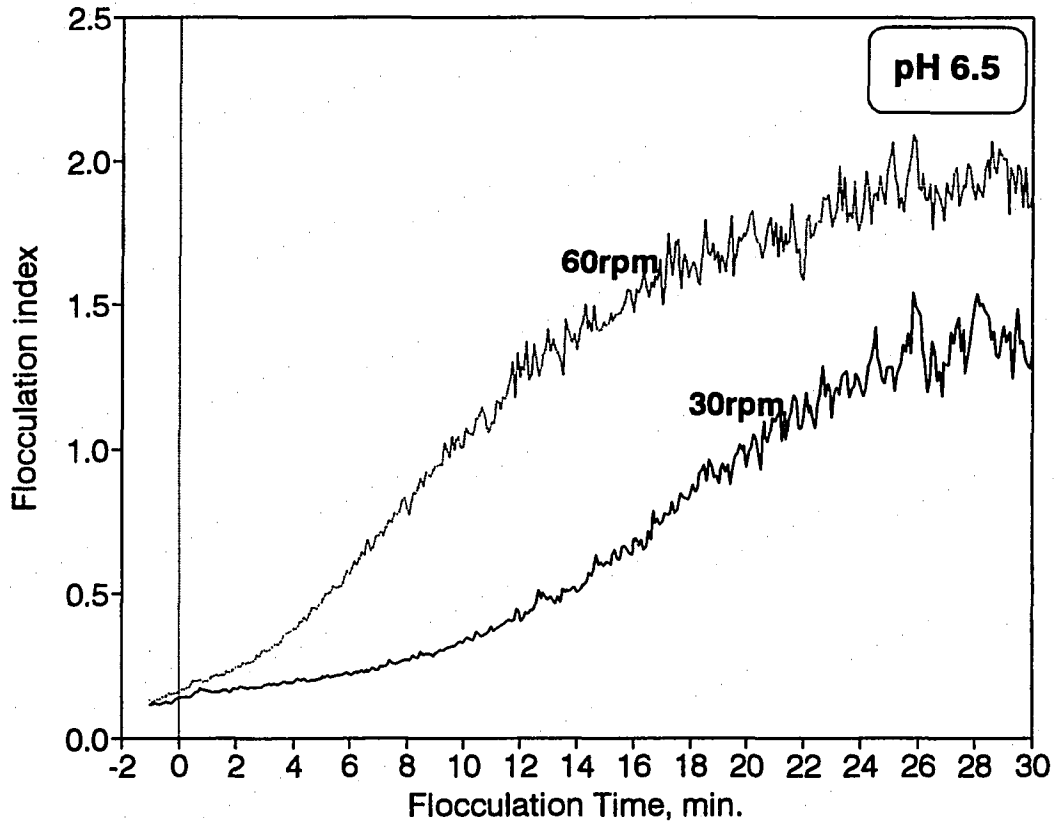
Figure 5.15. Effect of flocculation mixing intensity on the rate of flocculation (pH: 6.5, clay: 25 mg/L, dose: 5 mg/L)

index obtained from the PDA, however, shows that with a lower velocity gradient, the rate of

forming aggregates is slower initially, but eventually it overtakes the performance at higher

mixing intensity and exceeds it. It was found at pH 6.0 that the flocs grew very slowly and the

flocs reached to the average maximum size of < 50 μm. Furthermore, the floc breakup test,

yet to be presented, demonstrated that the flocs formed at pH 6.0 were extremely weak.

Therefore, it can be seen that after the floc particles reached their ultimate size at 60 rpm, the

flocs could not withstand the high shear being imposed. On the other hand, the results

produced at pH 6.5 as shown in Figures 5.14 and 5.15 show that a substantial difference in

process kinetics is evident at pH 6.5 under the different mixing intensities. That is, higher

mixing intensity results in a more rapid disappearance of primary particles and rapid formation

of aggregates, as indicated by the curves made from the AIA and PDA, respectively.

Comparing the rates of flocculation at pH 6.0 and 6.5 suggests that there are important

chemical limits to particle aggregation. For example, the effect of mixing intensity on the rate

and extent of particle aggregation at pH 6.0 was less pronounced. It is also interesting to note

that the results of flocculation kinetics become significantly different for the different mixing

conditions over just a 0.5 pH unit difference.

Figures 5.16 to 5.19 represent a comparison of flocculation kinetics at different mixing

intensity at pH 6.8 and pH 8.0, respectively, under the same experimental conditions as at pH

6.0 and 6.5. Note in these figures that under these two different intensities of flocculation,

measurable differences of flocculation kinetics are still observed during the 30 min of

flocculation time. The flocculation index results show a substantial difference in process
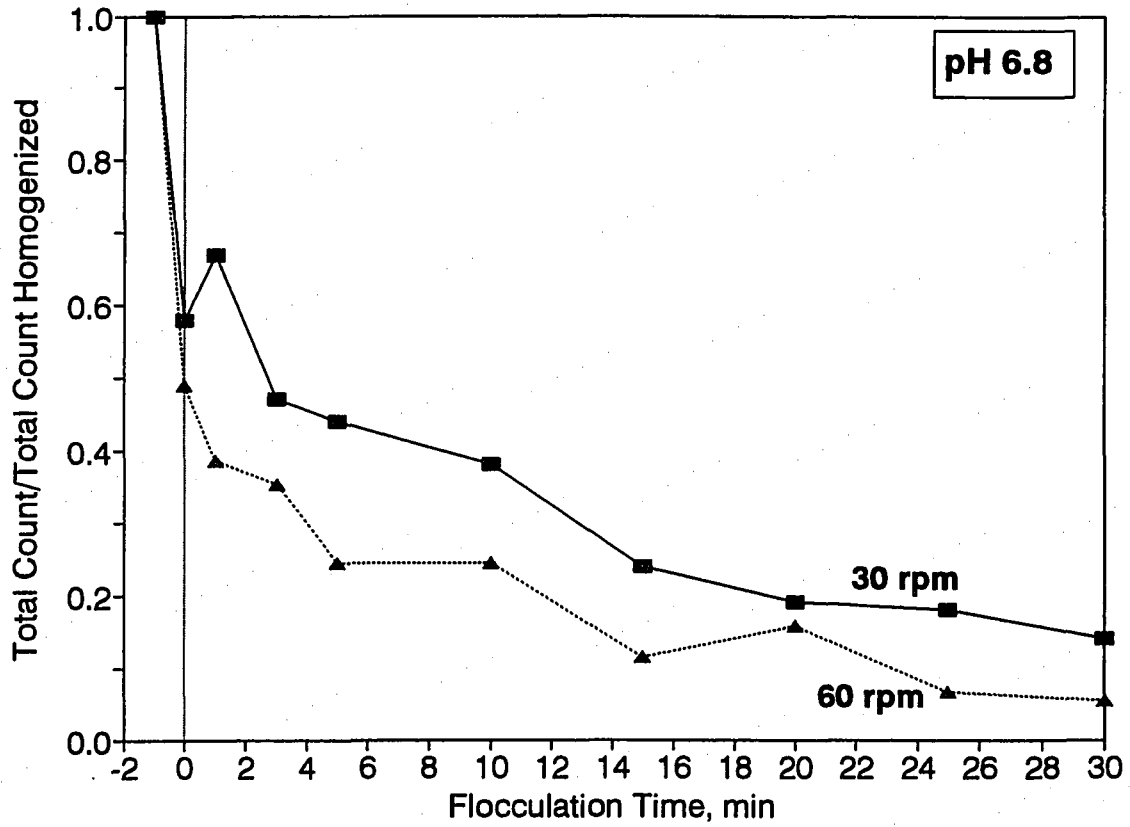
Figure 5.16. Effect of flocculation mixing intensity on the rate of flocculation (pH: 6.8, clay: 25 mg/L, dose: 5 mg/L)
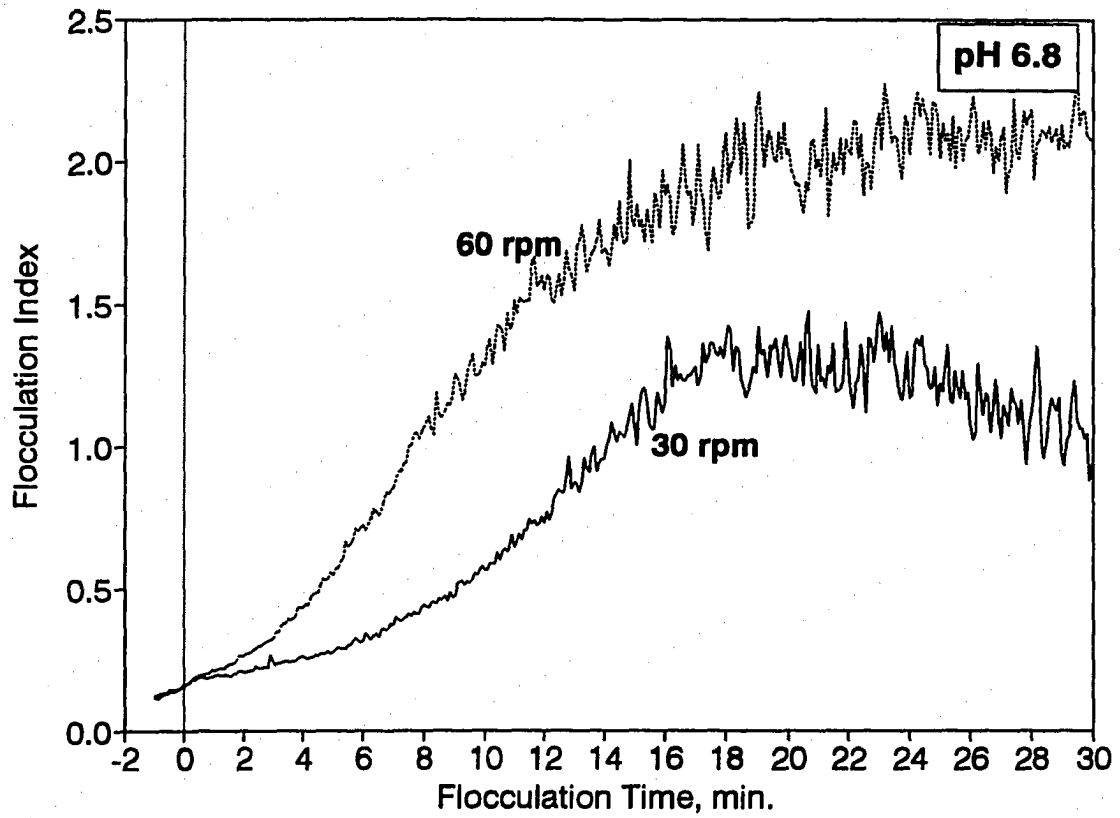
Figure 5.17. Effect of flocculation mixing intensity on the rate of flocculation (pH: 6.8, clay: 25 mg/L, dose: 5 mg/L)
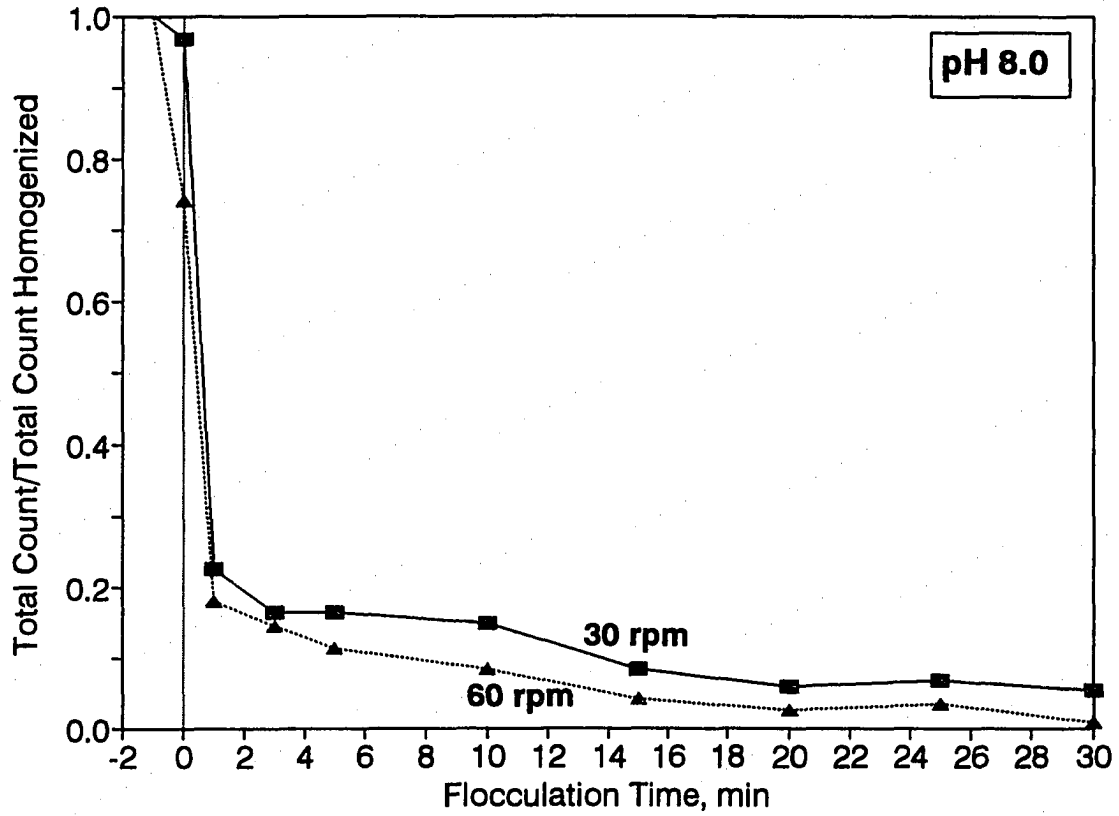
Figure 5.18. Effect of flocculation mixing intensity on the rate of flocculation (pH: 8.0, clay: 25 mg/L, dose: 5 mg/L)
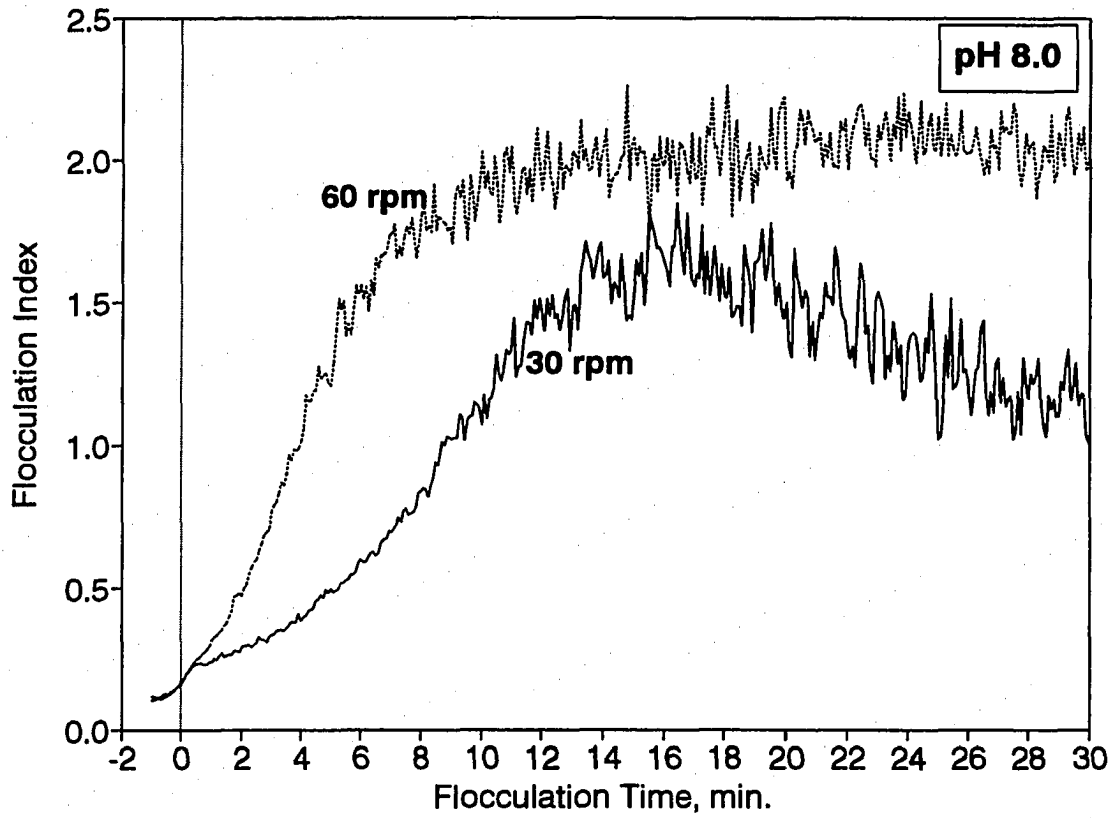
Figure 5.19. Effect of flocculation mixing intensity on the rate of flocculation (pH: 8.0, clay: 25 mg/L, dose: 5 mg/L)

kinetics at both pH 6.8 and 8.0 at the different mixing intensities; whereas the observed

differences of the rate of flocculation expressed by the disappearance of primary particles

become smaller as pH increases. Comparison of the flocculation kinetics data obtained by

using the AIA with the PDA showed that the increase in mixing speed caused an decrease in

the number of primary particles, but, it also caused a decrease in the number of larger flocs.

For example, under the favorable flocculation conditions at pH 6.8 and 8.0, the average

maximum size of flocculating particles reached to > 500 μm at 30 rpm and < 250 μm at 60

rpm.

The flocculation kinetics data, thus far presented, as shown in Figures 5.8 to 5.19

demonstrated that both the particle size distribution data obtained from the AIA and the on-

line measurement of turbidity fluctuation by the PDA provided reliable and sensitive

indications of flocculation kinetics, as evidenced by the rate of disappearance of primary

particles and the rate of aggregation of particles. The AIA gave the best indication of the rate

of primary particle disappearance; whereas, the PDA flocculation index gave the best

indication of the rate of larger floc formation.

Figures 5.20 and 5.21 present the rate of flocculation over the pH range 6.0 to 8.0 for

50 and 100 mg/L of clay concentration at 30 and 45 rpm of slow mixing intensities,

respectively. At these higher clay conditions, again, the dramatic impact of pH on flocculation

kinetics is apparent; resulting in steeper slopes (i.e., more rapid flocculation) at the three

higher pH levels. These results show that flocculation occurred rapidly during the first few

minutes of the process at the three higher pH levels. As the particles became larger and the
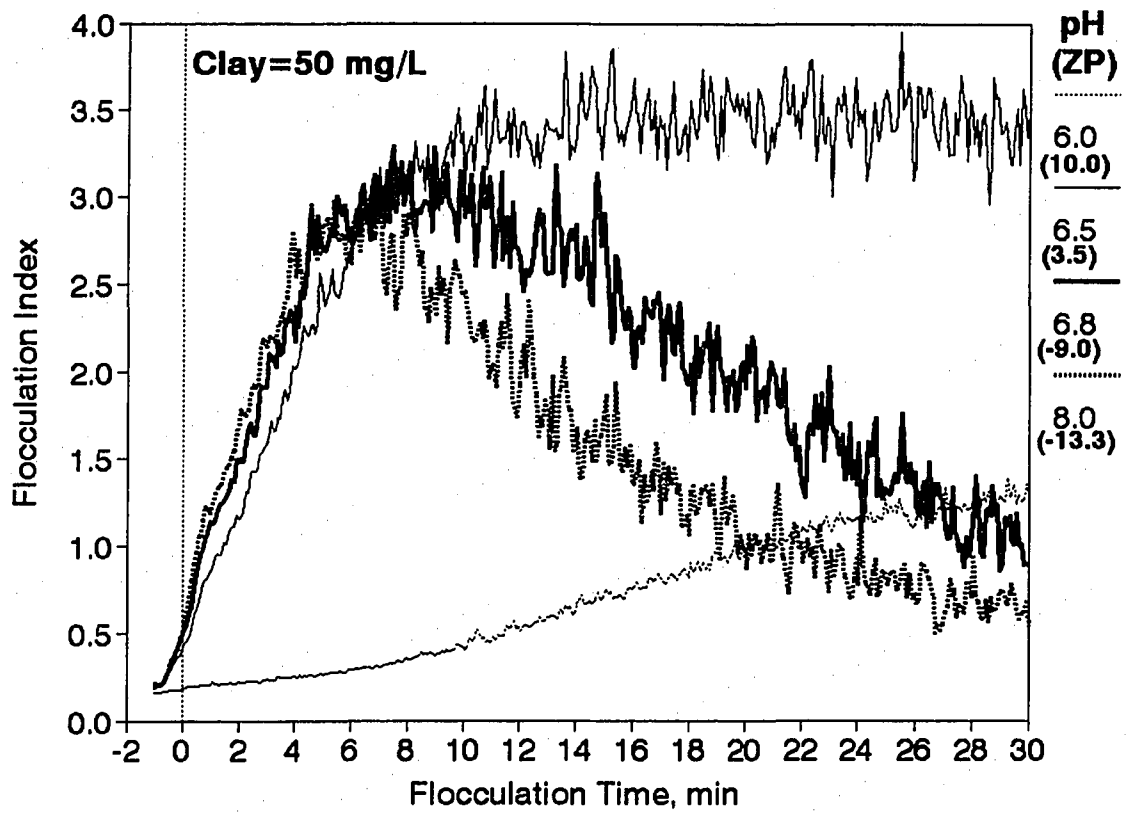
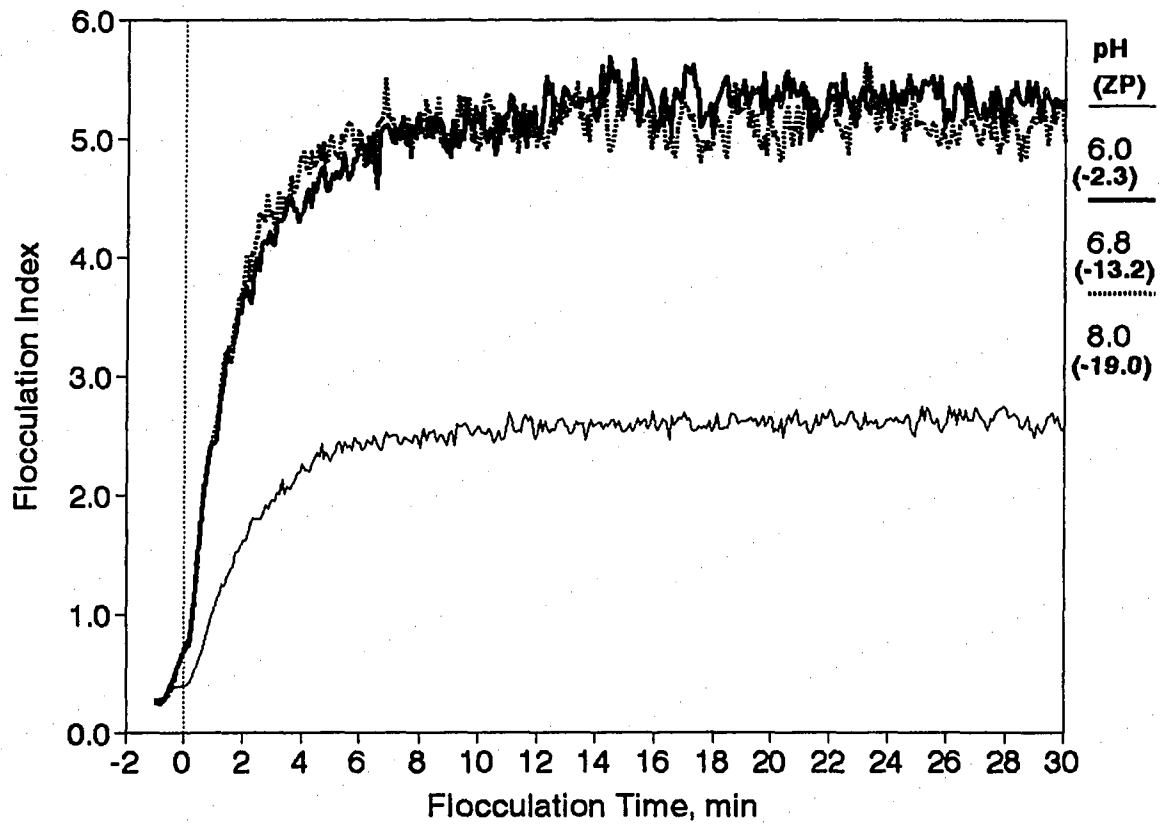Figure 5.20. Effect of pH on the rate of flocculation (clay: 50 mg/L, dose: 5 mg/L, 30 rpm)

Figure 5.21. Effect of pH on the rate of flocculation (clay: 100 mg/L, dose: 5 mg/L,45 rpm)

concentrations of particles in suspension was reduced, the kinetics of flocculation was slowed

down owing to decrease in particle collision frequency.

It should be noted in Figure 5.20 that the marked decrease in the flocculation index at

pH 6.8 and 8.0 starting at 6 to 8 minutes is due to sedimentation of the larger floc at this

mixing intensity. It is apparent that the largest flocs were produced at pH 8.0, a fact that was

confirmed using a low power hand held microscope to observe the floc. For example, the

observed average maximum size of flocs was around 600 μm and 800 μm at pH 6.8 and 8.0,

respectively. The loss of these floc particles due to settling also diminishes the collision

opportunities with remaining primary particles. This problem of settling of larger floc is largely

absent in Figure 5.21 due to higher mixing intensity. It is noted for 50 mg/L clay concentration

that the rate of flocculation at pH 6.0 is substantially slower than at higher pH, probably

caused either by the restabilization due to charge reversal or by insufficient amount of iron

precipitates which can provide enhanced particle-particle interaction. At higher pH, the

difference in the kinetics is diminished. For 100 mg/L of clay concentration as shown in Figure

5.21, the ZP values indicate that complete charge neutralization was not achieved, nor

necessary, at 5 mg/L of coagulant dose. Thus, the improvement of flocculation kinetics with

increasing suspension pH is evident in spite of a more negative charged particles obtained at

the higher pH.

An interesting feature in the flocculation index plots shown in Figure 5.21 is the

different maximum flocculation index reached at different pH. The maximum in the observed

flocculation index indicates that the flocs eventually reach a limiting size due to the

comparative rates of floc aggregation and breakup, depending on the mixing intensity and the floc strength. Therefore, the substantial difference in maximum flocculation index observed at between pH 6.0 and 6.8 may indicate that the difference in floc strength is strongly dependent on the system chemistry, such as solution pH in this case. For example, the flocs formed at pH 6.0 are much weaker than those formed at the higher pH's.

Comparing flocculation kinetics and ZP values, thus far presented, observed at between pH 6.0 and higher pH's may suggest that the poorer kinetics at pH 6.0 was caused either by the restabilization of particles or by lack of iron precipitate solids, or by both factors. To evaluate this issue, the surface charges of clay particles were brought to complete neutralization by using 1 mg/L of coagulant dose at pH 6.0. The results are presented in Figures 5.22 and 23. The ZP value under these experimental conditions was near zero (ZP= -1.0 mV). As shown in Figure 5.22, under the different mixing intensities, a substantial difference in the rate of disappearance of primary particles is apparent; whereas, the difference in the rate of floc growth is insignificant , as shown in the changes in flocculation index in Figure 5.23. In the aspect of floc growth as evidenced in Figure 5.23, the rate of floc growth is quite slow even under the conditions of the favorable surface charge and the enhanced particle transport due to the higher intensity of flocculation. Therefore, these results suggest that complete charge neutralization, even with the help of better mixing conditions, is not sufficient to improve the rate of aggregation of particles. This demonstrates, once again, the important role of iron precipitate in enhancing flocculation kinetics.

In order to elucidate the influence of the coagulation mechanism on the rate of flocculation, the flocculation kinetics for 50 mg/L clay concentration are compared using
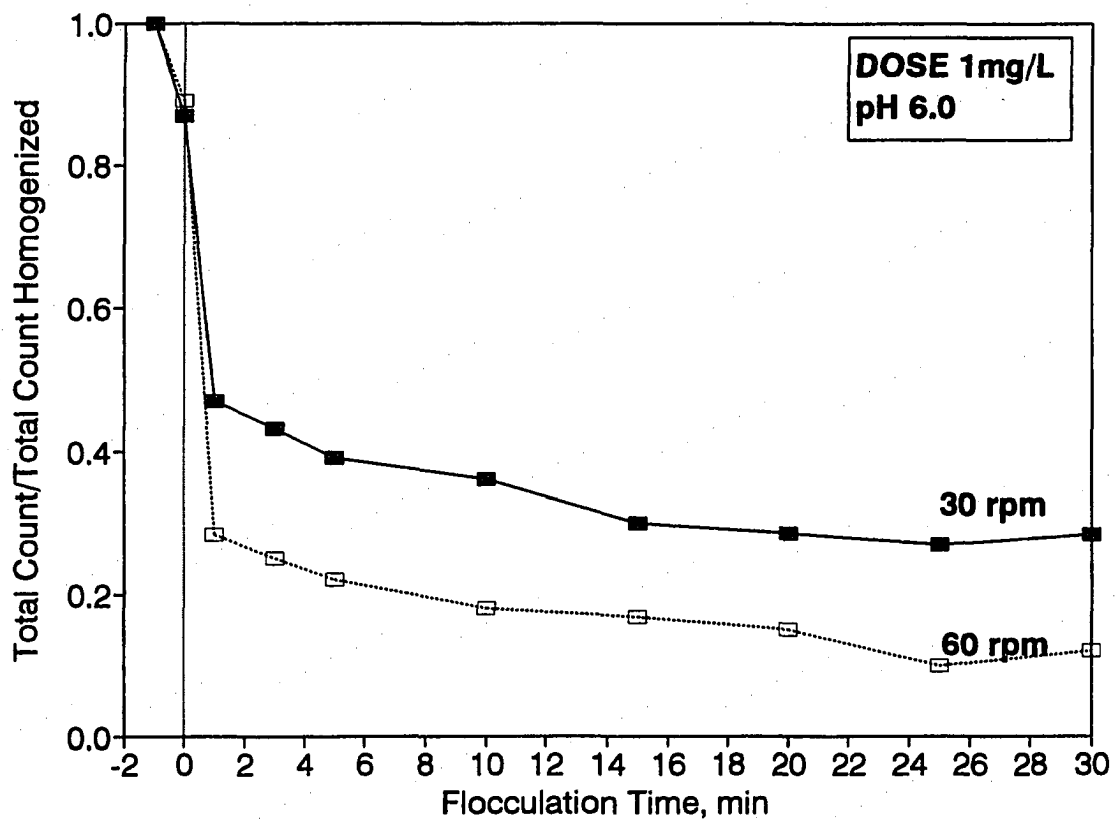
Figure 5.22. Effect of flocculation mixing intensity on the rate of flocculation (pH: 6.0, clay: 25 mg/L, dose: 1 mg/L)
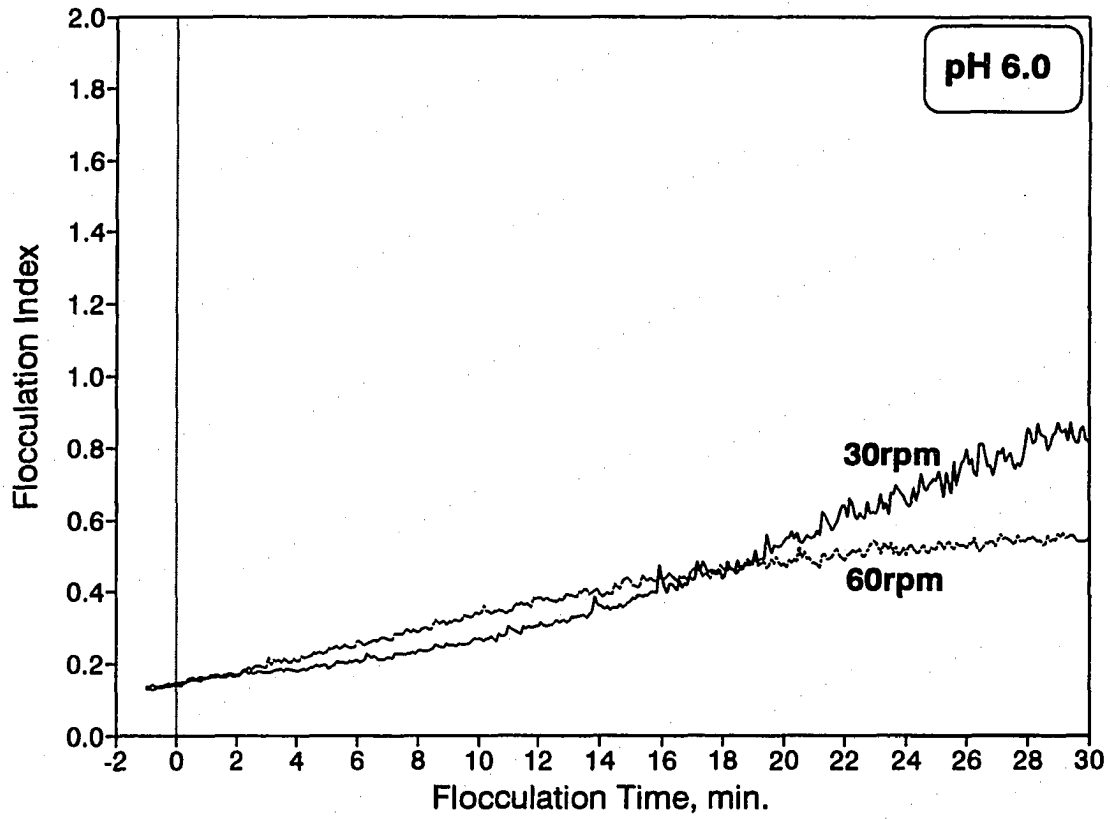
Figure 5.23. Effect of flocculation mixing intensity on the rate of flocculation (pH: 6.0, clay: 25 mg/L, dose: 1 mg/L)

different coagulant dosages at pH 6.0 as shown in Figure 5.24. The curves in this figure

indicate that particle aggregation is slightly more rapid at 2 mg/L dose than 1 mg/L dose. At

or above 3 mg/L dose, the rate of flocculation is significantly reduced, probably attributed to

charge restabilization of particles in suspension. This result confirmed that the overall process

of particle aggregation at pH 6.0 was caused mainly by adsorption-destabilization of the clay

suspension by the addition of hydrolyzed Fe(III) species. It is also interesting to note that a

substantial difference in the rate of flocculation was observed in just 1 mg/L of coagulant

dosage difference between 2 and 3 mg/L. This suggests that under the A/D coagulation

mechanism predominant at pH 6.0, the efficient flocculation is very sensitive to the amount of

coagulant dosage applied to the clay suspension.

Comparison between experimental results presented thus far leads to the following

conclusion. Under the different clay concentrations investigated, the chemical conditions that

cause rapid precipitation of Fe(III) species and subsequent aggregation of particles are

significantly more important than charge neutralization caused by soluble hydrolyzed Fe(III)

products. The mechanism of destabilization caused mainly by the interaction between the clay

particles and the soluble Fe(III) hydrolysis products would only be important in the

aggregation of particles at lower pH.

5.2.2 Effects of sulfate ion

Figure 5.25 illustrates the ZP changes of kaolin particles without adding coagulant at

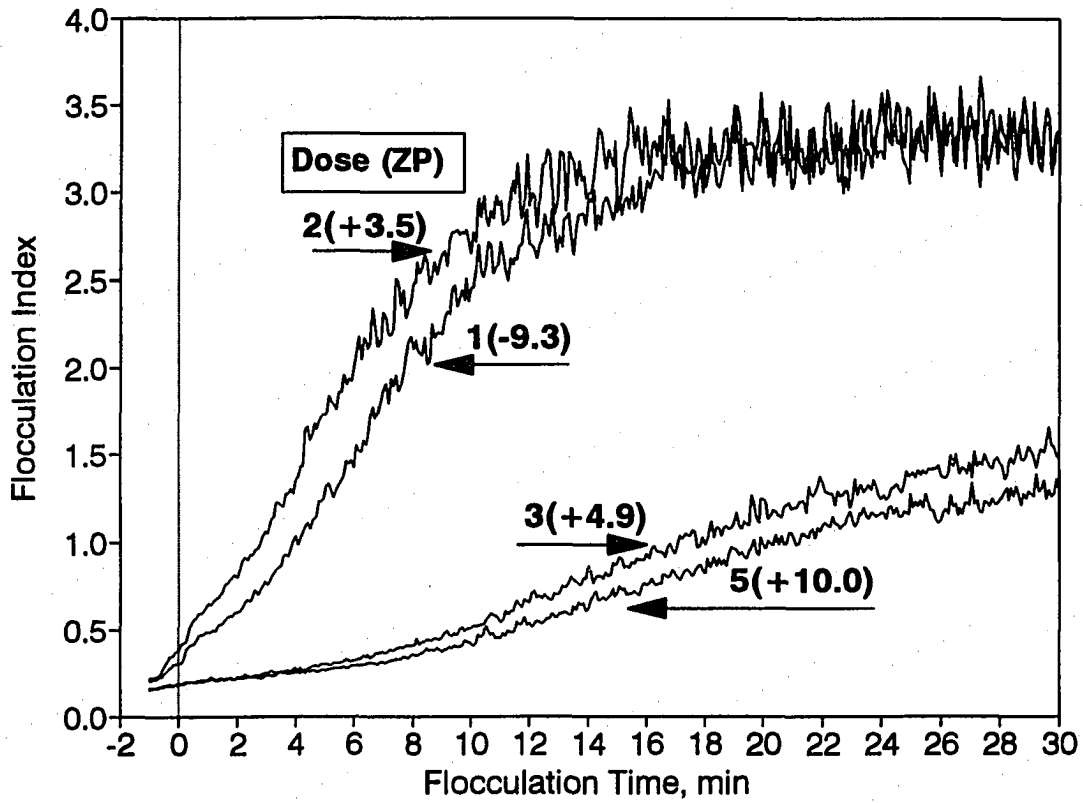various pH values; in addition, the ZP of kaolin particles in the presence of 10^{-3} M of sulfate

Figure 5.24. Effect of coagulant dose on the rate of flocculation (pH: 6.0, clay: 50 mg/L, flocculation: 30 rpm)
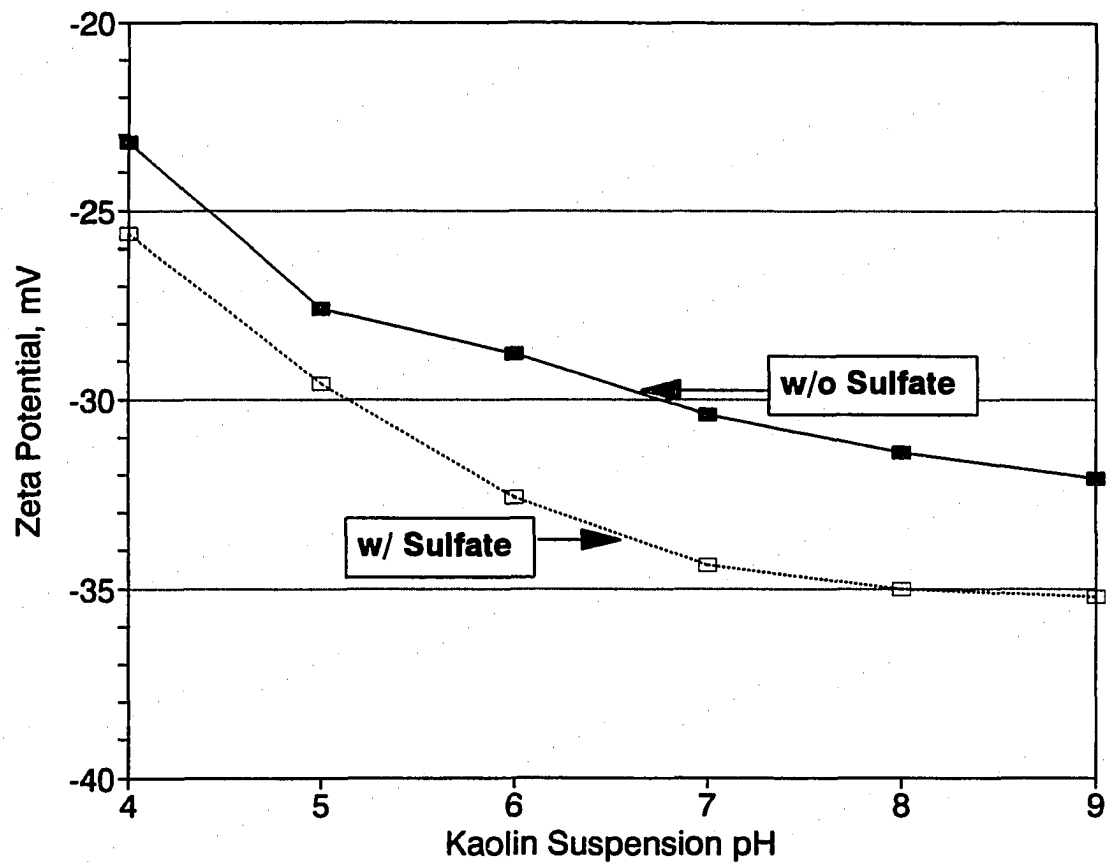
Figure 5.25. Zeta potential of kaolin as a function of suspension pH without and with 10^{-3} M sulfate ion

ion without adding coagulant in the same test water is also plotted. Each ZP value in the plots represents the average of triplicate measurement. Total ionic strength was maintained 5 X 10^{-3} M with an addition of appropriate amount of NaNO₃ in distilled water. In the preliminary tests, the ions dissolved by the addition of NaNO₃ have been found to be an indifferent electrolyte ions which do not cause any significant changes on the surface charges of particles because they are not specifically adsorbed on the particle surface. The ZP values in Figure 5.25 indicate that the sulfate ion reduces the magnitude of the ZP of kaolin almost uniformly, approximately 3 to 4 mV increase in negative ZP over the entire pH range studied. The decrease in ZP which occurs due to the addition of sulfate ion suggests that the sulfate ions are able to adsorb onto the surface of kaolin particles in the absence of coagulant. However, in the absence of coagulant, the influence of pH on the extent of adsorption of sulfate on kaolin particles appears to be insignificant. As mentioned earlier in Section 4, the changes in ionic strength between 10^{-3} to 10^{-2} M with the addition of NaNO₃ alone did not affect the ZP values of kaolin particles and did not induce any coagulation of kaolin particles.

Most of the comparisons of flocculation kinetic results presented herein are based on the rate of changes in flocculation index and ZP values as a function of suspension pH and sulfate concentrations to investigate the effect of sulfate on coagulation mechanism and flocculation index.

Figures 5.26 and 5.27 represent the rate of flocculation expressed by the flocculation index against mixing time without and with the addition of 10^{-3} M SO_4^{2-} using 25 mg/L clay concentration at different pH levels. In fact, Figure 5.26 was already presented earlier as a Figure 5.9 in which the dramatic impact of suspension pH on the rate of flocculation was
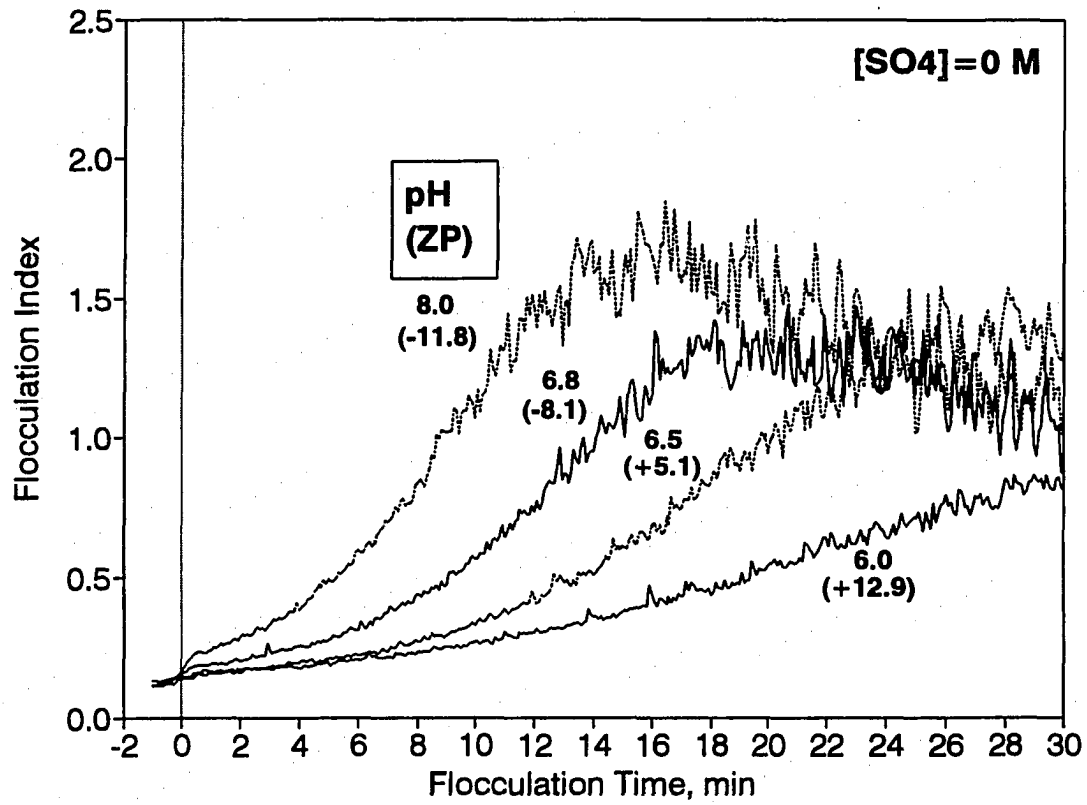
Figure 5.26. Effect of sulfate on the rate of flocculation (clay: 25 mg/L, dose: 5 mg/L, 30 rpm); without using sulfate
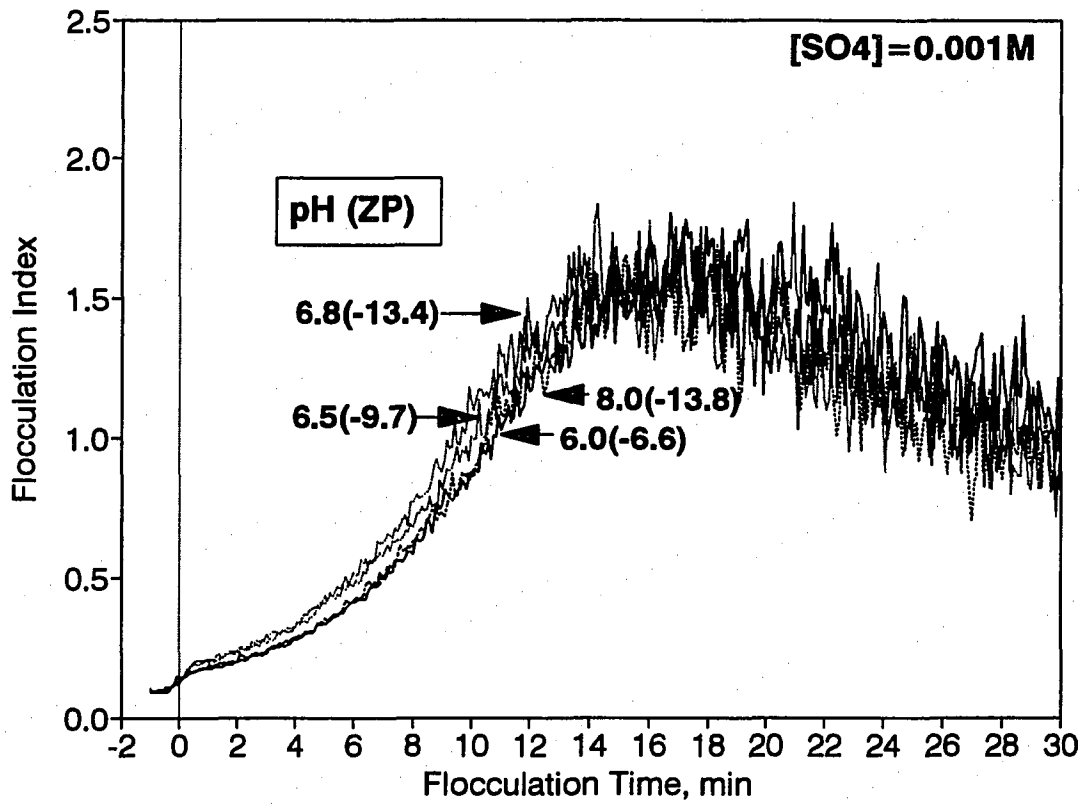
Figure 5.27. Effect of sulfate on the rate of flocculation (clay: 25 mg/L, dose: 5 mg/L, 30 rpm); using 0.001 M SO_4^{2-}

demonstrated. It is noteworthy that in the presence of 10^{-3} M SO_4^{2-}, the dramatic impact of suspension pH on the rate of flocculation is substantially eliminated as shown in Figure 5.27. As noted in the figures, the sulfate eliminates the positive ZP at lower pH and slightly increases the negative ZP at higher pH levels. The plots in Figure 5.27 indicate that the kinetics at all pH levels converge on the best kinetics observed in Figure 5.26. It is also noted that the negative ZP values resulting from the sulfate addition did not impair flocculation kinetics. Another interesting feature in the flocculation index curves and the ZP values in each curve as shown in Figures 5.26 and 5.27 is that the dramatic impact of sulfate on flocculation kinetics and the reduction of ZP induced by the addition of sulfate ion are quite different at different pH levels. Thus, more significant impact on flocculation kinetics and more reduction in ZP are apparent at the more acidic pH level, which suggests that the influence of sulfate ion on surface charge of flocs is greater at lower pH values.

Plots of flocculation index as a function of flocculation time for 50 mg/L kaolin are presented in Figures 5.28 and 5.29 at pH 6.0 and 6.5, respectively. In addition, Figures 5.28 and 5.29 contain the evidences of floc strength at different sulfate concentrations. For the floc breakup test, as described in Section 4 previously, the flocs formed during 30 min of flocculation time were subjected to 2 min of 250 rpm of mixing intensity, which is used for rapid mixing to cause partial breakup. Therefore, the beginning of the floc breakup process appears in the figures after 30 min of flocculation time. The plots in Figures 5.28 and 5.29 show, once again, the pronounced effect of sulfate on the rate of flocculation. At pH 6.0 in Figure 5.28, the presence of 10^{-3} M sulfate greatly speeds up the rate of flocculation; whereas, at pH 6.5 in Figure 5.29, it has little impact on flocculation kinetics. It is noted in Figure 5.28
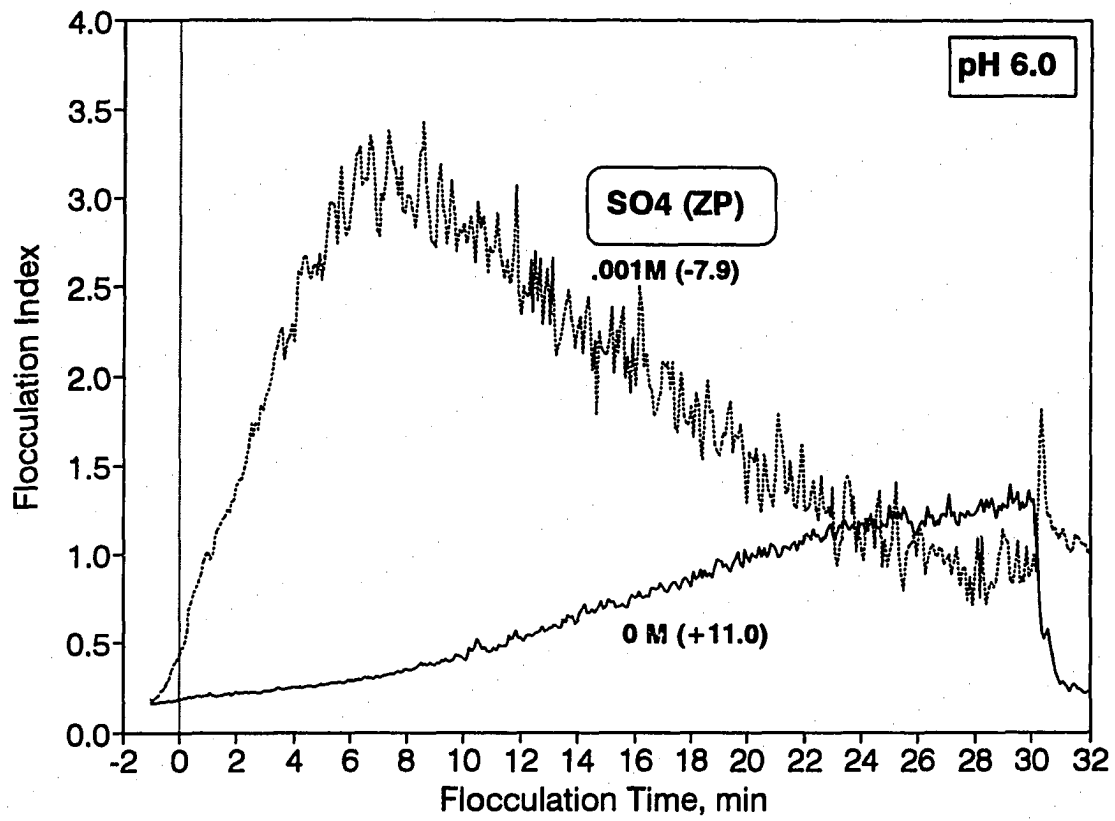
Figure 5.28. Effect of sulfate on the rate of flocculation (pH 6.0, clay: 50 mg/L, dose: 5 mg/L, 30 rpm)
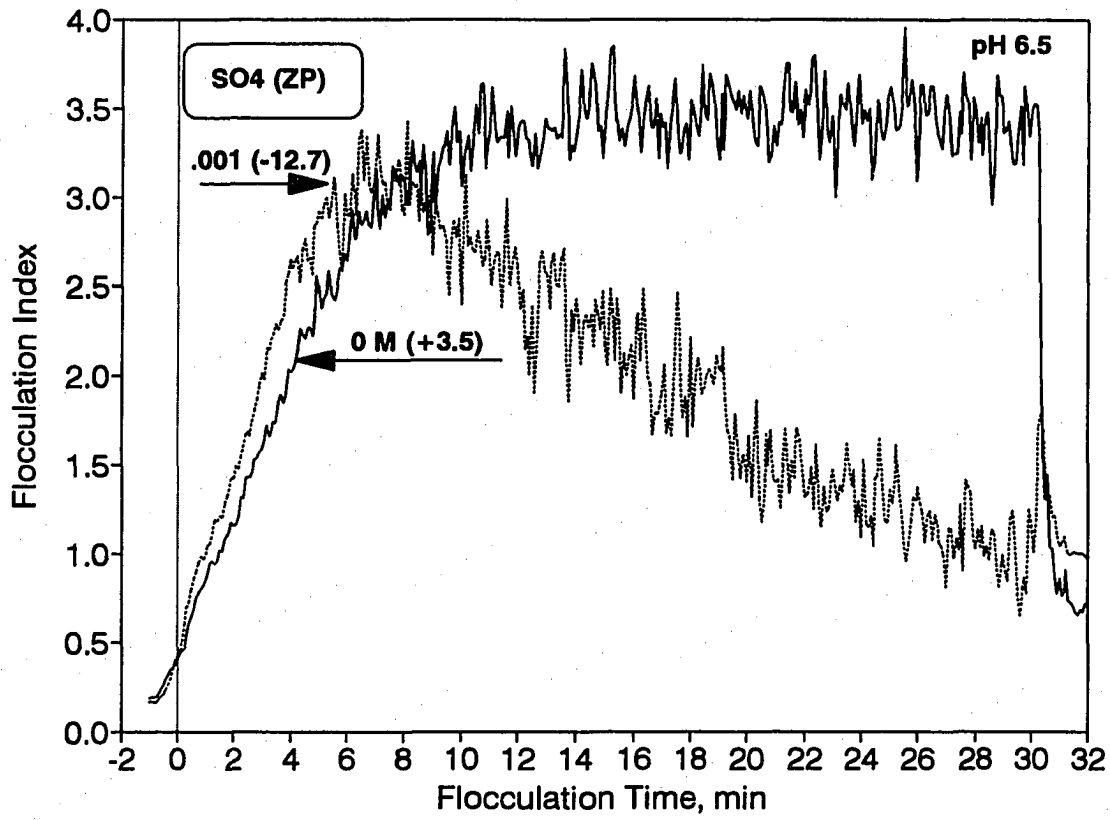
Figure 5.29. Effect of sulfate on the rate of flocculation (pH 6.5, clay: 50 mg/L, dose: 5 mg/L, 30 rpm)

that in the absence of sulfate, the maximum flocculation index was not attained until 30 min after starting flocculation. But, in the presence of sulfate, the flocculation index was reached maximum at about 7 min of flocculation time followed by a substantial decrease, which is mainly caused by the settling of bigger sized flocs during the flocculation process. However, Figure 5.29 shows that even though the sulfate did not cause significant impact on the initial rate of flocculation, it had substantial impact on the shape of flocculation index curve after 8 min of flocculation time. Since the settled flocs lead to the decrease in flocculation index, much more flocs appears to settle down in the presence of sulfate, suggesting heavier flocs formed in the presence of sulfate. Comparison of Figures 5.28 and 5.29 shows that the flocculation kinetics on the acidic side are greatly improved if an appropriate amount of sulfate ion is present. It is noteworthy that the breakup data presented in Figures 5.28 and 5.29 show that the flocs formed at faster kinetic conditions in the presence of sulfate were stronger than the those formed without sulfate. This is evident by higher flocculation index values after the breakup operation.

Plots of flocculation index as a function of flocculation time for 50 mg/L kaolin are presented in Figures 5.30 and 5.31 at pH 6.8 and 8.0, respectively, but otherwise under the same experimental conditions as at pH 6.0 and 6.5. As shown in these figures, as the flocculation process proceeds, the flocculation index substantially increases rapidly up to a certain maximum values as a result of fast growing of flocs. The plots in the figures indicate that the dramatic impact of sulfate ion on the rate of flocculation, which was apparent at pH 6.0 and 6.5, is not evident at higher pH levels. Furthermore, Figure 5.31 shows that the presence of sulfate becomes detrimental to the rate of flocculation at pH 8.0. Once again, the
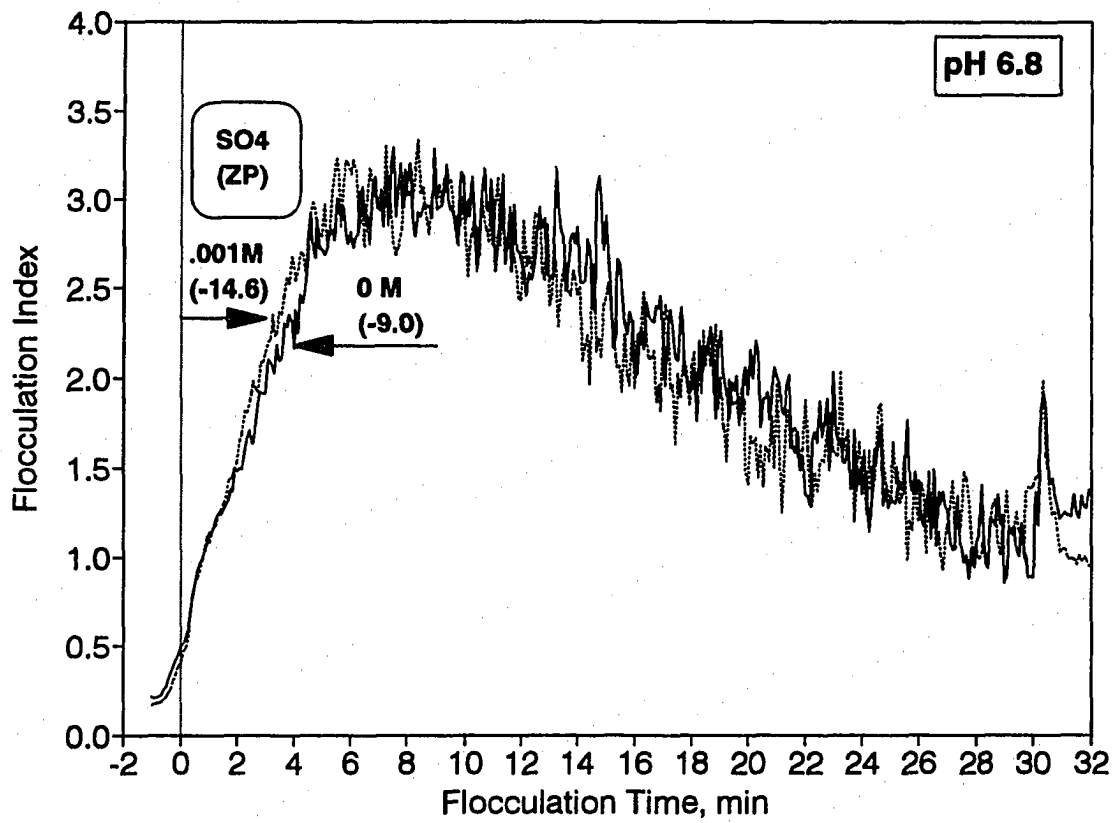
Figure 5.30. Effect of sulfate on the rate of flocculation (pH 6.8, clay: 50 mg/L, dose: 5 mg/L, 30 rpm)
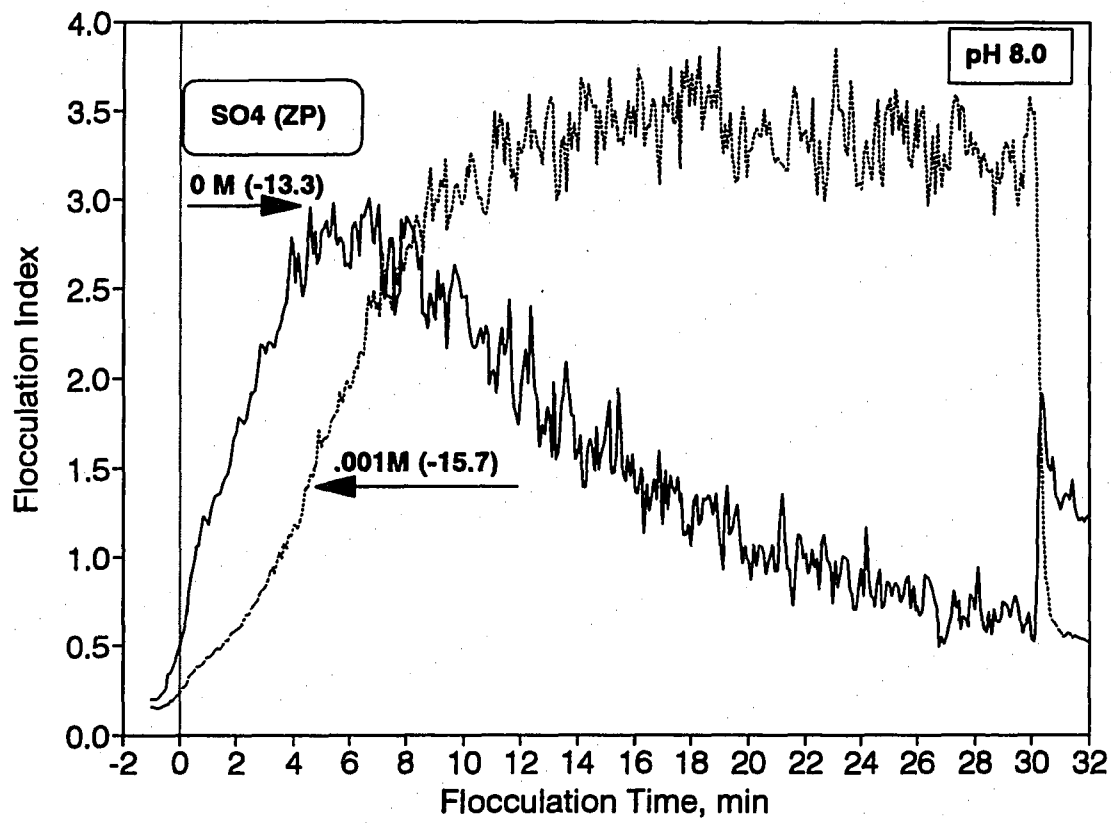
Figure 5.31. Effect of sulfate on the rate of flocculation (pH 8.0, clay: 25 mg/L, dose: 5 mg/L, 30 rpm)

ZP values in Figures 5.30 and 5.31 indicate that the ZP of the particles becomes substantially more negative when sulfate is present. However, the changes in ZP did not affect the rate of flocculation at pH 6.8, but rather adversely affected the rate of flocculation at pH 8.0. These results suggest that there might be a certain limit of critical ZP ranges and pH levels at which the presence of sulfate is beneficial to the aggregation of particles. It is also interesting to note that the presence of sulfate which helped form stronger flocs at pH 6.0 and 6.5 deteriorated the strength of flocs formed at pH 6.8 and 8.0. Therefore, comparing the floc breakup data observed at pH 6.0 and 6.5 with those at pH 6.8 and 8.0 suggests that the effectiveness of sulfate to strengthen the flocs also greatly varied with pH range.

Through the discussion from the preceding data, it is obvious that sulfate ion added into the kaolin suspension played an important role in the flocculation process, not only improving flocculation kinetics at more acidic pH levels but also significantly changing surface charge of particles. This brings us to the question how sulfate ion influences flocculation kinetics. There were two important roles of sulfate on the coagulation process when using a metal salt coagulant:

- Sulfate may destabilize a suspension already restabilized by an excess adsorption of highly positive charged species
- Sulfate may enhance the rate and extent of metal hydroxide precipitation

To evaluate the relative importance of these two roles, the net negative charge of 50 mg/L kaolin was brought to near neutral ZP and less negative ZP using 2 mg/L of coagulant

dose at pH 6.0 and 6.5 either with or without adding 10^{-3} M sulfate into the clay suspension. Two additional observations were also utilized in these experiments. The supernatant turbidity during sedimentation after 30 min of flocculation and the changes in aggregates volume distributions during the flocculation process were observed to gather additional evidence on the differences in the flocculation kinetics and the reliability of flocculation index used in this study. As shown in Figure 5.32, at pH 6.0, the use of sulfate in the flocculation process results in more negative charges of particles but results in a faster rate of flocculation. However, the pronounced influence of sulfate on flocculation process disappeared with just 0.5 unit increase in pH, as evident in Figure 5.33, even though it still significantly affected surface charges of particles. The ZP values observed at pH 6.0 indicate that the flocculation kinetics was much faster at far more negative ZP values under the same coagulant dose applied. Therefore, it may be concluded that the kinetics of flocculation could be improved mainly by enhanced formation of Fe(III) precipitate attributed to the addition of sulfate, and thereby, better particle collision frequency, but not by favorable surface charges (i.e., ZP close to zero) for flocculation. At pH 6.5, the observation that the flocculation kinetics are indifferent to the presence of sulfate may be explained by considering the mechanism of coagulation at this pH. The clay particles are probably destabilized by the interaction with iron hydroxide precipitates to some extent at pH 6.5, at which the sulfate could not help the formation of additional iron precipitate. Our experimental results confirm those of earlier investigations which suggest the effect of sulfate as follows:
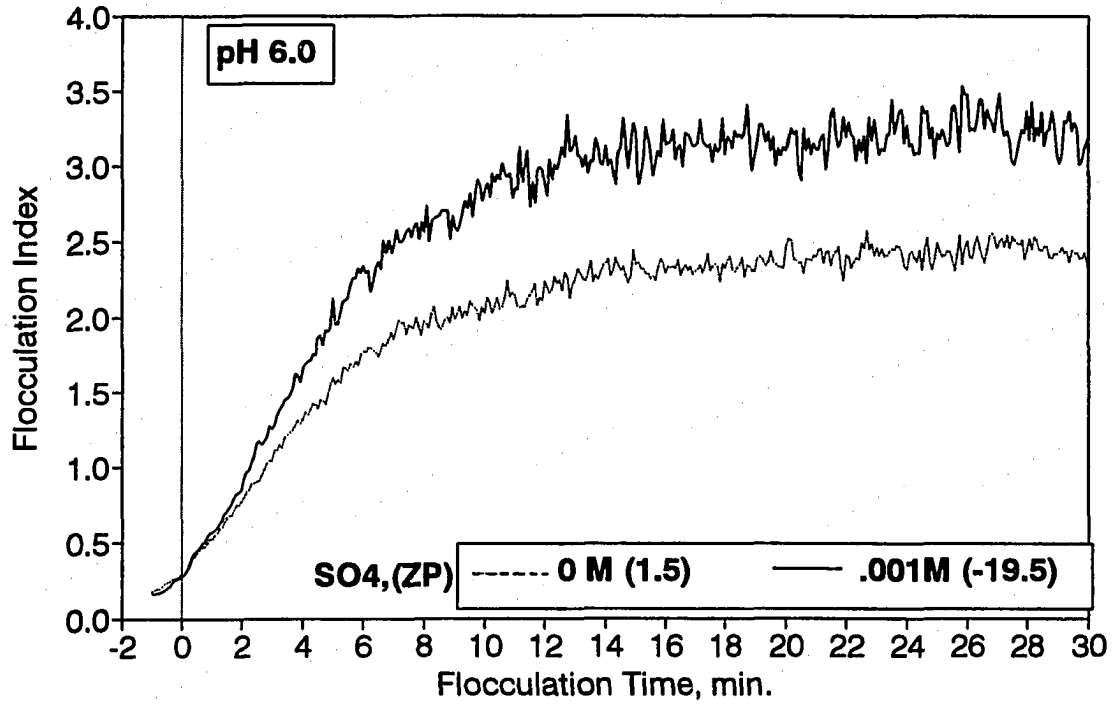
Figure 5.32. Effect of sulfate on the rate of flocculation (pH: 6.0, clay: 50 mg/L, dose: 2 mg/L, 45 rpm)
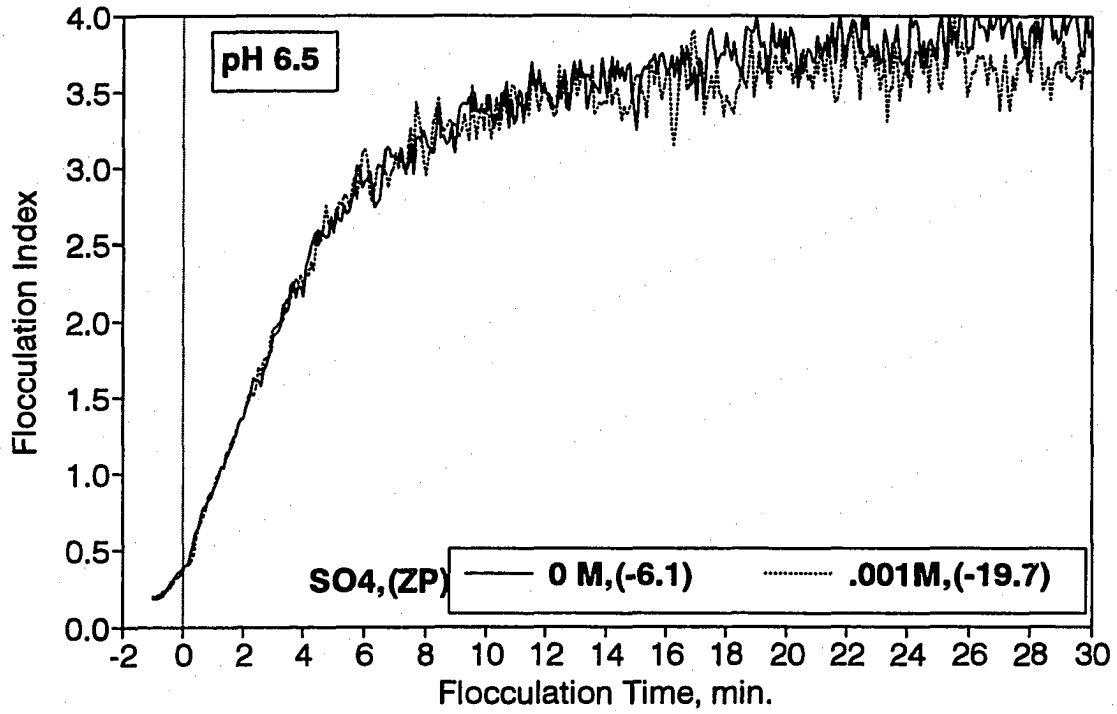
Figure 5.33. Effect of sulfate on the rate of flocculation (pH: 6.5, clay: 50 mg/L, dose: 2 mg/L, 45 rpm)

Insoluble aluminum hydroxo sulfato precipitate forms at a pH lower than necessary for the formation of the insoluble aluminum hydroxide since a lesser hydroxide ion concentration is required. Upon increasing pH, since sulfate ion is less basic than hydroxyl ion and is replaced by it with increasing pH, sulfate ion does not appreciably affect the complexion on the basic side (Hanna and Rubin, 1970, p. 321).

Figures 5.34 and 5.35 present the supernatant turbidity during sedimentation after 30 min of flocculation and the changes in aggregates volume distributions during the flocculation process. These experimental results were obtained during the same experiment presented in Figure 5.34 to illustrate the clear difference of flocculation kinetics and the reliability of flocculation index used in this study. The aggregates volume distribution were attained from the AIA using a low magnification setting (36x) of the microscope. Figure 5.34 indicates that the flocs formed under the conditions of better flocculation kinetics settled much faster. This result shows that the sulfate ion markedly improves the performance of flocculation under these experimental conditions. The difference in floc volume distribution at the different experimental conditions is shown in Figure 5.35. In general, Figure 5.35 shows that the presence of sulfate during the progress of flocculation resulted in a decrease in the volume of smaller particles and an increase in the volume of larger particles. This shift in the floc volume distribution indicates that the extent of changes in floc growth caused by the presence of sulfate ion is significant. These results shown in Figures .5.34 and 5.35 also demonstrate the reliable use of flocculation index as a means to study flocculation kinetics.
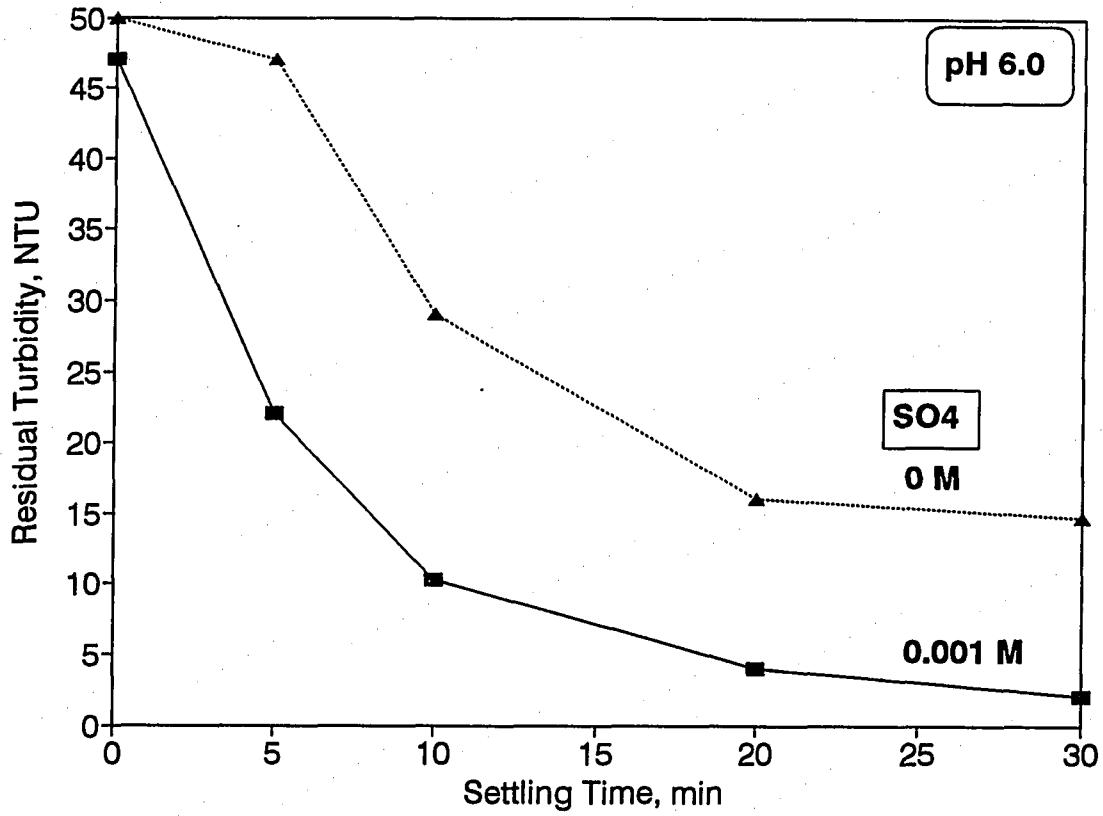
Figure 5.34. Effect of sulfate on the changes in residual turbidity against settling time (pH: 6.0, clay: 50 mg/L, dose: 2 mg/L, 45 rpm)
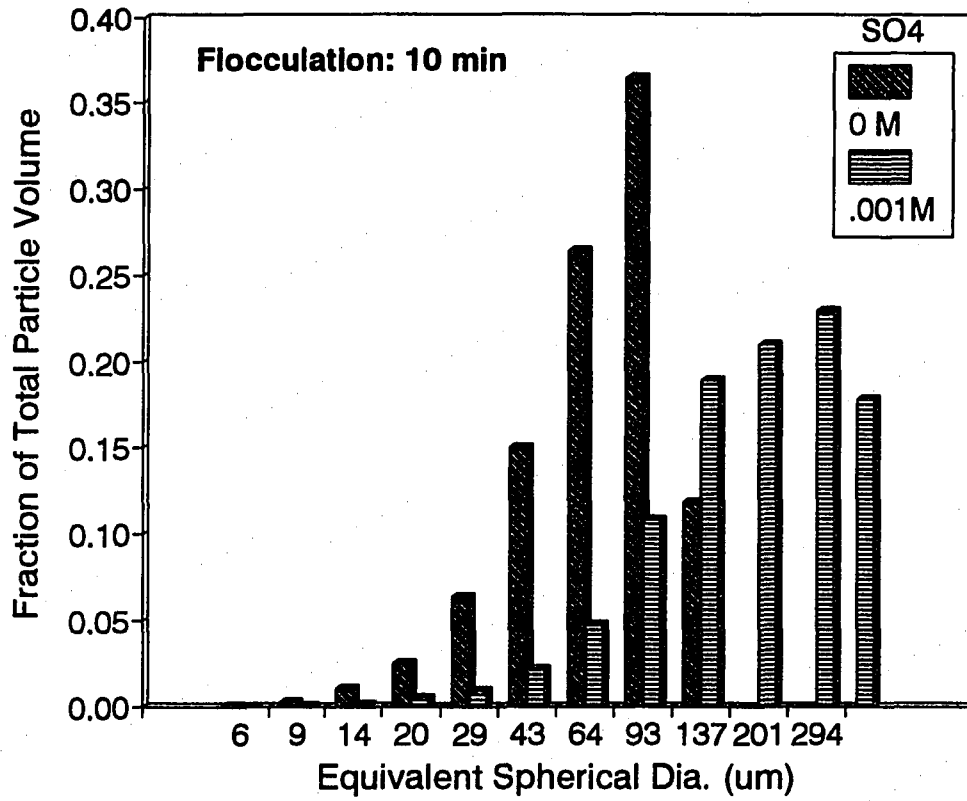
Figure 5.35. Effect of sulfate on the particle volume distributions of 10min flocculated suspensions. (pH: 6.0, clay: 50 mg/L, dose: 2 mg/L, 45 rpm)

Figures 5.36 and 5.37 show the experimental results for flocculation kinetics under different sulfate concentration at pH 6.0 and 8.0 using coagulant dose 1 and 5 mg/L, respectively. For these experimental results, some experimental parameters were chosen with caution so as to demonstrate the influence of sulfate on flocculation kinetics. The coagulant dosage of 1 mg/L was applied at pH 6.0 to bring about optimum destabilization conditions under A/D mechanism, i.e., ZP of particles was maintained to close to zero. In addition, 45 rpm of mixing intensity was applied during flocculation process to avoid any significant settling of flocs during the flocculation period. At pH 6.0 as shown in Figure 5.36, the presence of sulfate ion greatly speeds up the rate of flocculation. The increase in sulfate concentration beyond 3×10^{-4} M did not induce further improvement in flocculation kinetics, even though the higher concentrations of sulfate ion did increase the negative ZP values significantly. At pH 6.0, it is noteworthy that the flocculation kinetics is much better at higher negative charges caused by the addition of SO_4^{2-}. This result suggests that the better flocculation kinetics at poorer surface charge conditions may be explained by the enhanced particle collision opportunities with help of additional Fe(III) precipitates in the presence of sulfate. This confirms the results reported by several researchers who indicated that sulfate increased the amount of precipitate formation and enhanced the rate of precipitation from the metal salt coagulants. In contrast, as shown in Figure 5.37, the flocculation data at pH 8.0 indicate that the influence of sulfate on flocculation kinetics is essentially negligible at higher pH. This observation may be explained by a decreased adsorption of sulfate ion on particle surfaces at higher pH. The ZP measurements confirmed this conclusion. Thus, the changes in
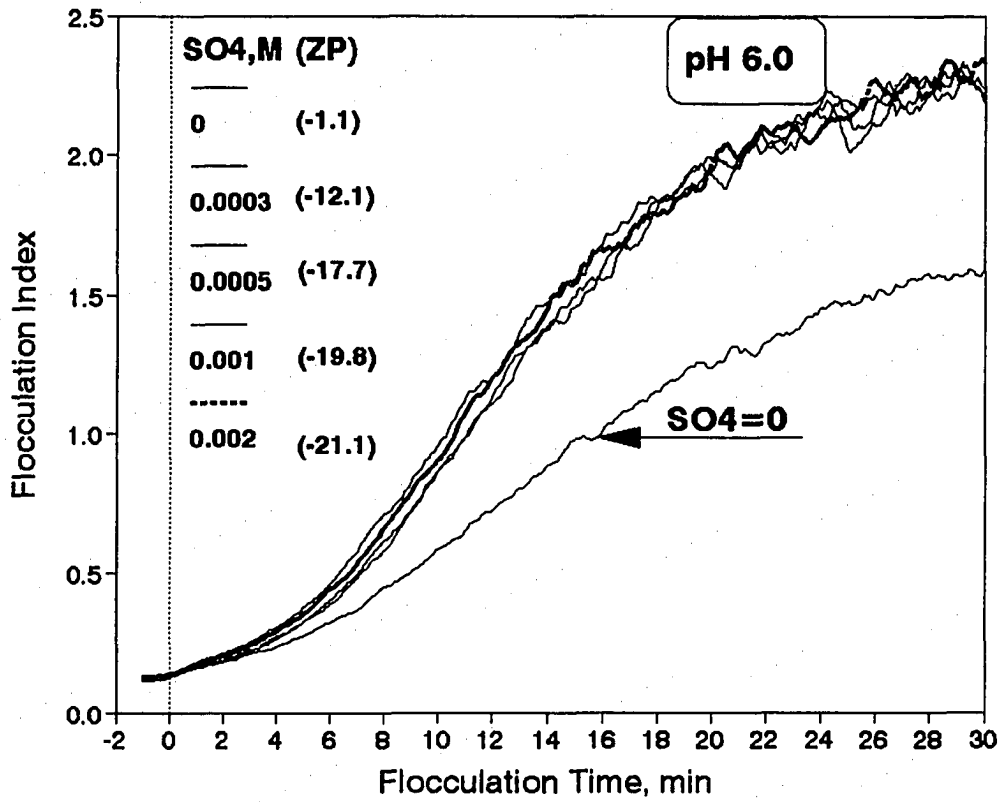
Figure 5.36. Effect of sulfate concentration on the rate of flocculation (pH: 6.0, clay: 25 mg/L, dose: 1 mg/L, 45 rpm)
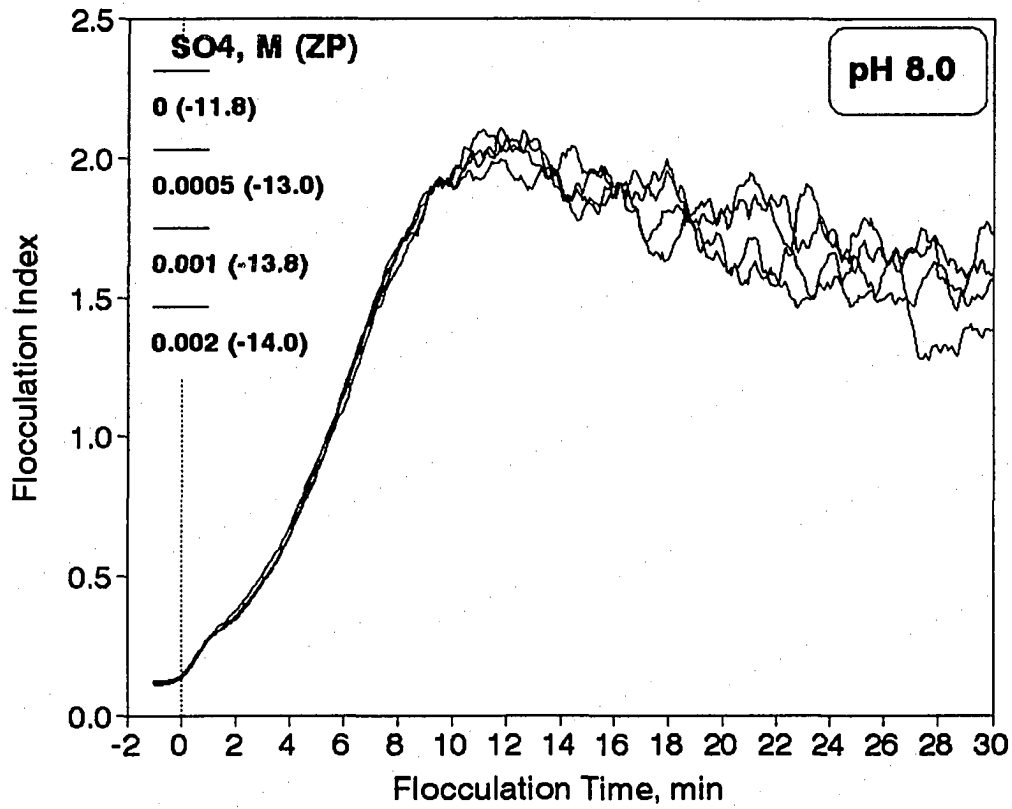
Figure 5.37. Effect of sulfate concentration on the rate of flocculation (pH: 8.0, clay: 25 mg/L, dose: 5 mg/L, 45 rpm)

surface charges of particles by the addition of sulfate at pH 8.0 were minimal compared to those at pH 6.0. The decrease in the amount of adsorbed sulfate at the higher $[OH^-]/[Al]$ ratio was noted by de Hek et al. (1978) and Dzombak and Morel (1991).

The effect of sulfate on the flocculation rate for higher clay concentration, 100 mg/L under the same experimental conditions except at pH 6.0 and 6.8, is shown in Figures 5.38 and 5.39, respectively. Again, these results clearly demonstrate the influence of pH on the degree of sulfate ion adsorption and the extent of changes in flocculation kinetics by sulfate ion. As shown in these figures, it is noted that the dramatic impact of sulfate on the rate of flocculation, which was observed at pH 6.0, was not evident at pH 6.8, even with the high clay concentration. Thus, the influence of sulfate on the flocculation process disappeared with 0.8 unit of pH change, even though it still significantly affected surface charges of particles. Once again, the ZP values in Figure 5.38 indicate that the flocculation kinetics is much faster at far more negative ZP values under the same applied coagulant dose. It is noteworthy that under high clay concentration, which may provide better particle collision frequency, the kinetics of flocculation was still improved by enhanced formation of precipitates attributed to the addition of sulfate, but not by favorable surface charges of particles (i.e., the ZP close to zero without sulfate) for flocculation. This result suggests that heterocoagulation and/or enmeshment interactions between clay particles and iron precipitates appear important for rapid flocculation kinetics under the all clay concentrations investigated herein.
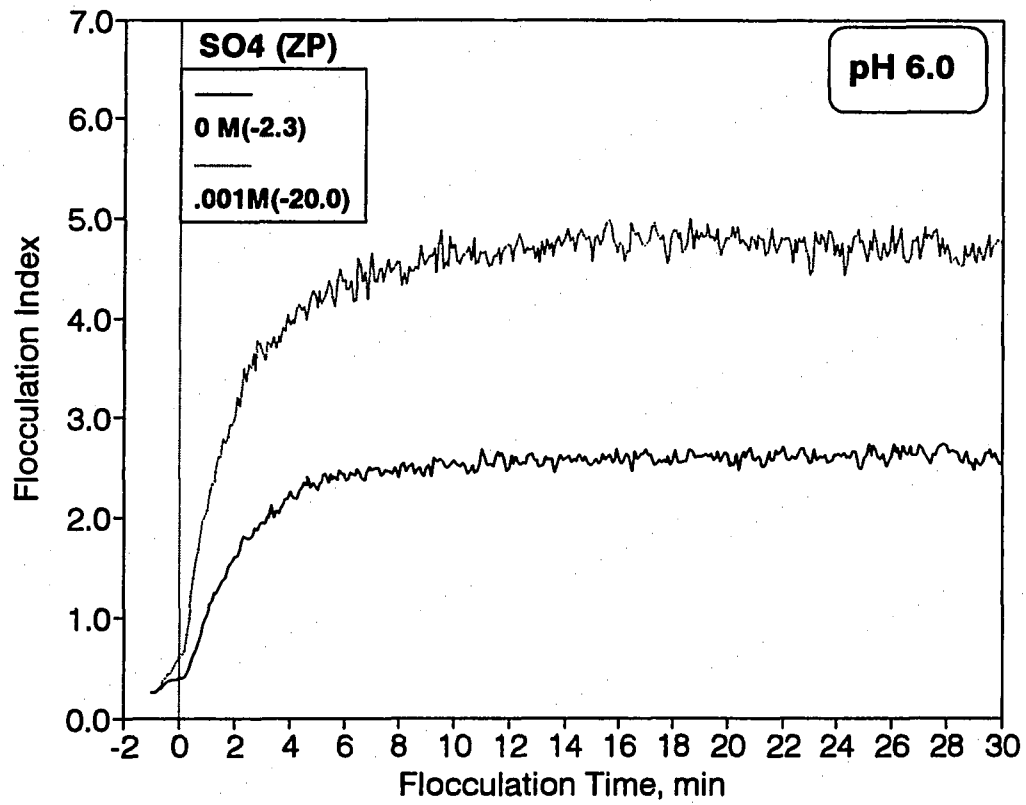
Figure 5.38. Effect of sulfate on the rate of flocculation (pH 6.0, clay: 100 mg/L, dose: 5 mg/L, 45 rpm)
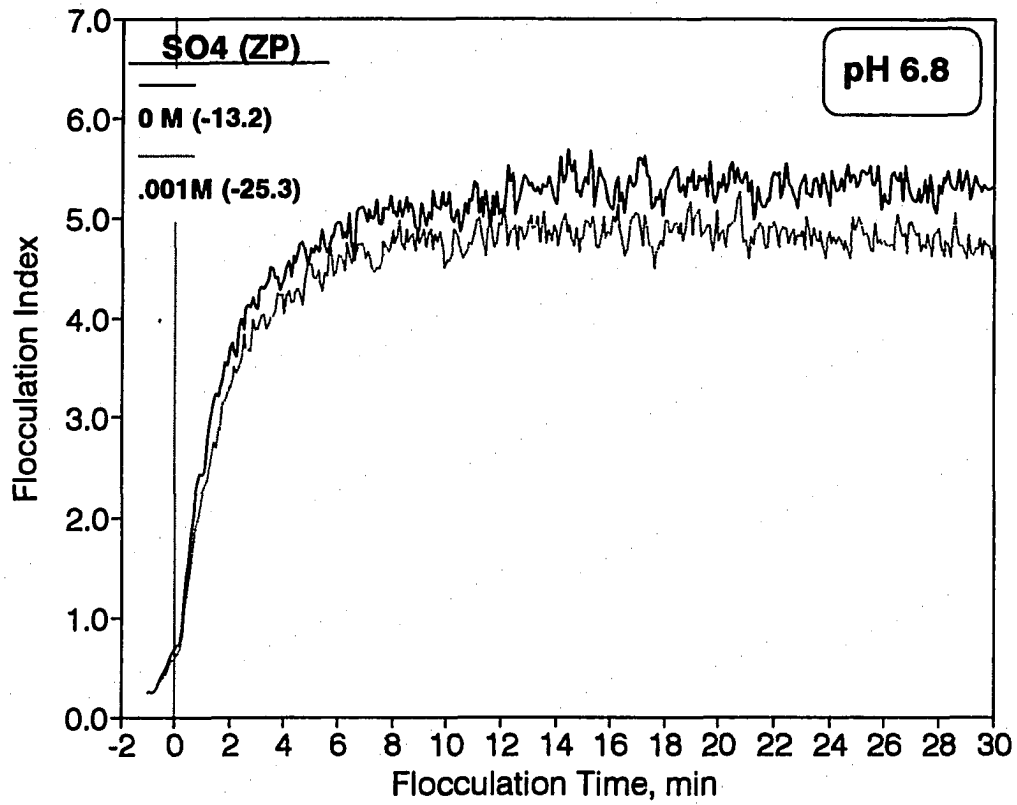
Figure 5.39. Effect of sulfate on the rate of flocculation (pH 6.8, clay: 100 mg/L, dose: 5 mg/L, 45 rpm)

4.2.3 Effects of temperature

Most of the experimental results for flocculation kinetics at two different temperatures to be presented compare the flocculation kinetics while maintaining a constant pH in the experiments at two temperatures, or while maintaining a constant pOH in the experiments at two temperatures. Recently, constant pOH has been found to be a more appropriate parameter than pH for correcting system chemistry for changes in temperature (Hanson and Cleasby, 1990; van Benchoten and Edzwald, 1990a). This observation can be supported intuitively. As temperature drops, and hence, the ion product of water changes, one would expect that the pH of the system should be adjusted to maintain the activity of hydroxyl ion constant because the Fe(III) species of importance in flocculation with a ferric coagulant are various hydroxide polymeric species or hydroxide precipitate. Maintaining a constant pOH at two temperatures results in a different pH at the second temperature. For example, a change in the water temperature from 23 °C to 5 °C results in a change in the ion product of water, K_w from $10^{-14.06}$ to $10^{-14.73}$. As a result, for example, the pH 6.8 at 23 °C results in a pH 7.5 at 5 °C to maintain constant pOH 7.26 (i.e., at 23 °C, $pOH = pK_w - pH = 14.06 - 6.8 = 7.26$, whereas at 5 °C, $pH = pK_w - pOH = 14.73 - 7.26 = 7.47$). To illustrate the influence of temperature on solution pH to maintain constant pOH, Table 5.2 and Figure 5.40 were made based on a temperature dependent equation for K_w. Included in Figure 5.40 are the representative pOH lines selected to find out pH values chosen for this study. For example, if pH 6.8 is selected as a test pH at 23 °C, entering the graph at pH 6.8 and 23°C falls on the

Table 5.2. Conversion table of pH adjusted at a specified temperature for constant pOH

Temp. C	25	24	23	20	15	10	5	0
pKw*	13.99	14.03	14.06	14.17	14.34	14.53	14.73	14.94
pOH	pH	pH	pH	pH	pH	pH	pH	pH
8.56	5.43	5.47	5.50	5.60	5.78	5.97	6.17	6.38
8.46	5.53	5.57	5.60	5.70	5.88	6.07	6.27	6.48
8.36	5.63	5.67	5.70	5.80	5.98	6.17	6.37	6.58
8.26	5.73	5.77	5.80	5.90	6.08	6.27	6.47	6.68
8.16	5.83	5.87	5.90	6.00	6.18	6.37	6.57	6.78
8.06	5.93	5.97	6.00	6.10	6.28	6.47	6.67	6.88
7.96	6.03	6.07	6.10	6.20	6.38	6.57	6.77	6.98
7.86	6.13	6.17	6.20	6.30	6.48	6.67	6.87	7.08
7.76	6.23	6.27	6.30	6.40	6.58	6.77	6.97	7.18
7.66	6.33	6.37	6.40	6.50	6.68	6.87	7.07	7.28
7.56	6.43	6.47	6.50	6.60	6.78	6.97	7.17	7.38
7.46	6.53	6.57	6.60	6.70	6.88	7.07	7.27	7.48
7.36	6.63	6.67	6.70	6.80	6.98	7.17	7.37	7.58
7.26	6.73	6.77	6.80	6.90	7.08	7.27	7.47	7.68
7.16	6.83	6.87	6.90	7.00	7.18	7.37	7.57	7.78
7.06	6.93	6.97	7.00	7.10	7.28	7.47	7.67	7.88
6.96	7.03	7.07	7.10	7.20	7.38	7.57	7.77	7.98
6.86	7.13	7.17	7.20	7.30	7.48	7.67	7.87	8.08
6.76	7.23	7.27	7.30	7.40	7.58	7.77	7.97	8.18
6.66	7.33	7.37	7.40	7.50	7.68	7.87	8.07	8.28
6.56	7.43	7.47	7.50	7.60	7.78	7.97	8.17	8.38
6.46	7.53	7.57	7.60	7.70	7.88	8.07	8.27	8.48
6.36	7.63	7.67	7.70	7.80	7.98	8.17	8.37	8.58
6.26	7.73	7.77	7.80	7.90	8.08	8.27	8.47	8.68
6.16	7.83	7.87	7.90	8.00	8.18	8.37	8.57	8.78
6.06	7.93	7.97	8.00	8.10	8.28	8.47	8.67	8.88

* Equation used: $\text{Log } Kw = -4470.99/T + 6.0875 - 0.01706T$ (T= temperature in $K = 273.15$) (Stumm, 1981)
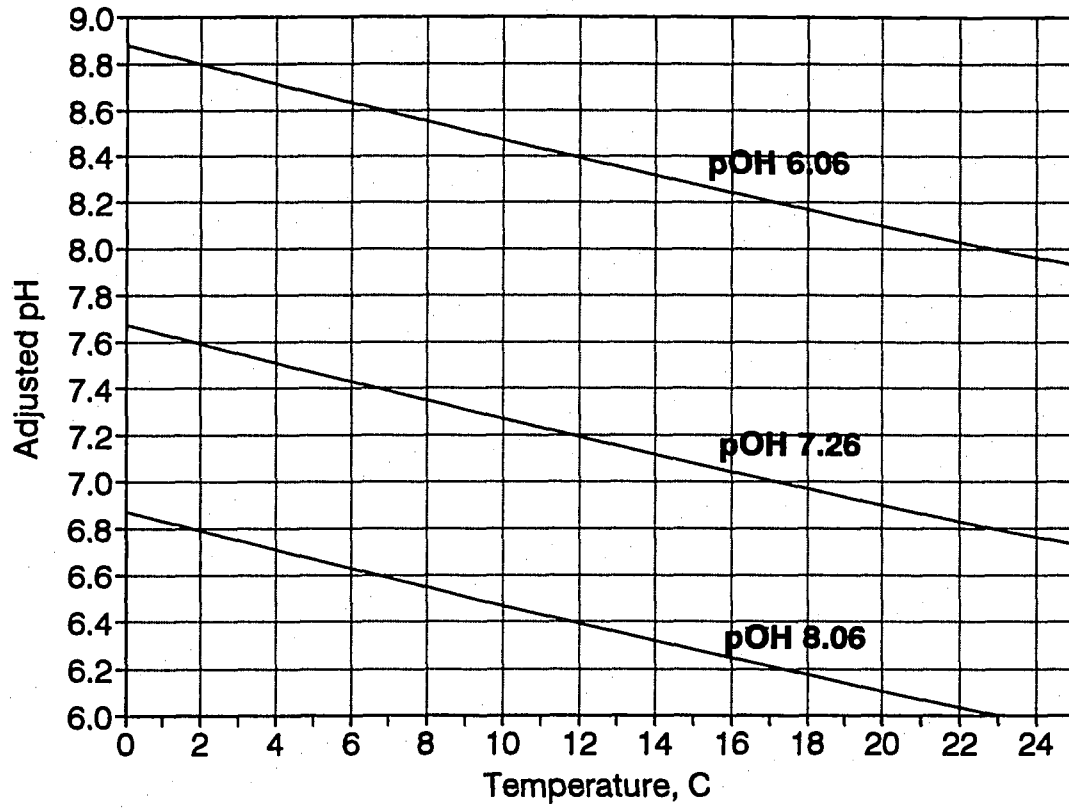
Figure 5.40. Adjusted pH at a specified temperature to the appropriate pH for constant pOH at another temperature

pOH 7.26 line. Following that line to 5°C, the ordinate reads pH 7.5. This is the pH needed to maintain pOH constant at 5 °C.

Figures 5.41 and 5.42 present the experimental results for flocculation kinetics at room temperature (23 ± 1 °C) versus 5 °C including the effect of altering system chemistry at 5 °C by maintaining constant pH or constant pOH. Included in these figures are baseline data at pH 6.8 at 23 °C compared with data collected at 5 °C. For comparison, once again, the rate of flocculation process was evaluated by determining the changes in total particle count fraction (Figure 5.41) and the changes in flocculation index (Figure 5.42) in the flocculating suspension at various times during the course of process. In experiments at low temperature, the rotating speed (rpm) of the stirring paddles was maintained constant at different temperatures so as to produce a constant power input, resulting in a little lower G at low temperature. Overall, Figures 5.41 and 5.42 show that low temperature had a detrimental kinetic effect on flocculating process, slowing the disappearance of primary particles and the growth of aggregates. When comparing flocculation kinetics as evidenced by the rate of disappearance of primary particles at a baseline pH 6.8, as shown in Figure 5.41, the low water temperature did not impair the kinetics of flocculation substantially when holding pOH constant. However, Figure 5.42 indicates a significant detrimental effect on flocculation kinetics at low temperature, even when maintaining constant pOH. It is noteworthy that the ZP values for each curve show that Fe(III) coagulant at low temperature is much more effective at charge neutralization of clay particles than at high temperature.

Figures 5.43 and 5.44 present the impact of low water temperature on the rate of flocculation at a baseline pH 8.0, but otherwise under the same experimental conditions as at
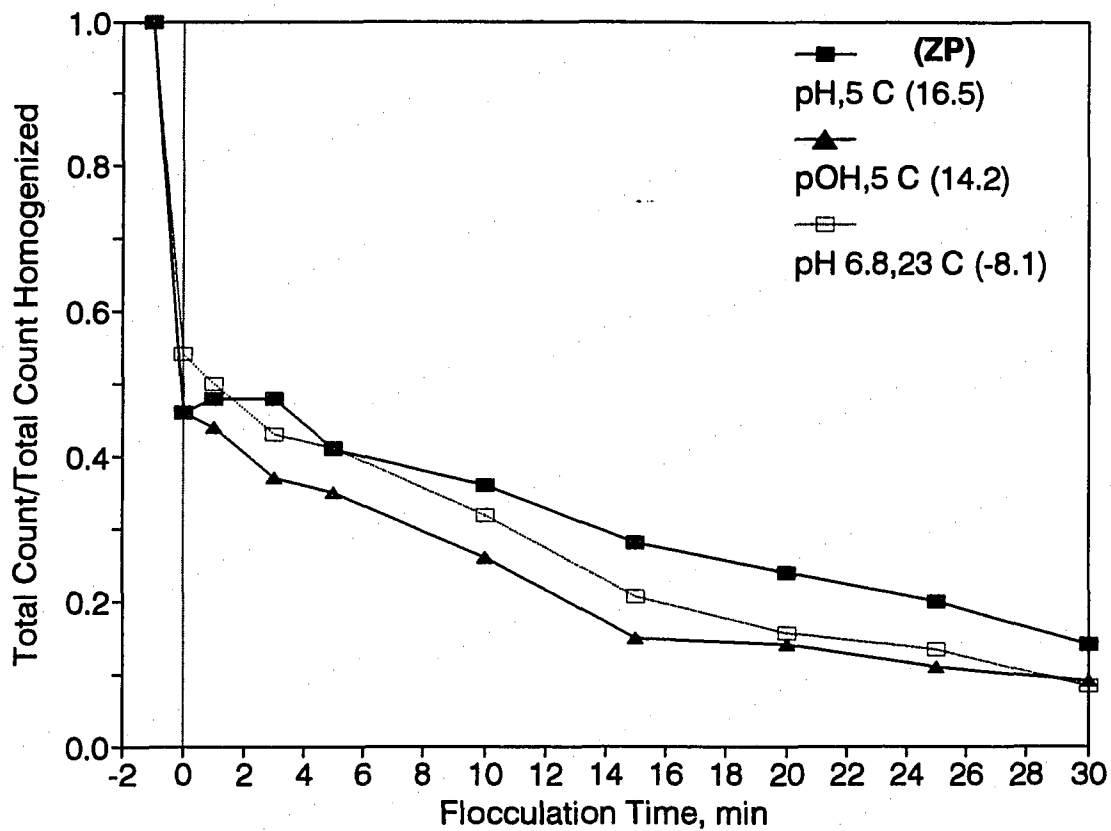
Figure 5.41. Effect of temperature and system chemistry on the rate of flocculation
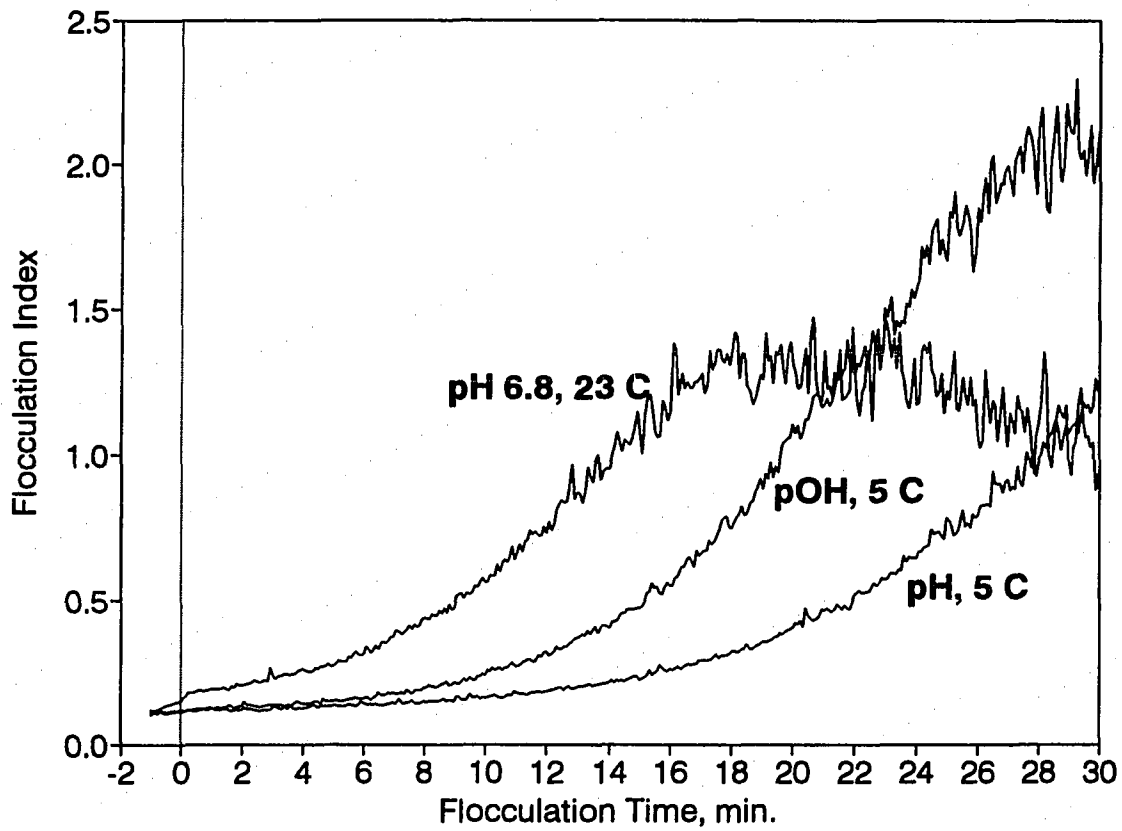(baseline 23 °C at pH 6.8, clay: 25 mg/L, dose: 5 mg/L, 30 rpm)

Figure 5.42. Effect of temperature and system chemistry on the rate of flocculation
(baseline 23 °C at pH 6.8, clay: 25 mg/L, dose: 5 mg/L, 30 rpm)

pH 6.8 shown in Figures 5.41 and 5.42. It is noted that Fe(III) coagulant at 5 °C does not result in flocculating kaolin particles as well as at room temperature, and altering system chemistry by adjusting pH was not capable of improving flocculation kinetics. At pH 8.0, once again, the low temperature significantly affected the surface charge of particles, as evidenced by the reversal of surface charge at 5 °C. The significant changes in ZP with temperature suggest that the low temperature played an important role in the manner in which the Fe(III) coagulant hydrolyzes, probably production of more highly positive charged Fe(III) species. Comparison of the results at pH 8.0 with those at pH 6.8 shows a different effect of using constant pOH at low temperature on flocculation kinetics. It is evident that holding constant pOH at low temperature did not improve the flocculation kinetics in Figures 5.43 and 5.44 compared with holding constant pH at cold temperature. In fact, the flocculation index was slightly worse with constant pOH in Figure 5.44. However, comparing Figures 5.41 and 5.42 with Figures 5.43 and 5.44, it is apparent that use of constant pOH is favorable below a certain pH level, in the more acidic pH range. Overall, poorer flocculation kinetics performance accompanying low water temperature may be due to slowing the hydrolysis and precipitation reactions of Fe(III) in water, as evidenced by the greater effectiveness of Fe(III) coagulant in the charge neutralization of the negatively charged kaolin particles, and due to slowing of the formation of bigger sized flocs, as evidenced by the slower increase of flocculation index as shown in Figure 5.44.

The results obtained under the same experimental conditions, except using 50 mg/L of clay, are plotted at pH 6.8 and 8.0 in Figures 5.45(a) and (b), respectively. As shown in these figures, again, low temperature had a pronounced detrimental effect on flocculation kinetics at
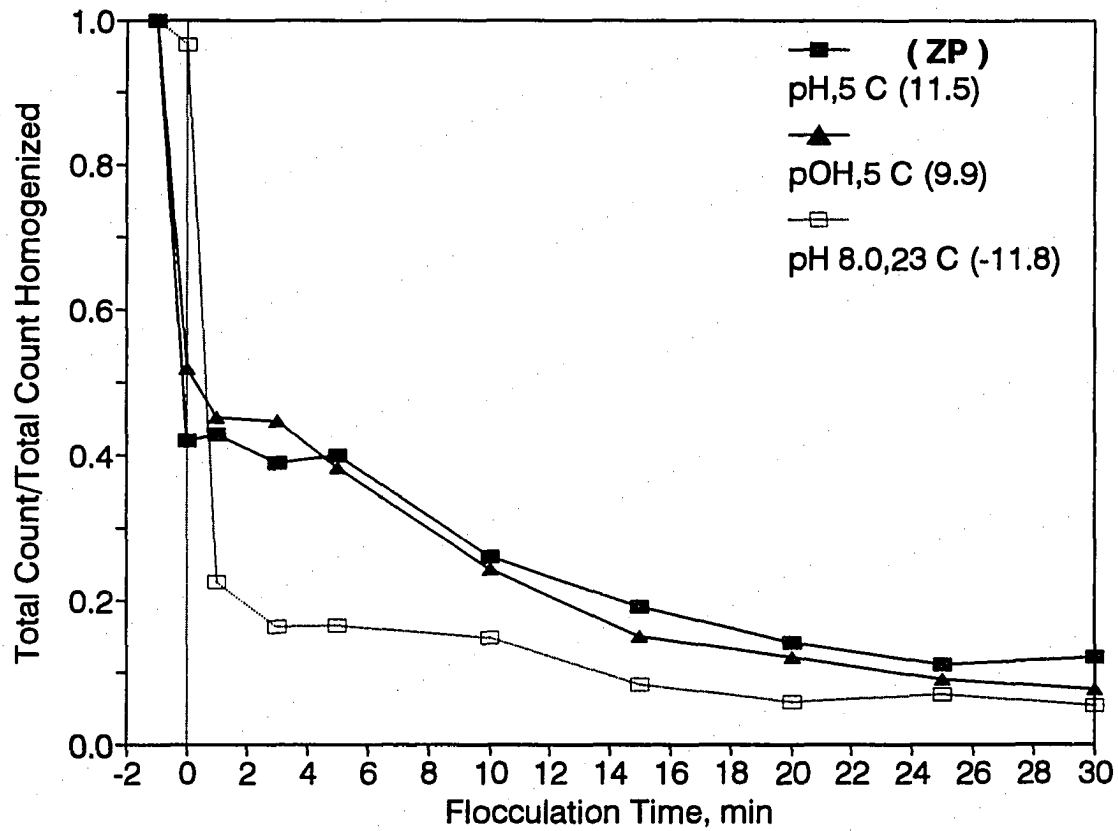
Figure 5.43. Effect of temperature and system chemistry on the rate of flocculation
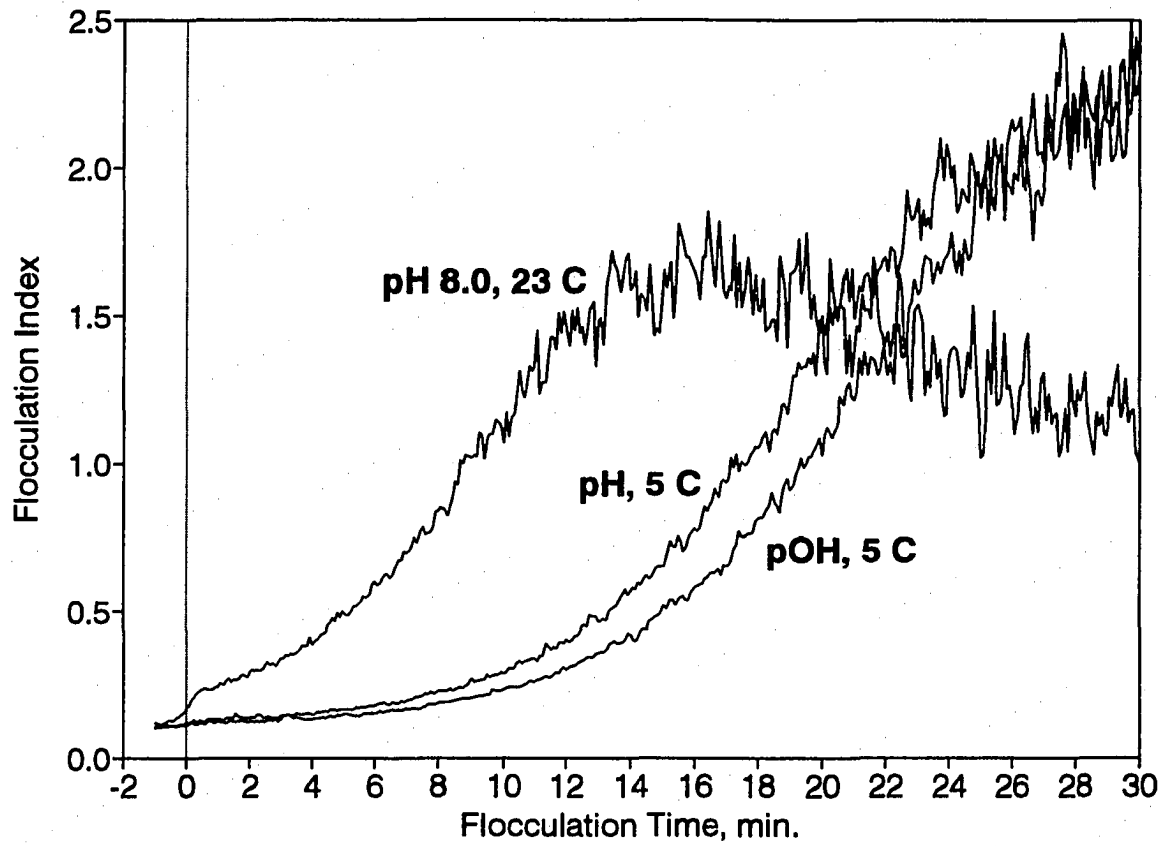(baseline 23 °C at pH 8.0, clay: 25 mg/L, dose: 5 mg/L, 30 rpm)

Figure 5.44. Effect of temperature and system chemistry on the rate of flocculation (baseline 23 °C at pH 8.0, clay: 25 mg/L, dose: 5 mg/L, 30 rpm)
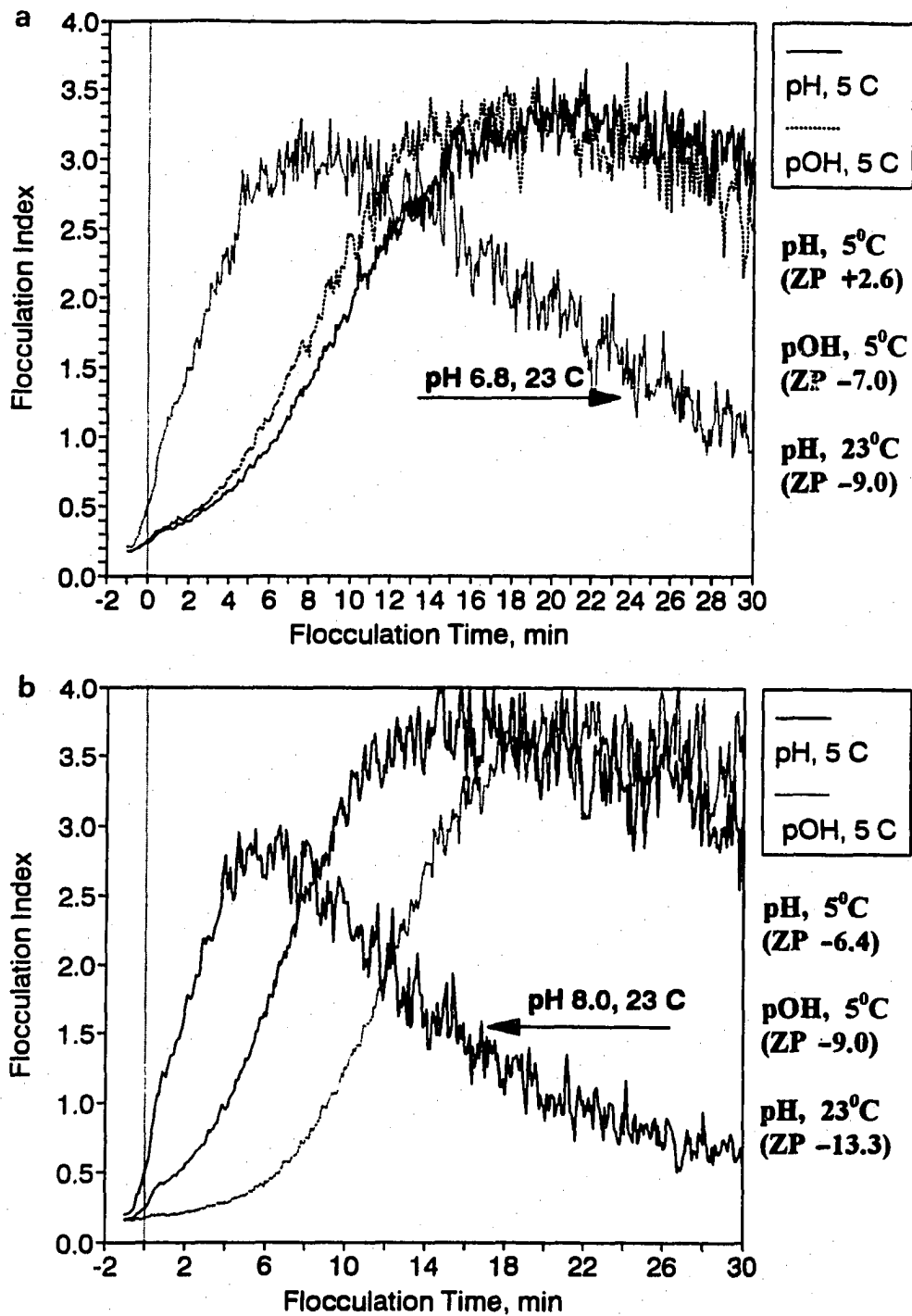
Figure 5.45. Effect of temperature and system chemistry on the rate of flocculation (clay: 50 mg/L, dose: 5 mg/L, 30 rpm); (a) baseline 23 °C at pH 6.8, (b)   baseline 23 °C at pH 8.0

both pH 6.8 and 8.0. Also, under this higher particle concentration, it was apparent at the

more acidic pH that there was only a slight benefit for holding pOH constant at the lower

temperature. At the higher pH, as evident in Figure(b), maintaining constant pOH at cold

temperature was detrimental to the growth of flocs. It is noteworthy that at low temperature,

the increase in the flocculation index is very slow, particularly during the first around 5 min,

indicating slower flocculation in the early phase of flocculation. In this case, it may be

explained that the formation of Fe(III) precipitate becomes slower at low temperature,

evidenced by the attainment of the higher positive charge (or less negative charge) at low

temperature. Francois and Bekaert (1986) also reported that slowed floc growth at low

temperature (5 °C) might be due to slowing the formation of insoluble Al hydroxides or poor

homogeneous distribution of the insoluble hydroxide throughout clay suspension. While

investigating the impact of cold water temperature on flocculation kinetics by means of

measuring the rate disappearance of primary particles, Hanson and Cleasby (1990) also

noticed that an increased lag phase in the rate of disappearance of primary particles was

evident, and poorer flocculation kinetics were observed at 5 °C compared with than at 20 °C.

In order to elucidate the effects of altering system chemistry at low temperature by

maintaining constant pOH, Figures 5.46 to 5.49 present a flocculation kinetics comparison

performed using 10 mg/L of coagulant dose at 5 °C to confirm the experimental results

performed using 5 mg/L of coagulant dose presented in Figures 5.41 to 5.45. First, Figures

5.46 and 5.47 compare flocculation kinetics at 5 °C using constant pH or pOH using 25 mg/L

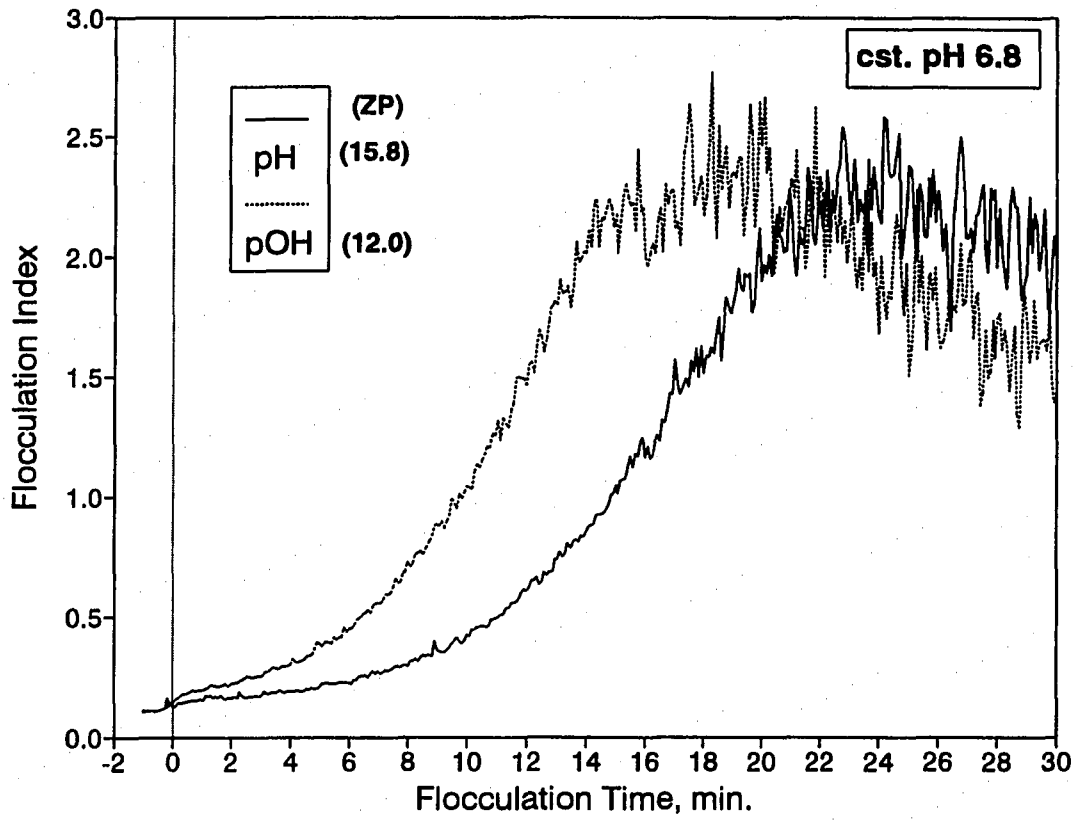clay at a baseline pH of 6.8 and 8.0, respectively. Once again, maintaining constant pOH

Figure 5.46. Effect of system chemistry on the rate of flocculation at 5 °C (constant pH: 6.8, clay: 25 mg/L, dose: 10 mg/L, 30 rpm)
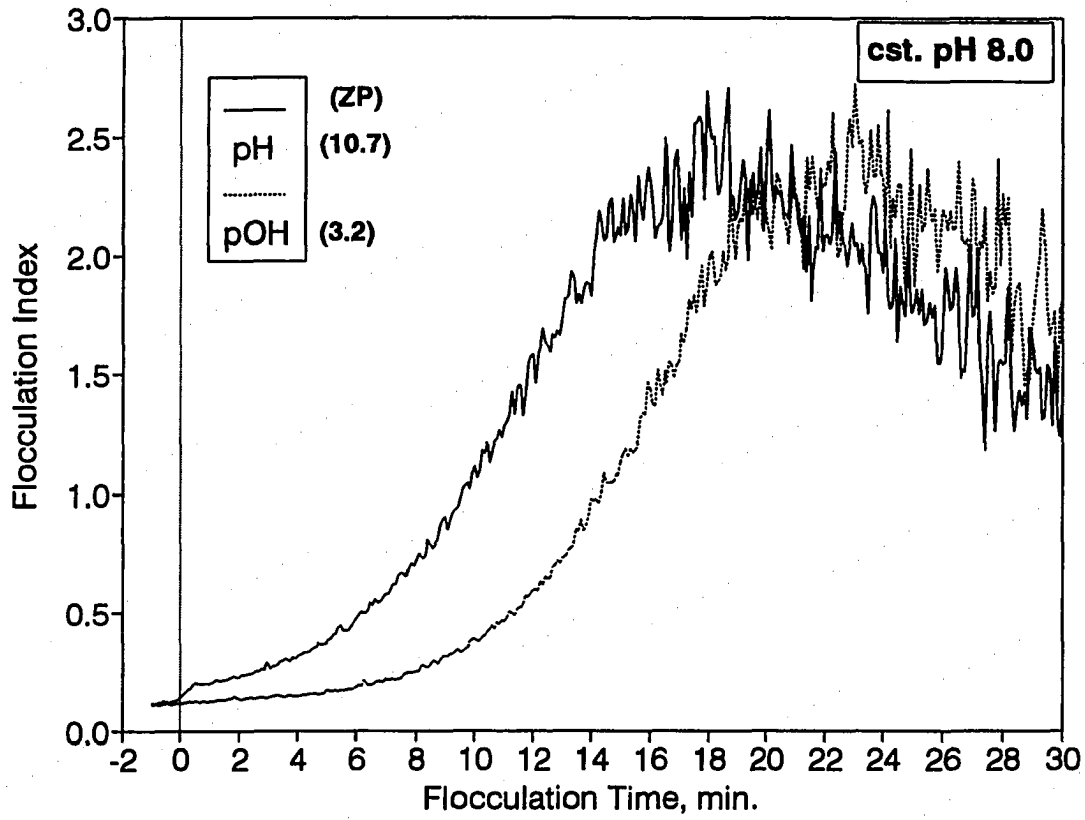
Figure 5.47. Effect of system chemistry on the rate of flocculation at 5 °C (constant pH: 8.0, clay: 25 mg/L, dose: 10 mg/L, 30 rpm)
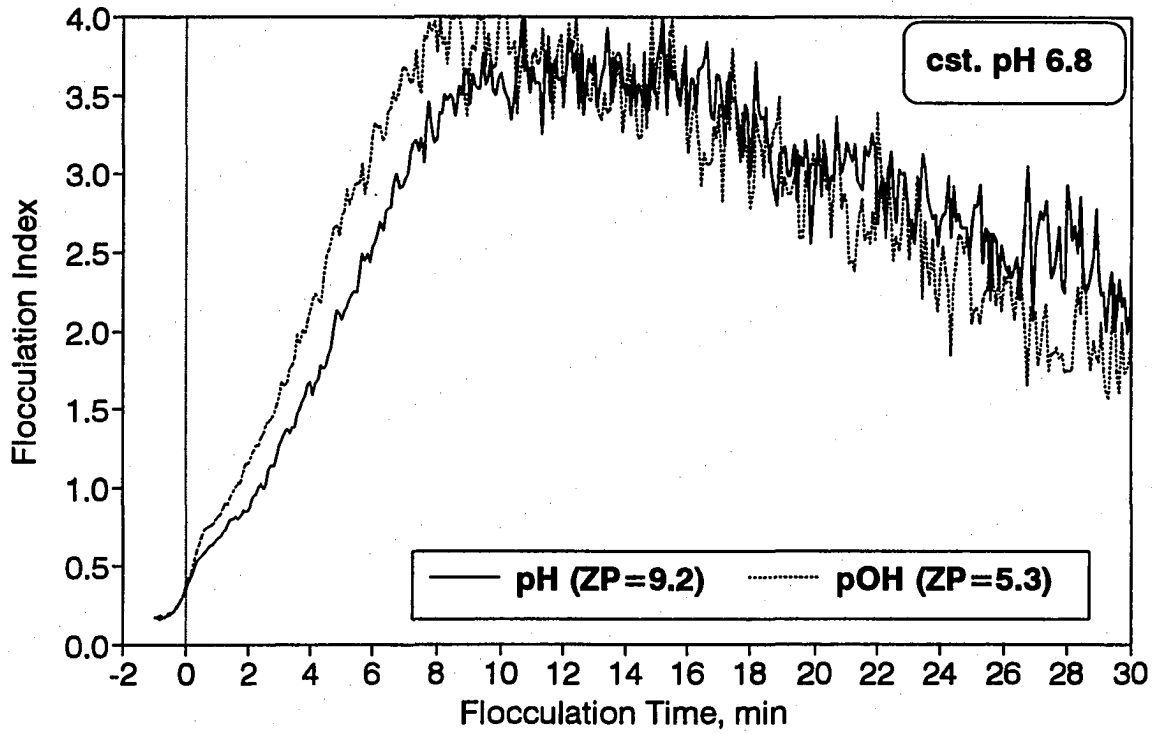
Figure 5.48. Effect of system chemistry on the rate of flocculation at 5 °C (constant pH: 6.8, clay: 50 mg/L, dose: 10 mg/L, 30 rpm)
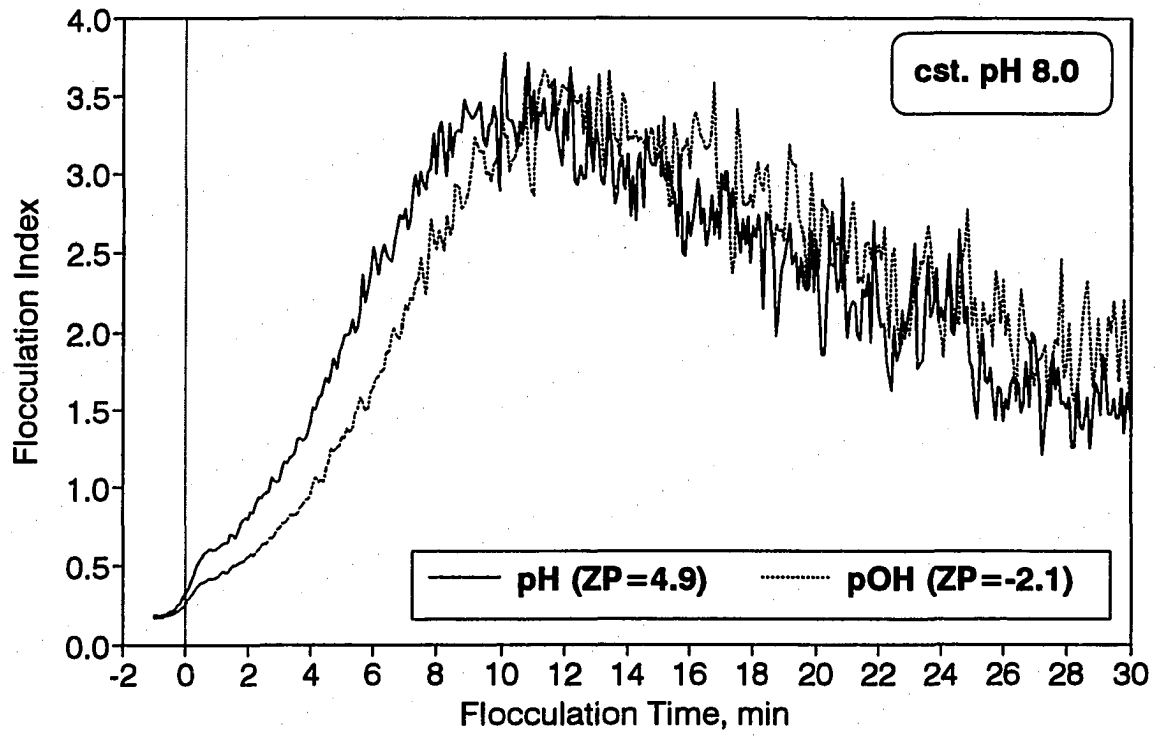
Figure 5.49. Effect of system chemistry on the rate of flocculation at 5 °C (constant pH: 8.0, clay: 50 mg/L, dose: 10 mg/L, 30 rpm)

significantly improved the rate of flocculation at pH 6.8, but it impaired the rate of flocculation at pH 8.0. Furthermore, its adverse impact on flocculation kinetics became greater with 10 mg/L of coagulant dose than with 5 mg/L of coagulant dose. Second, Figures 5.48 and 5.49 compare flocculation kinetics at constant pH and pOH using 50 mg/L clay at a baseline pH of 6.8 and 8.0, respectively. Also, under this high clay concentration and coagulant dose, it is apparent at the more acidic pH studied (pH = 6.8) that there is substantial benefit for holding pOH constant at the low temperature. However, at pH 8.0, the detrimental effect of using constant pOH is still evident but the detriment is reduced. It is also noted from the comparison of Figures 5.47 with 5.49 that comparison of the ZP values at pH 8.0 for both 25 and 50 mg/L clay concentrations does not yield any information for an optimum surface charges of the flocculation process at low temperature. As an evidence, poorer flocculation occurred at constant pOH in spite of the existence of ZP values closer to zero at both clay concentrations.

Figures 5.50 and 5.51 present the impact of low temperature on the rate of flocculation for 100 mg/L clay concentration at different suspension pH using 5 and 10 mg/L of coagulant dose, respectively. For Figure 5.51, the coagulant dose was increased to 10 mg/L to avoid possible underdosed condition for the higher clay concentration of 100 mg/L. As shown in Figures 5.50 and 5.51, again, a decrease in temperature has a significant effect on the rate of flocculation, increasing the time of formation of aggregates. The adverse impact of low temperature on the flocculation rates was most severe at constant pH using both 5 and 10 mg/L of dosages. It is also noted from Figure 5.50 using 5 mg/L coagulant dose that while constant pOH (pH = 7.5 at 5 °C) or increasing pH up to 8.0 with 5 mg/L of coagulant dose
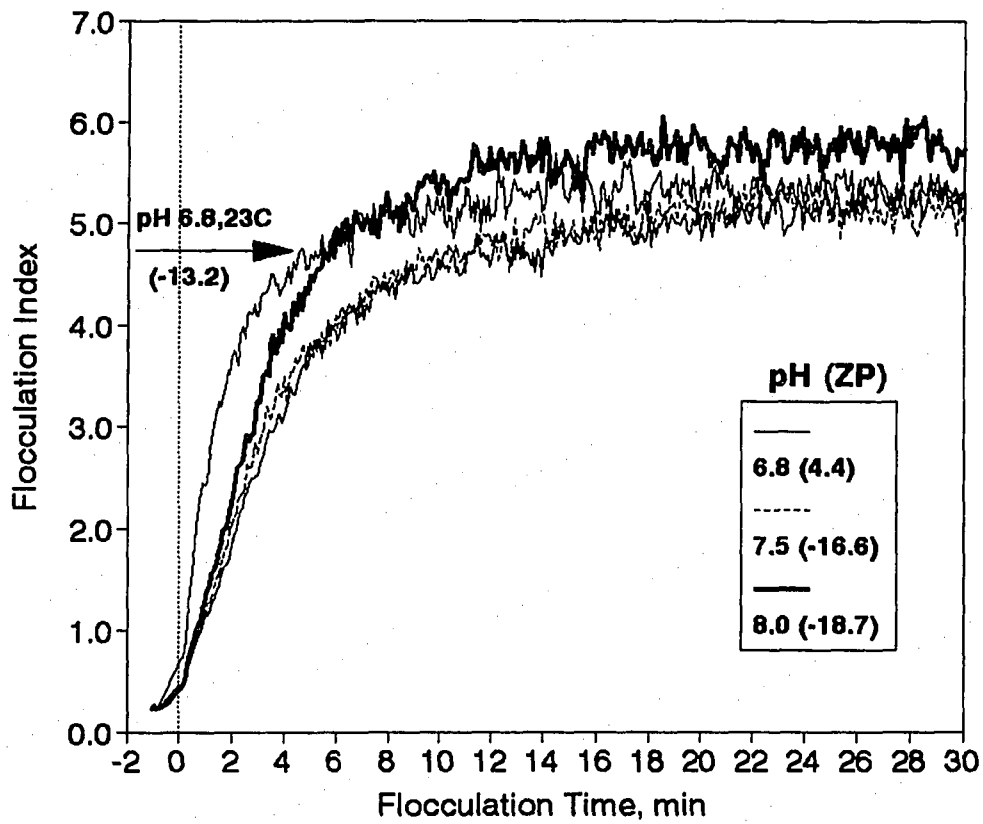
Figure 5.50. Effect of temperature and system chemistry on the rate of flocculation
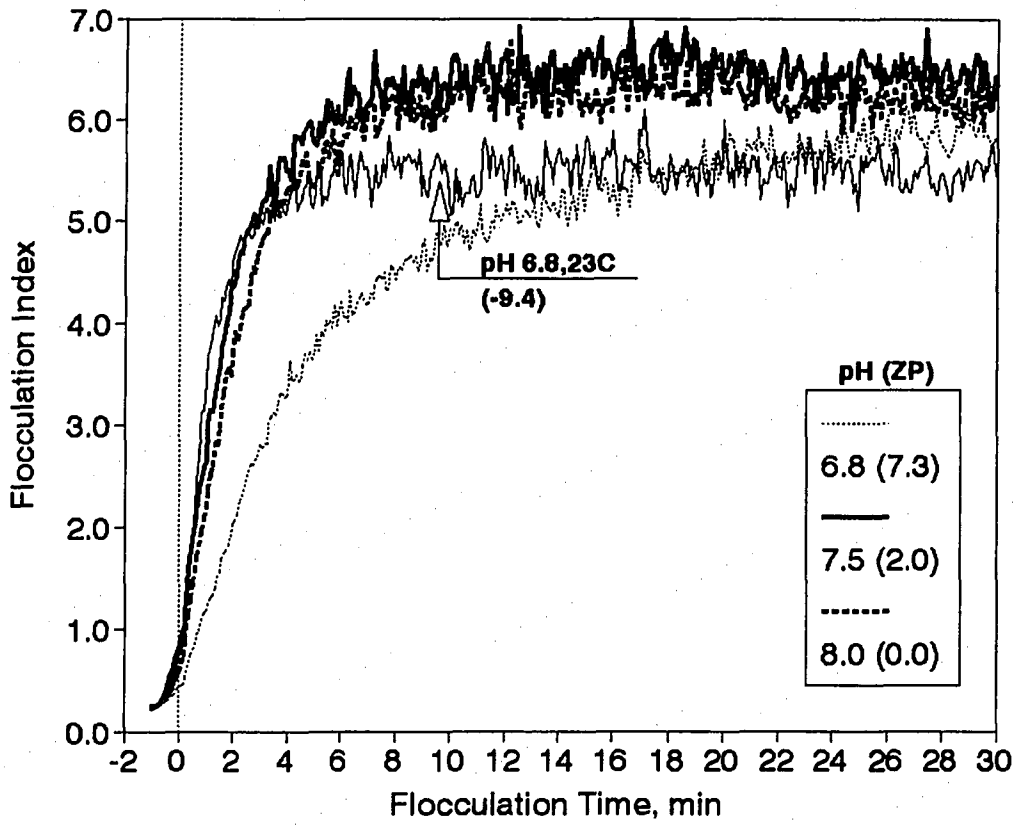(baseline 23 °C at pH 6.8, clay: 100 mg/L, dose: 5 mg/L, 45 rpm)

Figure 5.51. Effect of temperature and system chemistry on the rate of flocculation
(baseline 23 °C at pH 6.8, clay: 100 mg/L, dose: 10 mg/L, 45 rpm)

outperforms constant pH at low temperature, it does not outperform the flocculation kinetics

at room temperature. However, Figure 5.51 using 10 mg/L coagulant dose shows that when

either maintaining constant pOH or increasing pH up to 8.0 at low temperature resulted in

almost comparable flocculation as 23 °C baseline condition. The ZP values shown in Figures

5.50 and 5.51 indicate that the effect of low temperature on the surface charges of particles

was significant at this high clay concentration, too. Comparison of these results for 100 mg/L

clay suspension with those for 25 and 50 mg/L clay suspensions shown previously (all at the

pH 6.8 baseline condition) indicates that at higher clay concentration, the adverse impact of

cold temperature on flocculation kinetics can be significantly reduced either by using constant

pOH or increasing pH. Especially, the initial slow growth phase of flocs, which was apparent

at lower clay concentrations, is appreciably diminished. Lee and Gregory (1990) also observed

that under favorable coagulation conditions, such as optimum polymer dose and higher

molecular mass of cationic polymer, the initial 'lag time' for the flocculation index became

shorter. It is interesting to note the shape of curves in Figures 5.50 and 5.51 that at 5 °C, the

rate of flocculation starts out slower but overtakes the rate at 23 °C after 5 min of flocculation

period. As discussed earlier, the flocculation index changes with the square root of particle

number concentration and with first power of the scattering cross section so that it is

influenced much more by the size of flocs rather than the number concentration. According to

the microscopic observation, the greater flocculation index observed at 5 °C after 5 min was

due to greater number concentration of rather "open" or "stringy" aggregates. In contrast, the

flocs formed at 23 °C were observed to be less in number concentration but rather larger and more compact.

The supernatant turbidity data as shown in Figure 5.52 would serve as an indirect evidence of the above microscopic observation. The data in Figure 5.52 were obtained from the measurement of the supernatant turbidity during a sedimentation period following 30 min of flocculation, which was the same test as presented in Figure 5.51. This settling data show that the flocs formed at 23 °C is settled much faster than the flocs formed at 5 °C. Even though the decreased settling rate at 5 °C was influenced by an increase in the viscosity of water, it could also be due partly to the characteristic of flocs. Thus, higher number concentration of smaller flocs with open and less dense structures could cause the slow settling rate. Anyhow, it is evident that low temperature deteriorated the extent to which particles are aggregated during flocculation process, and thereby the efficient removal of turbidity during sedimentation.

To find out how to improve the rate of flocculation at cold temperature, some tests were carried out by increasing either coagulant dose or slow-mixing intensity. Figures 5.53 to 5.56 show the experimental results for flocculation kinetics at 5 °C by presenting the effect of applying higher intensity of slow mixing and the effect of increasing coagulant dose. Figures 5.53 - 5.54 and 5.55 - 5.56 represent the data for 25 and 50 mg/L clay concentration, respectively. For comparison, the data obtained at 5 °C using 5 mg/L coagulant dose are used as a baseline, and the data obtained at constant pH are presented. All of these data for 25 and 50 mg/L clay concentration show that both at pH 6.8 and 8.0, when either excess of coagulant is added or increased slow mixing intensity is applied, the rate of flocculation improves. These
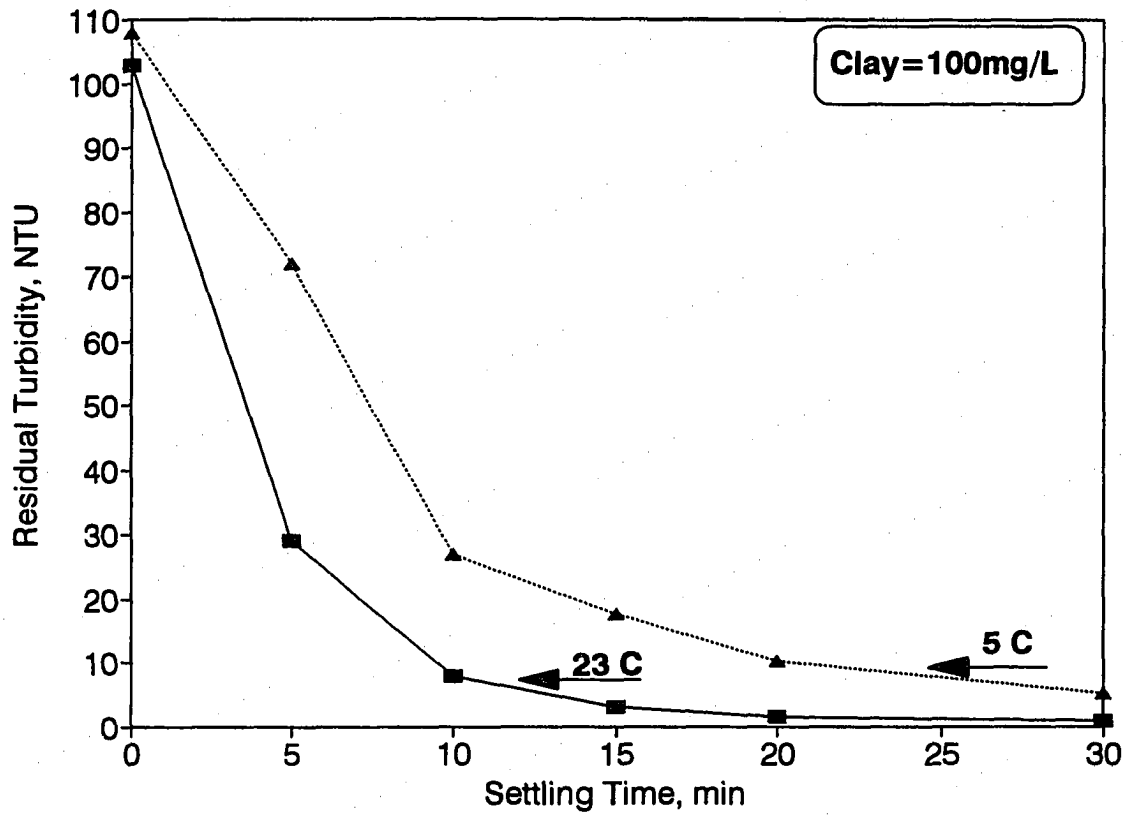
Figure 5.52. Effect of temperature on the changes in residual turbidity against settling time (pH: 6.8, clay: 100 mg/L, dose: 10 mg/L, 45 rpm)

Figure 5.53. Effect of mixing intensity and coagulant dose on the rate of flocculation at 5 °C (pH=6.8, clay: 25 mg/L)

Figure 5.54. Effect of mixing intensity and coagulant dose on the rate of flocculation at 5 °C (pH=8.0, clay: 25 mg/L)
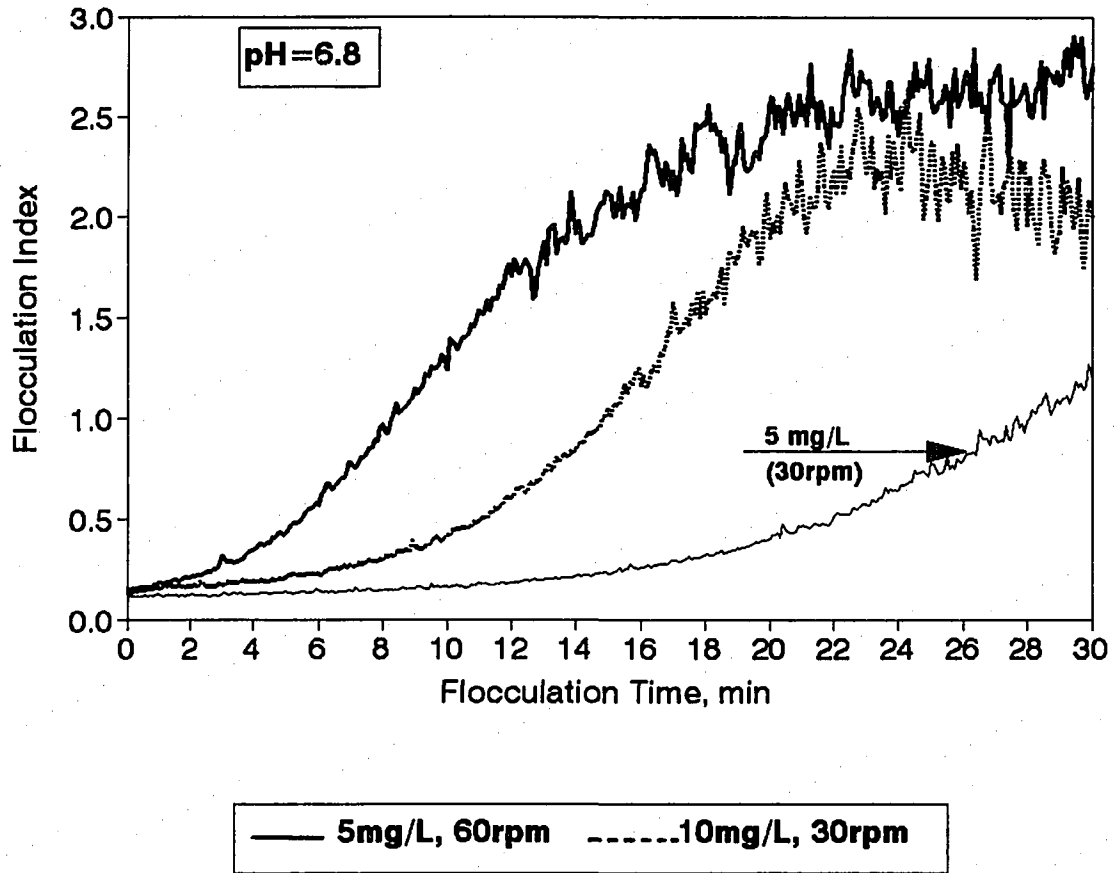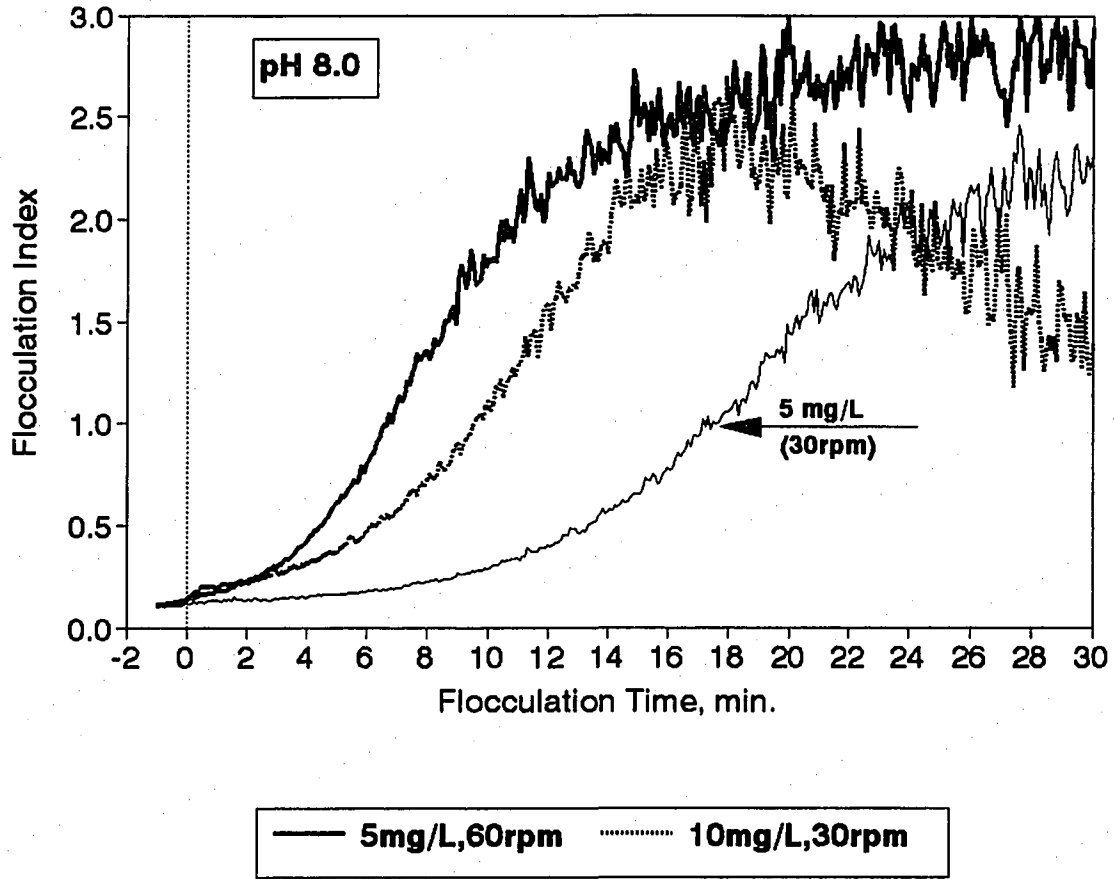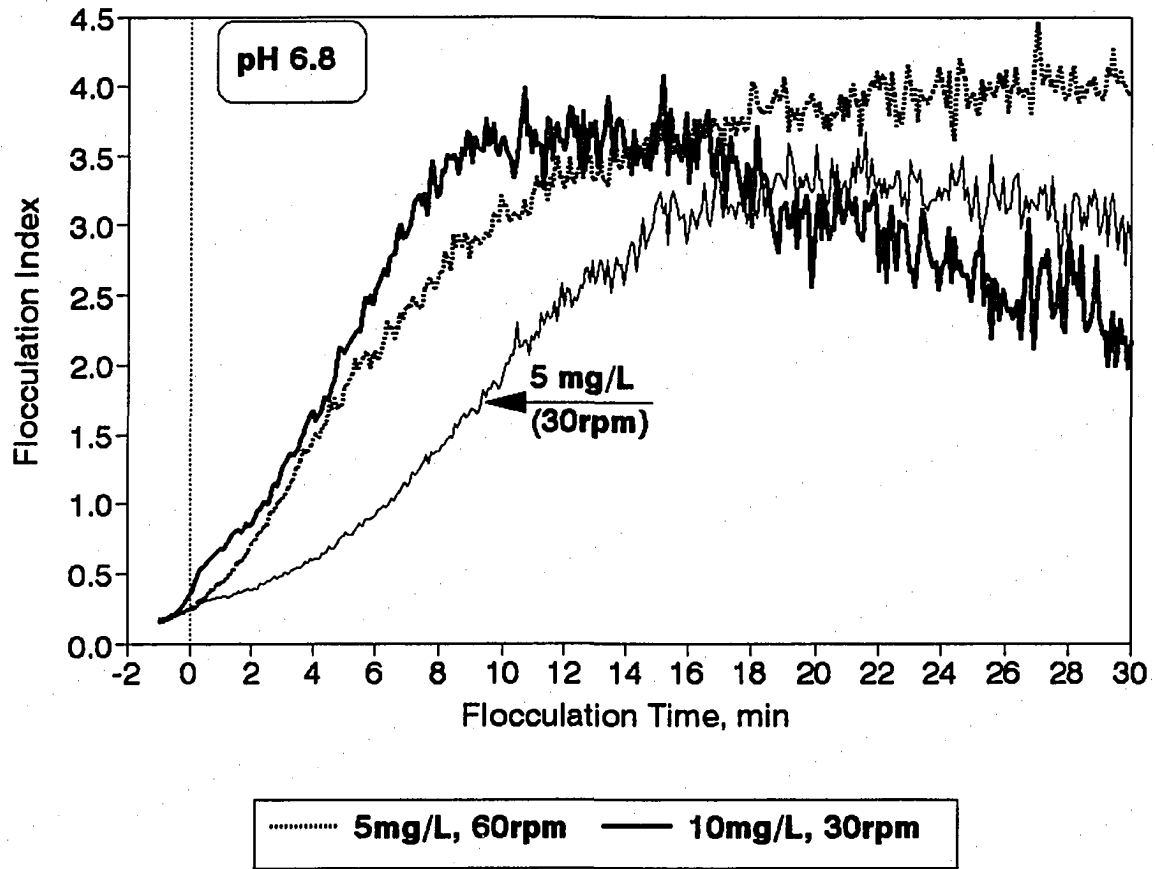
Figure 5.55. Effect of mixing intensity and coagulant dose on the rate of flocculation at 5 °C (pH=6.8, clay: 50 mg/L)
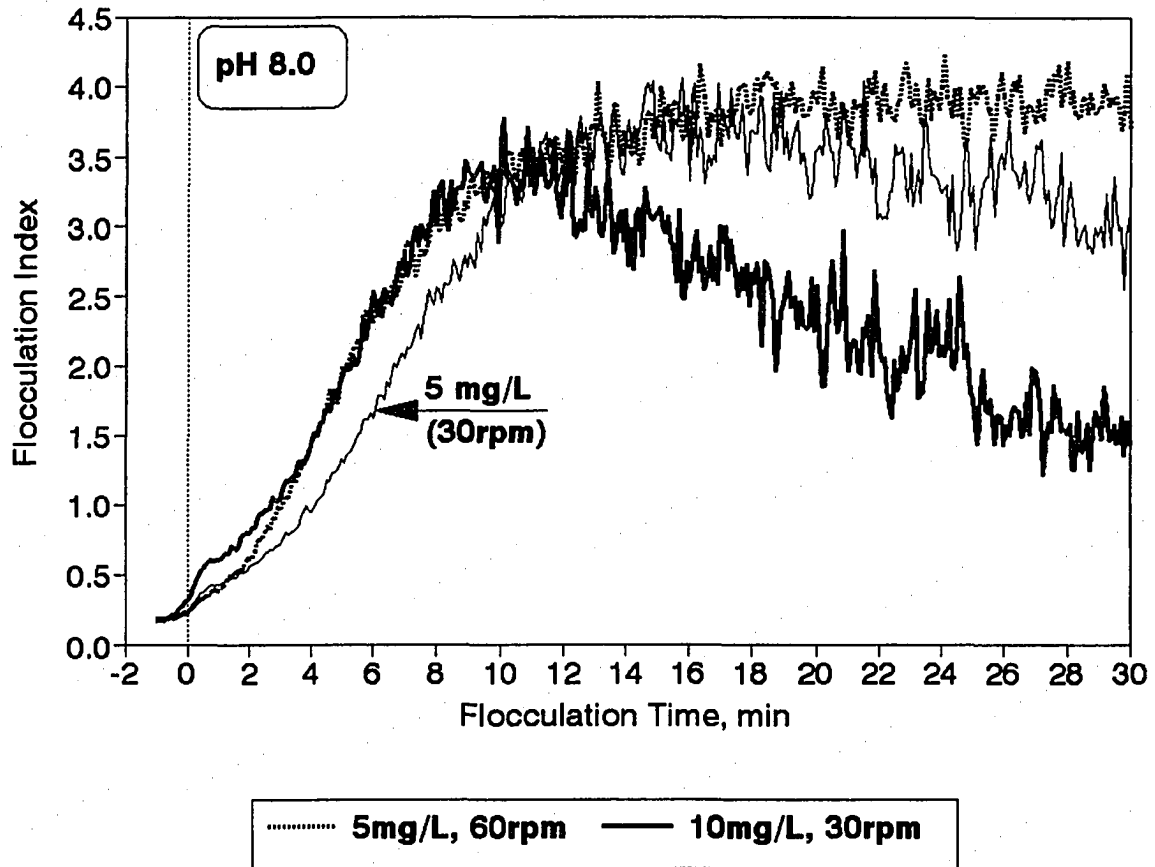
Figure 5.56. Effect of mixing intensity and coagulant dose on the rate of flocculation at 5 °C (pH=8.0, clay: 50 mg/L)

results suggest that both at pH 6.8 and 8.0, increasing either the coagulant dose or the mixing intensity at low temperature can partially overcome the detrimental impact of cold temperature on the process of flocculation. Probably, the improvement in flocculation was accomplished by the increased interparticle collision rate which can be caused by the additional formation of Fe(III) precipitate at higher coagulant dosage and by the enhanced particle transport at higher mixing intensity. Comparison of the data for 25 mg/L clay concentration (Figures 5.53 and 5.54) with the data for 50 mg/L clay concentration (Figures 5.55 and 5.56) indicates that at higher particle concentration, the improvement of flocculation kinetics is less dramatic by either alternative method. Thus, the increased interparticle collision rate seemed to be more beneficial to enhancing flocculation kinetics at the lower clay concentration.

Figures 5.57 and 5.58 present another way to improving the rate of flocculation at low temperature by extending the rapid mixing period up to 2 min at pH 6.8 and 8.0, respectively. Comparison of the results at pH 6.8 with those at pH 8.0 indicates different effects of extending rapid mixing period. For example, at pH 6.8, the flocculation kinetics at low temperature was substantially improved by extending the rapid mixing period using either constant pH or pOH. But, at pH 8.0, extending rapid mixing period at low temperature was beneficial to the aggregation of particles only when pH was maintained constant. The adverse effect of using constant pOH on flocculation kinetics at pH 8.0 became even greater when using the extended rapid mixing period. It is noteworthy at pH 6.8 that the initial lag, which
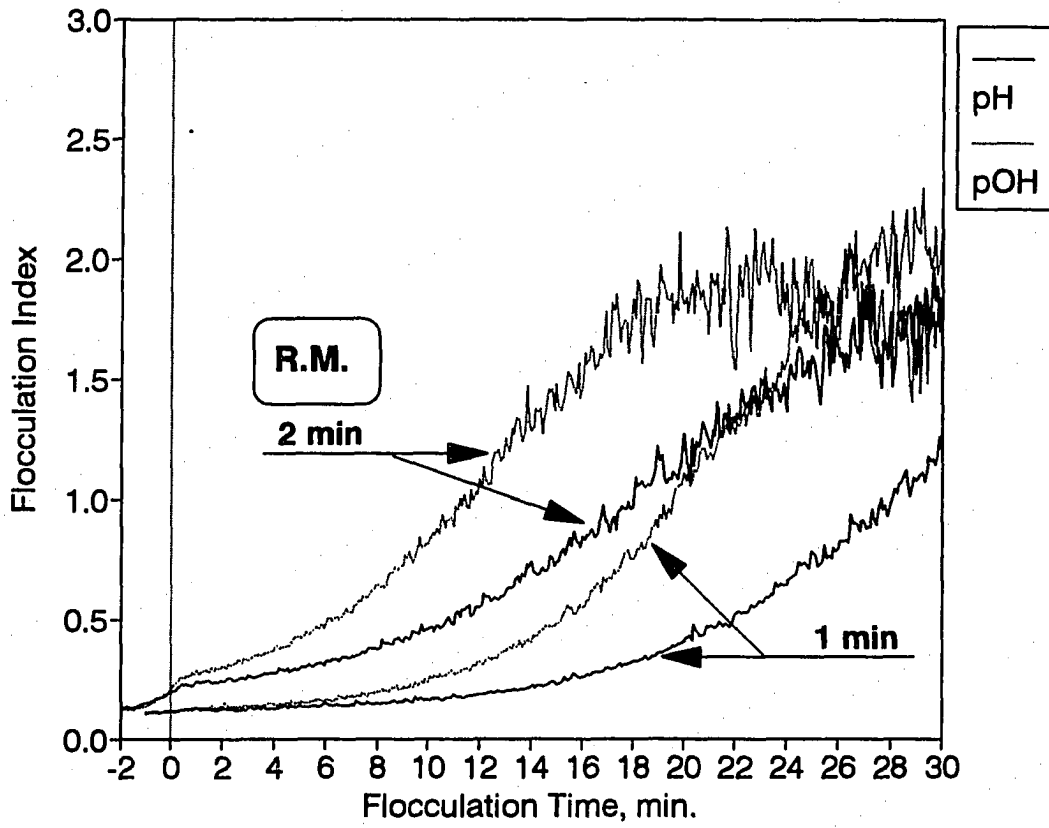
Figure 5.57. Effect of rapid mixing duration and system chemistry on the rate of flocculation at 5 °C (pH=6.8, clay: 25 mg/L, dose: 5 mg/L, 30 rpm)
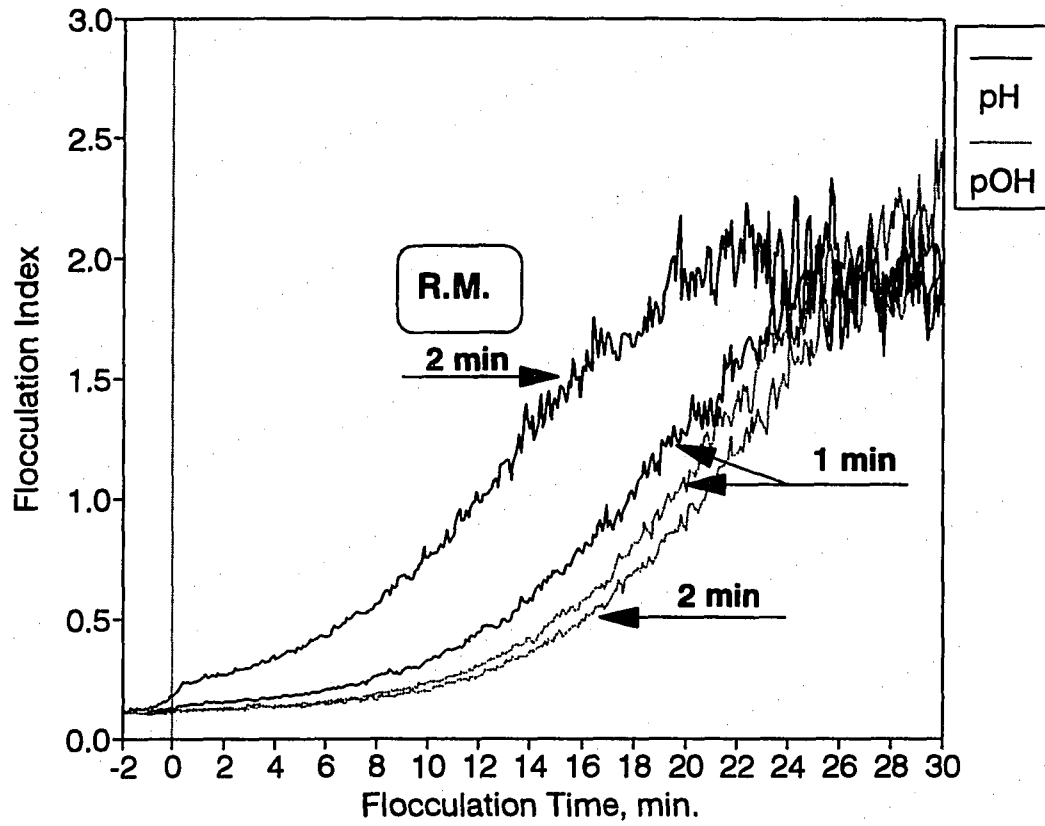
Figure 5.58. Effect of rapid mixing duration and system chemistry on the rate of
flocculation at 5 °C (pH=8.0, clay: 25 mg/L, dose: 5 mg/L, 30 rpm)

was evident at 5 °C with 1 min of rapid mixing, was substantially shortened with 2 min of rapid mixing.

It has been found from the experimental results that the sulfate ion played important role in the flocculation process. The sulfate ion added to the clay suspension greatly accelerated flocculation kinetics, particularly in the more acidic pH levels, not only by enhancing the extent and rate of Fe(III) precipitate formation but also suppressing the high positive surface charge of particles. In contrast, low temperature has been found to influence the chemical aspects of Fe(III) coagulation, by slowing the hydrolysis-precipitation process and thereby affecting surface charge of clay plus Fe(III) particles after rapid mixing. These evidences might lead to the hypothesis that sulfate ion can promote the hydrolysis-precipitation reaction slowed at low temperature, possibly enhancing flocculation kinetics at low temperature. To study this hypothesis, an appropriate amount of sulfate was added in the clay suspension at low temperature to confirm its effect on the flocculation process at cold temperature. These experiments were designed to compare the alternation of the system chemistry either by using constant pOH or adding sulfate ion at pH 6.8 and at 5 °C. The results presented in Figures 5.59 and 5.60 include simultaneous observation of flocculation kinetics using the AIA and PDA. As shown in Figures 5.59 and 5.60 with a baseline pH of 6.8 at 5 °C, more effective flocculation is accomplished while holding constant pOH and/or adding 10^{-3} M sulfate ion than by using constant pH without sulfate ion. At constant pH, comparison of the flocculation rates observed between with and without using sulfate ion shows that the sulfate ion significantly affects the flocculation process at low temperature at this baseline pH,
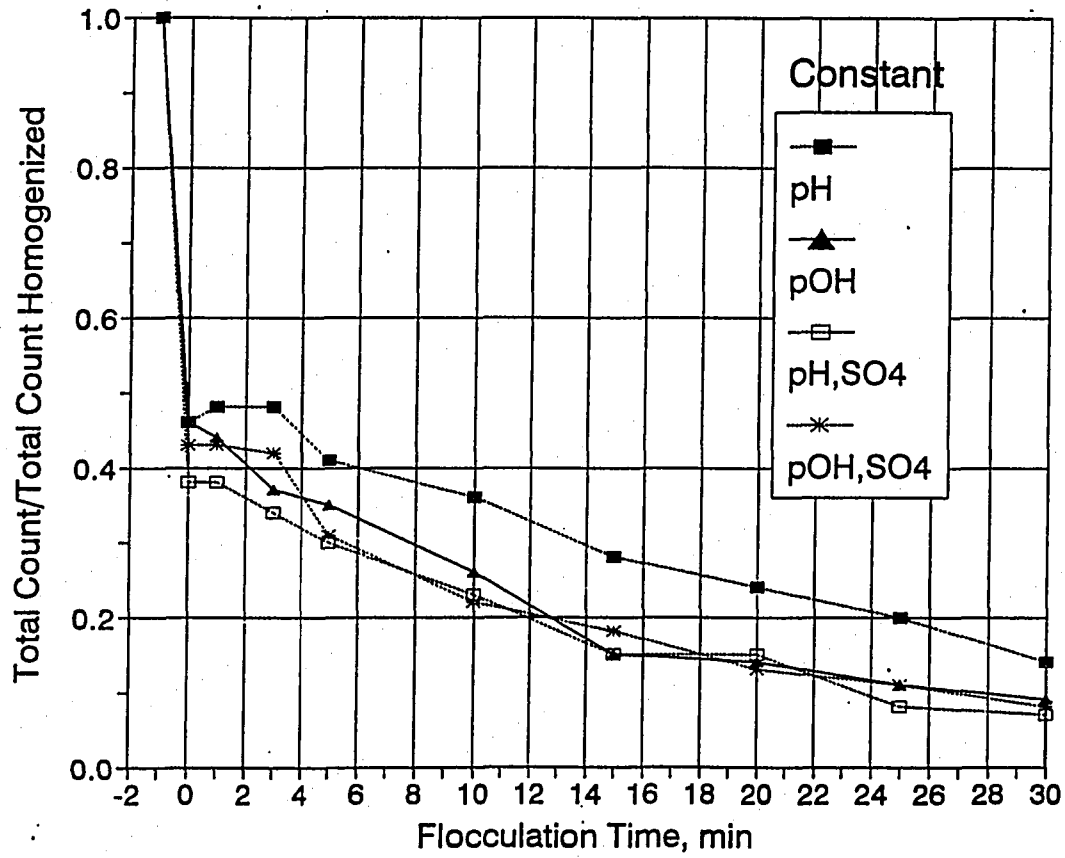
Figure 5.59. Effect of system chemistry on the rate of flocculation at 5 °C (constant pH: 6.8, clay: 25 mg/L, dose: 5 mg/L, 30 rpm); total particle count fraction vs. time
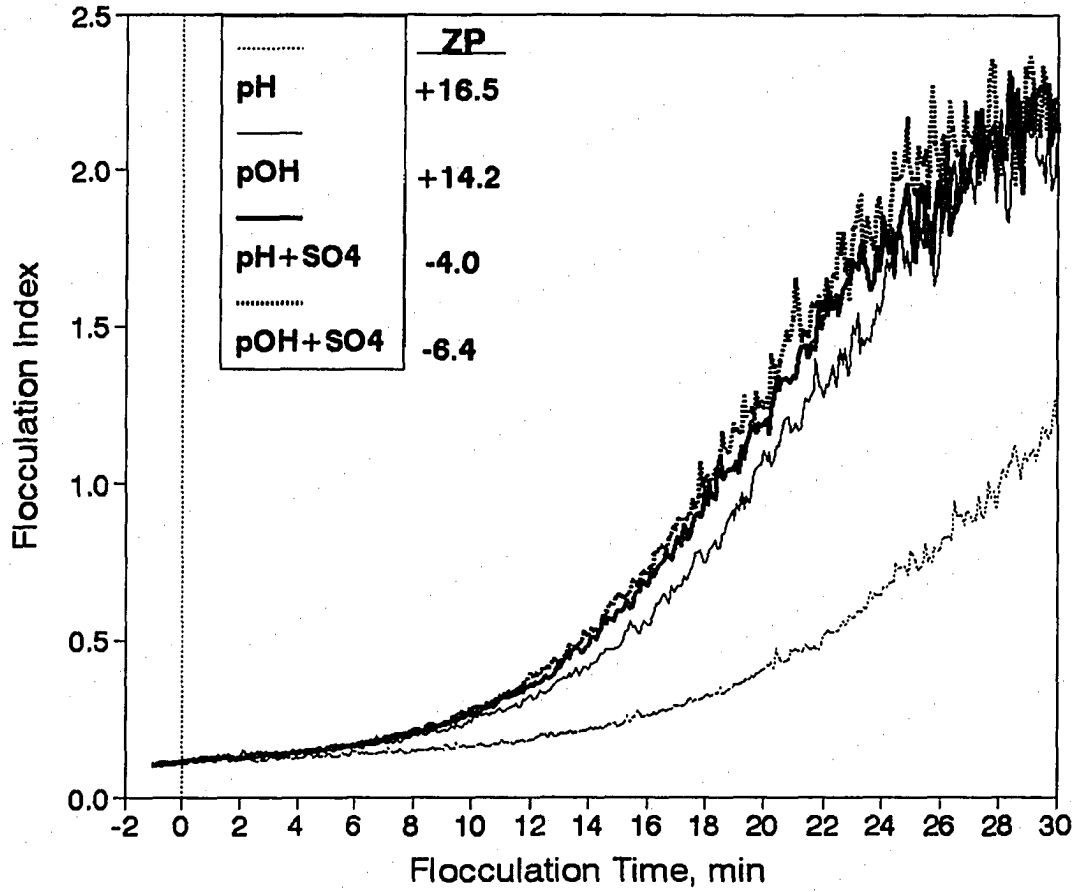
Figure 5.60. Effect of system chemistry on the rate of flocculation at 5 °C (constant pH: 6.8, clay: 25 mg/L, dose: 5 mg/L, 30 rpm); flocculation index vs. time

too, not only enhancing the rate of flocculation, also lowering surface charges of particles. However, use of sulfate ion at constant pH or pOH has a slightly greater effect on flocculation kinetics than maintaining constant pOH alone, although the sulfate ion brought down the high positive ZP to close to zero.

Figure 5.61 presents the effect of system chemistry on flocculation kinetics at pH 8.0, but otherwise with the same experimental conditions as at pH 6.8 in Figure 5.60. Note in this figure that neither of the two ways of altering system chemistry is capable of improving the flocculation kinetics at low temperature. Although sulfate ion causes significant changes of ZP values, it does not enhance the flocculation kinetics at pH 8.0 and 5 °C. This result shows a different effect of applying sulfate ion at low temperature on flocculation kinetics. Comparison of the results at pH 8.0 with those at pH 6.8 indicates that at low temperature, once again, the sulfate ion appears favorable for the aggregation of kaolin particles at the more acidic pH levels, i.e., pH 6.8 in this study.

Figures 5.62 and 5.63 show the comparison of the alternation of system chemistry by either holding constant pOH or adding 10^{-3} M sulfate ion at 5 °C. These results were obtained with a high-turbidity water (50 mg/L kaolin) using a high coagulant dose (10 mg/L) at pH 6.8 and 8.0 to investigate the influence of sulfate at low temperature on flocculation kinetics. As evidenced previously, the uses of higher coagulant dose and higher particle concentration have been found to provide more favorable flocculation kinetics at low temperature. First, at pH 6.8, noted in Figure 5.62 that maintaining constant pOH slightly improved flocculation kinetics. However, the use of sulfate at constant pH or pOH does not change the flocculation

Figure 5.61. Effect of system chemistry on the rate of flocculation at 5 °C (constant pH: 8.0, clay: 25 mg/L, dose: 5 mg/L, 30 rpm); flocculation index vs. time

Figure 5.62. Effect of system chemistry on the rate of flocculation at 5 °C (constant pH: 6.8, clay: 50 mg/L, dose: 10 mg/L, 30 rpm); flocculation index vs. time
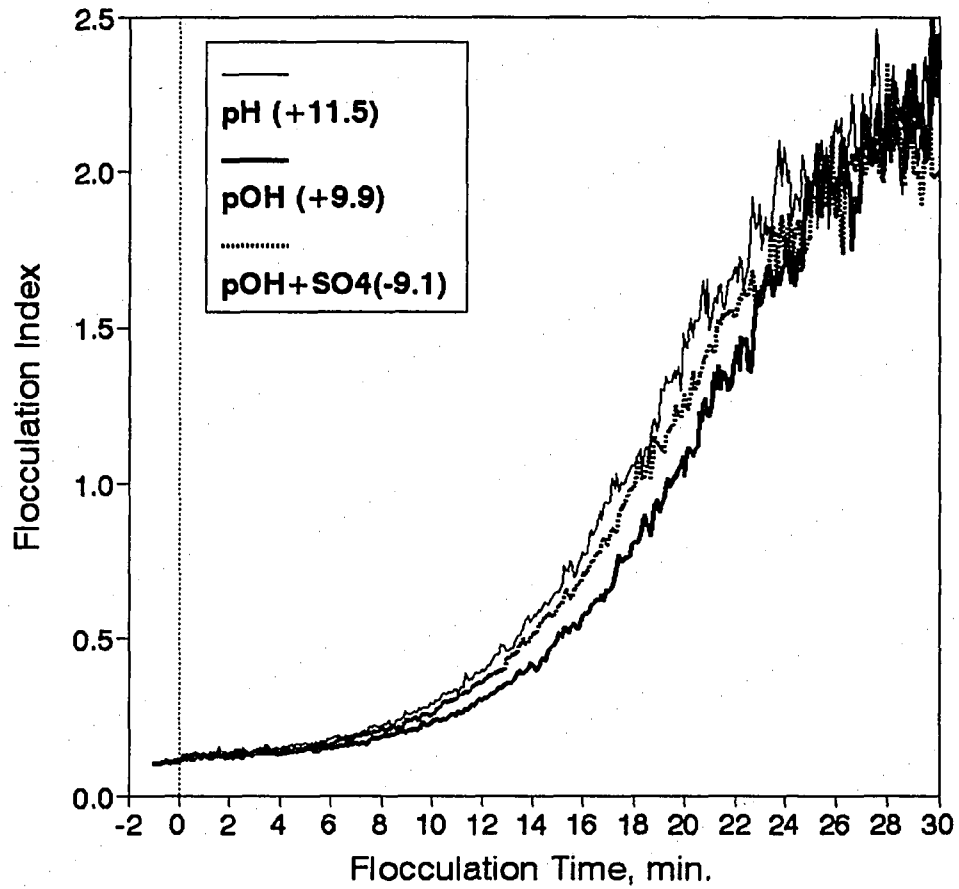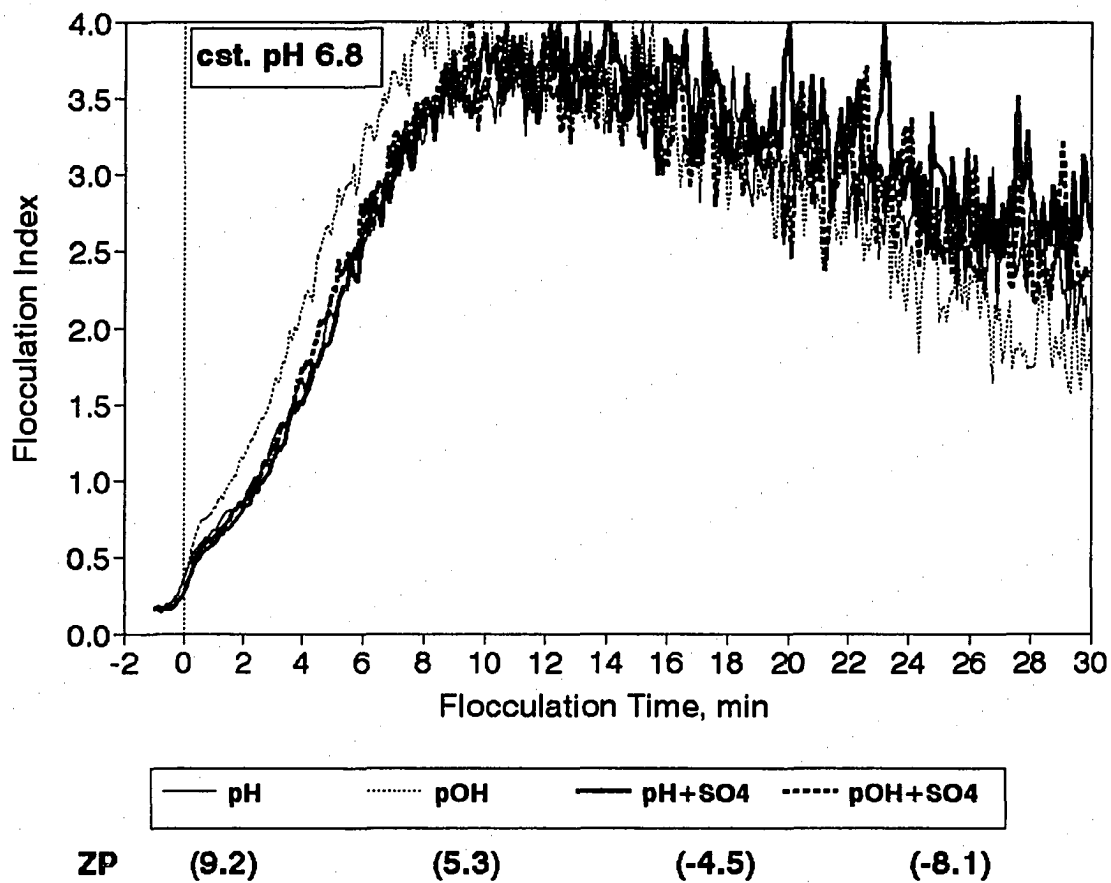
Figure 5.63. Effect of system chemistry on the rate of flocculation at 5 °C (constant pH: 8.0, clay: 50 mg/L, dose: 10 mg/L, 30 rpm); flocculation index vs. time

kinetics, although sulfate causes significant changes in surface charge of particles. Second, at pH 8.0 as shown in Figure 5.63, the use of sulfate at constant pH slightly improved flocculation kinetics. But, maintaining constant pOH without adding sulfate results in the ZP value closer to zero (-2.1 mV), it has a detrimental effect on flocculation kinetics. Overall, the influence of sulfate on flocculation kinetics at low temperature was reduced under the better flocculation conditions provided by increased coagulant dose and kaolin concentration.

Figure 5.64 presents the influence of sulfate ion on the rate of flocculation at low temperature using 50 mg/L kaolin at pH 6.0. As shown in the flocculation index curves, the rate of flocculation is greatly improved in the presence of sulfate at low temperature. The addition of sulfate into the clay suspension significantly affected the rate and extent of iron precipitate formation at pH 6.0, and hence it greatly reduced the highly positive ZP value. Therefore, the increased quantity of iron hydroxide and the neutralization of excess positive charge of particles due to the addition of sulfate enhanced interparticle collision frequency during flocculation process, and thereby improved the rate of floc growth.

Figure 5.65 shows the effect of sulfate ion on flocculation kinetics at pH 6.5 and 5 °C. Included in the figure is a baseline curve at pH 6.5 and 23 °C compared with curves obtained at 5 °C. The pH of 6.5 at 23 °C results in a pH of 7.2 at 5 °C to maintain constant pOH. In Figure 5.65, the applied coagulant dosage was reduced to 2 mg/L to avoid possible restabilization at higher coagulant dosage accompanied by highly positive charge of particles. The ZP at the 23 °C baseline condition was -6.1 mV. Figure 5.65 shows that the rate of flocculation was dramatically improved at 5 °C by maintaining constant pOH and/or adding

Figure 5.64. Effect of system chemistry on the rate of flocculation at 5 °C (constant pH: 6.0, clay: 50 mg/L, dose: 5 mg/L, 30 rpm); flocculation index vs. time
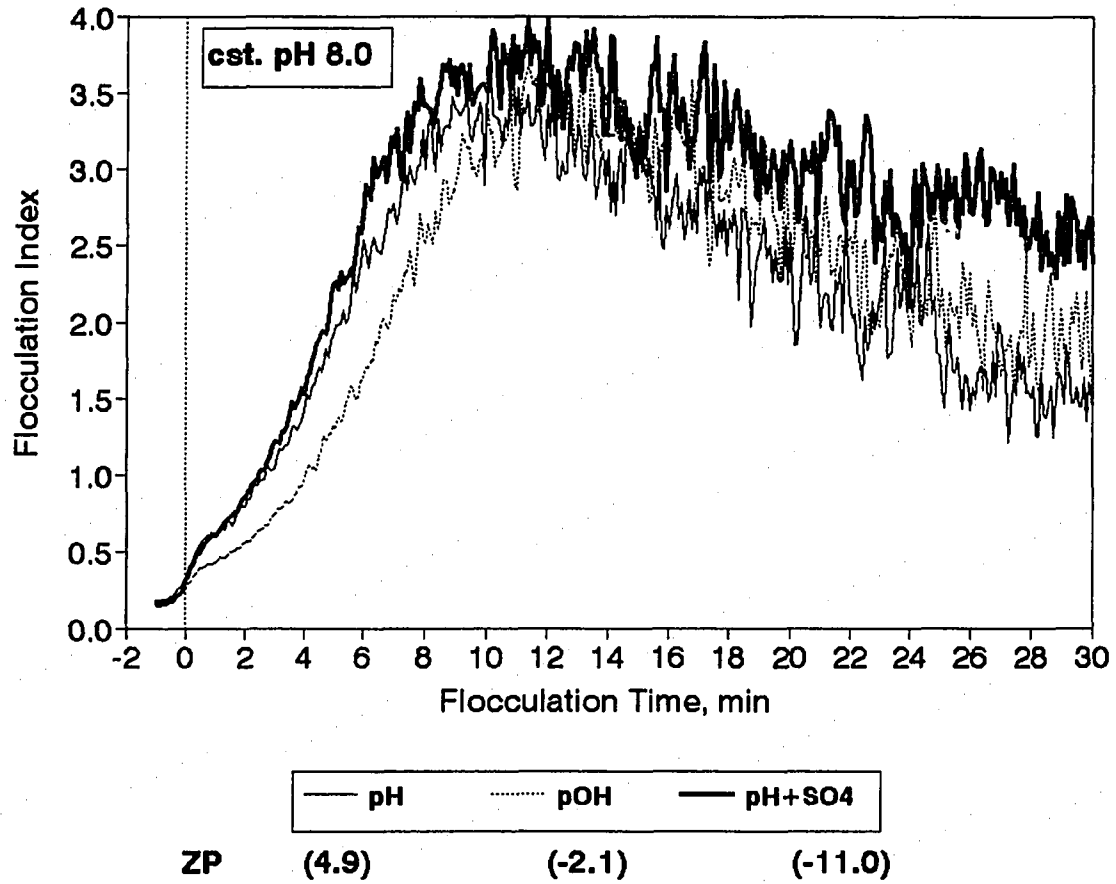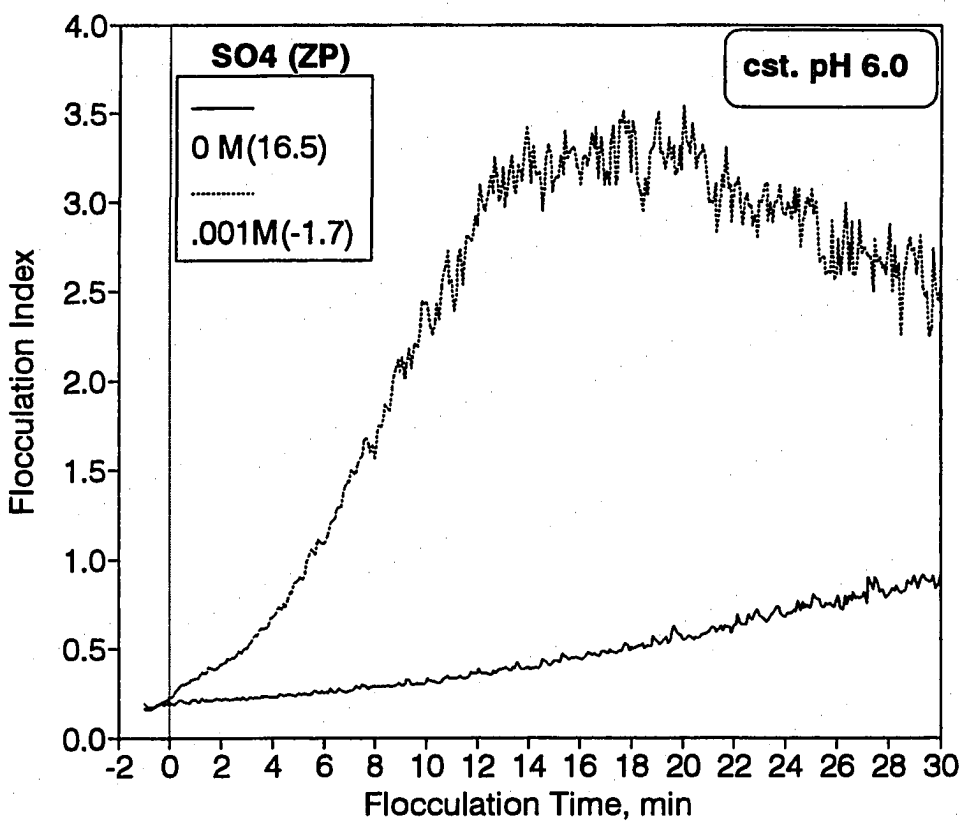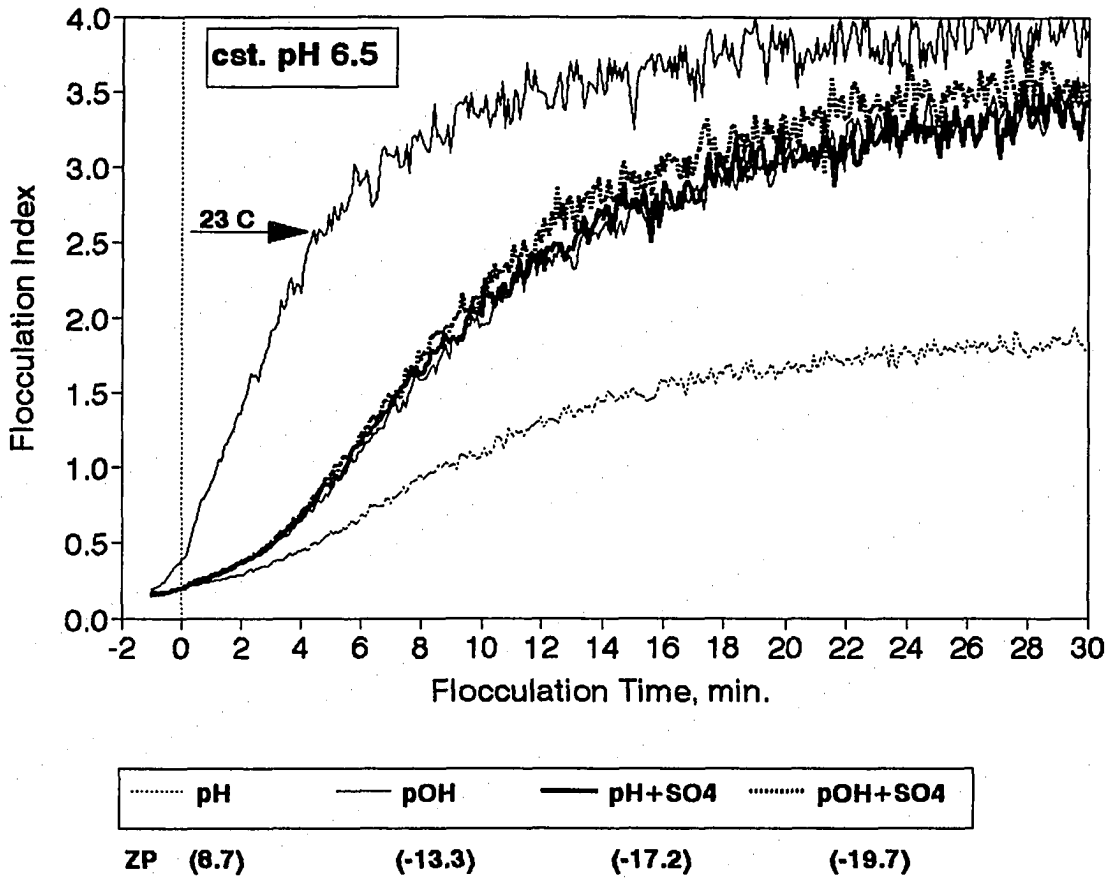
234

Figure 5.65. Effect of system chemistry on the rate of flocculation at 5 °C (constant pH: 6.5, clay: 50 mg/L, dose: 2 mg/L, 45 rpm); flocculation index vs. time

sulfate. But, sulfate did not induce substantial further improvement of flocculation kinetics compared with maintaining constant pOH alone, although it distinctly affects the ZP of particles. Comparing the flocculation kinetics observed between 5 and 23 °C, it is apparent that even the best performance at cold temperature did not reach the performance at 23 °C. Cold water temperature significantly influenced the extent to which aggregates were formed, and it certainly influenced the chemical kinetics so that the ZP of the particles and optimum pH are strongly affected. In general, comparison of the experimental data for the effect of sulfate at different pH, as shown in Figures 5.62 to 5.65, indicates that cold temperature flocculation kinetics on the more acidic side of flocculation was greatly improved if an adequate amount of sulfate is present, but it did not match the kinetics at room temperature.

Once again, to experimentally verify the distinct difference in flocculation kinetics and the reliability of flocculation index curve, the changes in aggregates volume distribution and supernatant turbidity during settling after flocculation are presented in Figures 5.66 and 5.67. These experimental data were obtained during the same experiment presented in Figure 5.65. Again, the aggregates volume distribution were determined by particle size measurement using the AIA equipped with a low magnification (36x) of the microscope. Figure 5.66(a) presents the comparison of the changes in fractional aggregate volume for a suspension after 10 and 20 minutes of flocculation at pH 6.5 and 5 °C; whereas, Figure 5.66(b) presents the results after 10 min of flocculation at different experimental conditions. First, as shown in Figure 5.66(a), the differential volume distribution indicates that a significant changes occurred between 10 min to 20 min of flocculation duration. For example, as the flocculation proceeds, the
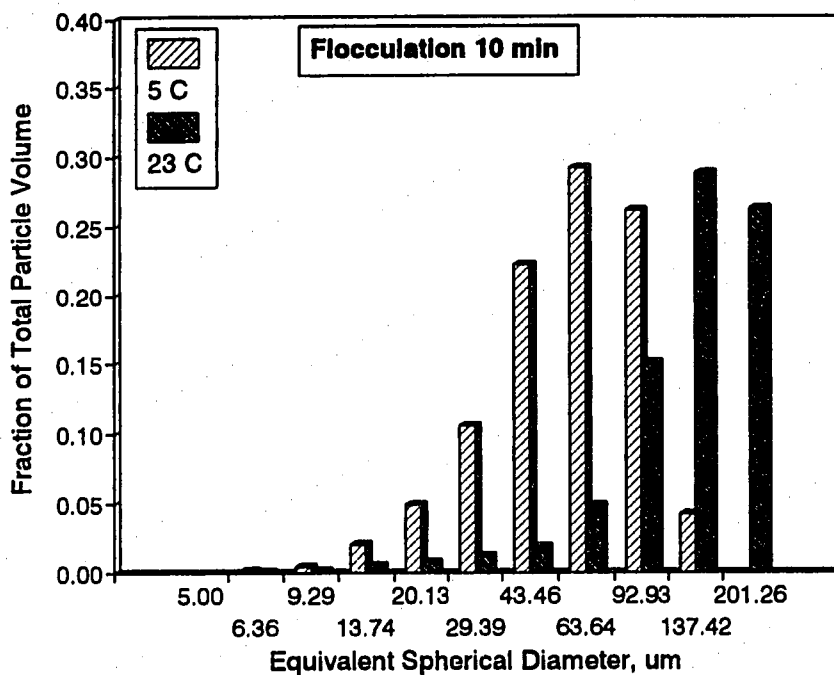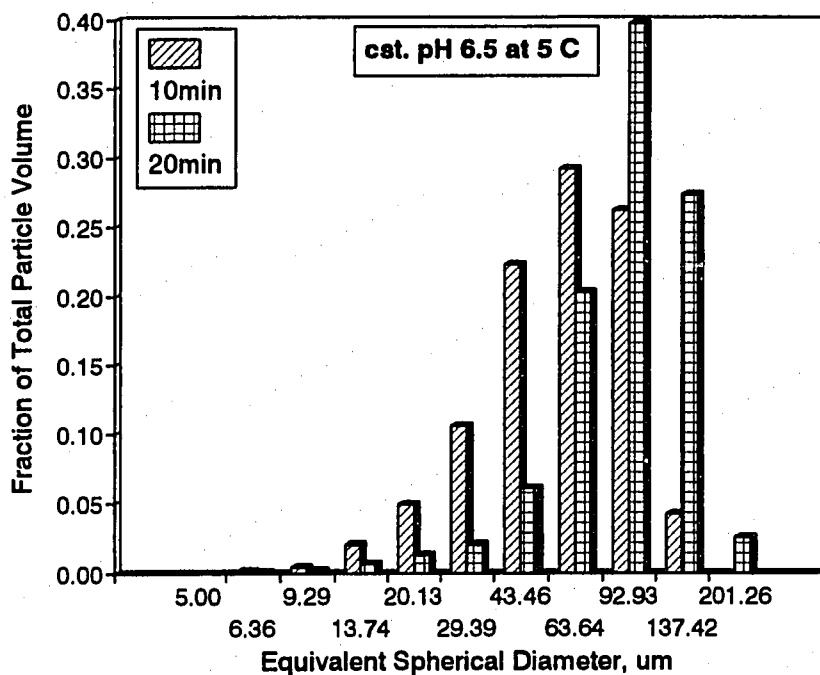
Figure 5.66. Changes in particle volume distributions (constant pH: 6.5, clay: 50 mg/L, dose: 2 mg/L, 45 rpm);(a) at different flocculation time at pH 6.5 and 5 °C, 10 min vs. 20 min,(b)at 10 min flocculation time, pH 6.5 at 23 °C vs. constant pOH at 5 °C

aggregates substantially grow in the bigger size range. Second, as shown in Figure 5.66(b), the shift in the size range containing the largest fractional volume of aggregates indicates that a significantly different degree of flocculation occurred at the warmer temperature. That is, the faster flocculation kinetics attained at 23 °C resulted in an increase in the volume of larger aggregates. As evidenced in Figures 5.66(a) and (b), the aggregate volume distribution determined by particle size measurement, once again, demonstrated the reliable indication of the differences in flocculation kinetics represented by the flocculation index curves.

Figure 5.67 presents the changes in supernatant turbidity during sedimentation at different experimental conditions, i.e., pH 6.5 at 23 °C versus constant pOH at 5 °C. These experimental data were also obtained during the same experiment presented in the prior Figure 5.65. As shown in this figure, the faster flocculation kinetics evidenced at 23 °C in the prior Figure 5.65 results in the formation of flocs that settled much more rapidly. However it should be considered that the increased viscosity of water at 5 °C also had a detrimental effect on settling of the flocs. Comparison of Figures 5.65 and 5.66(b) with 5.67 demonstrated that cold water temperature impaired the growth of flocs during flocculation process and removal of turbidity during sedimentation.

Figures 5.68 and 5.69 present the influence of sulfate ion on flocculation kinetics at 5 °C for 100 mg/L clay concentration using 10 mg/L coagulant dose at pH 6.8 and 8.0, respectively. At pH 6.8, noted in Figure 5.68, the addition of sulfate at low temperature results in an improvement of flocculation kinetics and reduction of highly positive ZP of particles. However, at pH 8.0 as shown in Figure 5.69, the pronounced influence of sulfate on
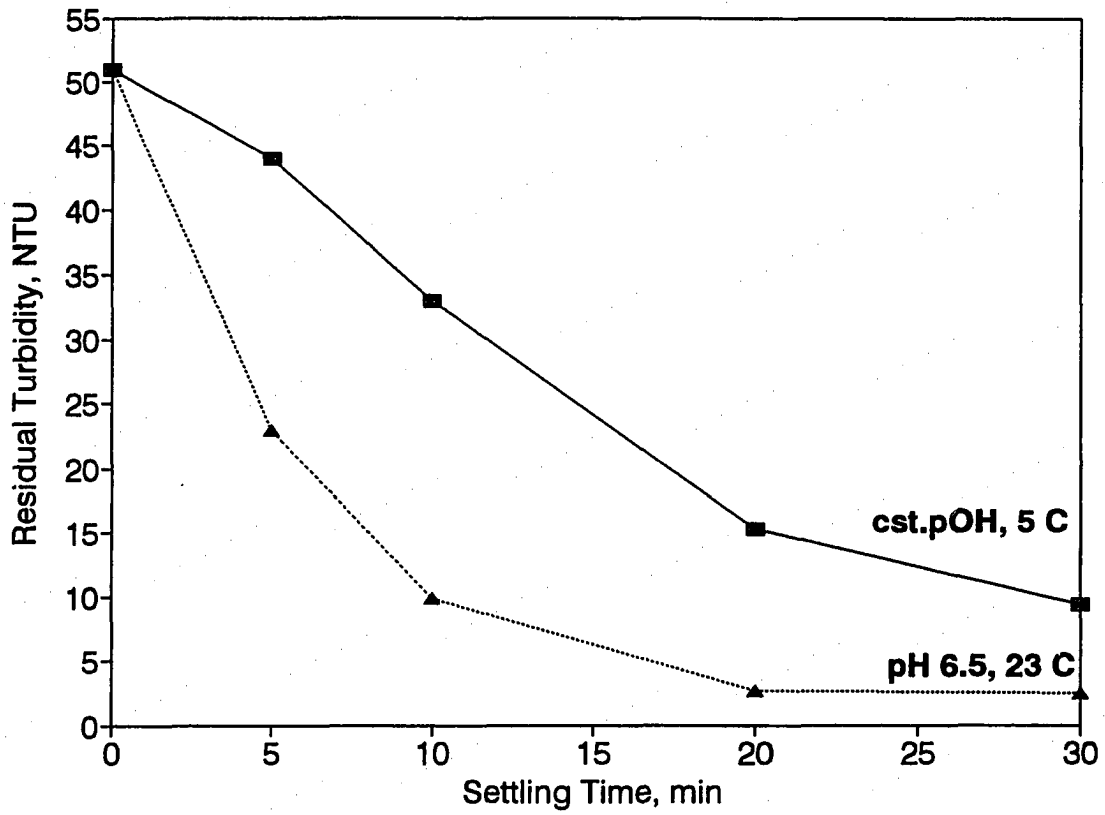
Figure 5.67. Effect of temperature on the changes in residual turbidity against settling time (constant pH: 6.5, clay: 50 mg/L, dose: 2 mg/L, 45 rpm)
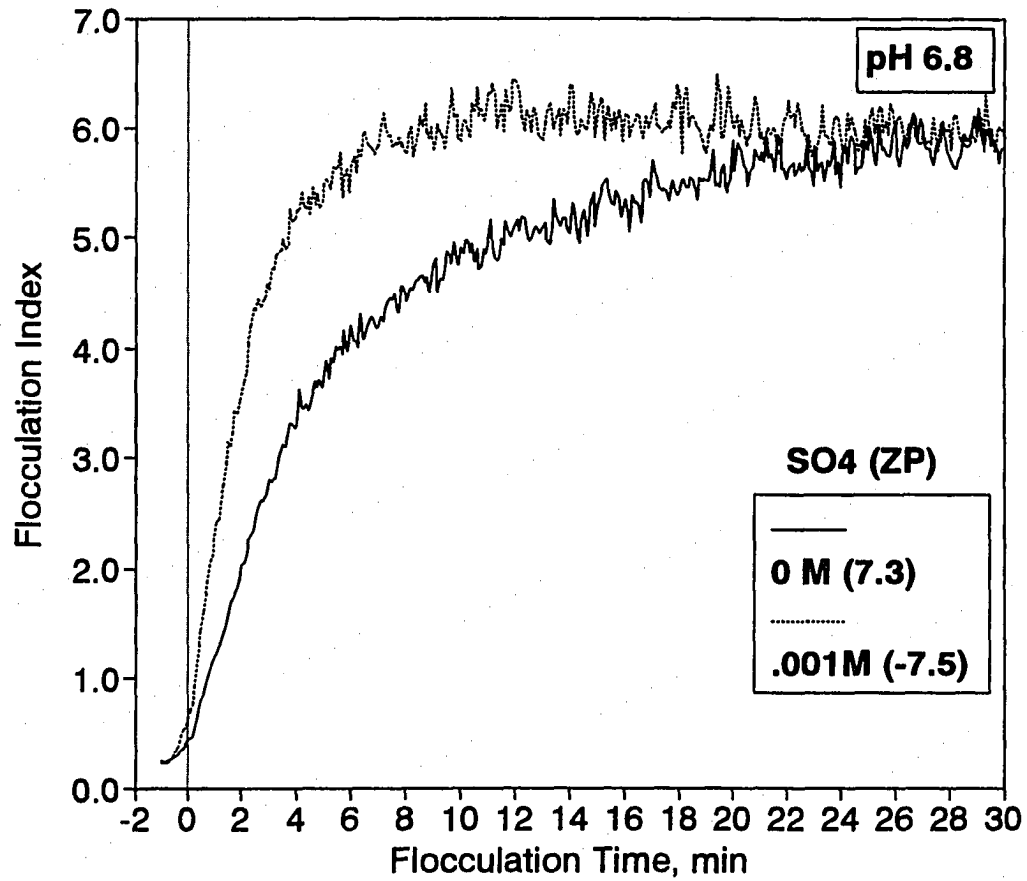
Figure 5.68. Effect of system chemistry on the rate of flocculation at 5 °C (constant pH: 6.8, clay: 100 mg/L, dose: 10 mg/L, 45 rpm); flocculation index vs. time
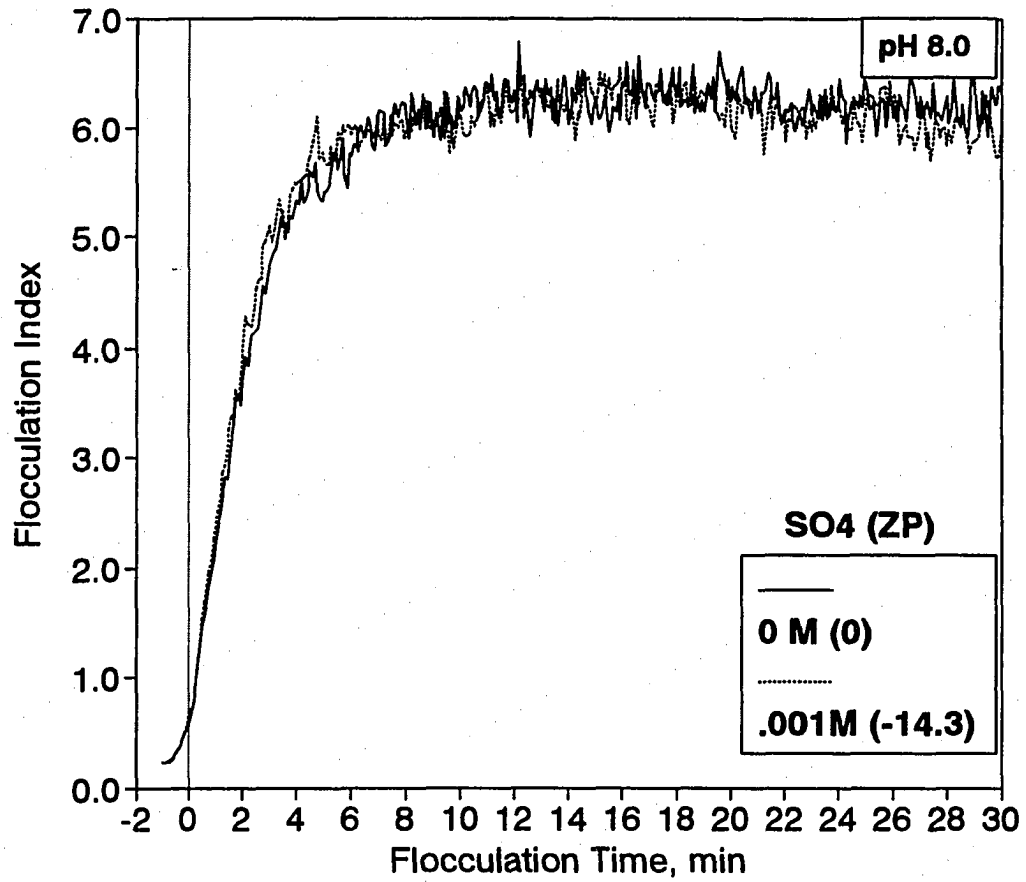
Figure 5.69. Effect of system chemistry on the rate of flocculation at 5 °C (constant pH: 8.0, clay: 100 mg/L, dose: 10 mg/L, 45 rpm); flocculation index vs. time

flocculation kinetics disappeared, although it still significantly changes the ZP of particles. Comparison of Figure 5.68 with Figure 5.69, once again, shows that the presence of sulfate at low temperature has a beneficial effect on flocculation kinetics for higher clay concentration, too, especially at lower pH value. Therefore, it can be concluded that the presence of sulfate extends the optimum range of rapid flocculation kinetics to lower pH levels over the entire range of clay concentration studied, 25 to 100 mg/L.

242

6. CONCLUSIONS

This research focused on the use of a Fe(III) coagulant to make quantitative studies of the rate at which flocculation processes occur, the factors upon which these rates depend, and the mechanisms involved. Both the particle size distribution data obtained from the Automatic Image Analysis (AIA) system and the measurement of the degree of turbidity fluctuation in a flowing suspension obtained from the Photometric Dispersion Analyzer (PDA) were used to measure flocculation kinetics. The effects of sulfate addition (from 0 to 2×10^{-3} M), pH (from 6.0 to 8.7), clay concentration (from 5 to 500 mg/L), temperature (5 and 23 °C), and mixing energy input (from 30 to 60 rpm slow mixing speed) were studied. In the following conclusions, general aspects flocculation kinetics are considered first. Second, the effect of sulfate ion on flocculation kinetics is considered. Finally, the effect of temperature on flocculation kinetics is presented.

6.1 Flocculation Kinetic Studies

1. Both the particle size distribution data obtained from the AIA and the on-line measurement of turbidity fluctuation by the PDA provided reliable and sensitive indications of flocculation kinetics, as evidenced by the rate of disappearance of primary particles and the rate of aggregation of particles. The AIA at high magnification gave the best indication of the primary particle disappearance, whereas, the PDA ratio values (i.e.,

the flocculation index) gave the best indication of the larger floc formation. The AIA at low magnification was also useful in observing the floc size distribution at various times during flocculation.

2. There were marked increases in the speed of flocculation with pH increase in experiments between pH 6.0 and 8.0 in the absence of sulfate ion.

3. Below a specific lower limit of pH, the use of higher mixing intensity or more complete charge neutralization did not improve the rate of flocculation. This was observed in the absence of sulfate over the range of clay concentrations from 25 to 100 mg/L.

4. The effect of clay concentration on flocculation kinetics was evident. Higher clay concentrations resulted in more rapid rate of flocculation, especially during the first few minutes of the flocculation process. The effect of pH on the rate of flocculation was substantially reduced at higher clay concentrations over the pH range 6.5 to 8.0. But, at pH 6.0, the rate of flocculation was very slow regardless of the clay concentrations used.

5. The differences in the supernatant turbidity during sedimentation following flocculation, and the changes in aggregate volume distributions during the flocculation process obtained by the AIA analysis provided additional evidence about the differences in the flocculation kinetics, and demonstrated the reliability of the flocculation index (obtained by the PDA

analysis) as a useful indicator of flocculation kinetics.

6.2 Effect of Sulfate on Flocculation Kinetics

1. Sulfate ion added to the kaolin suspension played an important role in the flocculation process, not only in improving flocculation kinetics at more acidic pH levels (pH 6.0 to 6.8) but also in changing surface charge of particles.

2. Over the entire range of clay concentrations investigated, the impact of sulfate ion on flocculation kinetics and reduction of ZP of particles was quite variable at different pH levels. The impact on flocculation kinetics and reduction in ZP of the clay particles was more dramatically beneficial in the more acidic pH range (pH 6.0 to 6.8) and at the lower clay concentrations.

3. The kinetics of flocculation were improved mainly by the enhanced rate and extent of Fe(III) precipitation attributed to the addition of sulfate, and thereby, better interparticle collision frequency, but little by the charge reductions resulting from the sulfate addition.

4. The increase in sulfate concentration beyond 3×10^{-4} M (up to 2×10^{-3} M) did not induce further improvement in flocculation kinetics, although the higher concentrations of sulfate ion substantially increased the negative ZP value of particles.

6.3 Effect of Temperature on Flocculation Kinetics

1. Low water temperature had the pronounced effect on flocculation kinetics over the range of clay concentration studied from 25 to 100 mg/L, slowing the rate of flocculation and enhancing the charge neutralizing ability of Fe(III) coagulant. The detrimental effect was most notable at lower clay concentrations, in the absence of sulfate ion, and with the pH held constant at the cold temperature, and in the formation of larger aggregates as revealed by the PDA analysis.

2. The use of constant pOH at 5 $^{\circ}$C to adjust water chemistry for temperature change was found to be partially effective for reducing the impact of low temperature on flocculation kinetics, but only in the more acidic pH range studied (pH 6.5 and 6.8). But the improved performance did not reach the performance at room temperature.

3. The addition of sulfate ion into clay suspension resulted in an improvement of flocculation kinetics at low temperature over the range of clay concentration investigated (25 to 100 mg/L), especially in the more acidic pH range studied (pH 6.0 to 6.8). The benefits were also most dramatic at the lower clay concentrations studied. But, the improved performance did not reach the performance at room temperature.

4. The addition of sulfate ion had beneficial effects similar to those obtained by maintaining constant pOH on improving the rate of flocculation at low temperature. But, the addition

of sulfate ion, in addition to maintaining constant pOH, did not induce substantial further improvement of flocculation kinetics compared with maintaining constant pOH alone.

5. Three experimental provisions were found to partially offset the detrimental effect of low temperature on flocculation kinetics; (1) increasing the coagulant dosage, (2) moderately increasing the slow mixing intensity, and (3) extending the rapid mixing period. However, the optimization of the combination of these provisions would be necessary in a case by case basis, particularly depending on pH.

BIBLIOGRAPHY

American Water Works Association (1971). Water Quality and Treatment, Third Edition, McGraw-Hill, New York.

American Water Works Association (1990). Water Quality and Treatment, Fourth Edition, McGraw-Hill, New York.

AWWA Coagulation Committee (1989). Committee report: Coagulation as an Integrated Water Treatment Process, Jour. Am. Water Works Assoc., 81, 10: 72-78.

Amirtharajah, A. (1987). Rapid Mixing and The Coagulation Process, Presented at The AWWA Annual Conference, Kansas City, MO.

Amirtharajah, A. and Mills K. M. (1982). Rapid-Mix Design for Mechanisms of Alum Coagulation, Jour. Am. Water Works Assoc., 74, 4: 210-216.

Amirtharajah, A. and O'Melia C. R. (1990). Coagulation Process: Destabilization, Mixing, and Flocculation In Water Quality and Treatment, 4th edition, McGraw-Hill.

Apps, J. A. and Neil, J. M. (1990). Solubilities of Aluminum Hydroxides and Oxyhydroxides in Alkaline Solutions: Correlation with Thermodynamic Properties of $Al(OH)_4^-$ In Chemical Modelling of Aqueous Systems II, Melchioral, D. C. and Bassett, R. L., Eds, American Chemistry Society Symposium Series 416.

Argaman, Y. and Kaufman, W. J. (1968). Turbulence in Orthokinetic Flocculation, SERL Report No. 68-5. Sanitary Engineering Research Laboratory, University of California, Berkeley, Calif., July.

Baes, C. f. and Mesmer, R. E. (1976). The Hydrolysis of Cations. John Wiley and Sons, New York.

Bottero, J. Y. and Bersillon, J. L. (1989) Aluminum and Iron(III) Chemistry: Some Implications for Organic Substance Removal In Aquatic Humic Substances, Suffet, I. H. and MacCarthy, P., Eds, Advances in Chemistry Series 219, American Chemistry Society, Washington, D.C. : 425-442.

Bratby, J. R. (1981). Interpretating Laboratory Results for the Design of Rapid Mixing and Flocculation Systems, Jour. Am. Water Works Assoc., 73, 6: 318-325.

Camp, T. R., Root, B. A., and Bhoota, B. V. (1940). Effects of Temperature on the Rate of Floc Formation, Jour. Am. Water Works Assoc., 32, 11: 1913-1927.

Camp, T. R. and Stein, P.C. (1943). Velocity Gradients and Internal Work in Fluid Motion, Jour. Boston Society of Civil Engineers, 30, 10: 219-237.

Carroll, B. A. and Hawkes, M. J. (1991). Operational experiences of Converting from Aluminum to Iron Coagulation at a Water Supply Treatment Works, Water Supply, 9, 9: 53-58.

Clark, M. M. (1985). Critique of Camp and Stein's RMS Velocity Gradient, Jour. Envir. Engr. Div., 111, 12: 741-754.

Cleasby, J. L. (1984). Is Velocity Gradient a Valid Turbulent Flocculation Parameter ?, Jour. Envir. Engr. Div., 110, 10: 875-897.

Cleasby, J. L., Sindt, G., Dhamarajah, H., and Baumann, E. R. (1989). Design and Operation Guidelines for Optimization of the High Rate Filtration Process, Am. Water Works Assoc. Research Foundation.

Crumbliss, A. L. and Garrison, J. M. (1988). A Comparison of Some Aspects of the Aqueous Coordination Chemistry of Aluminum(III) and Iron(III), Comments on Inor. Chem., 8, 1: 1-26.

Davis, J. A. and Leckie, J. O. (1978). Effect of Adsorbed Complexing Ligands on Trace Metal Uptake by Hydrous Oxides, Environ. Sci. Tech., 2: 1309-1315.

De Hek, H., Stol, R. J. and De Bruyn, P. L. (1978). Hydrolysis - Precipitation Studies of Aluminum(III) Solutions. 3. The Role of the Sulfate Ion, Jour. Colloid Inter. Sci., 64, 3: 72-89.

Dempsey, B. A. (1987). Chemistry of Coagulants. In Am. Water Works Assoc. Seminar Proceedings: Influence of Coagulation on the Selection, Operation, and Performance of Water Treatment Facilities. Am. Water Works Assoc., Denver, June: 19-30.

Dentel, S. K. (1987). Optimizing Coagulant Additions From Laboratory and Field Test Methods. In Am. Water Works Assoc. Seminar Proceedings: Influence of Coagulation on the Selection, Operation, and Performance of Water Treatment Facilities. Am. Water Works Assoc., Denver, June: 49-88.

Dentel, S. K. and Gossett, J. M. (1988). Mechanisms of Coagulation with Aluminum Salts, Jour. Am. Water Works Assoc., 80, 4: 187-198.

Dousma, J. and de Bruyn, P. L. (1976). Precipitation Studies of Iron Solutions II. Model for Hydrolysis and Precipitation from Fe(III) Nitrate Solutions, Jour. Colloid Inter. Sci., 56: 527-538.

Dousma, J, den Ottelander, D., and de Bruyn, P.L. (1979). The Influence of Sulfate Ions on the Formation of Iron(III) Oxides, Jour. Inorg. Nucl. Chem., 41: 1565-1568.

Driscoll, C. T. and Letterman, R. D. (1988). Chemistry and Fate of Al(III) in Treated Drinking Water, Jour. Envir.Engrg. Div., ASCE, 114, 2: 21-37.

Dzombak, D.A.and Morel, F.M.M.(1990). Surface Complexation Modeling, Hydrous Ferric Oxide, John Wiley & Sons, NY.

Flynn, C. M. (1984). Hydrolysis of Inorganic Iron(III) Salts, Chemical Review, 84: 31-41.

Francois, R.J. and Bekaert, N.V.(1986). Influence of Mixing Parameters and Water Quality on the Flocculation of Kaolinite with Aluminum Sulfate, In Chemistry for Protection of the Environment 1985. Proceedings of the 5th International Conference, Leuven, Belgium, 9-13, Sept. 1985.

Ghominy, H. F., Shafik, S. S., Mikhail, E. M., and Misak, N. Z. (1993). On the Sorption of Anions by Ferric Oxide Gel 1. Aqueous Medium, Colloids and Surfaces, 71: 91-97.

Gregory, J. (1985). Turbidity fluctuations in flowing suspensions, Jour. Colloid Inter. Sci., 105, 2: 357-371.

Gregory, J. (1989). Fundamentals of Flocculation, Critical Reviews in Environmental Control, 19, 3: 185-230.

Gregory, J. and Lee, S. Y. (1990). The effect of Charge Density and Molecular Mass of Cationic Polymers on Flocculation Kinetics in Aqueous Solution, Jour. Water SRT-Aqua., 39, 4: 265-274.

Gregory, J. and Nelson, D. W. (1986). Monitoring of Aggregates in flowing Suspensions, Colloids and Surfaces, 18: 175-188.

Haarhoff, J. and Cleasby, J. L. (1988). Comparing Aluminum and Iron Coagulants for In-line Filtration of Cold Water, Jour. Am. Water Works Assoc., 80, 4: 168-175.

Hahn, H. H. and Stumm, W. (1968). Kinetics of Coagulation with Hydrolyzed Al(III), Jour. Colloid Inter. Sci., 28, 9: 134-144.

Hahn, H. H. and Stumm, W. (1968). Coagulation by Al(III): The role of Adsorption of Hydrolyzed Aluminum in the Kinetics of Coagulation, In Adsorption From Aqueous Solution. Weber, W. J. and Matijevic, E. Eds. American Chemical Society Publishers, Washington, D.C.

Han, M. and Lawler, D. F. (1992). The (Relative) Insignificance of G in Flocculation, Jour. Am. Water Works Assoc., 84, 10: 79-91.

Hanna, Jr. G.P. and Rubin, A. J. (1970). Effect of Sulfate and Other Ions in Coagulation with Aluminum (III), Jour. Am. Water Works Assoc., 25, 5: 315-321.

Hanson, A. T. (1989). The Effect of Water Temperature and Reactor Geometry on Turbulent Flocculation. Ph.D. Dissertation, Library, Iowa State University, Ames, Iowa.

Hanson, A. T. and Cleasby, J. L. (1990). The Effect of Temperature on Turbulent Flocculation: Fluid Dynamics and Chemistry, Jour. Am. Water Works Assoc., 82, 11: 56-73.

Healy, T. W., James, R. O., and Cooper, R. (1968). The Adsorption of Aqueous Co(II) at the Silica-Water Interface, In Adsorption from Aqueous Solution, Advances in Chemistry Series, American Chemical Society.

Hem, J. D. and Roberson, C. E. (1990). Aluminum Hydrolysis Reaction and Products in Mildly Acidic Aqueous Systems, In Chemical Modelling of Aqueous Systems II, Melchioral, D. C. and Bassett, R. L., Eds. American Chemistry Society Symposium Series 416.

Hohl, H., Sigg, L., and Stumm, W. (1978). Characterization of Surface Chemical Properties of Oxides in Natural Waters: the role of specific adsorption in determining the surface charge. Paper presented at the symposium on Particulates in Water. 175th ACS National Meeting, Anaheim, CA.

Hunter, R. J. (1981). Zeta Potential in Colloid Science, Academic Press, NY.

Hunter, R. J. (1989). Adsorption from Solution. In Hunter, R. J. Ed. Foundations of Colloid Science, Volume II. Oxford University Press, NY.

Hutchison, W. and Foley, P. D. (1974). Operational and Experimental Results of Direct Filtration, Jour. Am. Water Works Assoc., 66, 2: 79-85.

Ives, J. K. (1978). Rate Theories In K. J. Ives, Ed. The Scientific Basis of Flocculation. NATO Advanced Study Institute Series, Series E, Applied Science-No. 27. Sijthoff and Noorhoff, Netherlands.

James, R. D. (1981). Surface Ionization and Complexation at the Colloid/Aqueous Electrolyte Interface. In Adsorption of Inorganics at Solid-Liquid Interfaces, Anderson, M. A. and Rubin, A. J., Eds. Ann Arbor Science Publishers, Inc., Michigan.

James, R. D. and Healy, T. W. (1972a). Adsorption of Hydrolyzable Metal Ions at the Oxide-Water Interface. I. Co(II) Adsorption on SiO_2 and TiO_2 as Model Systems, Jour. Colloid Inter. Sci., 40, 1: 42-52.

James, R. D. and Healy, T. W. (1972b). Adsorption of Hydrolyzable Metal Ions at the Oxide-Water Interface. II. Charge Reversal of SiO_2 and TiO_2 Colloids by Adsorbed Co(II), La(III), and Th(IV) as Model Systems, Jour. Colloid Inter. Sci., 40, 1: 53-63.

James, R. D. and Healy, T. W. (1972c). Adsorption of Hydrolyzable metal Ions at the Oxide - Water Interface. III. A Thermodynamic Model of Adsorption, Jour. Colloid Inter. Sci., 40, 1: 65-81.

Knight, R. J. and Sylva, R. N. (1974). Precipitation in hydrolyzed Iron(III) Solutions, Jour. Inorg. Nucl. Chem., 36: 591-597.

Knocke, W. R., West, C., and Hoehn, R. C. (1986). Effects of Low Temperature on the Removal of Trihalomethane Precursors by Coagulation, Jour. Am. Water Works Assoc., 78, 4: 189-195.

La Mer, V. K. (1964). Coagulation Symposium Introduction, Jour. Colloid Sci., 120: 1-16.

Lawler, D. F., O'Melia, C. R., and Tobiason, J. E. (1980). Integral Water Treatment Plant Design: From Particle Size to Plant Performance. In Kavanaugh M. C. and Leckie, J. O. Eds. Particulates in Water: Characterization, Fate, Effects, and Removal, American Chemical Society Publishers, Wa. D.C.

Lawler, D. F. (1993). Physical Aspects of Flocculation: from Microscale to Macroscale. In Separation of Particles from Water. Gregory, J. Ed. Pergamon Press: 165-180.

Leipold, C. (1934). Mechanical Agitation and Alum Floc Formation, Jour. Am. Water Works Assoc., 26, 8: 1070-1084.

Letterman, R. D. and Iyer, D. R. (1985). Modelling The Effects of Hydrolyzed Aluminum and Solution Chemistry on Flocculation Kinetics, Environ. Sci. and Tech., 19: 673.

Letterman, R. D. and Vanderbrook, S.G. (1983). Effect of Solution Chemistry on Coagulation with Hydrolyzed Al(III), Water Research, 17: 195-204.

Leprince, A., Fiessinger, F., and Bottero, J. Y. (1984). Polymerized Iron Chloride: An Improved Inorganic Coagulant, Jour. Am. Water Works Assoc., 76: 93-97.

Machesky, M. L. (1990). Influence of Temperature on Ion Adsorption by Hydrous Metal Oxides, In Chemical Modelling of Aqueous Systems II, Melchioral, D. C. and Bassett, R. L., Eds. American Chemistry Society Symposium Series 416.

Matijevic, E. (1973). Colloid Stability and Complex Chemistry, Jour. Colloid and Inter. Sci., 43, 2: 217-245.

Matijevic, E. and Janauer, G. E. (1966). Coagulation and Reversal of Charge of Lyophobic Colloids by Hydrolyzed Metal Ions. II. Ferric Nitrate, Jour. Colloid and Inter. Sci., 21: 197-223.

Matijevic, E. and Kolak, N. (1967). Coagulation of Lyophobic Colloids by Metal Chelates, Jour. Colloid Inter. Sci., 24: 441-450.

Matsui, Y. and Tambo, N. (1991). Online Floc Size Evaluation by Photometric Dispersion Analyzer, Water Supply, 9: 71-78.

Maulding, J. H. and Harris, R. H. (1968). Effect of Ionic Environmental and Temperature on the Coagulation of Color-Causing Organic Compounds with Ferric Sulfate, Jour. Am. Water Works Assoc., 60, 4: 460-476.

Mohtadi, M. F. and Rao, P. N. (1973). Effect of Temperature on Flocculation of Aqueous Dispersions, Water Research, 7, : 747-767.

Morel, F. M. M. (1983). Principles of Aquatic Chemistry, John Wiley and Sons, Inc.

Morel, F. M. M. and Hering, J. G. (1993). Principles and Applications of Aquatic Chemistry, John Wiley and Sons.

Morris, J. K. and Knocke, W. R. (1984). Temperature Effects on the Use of Metal-ion Coagulants for Water Treatment, Jour. Am. Water Works Assoc., 76, 3: 74-79.

Nordstrom, D. K. and May, H. M. (1989). Aqueous Equilibrium Data for Mononuclear Aluminum Species, In The Environmental Chemistry of Aluminum, Sposito, G. Ed. CRC Press, Boca Raton, FL: 29-54.

Nordstrom, D. K., Plummer, L. N., Langmuir, D., Busenberg, E., May, H. M., Jones, B. F., and Parkhurst, D. L. (1990). Revised Chemical Equilibrium Data for Major Water-Mineral Reactions and Their Limitations, In Chemical Modelling of Aqueous Systems II, Melchior, D. C. and Bassett, R. L. Eds. ACS Symposium Series 416, American Chemical Society, Washington, D.C.: 398-413.

O'Melia, C. R. (1978). Coagulation in Waste Water Treatment. In K. J. Ives, Ed. The Scientific Basis of Flocculation. Nato Advanced Study Institute Series, Series E, Applied Science-No. 27. Sijthoff and Noorhoff, Netherlands.

O'Melia C. R. (1987). Particle-Particle Interactions, In Aquatic Surface Chemistry. Stumm, W. Ed., John Wiley and Sons, N.Y.: 385-404.

O'Melia, C. R. and Stumm, W. (1967). Aggregation of Silica Dispersions by Iron(III), Jour. Colloid Inter. Sci., 23: 437-447

O'Melia, C. R., Gray, K. A., and Yao, C. H. (1989). Polymeric Inorganic Coagulants, Am. Water Works Assoc. Research Foundation.

Packham, R. F. (1965). Some Studies of the Coagulation of Dispersed Clays with Hydrolyzing Salts, Jour. Colloid Sci., 20: 81-92.

Parfitt, R. L. and Smart, R. C. (1978). The Mechanism of Sulfate Adsorption on Iron Oxides, Soil Sci. Soc. Am. Jour., 42:48-50.

Saffman, P. G. and Turner, J. S. (1956). On the Collision of Drops in Turbulent Clouds, Jour. Fluid Mechanics, 1, 1: 16-30.

Schindler, P. W. and Stumm, W. (1987). The Surface Chemistry of Oxides, Hydroxides, and Oxide Minerals In Aquatic Surface Chemistry. Stumm, W. Ed., John Wiley and Sons, N.Y.: 167-196.

Schneider, W. (1984). Hydrolysis of Iron(III) - Chaotic Olation versus Nucleation, Comments on Inorg. Chem., 3, 4: 205-223.

Schneider, W. and Schwyn, B. (1987). The Hydrolysis of Iron in Synthetic, Biological, and Aquatic Media, In Aquatic Surface Chemistry. Stumm, W. Ed. John Wiley and Sons, N.Y.: 167-196.

Sigg, L. and Stumm, W. (1981). The Interaction of Anions and Weak Acids with the Hydrous Goethite Surface, Colloids and Surfaces, 2:101-117.

Smith, R. W. and Hem, J. D. (1972) Effect of Aging on Aluminum Hydroxide Complexs in Dilute Aqueous Solutions, U.S.G.S. Water-Supply Paper 1827-D.

Snoeyink, V. J. and Jenkins, D. (1980). Water Chemistry. John Wiley and Sons, NY.

Sricharoenchaikit, P. and Letterman, R. D. (1987). Effect of Al(III) and Sulfate Ion on Flocculation Kinetics, Jour. Envir. Engr. Div., ASCE, 113, 10: 1120-1138.

Stumm, W. (1992). Chemistry of the Solid-Water Interface, Wiley-Interscience, NY.

Stumm, W. and Morgan, J. J. (1962). Chemical Aspects of Coagulation, Jour. Am. Water Works Assoc., 56, 1: 971-994.

Stumm, W. and Morgan, J. J. (1968). Stoichiometry of Coagulation, Jour. Am. Water Works Assoc., 60, 5: 514-539.

Stumm, W. and Morgan, J. J. (1981). Aquatic Chemistry. 2nd ed. John Wiley and Sons, NY.

Stumm, W. and O'Melia C. R. (1968). Stoichiometry of Coagulation, Jour. Am. Water Works Assoc., 60, 5: 514-539.

Sylva, R. N. (1972). The Hydrolysis of Iron(III), Reviews of Pure and Applied Chem., 22: 115-132.

Tang, H. and Stumm, W. (1987a). The Coagulation Behaviors of Fe(III) Polymeric Species, I. Preformed Polymers by Base Addition, Water Research, 21: 115-121.

Tang, H. and Stumm, W. (1987b). The Coagulation Behaviors of Fe(III) Polymeric Species, II. Preformed Polymers in Various Concentrations, Water Research, 21: 122-128.

Thompson, D. W. and Tahir, N. M. (1991). The Influence of a Smectite Clay on the Hydrolysis of Iron(III), Colloids and Surfaces, 60: 369-398.

Treweek, G. P. and Morgan, J. J. (1980). Prediction of Suspension Turbidities from Aggregate Size Distribution. In Kavanaugh M. C. and Leckie, J. O. Eds. Particulates in Water: Characterization, Fate, Effects, and Removal, American Chemical Society Publishers, Washington. D.C.

van Benschoten, J. E. and Edzwald J. K. (1990a). Chemical Aspects of Coagulation using Aluminum Salts-I. Hydrolytic Reactions of Alum and Polyaluminum Chloride, Water Research, 24, 12:1519-1526.

van Benschoten, J. E. and Edzwald J. K. (1990b). Chemical Aspects of Coagulation using Aluminum Salts-II. Coagulation of Fulvic Acid using Alum and Polyaluminum Chloride, Water Research, 24, 12: 1525-1535.

van der Woude, J. H. A. and de Bruyn, P. L. (1983). Formation of Colloidal Dispersions from Supersaturated Iron(III) Nitrate Solutions. Part I: Precipitation of Amorphous Iron Hydroxide, Colloids and Surfaces, 8: 55-78.

Velz, C. J. (1934). Influence of Temperature on Coagulation, Civil Engineering, 4, 7: 345-349.

Vik, E. A. and Eikebrokk, B. (1989). Coagulation Process for Removal of Humic Substances from Drinking Water, In Aquatic Humic Substances: Influence on Fate and Treatment of Pollutants, Suffet, I. H. and MacCarthy, P., A. Eds. Symposium by The American Chemical Society, Washington, D.C.: 385-408.

Weber, W. J. (1972). Physicochemical Processes for Water Quality Control, Wiley-Interscience, New York.

ACKNOWLEDGMENTS

APPENDIX

RESULTS OF 2 LITERS BATCH REACTOR TEST WITH

5 MG/L CLAY CONCENTRATION

Included in this Appendix are the experimental results of flocculation kinetic studies conducted in a 2 L square batch reactor identical to that used for jar tests. The experimental conditions are summarized as follows:

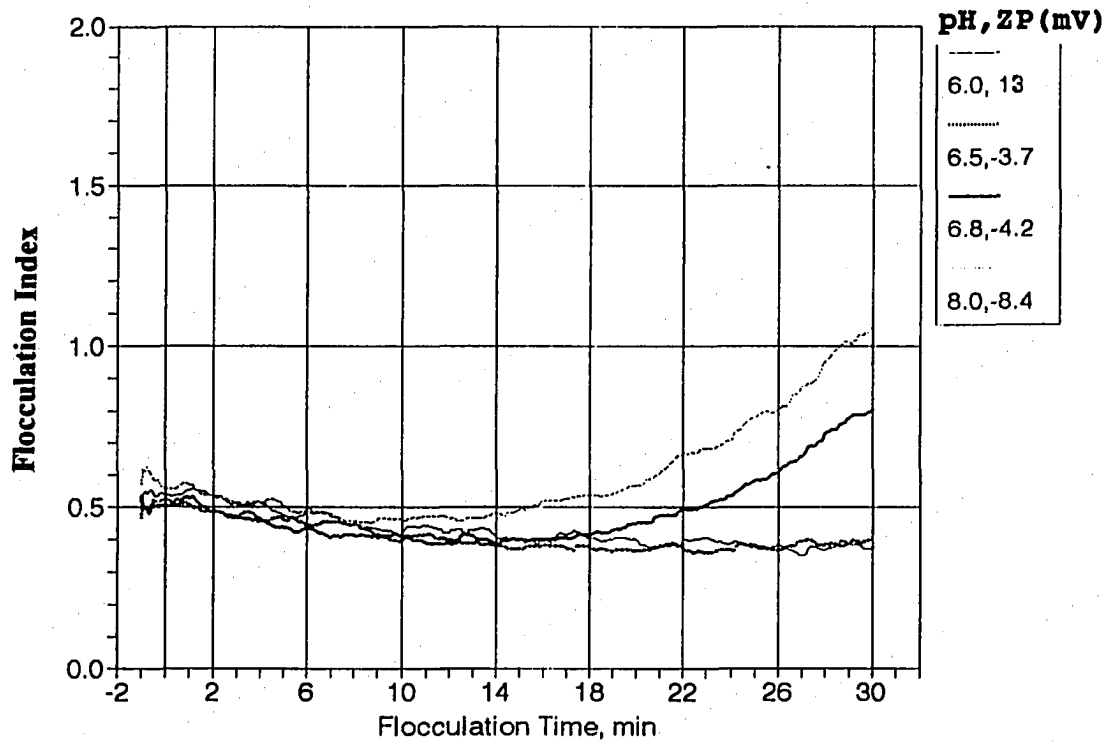| Parameters	Description
Clay Concentration	5 mg/L (5 NTU)
Dilution Water	distilled water
Ionic Strength	5×10^{-3} M (0.005 M $NaNO_3$)
Coagulant	stock solution, 0.25 M $Fe(NO_3)_3.9H_2O$
	dosing solution, 10 mg/mL $Fe(NO_3)_3.9H_2O$
Coagulant Dosage	5 mg/L as $Fe(NO_3)_3.9H_2O$
Rapid Mixing	250 rpm for 1 min.
Sulfate	0 to 10^{-3} M SO_4^{2-}
Temperature	room temperature (23 ± 1 °C)
RMS Gain Setting	200

Figure A.1. Effect of pH on the rate of flocculation (clay: 5 mg/L, dose: 5 mg/L)
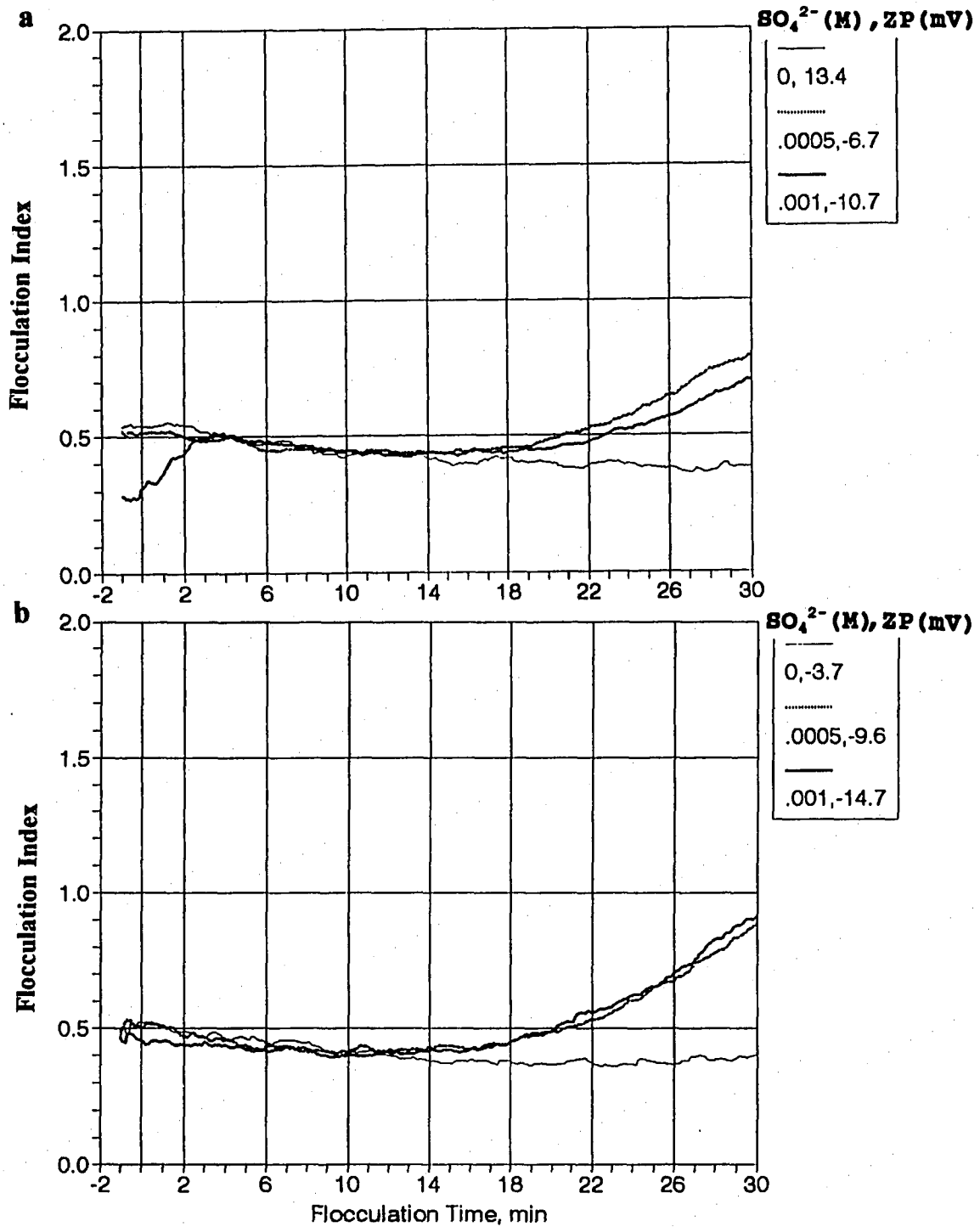
Figure A.2. Effect of sulfate concentration on the rate of flocculation
(clay: 5 mg/L, dose: 5 mg/L); (a) at pH 6.0, (b) at pH 6.5

a

Flocculation Index (y-axis: 0.0 to 2.0)

SO$_4^{2-}$(M),ZP(mV)

0,-4.2

.0005,-7.1

.001,-13.3

b

Flocculation Index (y-axis: 0.0 to 2.0)

Flocculation Time, min (x-axis: -2 to 30)

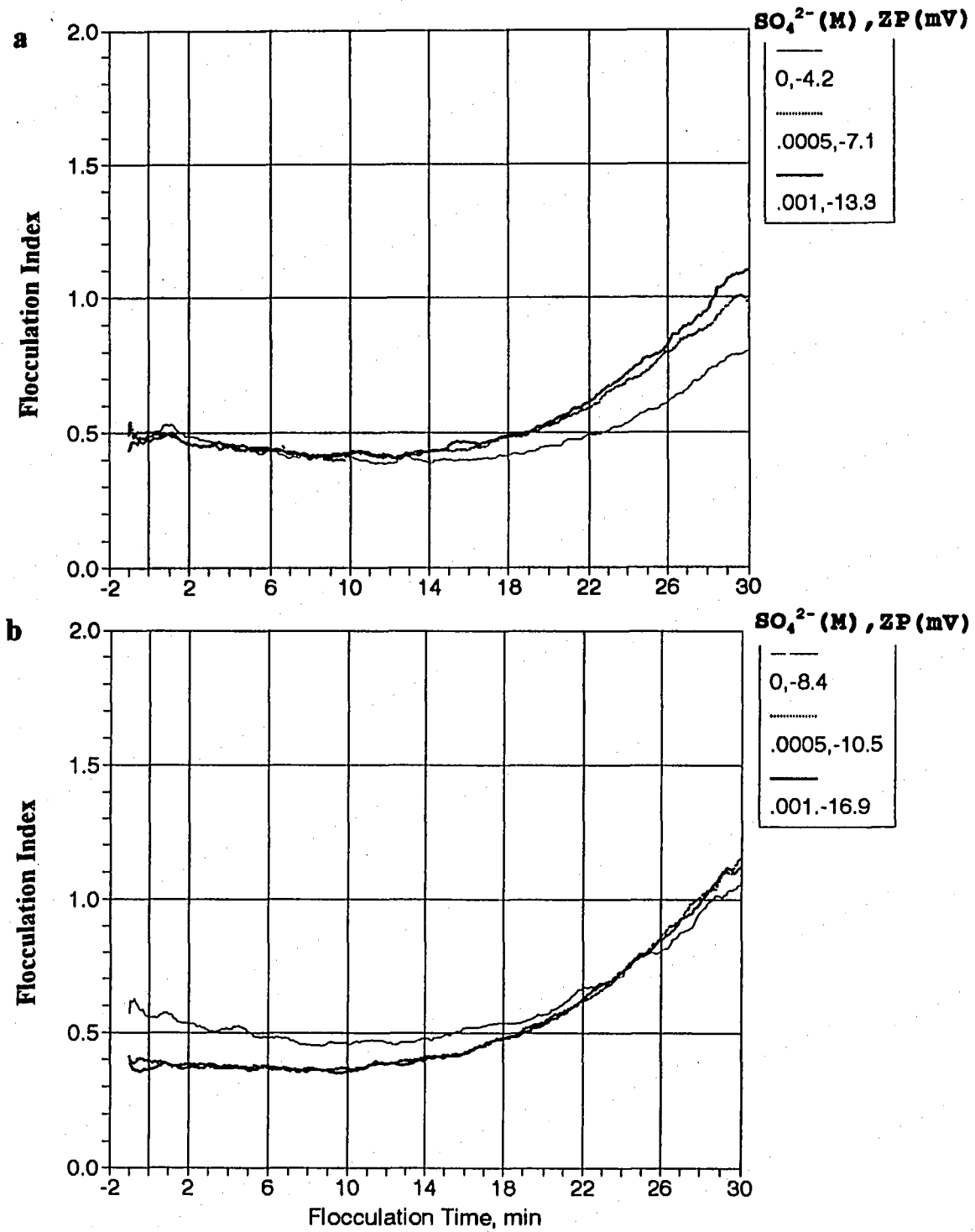SO$_4^{2-}$(M),ZP(mV)

0,-8.4

.0005,-10.5

.001.-16.9

Figure A.3. Effect of sulfate concentration on the rate of flocculation
(clay: 5 mg/L, dose: 5 mg/L); (a) at pH 6.8, (b) at pH 8.0